npg

Editorial

Celebrating the 80th anniversary of the Shanghai Institute of Materia Medica, Chinese Academy of Sciences (SIMM)

Jian DING

Editor-in-chief, Acta Pharmacologica Sinica

Acta Pharmacologica Sinica (APS) celebrates the 80-year anniversary of the establishment of SIMM by publishing this special issue to commemorate this event. APS, the official journal of the Chinese Pharmacological Society, has been published in association with SIMM since its launch in 1980. The founding editor-in-chief, Prof Guang-sheng DING, and many prominent SIMM scientists have served on the APS editorial board in the past. With consistent support from SIMM, APS has grown to be China's leading international journal in the fields of pharmacology and pharmacy, publishing high quality papers from all over the world. To commemorate the 80th anniversary of SIMM, APS has organized this special issue including perspective, review and original articles contributed by principle investigators from SIMM in various disciplines[1–12]. These articles highlight some of the research achievements accomplished at SIMM and provide an insight into the progress of drug research in China.

SIMM, established in 1932, is a comprehensive institute engaged in fundamental and applied research in drug discovery and development. Throughout its 80-year history, SIMM has trained many outstanding pharmaceutical scientists and technologists who have developed a number of new drugs that have made their mark in the international arena, such as artemisinin (anti-malarial), sodium dimercaptosuccinate (antidote against heavy metal poisonings), sobuzoxan (anti-tumor) and huperzine A (to treat Alzheimer's disease), to name a few. Since the implementation of the "Knowledge Innovation Program" at the Chinese Academy of Sciences, a series of major achievements have transpired in drug discovery: Antofloxacin hydrochloride is the first patented quinolone-class antibiotic agent discovered at SIMM following a relentless pursuit that lasted more than 10 years; and depsides salt from *Salvia miltiorrhiza* has emerged in prominence with the modernization of traditional Chinese medicine.

We remain confident that the achievements made by SIMM scientists during the past 80 years have laid a solid foundation to advance the drug discovery capabilities in China and that newly developed drugs will continue to be introduced to the international market in growing numbers. In tandem, APS will uphold its objective to publish excellent research being performed by both domestic groups and those abroad. Given the development of drug research in China and improved international cooperation, we believe that APS will remain as a platform for publishing high quality papers of key significance in the multidisciplinary field of pharmacology and related life sciences.

I hope this issue will appeal to the broad readership with an interest in the drug discovery and development efforts being performed in China. Join us in celebrating the 80th anniversary of SIMM and enjoy the articles in this special issue.

References

1   Miao ZH, Feng JM, Ding J. Newly discovered angiogenesis inhibitors and their mechanisms of action. Acta Pharmacol Sin 2012; 33: 1103–11.
2   Tang W, Zuo JP. Immunosuppressant discovery from *Tripterygium wilfordii* Hook f: the novel triptolide analog (5*R*)-5-hydroxytriptolide (LLDT-8). Acta Pharmacol Sin 2012; 33: 1112–8.
3   Wu WY, Wang YP. Pharmacological actions and therapeutic applications of *Salvia miltiorrhiza* depside salt and its active com — ponents. Acta Pharmacol Sin 2012; 33: 1119–30.
4   Ou-Yang SS, Lu JY, Kong XQ, Liang ZJ, Luo C, Jiang H. Computational drug discovery. Acta Pharmacol Sin 2012; 33: 1131–40.
5   Li Y. Qinghaosu (artemisinin): Chemistry and pharmacology. Acta Pharmacol Sin 2012; 33: 1141–6.
6   Yang SP, Yue JM. Discovery of structurally diverse and bioactive compounds from plant resources in China. Acta Pharmacol Sin 2012; 33: 1147–58.
7   Zhou ZF, Guo YW. Bioactive natural products from Chinese marine flora and fauna. Acta Pharmacol Sin 2012; 33: 1159–69.
8   Zhang HY. New insights into huperzine A for the treatment of

Alzheimer's disease. Acta Pharmacol Sin 2012; 33: 1170–5.

9   Bai DL, Chen WZ, Bo YX, Dong YL, Kang AL, Sun WK, *et al*. Discovery of N-(3,5-bis(1-pyrrolidylmethyl)-4-hydroxybenzyl)-4-methoxybenzene-sulfamide (sulcardine) as a novel anti-arrhythmic agent. Acta Pharmacol Sin 2012; 33: 1176–86.

10 Wu DD, Huang L, Zhang L, Wu LY, Li YC, Feng L. LLDT-67 attenuates MPTP-induced neurotoxicity in mice by up-regulating NGF expression. Acta Pharmacol Sin 2012; 33: 1187–94.

11 Wang YJ, Huang SL, Feng Y, Ning MM, Leng Y. Emodin, an 11β-hydroxysteroid dehydrogenase type 1 inhibitor, regulates adipocyte function *in vitro* and exerts anti-diabetic effect in *ob/ob* mice. Acta Pharmacol Sin 2012; 33: 1195–203.

12 Fang JP, Liu Y, Li J, Liao WF, Hu YH, Ding K. A novel small molecule, HK-156, inhibits lipopolysaccharide-induced activation of NF-κB signaling and improves survival in mouse models of sepsis. Acta Pharmacol Sin 2012; 33: 1204–16.

npg

Review

Newly discovered angiogenesis inhibitors and their mechanisms of action

Ze-hong MIAO*, Jian-ming FENG, Jian DING*

Division of Antitumor Pharmacology, State Key Laboratory of Drug Research, Shanghai Institute of Materia Medica, Chinese Academy of Sciences, Shanghai 201203, China

In the past decade, the success of angiogenesis inhibitors in clinical contexts has established the antiangiogenic strategy as an important part of cancer therapy. During that time period, we have discovered and reported 17 compounds that exert potent inhibition on angiogenesis. These compounds exhibit tremendous diversity in their sources, structures, targets and mechanisms. These studies have generated new models for further modification and optimization of inhibitory compounds, new information for mechanistic studies and a new drug candidate for clinical development. In particular, through studies on the antiangiogenic mechanism of pseudolaric acid B, we discovered a novel mechanism by which the stability of hypoxia-inducible factor 1α is regulated by the transcription factor c-Jun. We also completed a preclinical study of AL3810, a compound with the potential to circumvent tumor drug resistance to a certain extent. All of these findings will be briefly reviewed in this article.

Keywords: cancer therapy; angiogenesis inhibitor; antiangiogenic mechanism; hypoxia-inducible factor 1α; pseudolaric acid B; AL3810

Introduction

Angiogenesis drives tumor progression; in particular, angiogenesis is critical for the growth and metastasis of solid tumors[1-4]. The inhibition of tumor angiogenesis has therefore become an important strategy for cancer therapy. Several inhibitors of tumor angiogenesis, such as bevacizumab (Avastin), sorafenib (Nexavar) and sunitinib (Sutent), have been successfully used in the clinic to treat solid tumors[4]. This success has led to increased efforts to discover new angiogenesis inhibitors with different mechanisms of action and/or distinct chemical structures. During the past 10 years, we have discovered and reported on 17 compounds that demonstrate potent inhibition of angiogenesis (Table 1). In contrast to the inhibitors that are already employed for clinical purposes, these newly discovered antiangiogenic agents display intriguing diversity in their sources, chemical structures, antiangiogenic mechanisms, and molecular targets. This review will focus on these diverse characteristics of the 17 newly discovered antiangiogenic compounds, as well as the representative findings that have been produced by the mechanistic investigation and preclinical development of these compounds.

An overview of the 17 antiangiogenic compounds

In a search for new angiogenesis inhibitors, we performed extensive evaluations of thousands of natural products and synthetic or semi-synthetic compounds over the course of the past 10 years. From this process, 17 compounds were discovered to possess antiangiogenic activity (Table 1). The mechanisms of action of several of these compounds have been investigated, and one of these compounds, namely, AL3810, has been registered as an IND (investigational new drug) for cancer therapy in China.

Analyses of these 17 compounds indicate their diverse sources (Table 1). In particular, 7 of these inhibitors are derived from terrestrial sources, and 5 of these 7 compounds (pseudolaric acid B, triptolide, 10-hydroxycamptothecin, 11,11'-dideoxyverticillin and shiraiachrome A) are used in traditional Chinese medicine (TCM). It is also notable that quercetin is present both in many fruits and vegetables and in olive oil, red wine and tea. Of the remaining 10 compounds that were identified, 5 are marine-derived inhibitors, 3 of which [JG3, MDOS and *Grateloupia longifolia* polysaccharide (GLP)] are saccharides and 2 of which are saponins from sea cucumber. The final 5 inhibitors are chemically synthesized; these synthesized compounds are also representative of a great diversity of chemical structures, including terpenoids, alkaloids, flavonoids, saccharides, saponins and pyrido-pyrimidines, as shown in Table 1.
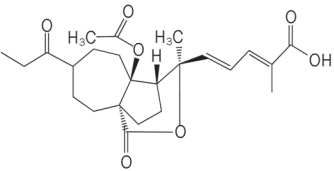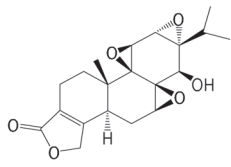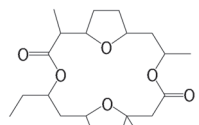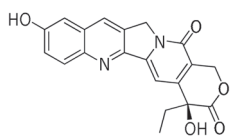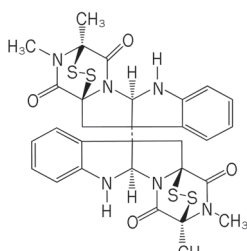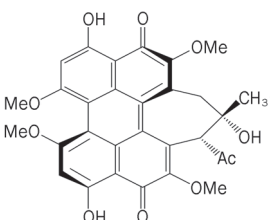
* To whom correspondence should be addressed.
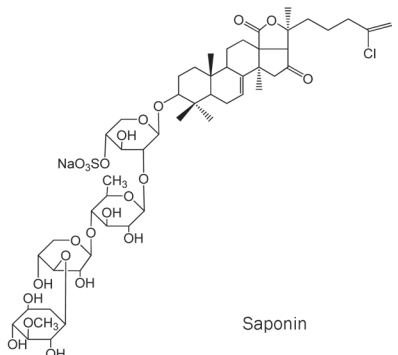E-mail zhmiao@mail.shcnc.ac.cn (Ze-hong MIAO);
      jding@mail.shcnc.ac.cn (Jian DING)
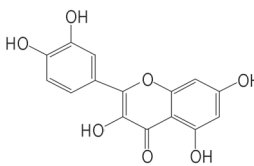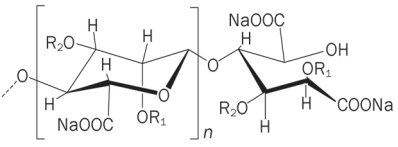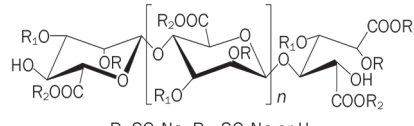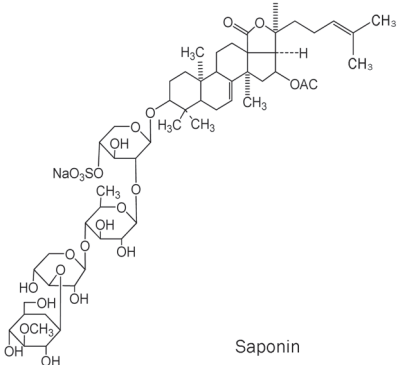
Table 1. Angiogenesis inhibitors discovered in the Shanghai Institute of Materia Medica since 2001.

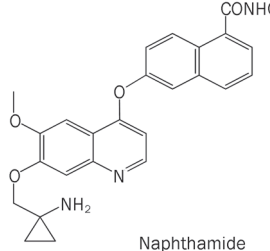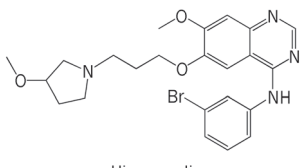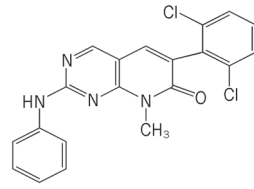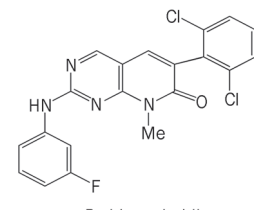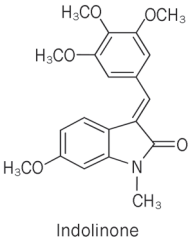| No	Inhibitors	Chemical structure	Origin	Targets	Antiangiogenic mechanisms	Refs
Terrestrial natural products						
1	Pseudolaric acid B	Iterpenoid	The root bark of *Pseudolarix amabilis*, a TCM	Microtubulin	1. To increase the phosphorylated c-Jun while reducing the non-phosphorylated c-Jun at Ser63/73, which impairs its function in stabilizing HIF-1α; 2. To reduce HIF-1α protein by promoting its proteasome-mediated degradation; 3. To abrogate hypoxia-induced VEGF secretion via reducing HIF-1α protein.	[16, 18, 22, 23]
2	Triptolide	Diterpenoid triepoxide	*Tripterygium wilfordii* Hook F, a TCM	XPB; RNAP II	1. To increase the levels of HIF-1α mRNA, but to reduce its transcriptional function; 2. To decrease mRNA levels of HIF-1α target genes including VEGF, BNIP3, and CAIX; 3. To lower the secretion of VEGF protein, and to reduce sprout outgrowth.	[20, 21]
3	MFTZ-1	Macrolide	An endophyte *Streptomyces* sp. Is9131 of *Magnolia hookeri*	Topoisomerase II	1. To reduce HIF-1α accumulation, irrelevant to its topoisomerase II inhibition; 2. To abrogate the HIF-1α-driven increase in VEGF mRNA; 3. To reduce constitutive, HIF-1α-independent VEGF secretion and concurrently antagonize inducible, HIF-1α-dependent VEGF secretion.	[17, 25]
4	10-Hydroxy-camptothecin	Alkaloid	*Camptotheca acuminata*, a TCM	Topoisomerase I	1. To inhibit proliferation, migration and tube formation of HMEC cells; 2. To inhibit angiogenesis in CAM assays; 3. To elicit apoptosis in HMEC cells.	[19]
5	11,11′-di-deoxyverti-cillin	Indole alkaloid	The fungus *Shiraia bambusicola*, a TCM	VEGF VEGFR	1. To antagonize the antiapoptotic effects of VEGF, and to inhibit VEGF-induced HUVEC migration and tube formation; 2. To completely block VEGF-induced microvessel sprouting and vessel growth; 3. To decrease VEGF secretion and to suppress VEGF-induced tyrosine phosphorylation of Flt-1 and KDR/Flk-1.	[6]
6	Shiraia-chrome A	Naphthoquinone	The fungus *Shiraia bambusicola*, a TCM	VEGFR-2; FGFR; PDGFR; EGFR	1. To suppress the autophosphorylation of VEGFR-2, FGFR, PDGFR, and EGFR; 2. To inhibit the proliferation, migration, and tube formation of HMEC; 3. To inhibit the formation of new microvessels in a rat aorta culture model as well as in the CAM assay.	[7]

No	Inhibitors	Chemical structure	Origin	Targets	Antiangiogenic mechanisms	Refs
7	Quercetin	Flavonoid	Many fruits and vegetables, as well as olive oil, red wine, and tea	MMP-2	1. To inhibit proliferation, migration, and tube formation of HMEC and HUVEC; 2. To display an antiangiogenic effect *in vivo*; 3. To decrease the expression and activity of MMP-2.	[29]

Marine-derived natural products

No	Inhibitors	Chemical structure	Origin	Targets	Antiangiogenic mechanisms	Refs
8	JG3	Sulfated oligosaccharide	Marine oligoman-nurarate blocks	Heparanase	1. To combat heparanase activity via binding to the KKDC and QPLK domains of the heparanase molecule; 2. To abolish heparanase-driven invasion, and to inhibit the release of heparan sulfate–sequestered bFGF from the extracellular matrix, and to repress subsequent angiogenesis; 3. To inactivate bFGF-induced bFGFR and ERK1/2 phosphorylation and to block bFGF-triggered angiogenic events by binding to bFGF.	[27, 42]
9	MDOS	R=SO₃Na, R₁=SO₃Na or H, R₂=CH₂CH(OH)CH₃ or Na, *n*=2–8 Sulfated oligosaccharide	Marine oligoman-nurarate blocks	HER2; EGFR; VEGFR; PDGFR; c-Kit; FGFR1; c-Src	1. To directly inhibit HER2, EGFR, VEGFR, PDGFR, c-Kit, FGFR1 and c-Src, with little impact on FGFR2; 2. To inhibit phosphorylation of PTKs, exemplified by HER2, EGFR and VEGFR2, and downstream molecules of Erk1/2 and AKT; 3. To act as an ATP competitive inhibitor via directly binding to the residues of entrance rather than those of the ATP-binding pocket.	[8]
10	*Grateloupia longifolia* polysaccharide	Sulphated polysaccharide (MW: $1.8×10^6$)	The marine alga *G longifolia*	Tissue factor	1. To decrease tissue factor at both mRNA and protein levels; 2. To inhibit proliferation of HMECs and HUVEC and tube formation and to reduce the number of migratory cells in a VEGF-independent manner; 3. To reduce new vessel formation and the vessel density in Matrigel plugs implanted in mice.	[30]
11	Philinopside E	Saponin	Sea cucumber (*pentacta quadrangularis*)	KDR	1. To inhibit KDR phosphorylation and downstream signaling; 2. To specifically interact with KDR extracellular domain, and to block its interaction with VEGF and the downstream signaling; 3. To markedly suppresses αvβ3 integrin-driven downstream signaling and as a result, to disturb the physical interaction between KDR and αvβ3 integrin in HMECs, followed by disruption of the actin cytoskeleton organization and decreased cell adhesion to vitronectin.	[9]

(To be continued)

No	Inhibitors	Chemical structure	Origin	Targets	Antiangiogenic mechanisms	Refs
12	Philinopside A	Saponin	Sea cucumber (*pentacta quad-rangularis*)	VEGFR; FGFR1; PDGFRβ; EGFR	1. To inhibit the proliferation, migration and tube formation of HMECs; 2. To suppress the formation of new microvessels in cultured rat aorta and angiogenesis in CAM assays; 3. To inhibit VEGFR, FGFR1, PDGFRβ, and EGFR.	[10]

Synthetic inhibitors

No	Inhibitors	Chemical structure	Origin	Targets	Antiangiogenic mechanisms	Refs
13	AL3810	Naphthamide	Synthetic	VEGFR1; VEGFR2; FGFR1; PDGFRβ	1. To inhibit VEGFR1, VEGFR2, FGFR1 and PDGFRβ; 2. To inhibit the autophosphorylation of VEGFR2, PDGFRβ, and FGFR1 in endothelial cells; 3. To exhibit potent antiangiogenesis activity, manifested by significant inhibition of microvessel outgrowth of rat arterial ring and CAM in *ex vivo* angiogenesis models.	[11, 31]
14	BB	Uinonazoline	Synthetic	EGFR	1. To selectively inhibit EGFR; 2. To abrogate autophosphorylation of the EGF-stimulated EGFR and phosphorylation of its key down-stream signaling molecules ERK and AKT in A549 cells; 3. To exhibit antiangiogenesis activity, as evidenced by antagonizing EGF-induced HMECS migration *in vitro*, blocking HMECS tube formation, and inhibiting microvessel sprouting from rat aortic rings.	[12]
15	TKI-28	Pyrido-pyrimidine	Synthetic	ErbB-2; EGFR; KDR; PDGFRβ; c-kit; c-Src	1. To inhibit ErbB-2, EGFR, KDR, PDGFRβ, c-kit and c-Src in cell-free systems; 2. To block their autophosphorylation and subsequently to downregulate phosphorylation of many downstream signaling proteins at the cellular level; 3. To inhibit cell proliferation driven by EGF, VEGF and PDGF, and cell migration and tube formation in HMECs.	[13]
16	TKI-31	Pyrido-pyrimidine	Synthetic	VEGFR2; PDGFRβ; c-kit; c-Src	1. To inhibit VEGFR2, PDGFRβ, c-kit and c-Src, showing no activity against VEGFR1 and EGFR; 2. To repress VEGF-induced phosphorylation of VEGFR2 in endothelial cells and PDGFBB-induced phosphorylation in fibroblast cells, leading to the inhibition of PI3K/Akt/mTOR, MAPK42/44 (ERK) and paxillin;	[14]

(To be continued)

No	Inhibitors	Chemical structure	Origin	Targets	Antiangiogenic mechanisms	Refs
					3. To suppress VEGF-induced endothelial cells proliferation, migration and their differentiation into capillary-like tube formation.	
17	C9	H₃CO, OCH₃ — H₃CO — H₃CO — O — CH₃ Indolinone	Synthetic	Microtubulin	1. To inhibit proliferation, migration and tube formation of endothelial cells, and angiogenesis in aortic ring and CAM assays; 2. To induce disassembly of microtubules in endothelial cells and to downregulate Raf-MEK-ERK signaling activated by pro-angiogenic factors; 3. To disrupt capillary-like networks and newly formed vessels *in vitro* and to rapidly decrease perfusion of neovasculature *in vivo*, and to induce endothelial cell contraction and membrane blebbing in neovasculature dependent on the Rho/Rho kinase pathway.	[24]

Abbreviations: BNIP3, BCL2/adenovirus E1B 19 kDa protein-interacting protein 3; CAIX, carbonic anhydrase IX; CAM, chick chorioallantoic membrane; EGFR, epidermal growth factor receptor; ERK, extracellular signal regulated kinase; bFGF, basic fibroblast growth factor; FGFR1, FGF receptor 1; HER2, human epidermal growth factor receptor-2; HIF-1α, hypoxia-inducible factor 1alpha; HMEC, human dermal microvasculature endothelial cells; HUVEC, human umbilical vein endothelial cells; KDR, receptor for vascular endothelial growth factor; MEK, MAPK/ERK kinase; MMP-2, matrix metalloproteinase-2; PDGFBB, platelet derived growth factor BB; PDGFR, platelet-derived growth factor receptor; RTK, receptor tyrosine kinase; VEGF, vascular endothelial growth factor; VEGFR, vascular endothelial growth factor receptor; TCM, traditional Chinese medicine.

The apparent differences in the sources and chemical structures of the 17 inhibitors are reflected in their distinct (potential) targets. These targets include angiogenic kinases (angiokinases), extracellular matrix (ECM) components and the hypoxia-inducible factor 1α (HIF-1α)-vascular endothelial growth factor (VEGF) axis, among others (Table 1, Figure 1). Moreover, the antiangiogenic activities of these compounds revealed in the *in vitro*, *ex vivo* and/or *in vivo* experimental models are mediated by distinct molecular signaling pathways (Figure 1).

Angiokinase inhibitors

Although many protein tyrosine kinases (PTKs) contribute to the angiogenic process, the VEGF-VEGF receptor (VEGFR) axis is the main target for clinical applications of antiangiogenic therapy[5]. Of the 17 compounds listed in Table 1, 9 compounds, namely, 11,11'-dideoxyverticillin, shiraiachrome A, MDOS, philinopside A, philinopside E, AL3810, BB, TKI-28, and TKI-31, were found to directly inhibit this axis[6–14] (Table 1 and Figure 1). The former 5 compounds are derived from natural products, whereas the latter 4 inhibitors are synthetic. These 9 compounds display different profiles of PTK inhibition, as they have distinct selectivity against various receptor and/or non-receptor tyrosine kinases, including human epi-
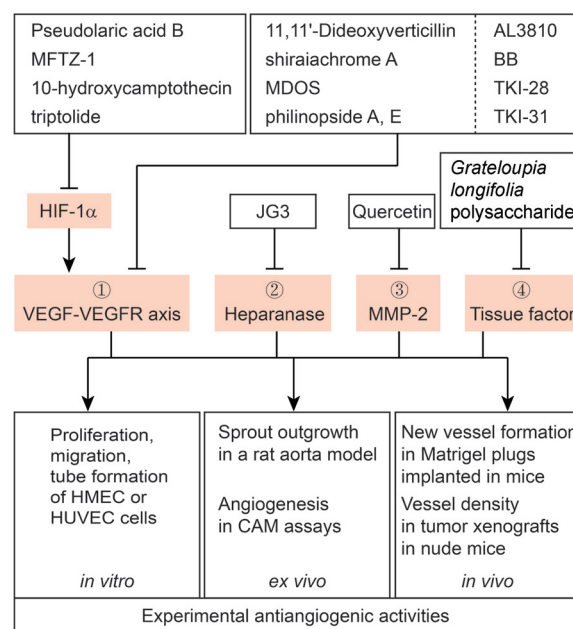

Figure 1. A schematic overview of molecular signaling that possibly mediates experimental antiangiogenic activities of the compounds discussed here.

dermal growth factor receptor 2 (HER2), epidermal growth factor receptor (EGFR), VEGFR, platelet-derived growth factor receptor (PDGFR), c-Kit, fibroblast growth factor receptor 1 (FGFR1) and/or c-Src. Nevertheless, all 9 of these compounds can directly suppress the critical angiokinase VEGFR, producing significant experimentally observed antiangiogenic effects as a result (Table 1 and Figure 1). In particular, AL3810 has been in clinical trials because it not only displays excellent anticancer and antiangiogenic activities but also demonstrates good pharmacokinetics and toxicity in preclinical studies[15, 16].

HIF-1α-VEGF axis inhibitors

We also found that of the 17 identified antiangiogenic compounds, 4 compounds, namely, pseudolaric acid B, MFTZ-1, 10-hydroxycamptothecin and triptolide, can indirectly inhibit the VEGF-VEGFR axis by decreasing cellular HIF-1α accumulation and thereby reducing VEGF expression and secretion[15–21] (Figure 1). We define these compounds to be HIF-1α-VEGF axis inhibitors. HIF-1α is a critical transcription factor that impacts tumor angiogenesis by regulating the expression of VEGF. HIF-1α has thus been proposed as a promising anticancer target.

The HIF-1α-VEGF axis inhibitors reduce the cellular amount of HIF-1α in different ways. Pseudolaric acid B targets microtubulin and causes its depolymerization[22, 23]. Pseudolaric acid B inhibits angiogenesis by reducing the stability of HIF-1α and thereby downregulating the VEGF-VEGFR axis[15, 16, 18]. However, there has been no direct evidence indicating any association between its antiangiogenic activity and its inhibition of microtubulin[23, 24]. By contrast, MFTZ-1 does not affect either the degradation of HIF-1α protein or the level of HIF-1α mRNA. Instead, MFTZ-1 can abrogate the HIF-1α-driven increase in VEGF mRNA and VEGF protein secretion, producing antiangiogenic effects. Specifically, MFTZ-1 can reduce constitutive, HIF-1α-independent VEGF secretion and concurrently antagonize inducible, HIF-1α-dependent VEGF secretion, in an effect that is independent of its inhibition of its primary target, topoisomerase II[17, 25]. The inhibition of angiogenesis by 10-hydroxycamptothecin[19] may be associated with this drug's suppression of HIF-1α expression, which occurs *via* the repression of topoisomerase I-dependent transcription. This mechanism of action is possibly similar to the mechanism that is used by topotecan, another camptothecin derivative[26]. In contrast to the previous 3 inhibitors, triptolide may enhance the levels of cellular HIF-1α mRNA and protein[20]. However, triptolide also causes the downregulation of VEGF expression and secretion[20], possibly because it binds to XPB (which is also known as ERCC3) and causes the degradation of RNA polymerase II[21], disrupting the transcriptional function of HIF-1α.

ECM component inhibitors

ECM components including heparanase and matrix metalloproteinase (MMP) are critically involved in the metastatic and angiogenic capabilities of tumor cells. Inhibitors targeting ECM components are increasingly emerging as promising agents for cancer therapy. We have discovered a series of compounds that inhibit tumor angiogenesis by targeting heparanase and MMP. Oligomannurarate sulfate (JG3), a novel oligosaccharide, was identified as a heparanase inhibitor. JG3 significantly inhibits tumor angiogenesis and metastasis, both *in vitro* and *in vivo*, by combating heparanase activity; in particular, this effect is mediated through the binding of JG3 to the KKDC and QPLK domains of heparanase. In addition, JG3 abolished heparanase-driven invasion, inhibited the release of basic fibroblast growth factor (bFGF) from the ECM and repressed subsequent angiogenesis[27]. By contrast, the antiangiogenic effects of quercetin were found to be associated with its downregulation of MMP-2[28]. In fact, however, other studies reveal complicated molecular mechanisms involved in the antiangiogenic activity of quercetin, including its inhibition of the synthesis and accumulation of the HIF-1α protein; this inhibition reduces the production and secretion of VEGF, as discussed above[29].

Other angiogenesis inhibitors

C9 and GLP exert antiangiogenic effects through relatively unique mechanisms of action (Table 1). C9 is a new microtubule-depolymerizing agent. In striking contrast to pseudolaric acid B, C9 elicits its antiangiogenic and vascular disrupting effects by inducing microtubule disassembly, the downregulation of Raf-MEK-ERK signaling and the reorganization of actin through the Rho/Rho kinase pathway[24]. GLP is a new type of polysaccharide isolated from the alga *G longifolia*. GLP causes obvious *in vitro* and *in vivo* antiangiogenic effects that are not associated with classical VEGF-VEGFR signaling. GLP decreases tissue factor at both the mRNA and protein levels, and this effect may be involved in the inhibition of angiogenesis by GLP[30].

Our findings provide the following beneficial clues to facilitate the future discovery of angiogenesis inhibitors: (1) Natural products are an important source of angiogenesis inhibitors. In particular, through drug discovery guided by therapeutic experiences from long-established TCM practices, inhibitors of angiogenesis could be obtained that have new chemical structures and unique mechanisms of action; examples of these sorts of inhibitors include pseudolaric acid B, triptolide, 11,11'-dideoxyverticillin and shiraiachrome A (Table 1). The original medicinal materials producing these compounds have long been used to either treat various angiogenesis-related diseases, such as rheumatoid arthritis, microbial skin diseases and psoriasis[7, 21, 23], or cause the early termination of pregnancies[23]. (2) Marine-derived compounds could be another important source of angiogenesis inhibitors, and certain compounds with specific types of chemical structures, such as saccharides, should be subjected to particular scrutiny; as demonstrated by JG3[27] and GLP[30], these compounds may exhibit unique modes of antiangiogenic activity. (3) Chemical synthesis, particularly if it is based on rational designs and modifications, is a common, frequently necessary method of generating compounds with possible medical applications; this principle is demonstrated by AL3810 in this instance[11, 31]

and is generally exemplified by a variety of clinically utilized drugs. (4) The compounds that we have discovered (Table 1) can be used as chemical models for further modification and optimization to improve their therapeutic potential as angiogenesis-inhibiting drugs for clinical use. (5) The known primary target(s) of certain compounds, such as pseudolaric acid B[15, 16, 18] and MFTZ-1[17], are not necessarily related to their antiangiogenic effects, indicating that unknown and potentially novel mechanism(s) are involved in these effects; these mechanisms merit further investigation.

The discovery that the stability of HIF-1α protein is regulated by c-Jun based on mechanistic studies of the antiangiogenic activity of pseudolaric acid B

Pseudolaric acid B is a diterpenoid isolated from the root bark of *Pseudolarix amabilis*[32]. Pseudolaric acid B has been demonstrated to both elicit potent anticancer effects by depolymerizing microtubulin[22, 23] and circumvent tumor multidrug resistance[22]. Detailed structure-activity studies have revealed that the components of pseudolaric acid B that are essential to its anticancer activity include a hydrophobic group (-CO_2 Me or -Me) at C-7, a Δ^7 double bond, an acyloxy (OAc) at C-4,3 and a side chain with a conjugated double bond and a hydrophilic terminal group[33]. Based on its traditional use in Chinese folk medicine for facilitating the early termination of pregnancy, we first discovered and reported that its antiangiogenic activity occurred because it accelerates the proteasome-executed degradation of the HIF-1α protein[18].

We previously reported that the activation of the transcription factor c-Jun plays a critical role in the circumvention of tumor multidrug resistance by salvicine[34, 35]. Based on those earlier findings, we investigated the effect of pseudolaric acid B and found that it could also drive c-Jun phosphorylation[16]. During our attempts to correlate HIF-1α protein degradation with the c-Jun phosphorylation induced by pseudolaric acid B, a novel mechanism was revealed in which c-Jun in its non-phosphorylated form regulates the stability of the HIF-1α protein[15, 16] (Figure 2).

HIF-1α is a transcription factor that drives neoangiogenesis by regulating the expression of various target genes, including the proangiogenic genes VEGF and VEGFR, in response to hypoxia during the growth of solid tumors[36]. The ubiquitination-mediated, proteasome-executed degradation constitutes a critical mechanism of regulating the stability of the cellular HIF-1α protein[37]. HIF-1α can be hydroxylated by an oxygen-sensitive prolyl hydroxylase at the Pro402 and Pro564 residues within its oxygen-dependent degradation domain (ODD)[38]. This hydroxylation will promote the ubiquitination of HIF-1α at Lys532, a process that is effectively mediated by the ubiquitin ligase known as the Von Hippel-Lindau tumor suppressor (pVHL)[39]. This ubiquitination then, in turn, leads to the reduced stability of HIF-1α by facilitating its degradation through the 26S proteasome[15] (Figure 2).

Our studies demonstrated that c-Jun binds to the ODD of HIF-1α protein, protecting HIF-1α from being ubiquitinated and thereby enhancing its stability by reducing its suscep-
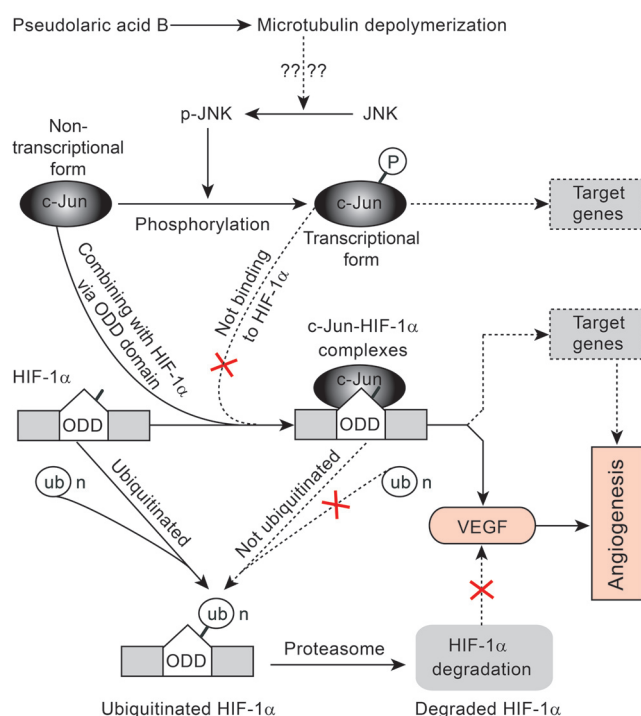

Figure 2. The antiangiogenic mechanism of pseudolaric acid B. Solid or broken lines indicate the relationships between the linked factors with direct experimental evidence (solid lines) or with logical possibility (broken lines) in the case of pseudolaric acid B.

tibility to the proteasome-executed degradation[15] (Figure 2). Notably, this binding requires the domains of c-Jun for DNA binding and heterodimerization but is independent of Ser63/73 phosphorylation. Further investigations have clarified that only non-phosphorylated c-Jun, *ie*, c-Jun without transcriptional activity, can bind to and protect HIF-1α[15, 16]. Relatively constant total levels of c-Jun are generally maintained within the cell. Pseudolaric acid B causes the increased phosphorylation of c-Jun, thus reducing the proportion of c-Jun that is in the Ser63/73-non-phosphorylated form. Consequently, the quantity of c-Jun that is able to bind to HIF-1α decreases, impairing the ability of c-Jun to stabilize HIF-1α[16] (Figure 2). Our findings constituted the first discovery of a function for the non-phosphorylated form of c-Jun; in accordance with these results, a function-converter model of c-Jun was proposed, in which Ser63/73 phosphorylation serves as a function converter that shifts c-Jun from its non-transcriptional functions to its transcriptional functions[16].

The development of AL3810 as a clinically promising angiokinase inhibitor

Various PTKs are aberrantly activated during tumor progression. Several of these PTKs, including VEGFR, PDGFR, and FGFR1, have been demonstrated to contribute to tumor angiogenesis[11, 31]. In recent years, we have discovered hundreds of compounds with inhibitory activities against different PTKs and have reported that 9 compounds exhibit potent antiangio-

genic effects (Table 1). Of these 9 compounds, AL3810 (also designated as E-3810)[31] demonstrates the greatest potential for clinical use.

AL3810 is a synthetic multitargeted PTK inhibitor that inhibits VEGFR1, VEGFR2, PDGFRα, PDGFRβ, and FGFR1 with IC_{50} values in the nanomolar range[11, 31]. In endothelial cells, AL3810 can suppress the autophosphorylation of VEGFR2, PDGFRβ and FGFR1. AL3810 thus displays apparent antiangiogenic activity in all of the tested *in vitro*, *ex vivo,* and *in vivo* models (Figure 1). Even at millimolar concentrations, however, AL3810 demonstrates no cytotoxic effects on cancer cell lines. Nevertheless, AL3810 can elicit broad-spectrum *in vivo* antitumor activity in human kidney, pancreas and liver cancer xenograft models; its activity appears to make it more potent than several commercially available multitargeted PTK inhibitors, such as sorafenib and Sutent. Moreover, its antitumor activity is closely correlated with its antiangiogenic activity[11, 31].

Notably, it appears that tumors do not easily become resistant to AL3810, as xenografted tumors re-grown after the withdrawal of AL3810 demonstrate a response to a second cycle of AL3810 treatment that is similar to the response observed for the first treatment cycle. By contrast, tumors re-grown after the withdrawal of sunitinib treatment display reduced sensitivity to a second cycle of treatment with sunitinib. However, these sunitinib-resistant tumors remain sensitive to AL3810[31]. Although this result requires further confirmation, particularly in the clinical context, and the mechanism underlying this result also must be clarified, its potential importance is obvious, particularly given that tumors are generally prone to becoming resistant to the PTK inhibitors that are currently in clinical use[40].

The oral bioavailability of AL3810 is excellent, reaching 31% in rats[11]. Moreover, the concentration of AL3810 in different tissues is higher than the concentration of AL3810 in the plasma of tumor-bearing nude mice. In particular, a 51.7-fold increase in the concentration of AL3810 was detected in the examined tumoral tissues when compared with that in plasma, demonstrating the high affinity of AL3810 to tumors[11]. In addition, AL3810 has a relatively long terminal half-life of approximately 4 h; this extended half-life may help explain its persistent antitumor effects[31]. All of these results indicate that AL3810 possesses a favorable pharmacokinetic profile.

The prominent advantages of AL3810, which include its potent antiangiogenic effect, its broad spectrum of antitumor activity, its ability to potentially circumvent the drug resistance of tumors and its favorable pharmacokinetic profile, make it an excellent candidate for development as an anticancer drug. AL3810 has already entered into clinical trials in Europe to assess its potential use for this application, and its clinical trials in China will be launched shortly[11, 31].

Concluding remarks

As an aspect of international efforts to explore new antiangiogenic compounds, we investigated the inhibition of angiogenesis by 17 compounds. These compounds have diverse origins,

structures, primary targets and mechanisms. Our findings provide new models for the further modification and optimization of antiangiogenic compounds, and new clues related to the examination of antiangiogenic mechanisms. Tumor drug resistance poses a challenge for the antiangiogenic agents that are in current use[41]. Therefore, one of the most urgent tasks in the future will be to both demonstrate the critical molecular mechanism(s) underlying the effects of AL3810 and accelerate the clinical development of AL3810 to meet the potential clinical need for agents that can circumvent this tumor drug resistance. The detailed dissection of the structure-effect relationships of certain compounds to analyze the relationships between their antiangiogenic mechanisms and their cytotoxicity and between their primary targets and their antiangiogenic mechanisms could be another important task to accomplish, as well; the elucidation of these relationships could generate new strategies for cancer therapy.

References

1　Zetter BR. The scientific contributions of M. Judah Folkman to cancer research. Nat Rev Cancer 2008; 8: 647–54.

2　Eichhorn ME, Kleespies A, Angele MK, Jauch KW, Bruns CJ. Angiogenesis in cancer: molecular mechanisms, clinical impact. Langenbecks Arch Surg 2007; 392: 371–9.

3　Fischer C, Mazzone M, Jonckx B, Carmeliet P. FLT1 and its ligands VEGFB and PlGF: drug targets for anti-angiogenic therapy? Nat Rev Cancer 2008; 8: 942–56.

4　Argyriou AA, Giannopoulou E, Kalofonos HP. Angiogenesis and antiangiogenic molecularly targeted therapies in malignant gliomas. Oncology 2009; 77: 1–11.

5　Tugues S, Koch S, Gualandi L, Li X, Claesson-Welsh L. Vascular endothelial growth factors and receptors: anti-angiogenic therapy in the treatment of cancer. Mol Aspects Med 2011; 32: 88–111.

6　Chen Y, Zhang YX, Li MH, Zhao WM, Shi YH, Miao ZH, *et al*. Antiangiogenic activity of 11,11'-dideoxyverticillin, a natural product isolated from the fungus *Shiraia bambusicola*. Biochem Biophys Res Commun 2005; 329: 1334–42.

7　Tong Y, Zhang X, Zhao W, Zhang Y, Lang J, Shi Y, *et al*. Anti-angiogenic effects of Shiraiachrome A, a compound isolated from a Chinese folk medicine used to treat rheumatoid arthritis. Eur J Pharmacol 2004;

494: 101–9.

8 Ma J, Xin X, Meng L, Tong L, Lin L, Geng M, *et al*. The marine-derived oligosaccharide sulfate (MdOS), a novel multiple tyrosine kinase inhibitor, combats tumor angiogenesis both *in vitro* and *in vivo*. PLoS One 2008; 3: e3774.

9 Tian F, Zhu CH, Zhang XW, Xie X, Xin XL, Yi YH, *et al*. Philinopside E, a new sulfated saponin from sea cucumber, blocks the interaction between kinase insert domain-containing receptor (KDR) and alpha-vbeta3 integrin via binding to the extracellular domain of KDR. Mol Pharmacol 2007; 72: 545–52.

10 Tong Y, Zhang X, Tian F, Yi Y, Xu Q, Li L, *et al*. Philinopside A, a novel marine-derived compound possessing dual anti-angiogenic and anti-tumor effects. Int J Cancer 2005; 114: 843–53.

11 Zhou Y, Chen Y, Tong L, Xie H, Wen W, Zhang J, *et al*. AL3810, a multi-tyrosine kinase inhibitor, exhibits potent anti-angiogenic and antitumor activity via targeting VEGFR, FGFR, and PDGFR. J Cell Mol Med 2012. doi: 10.1111/j.1582-4934.2012.01541.x.

12 Sun QM, Miao ZH, Lin LP, Gui M, Zhu CH, Xie H, *et al*. BB, a new EGFR inhibitor, exhibits prominent anti–angiogenesis and antitumor activities. Cancer Biol Ther 2009; 8: 1640–7.

13 Guo XN, Zhong L, Tan JZ, Li J, Luo XM, Jiang HL, *et al*. *In vitro* pharmacological characterization of TKI-28, a broad-spectrum tyrosine kinase inhibitor with anti-tumor and anti-angiogenic effects. Cancer Biol Ther 2005; 4: 1125–32.

14 Zhong L, Guo XN, Zhang XH, Sun QM, Tong LJ, Wu ZX, *et al*. TKI-31 inhibits angiogenesis by combined suppression signaling pathway of VEGFR2 and PDGFRbeta. Cancer Biol Ther 2006; 5: 323–30.

15 Yu B, Miao ZH, Jiang Y, Li MH, Yang N, Li T, *et al*. c-Jun protects hypoxia-inducible factor-1alpha from degradation via its oxygen-dependent degradation domain in a nontranscriptional manner. Cancer Res 2009; 69: 7704–12.

16 Yu B, Li MH, Wang W, Wang YQ, Jiang Y, Yang SP, *et al*. Pseudolaric acid B-driven phosphorylation of c-Jun impairs its role in stabilizing HIF-1alpha: a novel function-converter model. J Mol Med (Berl) 2012; 90: 971–81.

17 Dai M, Miao ZH, Ren X, Tong LJ, Yang N, Li T, *et al*. MFTZ-1 reduces constitutive and inducible HIF-1alpha accumulation and VEGF secretion independent of its topoisomerase II inhibition. J Cell Mol Med 2010; 14: 2281–91.

18 Li MH, Miao ZH, Tan WF, Yue JM, Zhang C, Lin LP, *et al*. Pseudolaric acid B inhibits angiogenesis and reduces hypoxia-inducible factor 1alpha by promoting proteasome-mediated degradation. Clin Cancer Res 2004; 10: 8266–74.

19 Xiao D, Tan W, Li M, Ding J. Antiangiogenic potential of 10-hydroxy-camptothecin. Life Sci 2001; 69: 1619–28.

20 Zhou ZL, Luo ZG, Yu B, Jiang Y, Chen Y, Feng JM, *et al*. Increased accumulation of hypoxia-inducible factor-1alpha with reduced transcriptional activity mediates the antitumor effect of triptolide. Mol Cancer 2010; 9: 1–11.

21 Zhou ZL, Yang YX, Ding J, Li YC, Miao ZH. Triptolide: structural modifications, structure-activity relationships, bioactivities, clinical development and mechanisms. Nat Prod Rep 2012; 29: 457–75.

22 Wong VK, Chiu P, Chung SS, Chow LM, Zhao YZ, Yang BB, *et al*. Pseudolaric acid B, a novel microtubule-destabilizing agent that circumvents multidrug resistance phenotype and exhibits antitumor activity *in vivo*. Clin Cancer Res 2005; 11: 6002–11.

23 Tong YG, Zhang XW, Geng MY, Yue JM, Xin XL, Tian F, *et al*. Pseudolarix acid B, a new tubulin-binding agent, inhibits angiogenesis by interacting with a novel binding site on tubulin. Mol Pharmacol 2006; 69: 1226–33.

24 Ren X, Dai M, Lin LP, Li PK, Ding J. Anti-angiogenic and vascular disrupting effects of C9, a new microtubule-depolymerizing agent. Br J Pharmacol 2009; 156: 1228–38.

25 Xie CY, Zhu H, Lin LP, Miao ZH, Geng MY, Cai YJ, *et al*. MFTZ-1, an actinomycetes subspecies derived antitumor macrolide, functions as a novel topoisomerase II poison. Mol Cancer Ther 2007; 6: 3059–70.

26 Kummar S, Raffeld M, Juwara L, Horneffer Y, Strassberger A, Allen D, *et al*. Multihistology, target-driven pilot trial of oral topotecan as an inhibitor of hypoxia-inducible factor-1alpha in advanced solid tumors. Clin Cancer Res 2011; 17: 5123–31.

27 Zhao H, Liu H, Chen Y, Xin X, Li J, Hou Y, *et al*. Oligomannurarate sulfate, a novel heparanase inhibitor simultaneously targeting basic fibroblast growth factor, combats tumor angiogenesis and metastasis. Cancer Res 2006; 66: 8779–87.

28 Tan WF, Lin LP, Li MH, Zhang YX, Tong YG, Xiao D, *et al*. Quercetin, a dietary-derived flavonoid, possesses antiangiogenic potential. Eur J Pharmacol 2003; 459: 255–62.

29 Lee DH, Lee YJ. Quercetin suppresses hypoxia-induced accumulation of hypoxia-inducible factor-1alpha (HIF-1alpha) through inhibiting protein synthesis. J Cell Biochem 2008; 105: 546–53.

30 Zhang C, Yang F, Zhang XW, Wang SC, Li MH, Lin LP, *et al*. *Grateloupia longifolia* polysaccharide inhibits angiogenesis by downregulating tissue factor expression in HMEC-1 endothelial cells. Br J Pharmacol 2006; 148: 741–51.

31 Bello E, Colella G, Scarlato V, Oliva P, Berndt A, Valbusa G, *et al*. E-3810 is a potent dual inhibitor of VEGFR and FGFR that exerts anti-tumor activity in multiple preclinical models. Cancer Res 2011; 71: 1396–405.

32 Chiu P, Leung LT, Ko BC. Pseudolaric acids: isolation, bioactivity and synthetic studies. Nat Prod Rep 2010; 27: 1066–83.

33 Yang SP, Cai YJ, Zhang BL, Tong LJ, Xie H, Wu Y, *et al*. Structural modification of an angiogenesis inhibitor discovered from traditional Chinese medicine and a structure-activity relationship study. J Med Chem 2008; 51: 77–85.

34 Miao ZH, Ding J. Transcription factor c-Jun activation represses *mdr-1* gene expression. Cancer Res 2003; 63: 4527–32.

35 Miao ZH, Tang T, Zhang YX, Zhang JS, Ding J. Cytotoxicity, apoptosis induction and downregulation of MDR-1 expression by the anti-topoisomerase II agent, salvicine, in multidrug-resistant tumor cells. Int J Cancer 2003; 106: 108–15.

36 Weidemann A, Johnson RS. Biology of HIF-1alpha. Cell Death Differ 2008; 15: 621–7.

37 Semenza GL. Hydroxylation of HIF-1: oxygen sensing at the molecular level. Physiology (Bethesda) 2004; 19: 176–82.

38 Epstein AC, Gleadle JM, McNeill LA, Hewitson KS, O'Rourke J, Mole DR, *et al*. *C elegans* EGL-9 and mammalian homologs define a family of dioxygenases that regulate HIF by prolyl hydroxylation. Cell 2001; 107: 43–54.

39 Berra E, Ginouves A, Pouyssegur J. The hypoxia-inducible-factor hydroxylases bring fresh air into hypoxia signalling. EMBO Rep 2006; 7: 41–5.

40 Rosenzweig SA. Acquired resistance to drugs targeting receptor tyrosine kinases. Biochem Pharmacol 2012; 83: 1041–8.

41 Bergers G, Hanahan D. Modes of resistance to anti-angiogenic therapy. Nat Rev Cancer 2008; 8: 592–603.

42 Li QN, Liu HY, Xin XL, Pan QM, Wang L, Zhang J, *et al*. Marine-derived oligosaccharide sulfate (JG3) suppresses heparanase-driven cell adhesion events in heparanase over-expressing CHO-K1 cells. Acta Pharmacol Sin 2009; 30: 1033–8.

npg

Review

Immunosuppressant discovery from *Tripterygium wilfordii* Hook f: the novel triptolide analog (5*R*)-5-hydroxytriptolide (LLDT-8)

Wei TANG, Jian-ping ZUO*

Laboratory of Immunopharmacology, State Key Laboratory of Drug Research, Shanghai Institute of Materia Medica, Chinese Academy of Sciences, Shanghai 201203, China

The Chinese traditional herb *Tripterygium wilfordii* Hook f (TwHF) has been widely used in the treatment of autoimmune and inflammatory diseases. Over the past few decades, great efforts have been made to explore modern preparations of TwHF with higher efficacy, solubility, and lower toxicity. In this study, we reviewed several examples both of naturally occurring compounds and their derivatives in TwHF, and summarized the preclinical evaluations with regard to autoimmune and inflammatory diseases. All of the candidate compounds described herein have been or are currently in clinical trials. Although some studies encountered problems, the data still provided valuable references for future studies. (5*R*)-5-hydroxytriptolide (LLDT-8, Leitengshu) is a novel triptolide derivative with potent immunosuppressive and anti-inflammatory activities developed at Shanghai Institute of Materia Medica. Indeed, a Phase I clinical trial for this compound has been completed in rheumatoid arthritis patients. The results will provide the basis for the further exploration of this ancient herb and encourage the research and development of valuable traditional Chinese medicine.

Keywords: *Tripterygium wilfordii* Hook f; triptolide; (5*R*)-5-hydroxytriptolide (LLDT-8); autoimmune diseases; immunosuppressants; clinical trials

Introduction

For thousands of years, natural products have played an important role throughout the world in treating and preventing human diseases[1–5]. The discovery and development of immunosuppressants from natural sources have an impressive record: mycophenolic acid (MPA) and cyclosporin A (CsA), the fungal metabolites isolated in 1932[6] and 1970[7], respectively; rapamycin, found in 1975[8]; FK506, extracted from a culture filtrate of *Streptomyces tsukubaensis* in 1987[9, 10]; and fingolimod (FTY720), described in 1995[11]. Although the current industry model for drug discovery does not favor natural products, the resources are so vast as to seem unlimited, and these emerging tools will provide important discoveries, leading to new medicines[12]. Furthermore, the drugs already in use as immunosuppressants (*eg*, cyclophosphamide, methotrexate, azathioprine, cyclosporin) are associated with some significant problems, including toxicity, a lack of reversibility, and increased susceptibility to viral and other infections[13]. Indeed, exploring new and innovative immunosuppres-

sants from natural sources has now become a focus of intense research.

Tripterygium wilfordii Hook f (TwHF) and its extracts have been widely used in the treatment of autoimmune and inflammatory diseases, including rheumatoid arthritis (RA), systemic lupus erythematosus (SLE), and dermatomyositis (DM)[14–18], and have beneficial effects on tissue and organ transplantation[19, 20]. In 1993, the ethyl acetate (EA) extract of TwHF was entered into a Phase I study for the treatment of RA patients[21–25], and many clinical trials have tested triptolide for the treatment of RA and psoriasis[26, 27]. In addition, PG490-88/F60008 (Figure 1), a water-soluble prodrug of triptolide, has been approved for entry into a Phase I clinical trial for the treatment of solid tumors[28, 29].

The Shanghai Institute of Materia Medica (SIMM) has made great efforts to discover drugs from natural products that are of clinical value and have contributed to the treatment of autoimmune diseases, such as RA, SLE, and multiple sclerosis (MS). By combining basic and applied research efforts and through the collaboration between chemistry and biology, the SIMM has developed several series of immunosuppressive drug candidates against autoimmune diseases: LLDT-8 (Figure 1), a novel triptolide analog from the Chinese traditional herb
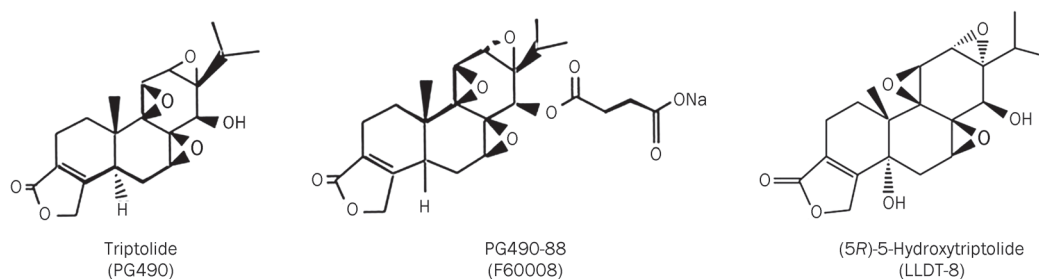
Figure 1. The structure of triptolide and its derivatives, PG490-88 (F60008) and LLDT-8.

TwHF, that will enter into a Phase II clinical trial involving RA patients in China[30-40]; SM934, a water-soluble derivative of artemisinin; and periplocoside E, a pregnane glycoside identified from *Periploca sepium* Bge.

This review focuses on the drug candidates isolated from TwHF. Regardless of the success or failure in treatment, the experience gained through the exploration and practice is invaluable.

TwHF, a representative Chinese medicinal herb showing immunosuppressive and anti-inflammatory activities

TwHF is a deciduous climbing vine that grows up to 12 meters and has brown, angular, downy twigs. The leaves are light green, smooth adaxially, and pale gray with light-colored hairs abaxially. As a well-known Chinese medicinal herb, TwHF is distributed widely in southern China, including Fujian, Zhejiang, and Anhui Provinces. The Chinese herb Lei Gong Teng is derived from the roots of TwHF and has been used in traditional Chinese medicine for more than two thousand years. The description of TwHF has been traced to the period of the Three Kingdoms (220–280 AD) when these plants were recorded as "Mangcao" in *Shennong's Chinese Materia Medica*. In the ensuing thousand years, much Chinese literature, including *Materia Medica of South Yunnan (dian nan ben cao)* and *Guidelines and details on roots and herbs (Bencao gangmu)* of the Ming dynasty, *Chinese herbal Iconographia Plantarum* of the Qing dynasty, and *Icons of Chinese medicinal plants* in the 20th century, has recorded the resources, efficacy and medicinal application of TwHF. Modern research on the pharmacology of TwHF focuses on active component identification, structure modification and novel derivative discovery.

For centuries, Chinese people have used TwHF and its extracts for the treatment of autoimmune and inflammatory diseases, including RA, SLE, and DM. Contemporary researchers have attempted to standardize the TwHF extract for further development and investigate its efficacy in autoimmune diseases, and some progress had been achieved in recent years. The ethyl acetate (EA) extract of TwHF was entered into a Phase I study that included 13 patients with established RA in 1993[21-25]. The EA extract of TwHF at dosages up to 570 mg/d appeared to be safe, and doses >360 mg/d were associated with clinical benefits in the patients with RA[21]. The dos-

age was normalized to previous extracts by assessing the content of triptolide and tripdiolide. A randomized, controlled, 24-week study was then conducted in 2004 in patients with active RA and 6 or more painful and swollen joints[22]. The results demonstrated that the treatment with a standardized extract from the peeled roots of TwHF administered (60 mg 3 times daily) over 24 weeks may be both effective and safe in treating patients with active rheumatoid arthritis.

With the recent technological developments in the isolation and structural identification of compounds, more than 100 components have been isolated from TwHF, with most of them having a potent therapeutic efficacy for a variety of autoimmune and inflammatory diseases. Among the reported active components from this herb, including triterpene, diterpene and macrocyclic alkaloids, the most noteworthy component is triptolide. Triptolide, an oxygenated diterpene, was identified as the most active component, accounting for the immunosuppressive effects of TwHF[41, 42]. Over the past few decades, much research has been conducted on the clinical use of triptolide for the treatment of autoimmune and inflammatory diseases, such as RA, SLE, nephritis[26, 43–52], psoriasis[27], and Crohn's disease[53], and kidney transplantation[54]. However the strong toxicity, particularly with regard to male reproductive toxicity, limits the application of triptolide to a great extent[55–58].

To identify more effective compounds with less toxicity and higher solubility, the structural modification of triptolide was studied, and derivatives were synthesized and evaluated for their biological activities. In the past few years, new water-soluble triptolide derivatives have been designed and synthesized, including PG490-88 or F60008. PG490-88 or F60008, a prodrug of triptolide, is converted to triptolide *in vivo* by plasma esterases following intravenous administration[59-67]. Table 1 summarizes the preclinical pharmacological study of triptolide and PG490-88/F60008 against autoimmune diseases and transplantation rejection. Although PG490-88 or F60008 has been approved for entry into a Phase I clinical trial for the treatment of solid tumors, two lethal events were observed in twenty patients, and the high inter-individual variability rendered PG490-88 or F60008 a far from optimal derivate of triptolide[28, 29].

(5*R*)-5-hydroxytriptolide (LLDT-8, Leitengshu), a novel triptolide analog in clinical trials

Great efforts have been made at the SIMM in the search for promising triptolide analogs with a low toxicity and relative high immunosuppressive activity, and a series of novel triptolide analogs have been successfully synthesized. We have identified one derivative, (5*R*)-5-hydroxytriptolide (LLDT-8, Leitengshu), which demonstrates potent immunosuppressive and anti-inflammatory activities[31]. Over the course of ten years, the biological activity of LLDT-8 has been evaluated, and the underlying mechanisms have been investigated with regard to many autoimmune and inflammatory diseases. The administration of LLDT-8 reduced the incidence and severity of collagen-induced arthritis in DBA/1 mice[33]. To assess the long-term effectiveness of LLDT-8, 3-month-treatment experiments were performed. The oral administration of LLDT-8 (0.125, 0.25, and 0.5 mg/kg, starting at 1 d before the booster immunization) consistently attenuated the severity of CIA compared with untreated mice. LDP, Leigongteng Duodai Pian, is the prescription drug of the extracts of TwHF used for treating RA in China. The preventive effect of LLDT-8 at a dose of 0.25 mg/kg was similar to LDP at 20 mg/kg in CIA mice. We also tested the therapeutic effect of LLDT-8 after the establishment of RA, and the inhibitory profile was persistent during the 3-month observation. LLDT-8 also exerted therapeutic effects on experimental autoimmune encephalomyelitis (EAE)[36], concanavalin A-induced acute hepatitis[37], graft-versus-host disease (GVHD)[32], allograft rejection[38], and bleomycin-induced lung fibrosis[39]. LLDT-8 effectively inhibited human T cell immune responses without affecting the NK cytotoxic activity, and this immunosuppressive activity was parallel to that observed for murine immunity[40]. The mechanism of LLDT-8 involves a variety of immune cells and molecules and includes limiting T cell function and proliferation, inhibiting macrophage activation, inducing regulatory T cell expansion, and interfering with IFN-γ-related signaling[31-40]. More importantly, compared to triptolide, LLDT-8 displayed a much lower toxicity both *in vitro* and *in vivo*. The CC_{50} value of LLDT-8 was 256.6±73.8 nmol/L, and the CC_{50} value of triptolide was 2.1±0.3 nmol/L in murine splenocytes. The immunosuppressive effects of LLDT-8 and triptolide were also tested in mitogen- and alloantigen-induced lymphocyte proliferation assays. The IC_{50} values of triptolide for inhibiting ConA-induced T lymphocyte proliferation, LPS-induced B lymphocyte proliferation, and mixed lymphocyte reaction (MLR) were 6.7±0.2, 8.6±2.8, and 2.7±0.6 nmol/L, respectively, with the IC_{50} values of triptolide being close to or even higher than the CC_{50} values. This result indicated that the activities of triptolide were largely dependent on its cytotoxicity. However, the IC_{50} values of LLDT-8 for inhibiting the lymphocyte proliferation caused by ConA, LPS, or MLR were lower than its CC_{50} values (IC_{50}=131.7±32.4, 171.5±17.3, and 38.8±5.1 nmol/L, respectively), thus excluding the possibility that the inhibitory activities of LLDT-8 were attributable to its cytotoxicity[31]. When administered in mice, the lethal dose for 50% of the animal test population of LLDT-8 is 9.3 mg/kg

(intraperitoneal), whereas that of triptolide is 0.86 mg/kg, with a 10-fold lower acute toxicity *in vivo*[30]. Table 2 summarizes the preclinical pharmacological study of LLDT-8 as an immunosuppressant drug candidate. Female RA patients who were over the 35 years of age and menopausal or did not have birth demands were enrolled in a tolerability and pharmacokinetic study. The tolerability and pharmacokinetic properties of LLDT-8 and its initial therapeutic efficacy were assessed and determined. According to the pharmacokinetic and pharmacodynamic results reported using experimental animals, the initial dose should be set at 0.25 mg/d. In accord with the dose escalation scheme, the highest dose could be set at 4 mg/d in the phase I clinical trial for LLDT-8[30]. The results of the clinical trial will provide the basis for the further exploration of this novel derivate of triplide and encourage the research and development of valuable traditional Chinese medicine.

Concluding remarks

Research on TwHF has long been an intense issue. During the past few decades, several drug candidates from this herb have been or are currently in clinical trials. However, it has been demonstrated that some compounds cannot be considered the optimal derivative of triptolide. For other compounds, for example, LLDT-8, we are still awaiting the results of the clinical studies. Regardless of the results of the trials, research on this important ancient medicinal herb will continue.

Acknowledgements

Abbreviations

TwHF, *Tripterygium wilfordii* Hook f; TCM, traditional Chinese medicine; LLDT-8, (5*R*)-5-hydroxytriptolide; RA, rheumatoid arthritis; SLE, systemic lupus erythematosus; DM, dermatomyositis; EA, ethyl acetate; MPA, mycophenolic acid; CsA, cyclosporin A; FTY720, fingolimod; MS, multiple sclerosis; EAE, experimental autoimmune encephalomyelitis; GVHD, graft-versus-host disease.

References

1 Drug discovery from Nature. Susanne Grabley, Ralf Thiericke. ISBN 3-540-64844-5 Springer-Verlag Berlin Heidelberg New York.
2 Paterson I, Anderson EA. The renaissance of natural products as drug candidates. Science 2005; 310: 451–3.
3 Koehn FE, Carter GT. The evolving role of natural products in drug discovery. Nat Rev Drug Discov 2005; 4: 206–20 .
4 Ganesan A. The impact of natural products upon modern drug discovery. Curr Opin Chem Biol 2008; 123: 306–17.
5 Newman DJ, Cragg GM, Snader KM . The influence of natural products upon drug discovery. Nat Prod Rep 2000; 17: 215–34 .
6 Oxford AE, Raistrick H. Studies in the biochemistry of micro-organisms: 3:5-Dihydroxyphthalic acid, a new product of the

Table 1. The preclinical pharmacological study of triptolide and PG490-88/F60008 against autoimmune diseases and transplantation rejection.

Compounds	Disease	Models	Regimens	Reported responses	Possible mechanism	Refs
Triptolide	Rheumatoid arthritis	Type II collagen-induced arthritis (CIA) in Lewis rats	Oral administration of 0.1 mg·kg^{-1}·d^{-1} for 28 d	Significant delay in time to onset of arthritis, as well as significantly decreased arthritis incidence, clinical arthritis severity score, histopathological arthritis severity score, and *in vivo* cell-mediated immunity to collagen	Suppressed cell-mediated immune responses	16
	Rheumatoid arthritis	Collagen-induced arthritis in DBA/1 mice	Oral administration (8, 16, and 32 μg·kg^{-1}·d^{-1}, started when the first clinical signs of disease were beginning, and continued for 21 d	Arthritis incidence was reduced in all groups after receiving triptolide (8–32 μg/kg), arthritis scores was suppressed at 16 and 32 μg/kg doses	Suppression of MMPs, up-regulation of TIMPs, interference with the gene expression of proinflammatory cytokines and PGE$_2$ production, inhibition of NF-κB	44
	Arthritis	Adjuvant-induced arthritis in rat	ip administrations from day 14–20 after immunization at a dose of 0.1, 0.2, and 0.4 mg·kg^{-1}·d^{-1}	Thickness index decreased in all administration groups and maximal inhibition occurred at a dose of 0.4 mg/kg	Over-expression of MCP-1, MIP-1α, and RANTES at both mRNA and protein levels were inhibited	45
	GVHD	C57BL/6 to BDF1 murine BMT model	Oral or intraperitoneal treatment for only 14 d	Prevented GVHD induction and development, produced long-term survival	Induction of anergy and a deviation away from a proinflammatory phenotype	52
	Transplantation	F344 donor to Lewis recipient rat cardiac transplantation	Intraperitoneal treatment at doses of 0.04, 0.08, 0.16, and 0.32 mg·kg^{-1}·d^{-1} starting on the day of transplantation	The median survival time (MST) was 8 d for placebo; 9.5, 11, 14, and 19 d for triptolide monotherapy at doses of 0.04, 0.08, 0.16, and 0.32 mg·kg^{-1}·d^{-1}, respectively	/	46
	Transplantation	Mouse model of cardiac transplantation	ip administration of 3 mg·kg^{-1}·d^{-1} of triptolide at d 0–7, 9, 11, 13, and 15 post transplantation	MST in vehicle group: 7.66±0.8 d, in triptolide group: 23.5±5.3 d	/	47
	Transplantation	Skin allograft rejection	0.1 mg·kg^{-1}·d^{-1}	Prolonged the graft survival when triptolide was given for 9 d after transplantation, but not before transplantation.	Inhibits lymphocyte activation at a relatively late stage	49
	Transplantation	Rat cardiac and renal allograft (from Brown Norway into the abdomen of Lewis rats)	ip dosing of 2.5, 5, 10, 20, or 30 mg·kg^{-1}·d^{-1} for 16 d; oral administration for 16 d at doses of 5, 10, or 30 mg·kg^{-1}·d^{-1} starting 1 d before transplantation	MST of heart allografts was significantly longer in ip dosing of 10, 20, or 30 mg·kg^{-1}·d^{-1}, also in oral administration at doses of 5, 10, or 30 mg·kg^{-1}·d^{-1} MSTs of renal allograft in ip dosing of 20, 30 mg·kg^{-1}·d^{-1} significantly longer	/	55
PG490-88 (F60008)	GVHD	Bone marrow and spleen cells transplantation (B10. D2 to BALB/c mice)	ip at 0.535 mg·kg^{-1}·d^{-1} for the first 3 weeks after transplantation	Protected from developing GVHD up to 100 d	Inhibition of alloreactive T cell expansion through interleukin-2 production	59
	Transplantation	MHC-mismatched renal transplanted into cynomolgus monkeys	0.03 mg·kg^{-1}·d^{-1} by gavage	PG490-88 monotherapy failed to prolong allograft survival	Inhibition of T-cell activation and a decrease in IFN-γ production and NF-AT/NF-κB activity	61
	Transplantation	Dog renal transplantation model	Oral administration at 0.06 mg·kg^{-1}·d^{-1}	Prolonged graft survival from a MST of 6 d to 11 d	Inhibition of complement activation and T-cell infiltration	62

(To be continued)

Compounds	Disease	Models	Regimens	Reported responses	Possible mechanism	Refs
	Transplantation	Chronic rejection in rat kidney (F344 to LEW rats)	0.5 mg·kg⁻¹·d⁻¹ for 10 d	Moderate histological changes on d 90	Suppression of intragraft gene expression	63
	Transplantation	Acute renal rejection across the ACI-to-LEW rat strain	Orally administered at 0.3, 0.5, or 1.0 mg·kg⁻¹·d⁻¹ d for 10 d	Dose-dependent prolongation of kidney allograft survival at 0.5 and 1.0 mg·kg⁻¹·d⁻¹	/	64
	Transplantation	Mouse heterotopic tracheal allograft model of obliterative airway disease	Intraperitoneal injection at 0.25 mg·kg⁻¹·d⁻¹	Attenuates airway obliteration and inhibits accumulation of inflammatory cells	Direct effect on DC or an indirect effect resulting from increased T-cell-mediated apoptosis to be elucidated	65
	GVHD	Murine allogeneic BMT model (B10.D2 to BALB/c)	ip administration at 0.0535 mg/mL daily for the first 3 weeks after BMT	Protected from lethal GVHD for more than 100 d	Induction of responding T cells anergy or TH_2 responses	59, 66
	Lung fibrosis	Bleomycin-induced lung fibrosis	ip administered at 0.25 mg/kg on the same day or 5 d after bleomycin installation	Blocks both inflammation and fibrosis in the bleomycin model of mouse lung fibrosis	Inhibition in TGF-β gene expression	67

Table 2. The preclinical pharmacological study of LLDT-8 as an immunosuppressant drug candidate.

Compounds	Disease	Models	Regimens	Reported responses	Possible mechanism	Refs
LLDT-8	Rheumatoid arthritis	Collagen-induced arthritis in DBA/1 mice	po administrations for 3 months (0.125, 0.25, and 0.5 mg/kg, starting from 1 d before booster immunization)	Attenuated the severity of CIA	Blockade of IFN-γ signaling, IFN-γ related cytokine and chemokine	33
	Multiple sclerosis	MOG 35-55 induced EAE in mice	1 mg·kg⁻¹·d⁻¹ LLDT-8 ip from the day of EAE induction	Reduced the incidence and severity of EAE	Suppression of T cell proliferation and activation	36
	GVHD	Allo-BMT murine model (BLAB/c, H-2d to C57BL/6, H-2b) of aGVHD	1 mg·kg⁻¹·d⁻¹ administered orally starting on day of allo-BMT until the end of experiment	Prevented weight loss and death, extended survival of allo-BMT mice	Increased the CD4⁺CD25⁺T cells and up-regulated Foxp3 expression	32
	Transplantation	Balb/c to C57BL/6 murine cardiac transplantation model	LLDT-8 (1, 0.25 mg·kg⁻¹·d⁻¹) was administered orally starting on the transfer day until the end of experiment	Induced the survival prolongation of allogeneic cardiac graft	Reduced expression of chemokines and its receptor	38
	Acute Hepatitis	ConA-induced hepatitis in mice	Pretreatment with 0.5, 1, or 2 mg/kg LLDT-8 (by ip) four times (on d -3, -2, -1, and 1 h before conA injection)	Significantly increased the survival rates to 83%, 86% and 100%, respectively	Blockade of IFN-γ/STAT1/IRF-1 signaling- and inflammatory mediators	37
	Lung fibrosis	Bleomycin-induced lung fibrosis	LLDT-8 (0.5, 1, and 2 mg/kg, ip) administered once daily for 7 or 14 consecutive days	Protective against bleomycin-induced lung fibrosis, alleviated the body weight loss and lung index increase caused by bleomycin, reduced neutrophils and lymphocytes in the BALF	Anti-inflammation, antioxidant, and cytokine inhibition	39

metabolism of glucose by Penicillium brevi-compactum and related species. Biochem J 1932; 26: 1902–6.

7 Petcher TJ, Weber H, Rüegger A. Crystal and molecular structure of an iodo-derivative of the cyclic undecapeptide cyclosporin A. Helv Chim Acta 1976; 14; 59: 1480–9.

8 Vézina C, Kudelski A, Sehgal SN. Rapamycin (AY-22,989), a new antifungal antibiotic. I. Taxonomy of the producing streptomycete and isolation of the active principle. J Antibiot (Tokyo) 1975; 28: 721–6.

9 Ochiai T, Nakajima K, Nagata M, Hori S, Asano T, Isono K. Studies of the induction and maintenance of long-term graft acceptance by treatment with FK506 in heterotopic cardiac allotransplantation in rats. Transplantation 1987; 44: 734–8.

10 Ochiai T, Nagata M, Nakajima K, Suzuki T, Sakamoto K, Enomoto K, et al. Studies of the effects of FK506 on renal allografting in the beagle dog. Transplantation 1987; 44: 729–33.

11 Adachi K, Kohara T, Nakao N, Aritac M, Chibac K, Mishina T, et al. Design, synthesis and structure-activity relationships of 2-substituted 2-amino-1,3-propanediols: Discovery of a novel immunosuppressant, FTY720. Bioorg Med Chem Lett 1995; 5: 853–6.

12 Li JW, Vederas JC. Drug discovery and natural products: end of an era or an endless frontier? Science 2009; 325: 161–5.

13 Allison AC. Immunosuppressive drugs: the first 50 years and a glance forward. Immunopharmacology 2000; 47: 63–83.

14 Tao X, Davis LS, Lipsky PE. Effect of an extract of the Chinese herbal remedy Tripterygium wilfordii Hook F on human immune responsiveness. Arthritis Rheum 1991; 34: 1274–81.

15 Asano K, Matsuishi J, Yu Y, Kasahara T, Hisamitsu T. Suppressive effects of Tripterygium wilfordii Hook f, a traditional Chinese medicine, on collagen arthritis in mice. Immunopharmacology 1998; 39: 117–26.

16 Gu WZ, Brandwein SR. Inhibition of type II collagen-induced arthritis in rats by triptolide. Int J Immunopharmacol 1998; 20: 389–400.

17 Gu WZ, Banerjee S, Rauch J, Brandwein SR. Suppression of renal disease and arthritis, and prolongation of survival in MRL-lpr mice treated with an extract of Tripterygium wilfordii Hook f. Arthritis Rheum 1992; 35: 1381–6.

18 Gu WZ, Brandwein SR, Banerjee S. Inhibition of type II collagen induced arthritis in mice by an immunosuppressive extract of Tripterygium wilfordii Hook f. J Rheumatol 1992; 19: 682–8.

19 Asano K, Yu Y, Kasahara T, Hisamitsu T. Inhibition of murine chronic graft-versus-host disease by the chloroform extract of Tripterygium wilfordii Hook f. Transpl Immunol 1997; 5: 315–9.

20 Wang J, Xu R, Jin R, Chen Z, Fidler JM. Immunosuppressive activity of the Chinese medicinal plant Tripterygium wilfordii: II. Prolongation of hamster-to-rat cardiac xenograft survival by combination therapy with the PG27 extract and cyclosporine. Transplantation 2000; 70: 456–64.

21 Tao X, Cush JJ, Garret M, Lipsky PE. A phase I study of ethyl acetate extract of the Chinese antirheumatic herb Tripterygium wilfordii hook F in rheumatoid arthritis. J Rheumatol 2001; 28: 2160–7.

22 Goldbach-Mansky R, Wilson M, Fleischmann R, Olsen N, Silverfield J, Kempf P, et al. Comparison of Tripterygium wilfordii Hook F versus sulfasalazine in the treatment of rheumatoid arthritis: a randomized trial. Ann Intern Med 2009; 151: 229–40, W49–51.

23 Tao X, Younger J, Fan FZ, Wang B, Lipsky PE. Benefit of an extract of Tripterygium Wilfordii Hook F in patients with rheumatoid arthritis: a double-blind, placebo-controlled study. Arthritis Rheum 2002; 46: 1735–43.

24 Cibere J, Deng Z, Lin Y, Ou R, He Y, Wang Z, et al. A randomized double blind, placebo controlled trial of topical Tripterygium wilfordii in rheumatoid arthritis: reanalysis using logistic regression analysis. J Rheumatol 2003; 30: 465–7.

25 Marks WH. Tripterygium wilfordii Hook F. versus Sulfasalazine in the treatment of rheumatoid arthritis: a well-designed clinical trial of a botanical demonstrating effectiveness. Fitoterapia 2011; 82: 85–7.

26 Jiang X. Clinical observations on the use of the Chinese herb Tripterygium wilfordii Hook for the treatment of nephrotic syndrome. Pediatr Nephrol 1994; 8: 343–4.

27 Han R, Rostami-Yazdi M, Gerdes S, Mrowietz U. Triptolide in the treatment of psoriasis and other immune-mediated inflammatory diseases. Br J Clin Pharmacol 2012; 74: 424–36.

28 Harousseau JL, Dombret H, Pigneux A, Michallet M, Brandely M. Phase I study of F60008, a triptolide derivative, in patients with refractory or relapsing acute leukemias. 13th Congress of the European Hematology Association (EHA); 2008: 2008.

29 Kitzen JJ, de Jonge MJ, Lamers CH, Eskens FA, van der Biessen D, van Doorn L, et al. Phase I dose-escalation study of F60008, a novel apoptosis inducer, in patients with advanced solid tumours. Eur J Cancer 2009; 45: 1764–72.

30 Liu J, Chen X, Zhang Y, Miao H, Liu K, Li L, et al. Derivatization of (5R)-hydroxytriptolide from benzylamine to enhance mass spectrometric detection: application to a Phase I pharmacokinetic study in humans. Anal Chim Acta 2011; 689: 69–76.

31 Zhou R, Zhang F, He PL, Zhou WL, Wu QL, Xu JY, et al. (5R)-5-hydroxy-triptolide (LLDT-8), a novel triptolide analog mediates immunosuppressive effects in vitro and in vivo. Int Immunopharmacol 2005; 5: 1895–903.

32 Tang W, Yang Y, Zhang F, Li YC, Wang JX, Zhu YN, et al. Prevention of graft-versus-host disease by a novel immunosuppressant, (5R)-5-hydroxytriptolide (LLDT-8), through expansion of regulatory T cells. Int Immunopharmacol 2005; 5: 1904–13.

33 Zhou R, Tang W, Ren YX, He PL, Zhang F, Fu YF, et al. (5R)-5-hydroxytriptolide (LLDT-8) prevented collagen-induced arthritis in DBA/1 mice via suppressing IFN-γ production and its related signaling. J Pharmacol Exp Ther 2006; 318: 35–44.

34 Zhou R, Wang JX, Tang W, He PL, Yang YF, Li YC, et al. (5R)-5-hydroxytriptolide inhibits IFN-gamma-related signaling. Acta Pharmacol Sin 2006; 27: 1616–21.

35 Zhou R, Zheng SX, Tang W, He PL, Li XY, Yang YF, et al. Inhibition of inducible nitric-oxide synthase expression by (5R)-5-hydroxytriptolide (LLDT-8) in interferon-γ and bacterial lipopolysaccharide stimulated macrophages. J Pharmacol Exp Ther 2006; 316: 121–8.

36 Fu YF, Zhu YN, Ni J, Zhong XG, Tang W, Zhou R, et al. (5R)-5-hydroxytriptolide (LLDT-8), a novel triptolide derivative, prevents experimental autoimmune encephalomyelitis via inhibiting T cell activation. J Neuroimmunol 2006; 175: 142–51.

37 Zhou R, Tang W, Ren YX, He PL, Yang YF, Li YC, et al. Preventive effects of (5R)-5-hydroxytriptolide on concanavalin A-induced hepatitis. Eur J Pharmacol 2006; 537: 181–9.

38 Tang W, Yang Y, Zhou R, Li YC, Wang JX, Yang YF, et al. (5R)-5-hydroxytriptolide (LLDT-8), a potential inhibitor of chemokine, prevents allograft rejection in full MHC-mismatched mouse cardiac transplantation. Transplantation 2006; 81: 927–33.

39 Ren YX, Zhou R, Tang W, Wang WH, Li YC, Yang YF, et al. (5R)-5-hydroxytriptolide (LLDT-8) protects against bleomycin-induced lung fibrosis in mice. Acta Pharmacol Sin 2007; 28: 518–25.

40 Zhou R, Tang W, He PL, Ren YX, Yang YF, Li YC, et al. (5R)-5-hydroxytriptolide inhibits the immune response of human peripheral blood mononuclear cells. Int Immunopharmacol 2009; 9: 63–9.

41 Chan MA, Kohlmeier JE, Branden M, Jung M, Benedict SH. Triptolide is more effective in preventing T cell proliferation and interferon-gamma production than is FK506. Phytother Res 1999; 13: 464–7.

42 Gu WZ, Chen R, Brandwein S, McAlpine J, Burres N. Isolation, purification, and characterization of immunosuppressive compounds from tripterygium: triptolide and tripdiolide. Int J Immunopharmacol 1995; 17: 351–6.

43 Kupchan SM, Court WA, Dailey RG Jr, Gilmore CJ, Bryan RF. Triptolide and tripdiolide, novel antileukemic diterpenoid triepoxides from *Tripterygium wilfordii*. J Am Chem Soc 1972; 94: 7194–5.

44 Lin N, Liu C, Xiao C, Jia H, Imada K, Wu H, *et al*. Triptolide, a diterpenoid triepoxide, suppresses inflammation and cartilage destruction in collagen-induced arthritis mice. Biochem Pharmacol 2007; 73: 136–46.

45 Wang Y, Wei D, Lai Z, Le Y. Triptolide inhibits CC chemokines expressed in rat adjuvant-induced arthritis. Int Immunopharmacol 2006; 6: 1825–32.

46 Li R, Takazawa K, Suzuki H, Hariya A, Yamamoto T, Matsushita S, *et al*. Synergistic effect of triptolide and tacrolimus on rat cardiac allotransplantation. Jpn Heart J 2004; 45: 657–65.

47 Liu Y, Chen Y, Liu FQ, Lamb JR, Tam PK. Combined treatment with triptolide and rapamycin prolongs graft survival in a mouse model of cardiac transplantation. Transpl Int 2008; 21: 483–94.

48 Tao X, Davis LS, Hashimoto K, Lipsky PE. The Chinese herbal remedy, T2, inhibits mitogen-induced cytokine gene transcription by T cells, but not initial signal transduction. J Pharmacol Exp Ther 1996; 276: 316–25.

49 Yang SX, Gao HL, Xie SS, Zhang WR, Long ZZ. Immunosuppression of triptolide and its effect on skin allograft survival. Int J Immunopharmacol 1992; 14: 963–9.

50 Lu H, Hachida M, Enosawa S, Li XK, Suzuki S, Koyanagi H. Immunosuppressive effect of triptolide *in vitro*. Transplant Proc 1999; 31: 2056–7.

51 Chen BJ. Triptolide, a novel immunosuppressive and antiinflammatory agent purified from a Chinese herb *Tripterygium wilfordii* Hook F. Leuk Lymphoma 2001; 42: 253–65.

52 Fidler JM, Ku GY, Piazza D, Xu R, Jin R, Chen Z. Immunosuppressive activity of the Chinese medicinal plant *Tripterygium wilfordii*. III. Suppression of graft-versus-host disease in murine allogeneic bone marrow transplantation by the PG27 extract. Transplantation 2002; 74: 445–57.

53 Ren J, Tao Q, Wang X, Wang Z, Li J. Efficacy of T2 in active Crohn's disease: a prospective study report. Dig Dis Sci 2007; 52: 1790–7.

54 Ji SM, Wang QW, Chen JS, Sha GZ, Liu ZH, Li LS. Clinical trial of *Tripterygium Wilfordii* Hook F in human kidney transplantation in China. Transplant Proc 2006; 38: 1274–9.

55 Wang J, Xu R, Jin R, Chen Z, Fidler JM. Immunosuppressive activity of the Chinese medicinal plant *Tripterygium wilfordii*. I. Prolongation of rat cardiac and renal allograft survival by the PG27 extract and immunosuppressive synergy in combination therapy with cyclosporine. Transplantation 2000; 70: 447–55.

56 Huynh PN, Hikim AP, Wang C, Stefonovic K, Lue YH, Leung A, *et al*. Long-term effects of triptolide on spermatogenesis, epididymal sperm function, and fertility in male rats. J Androl 2000; 21: 689–99.

57 Hikim AP, Lue YH, Wang C, Reutrakul V, Sangsuwan R, Swerdloff RS. Posttesticular antifertility action of triptolide in the male rat: evidence for severe impairment of cauda epididymal sperm ultrastructure. J Androl 2000; 21: 431–7.

58 Lue Y, Sinha Hikim AP, Wang C, Leung A, Baravarian S, Reutrakul V, *et al*. Triptolide: A potential male contraceptive. J Androl 1998; 19: 479–86.

59 Chen BJ, Liu C, Cui X, Fidler JM, Chao NJ. Prevention of graft-versus-host disease by a novel immunosuppressant, PG490-88, through inhibition of alloreactive T cell expansion. Transplantation 2000; 70: 1442–7.

60 Crews GM, Erickson L, Pan F, Fisniku O, Jang MS, Wynn C, *et al*. Down-regulation of TGF-beta and VCAM-1 is associated with successful treatment of chronic rejection in rats. Transplant Proc 2005; 37: 1926–8.

61 Chen G, Sun H, Arp J, Garcia B, Wang X, Wise Y, *et al*. A synergistic effect between PG490-88 and tacrolimus prolongs renal allograft survival in monkeys. Am J Transplant 2006; 6: 714–23.

62 Wang X, Sun H, Chen G, Liu W, Wise Y, Yung C, *et al*. Immunosuppression with a combination of pg490-88 and a subtherapeutic dose of FK506 in a canine renal allograft model. Transplantation 2005; 79: 1537–44.

63 Fisniku O, Pan F, Wynn C, Erickson LM, Crews G, Jang MS, *et al*. Protective effects of PG490-88 on chronic allograft rejection by changing intragraft gene expression profiles. Transplant Proc 2005; 37: 1962–4.

64 Pan F, Fisniku O, Wynn C, Erickson LM, Crews G, Jang MS, *et al*. PG490-88, a new immunosuppressant, effectively prevents acute and chronic rejection in rat renal allografts. Transplant Proc 2005; 37: 134–6.

65 Leonard CT, Soccal PM, Berry GJ, Doyle RL, Theodore J, Duncan SR, *et al*. PG490-88, a derivative of triptolide, attenuates obliterative airway disease in a mouse heterotopic tracheal allograft model. J Heart Lung Transplant 2002; 21: 1314–8.

66 Chen BJ, Chen Y, Cui X, Fidler JM, Chao NJ. Mechanisms of tolerance induced by PG490-88 in a bone marrow transplantation model. Transplantation 2002; 73: 115–21.

67 Krishna G, Liu K, Shigemitsu H, Gao M, Raffin TA, Rosen GD. PG490-88, a derivative of triptolide, blocks bleomycin-induced lung fibrosis. Am J Pathol 2001; 158: 997–1004.

npg

Review

Pharmacological actions and therapeutic applications of *Salvia miltiorrhiza* depside salt and its active components

Wen-yu WU, Yi-ping WANG*

State Key Laboratory of Drug Research, Shanghai Institute of Materia Medica, Chinese Academy of Sciences, Shanghai 201203, China

Salvia miltiorrhiza, a traditional medical herb known as danshen, has been widely used in China to improve blood circulation, relieve blood stasis, and treat coronary heart disease. *S miltiorrhiza* depside salt is a novel drug recently developed at the Shanghai Institute of Materia Medica; it contains magnesium lithospermate B (MLB) and its analogs, rosmarinic acid (RA) and lithospermic acid (LA), as active components. The drug has been used in the clinic to improve blood circulation and treat coronary heart disease. The pharmacological effects of the depside salt from *S miltiorrhiza* and its components have been extensively investigated. Experimental studies have demonstrated that magnesium lithospermate B possesses a variety of biological activities, especially protective effects in the cardiovascular system such as attenuation of atherosclerosis and protection against myocardial ischemia-reperfusion injury. Rosmarinic acid and lithospermic acid also show beneficial effects on the cardiovascular system. This paper reviews the recent findings regarding the mechanisms underlying the pharmacological actions of the active components of *S miltiorrhiza* depside salt, based on published works and our own observations.

Keywords: traditional Chinese medicine; *Salvia miltiorrhiza* depside salt; magnesium lithospermate B (lithospermic acid B or salvianolic acid B); rosmarinic acid; lithospermic acid; cardiovascular activities

Introduction

The dried roots of *Salvia miltiorrhiza*, a traditional medical herb known as danshen, are used in China for the treatment of coronary heart disease, hepatitis, menstrual disorders, menostasis, blood circulation diseases, and other cardiovascular diseases[1]. The chemical constitutents of *S miltiorrhiza* have been studied for more than 60 years, but research has been focused mainly on the lipophilic diterpenoid quinones. In recent decades, the pharmacological activities of the water-soluble components of *S miltiorrhiza* have been investigated, including the active constituents magnesium lithospermate B (MLB, also called salvianolic acid B), rosmarinic acid (RA), lithospermic acid (LA), prolithospermic acid, ammonium potassium lithospermate B, and magnesium salvianolate E oligomers of caffeic acids (Figure 1)[2]. Pharmacological studies have shown that water-soluble extracts from danshen can provide an alternative regimen for the prevention of ischemic heart disease[3].

In 2005, the State Food and Drug Administration (SFDA) of China approved a new drug application for *S miltiorrhiza* depside salt, with MLB, RA, and LA as the primary active compounds, for the treatment of chronic angina. A clinical study showed that intravenous infusion of *S miltiorrhiza* depside salt had an observable therapeutic effect in patients with the coronary heart disease angina pectoris[4]. In this article, we review the recent findings from our group and others in order to present the pharmacological profiles and therapeutic applications of the main components of *S miltiorrhiza* depside salt — MLB, RA, and LA — and the mechanisms underlying their clinical efficacy.

Pharmacokinetic properties of *S miltiorrhiza* depside salt

An understanding of the pharmacokinetics and bioavailability of herbal medicinal products can enable us to link data from pharmacological assays to clinical effects and also help in designing rational dosage regimens. The pharmacokinetic properties of *S miltiorrhiza* depside salt have been investigated using liquid chromatography-tandem mass spectrometry following intravenous administration in animals[5, 6] and healthy
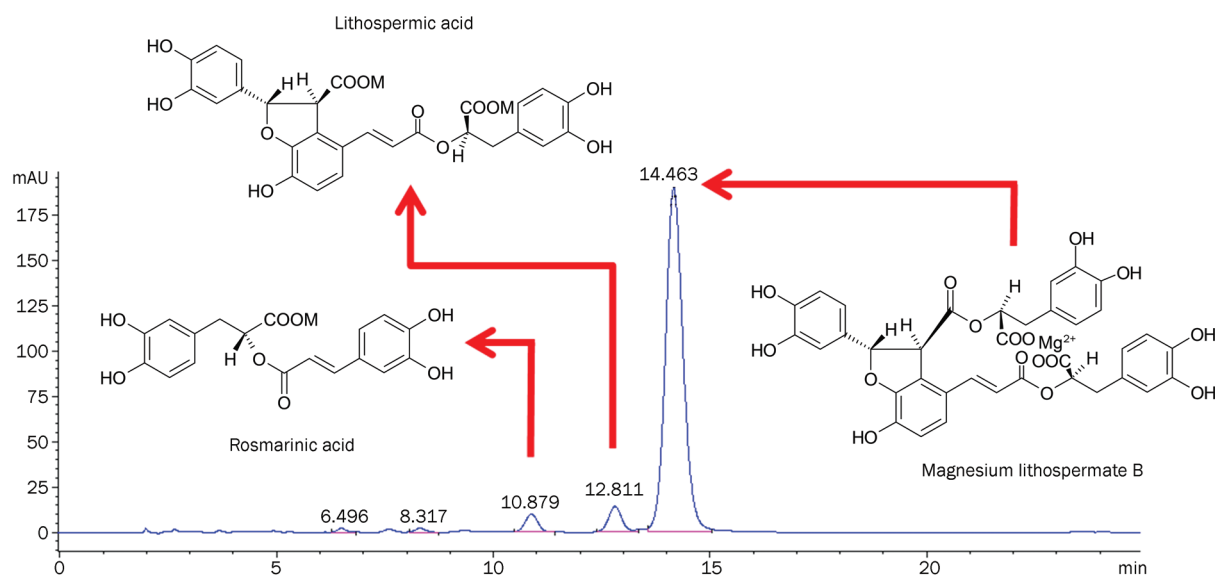
Figure 1. *Salvia miltiorrhiza* depside salt and its main components.

volunteers[7]. The bioavailability of MLB is extremely low; it has been calculated to be only 1.07%±0.43% in dogs[8] and 0.02% in rats[9]. The elimination time ($t_{1/2}$) of MLB, RA, and LA is 1.04, 0.75, and 2.0 h, respectively, in rats[5]; 0.71, 0.51, and 0.83 h in dogs[6]; and 2.33, 0.23, and 3.74 h in healthy Chinese volunteers[7], following intravenous administration of *S miltiorrhiza* depside salt. The pharmacokinetic properties of *S miltiorrhiza* depside salt are summarized in Table 1. Given that MLB has been shown to have low permeability through Caco-2 cell monolayers, its low bioavailability could be due to poor absorption and metabolism[10]. Overall, extensive metabolism, including a first-pass effect, poor absorption, and wide distribution contributed significantly to MLB's extremely low systemic bioavailability[9].

Cytochrome P450 isoenzymes (CYPs), the most important phase I enzymes in the metabolism of xenobiotics, are involved in the metabolism of most drugs. Recently, MLB was found to act as a weak inhibitor of CYP1A2 in human liver microsomes[11], to down-regulate CYP3A4 and CYP1A2 mRNA expression in the absence of rifampicin and to inhibit rifampicin-induced CYP3A4 mRNA expression in HepG2 cells[12]. However, Liu *et al* reported that MLB could significantly transactivate the CYP3A4 reporter gene construct in either HepG2 or Huh7 cells and the PXR mRNA expression in LS174T cells[13]. These data suggest that MLB may modulate the metabolism of the other drugs by induction or inhibition of specific drug-metabolizing enzymes. Additionally, the metabolism of MLB itself can be changed.

Pharmacological actions of magnesium lithospermate B (MLB)

Salvianolic acid B and lithospermic acid B were identified

Table 1. Pharmacokinetic properties of *S miltiorrhiza* depside salt.

Species (administration)	Doses	Pharmacokinetic parameters	MLB	RA	LA	References
Beagle dogs (iv)	6 mg/kg	T_{max} (h)	0.39±0.14	0.39±0.1	0.47±07	Li *et al*[6]
		C_{max} (mg/L)	9775±1576	874±131	308±40	
		$AUC_{(0-tn)}$ (mg·L^{-1}·h^{-1})	5097±871	460±68	171±27	
		$AUC_{(0-\infty)}$ (mg·L^{-1}·h^{-1})	5100±871	461±68	172±28	
		$MRT_{(0-\infty)}$ (h)	0.46±0.04	0.40±0.02	0.50±0.02	
		V/F (L/kg)	0.44±0.13	0.50±0.09	0.26±0.06	
		$T_{1/2\alpha}$ (h)	0.05±0.01	0.04±0.01	0.07±0.01	
		$T_{1/2\beta}$ (h)	0.71±0.32	0.51±0.18	0.83±0.48	
		CL/F (L·h^{-1}·kg^{-1})	0.39±0.20	0.72±0.20	0.27±0.13	
Rats (iv)	60 mg/kg	$AUC_{(0-tn)}$ (mg·h^{-1}·L^{-1})	51.6±12.4	6.6±1.8	25.5±2.3	Li *et al*[5]
		$AUC_{(0-\infty)}$ (mg·h^{-1}·L^{-1})	52.3±12.6	6.9±1.7	26.6±3.1	
		$MRT_{(0-\infty)}$ (h)	0.55±0.09	0.32±0.07	1.75±0.16	
		V (L/kg)	1.89±0.68	1.13±0.51	0.12±0.02	
		$T_{1/2\alpha}$ (h)	0.13±0.07	0.12±0.04	0.13±0.06	
		$T_{1/2\beta}$ (h)	1.04±0.09	0.75±0.14	2.00±0.60	
		CL (L·h^{-1}·kg^{-1})	1.09±0.26	1.02±0.32	0.04±0.01	
Human (iv)	100 mg/kg	C_{max} (mg/L)	4925±1861	174±61	361±101	Jia *et al*[7]
		T_{max} (h)	0.64±0.31	0.47±0.21	1.01±0.20	
		$t_{1/2}$ (h)	2.33±0.92	0.23±0.11	3.74±0.54	
		MRT (h)	1.16±0.62	0.54±0.07	4.24±1.59	
		AUC_{last} (ng·mL^{-1}·h^{-1})	4537±1265	129±28	1229±330	

$Ae_{0-24 h}$, excreted in 24-h urine sample as unchanged drug; AUC, area under the plasma level-time curve; C_{max}, maximum concentration of drug; CL, systemic clearance; MRT, mean retention time; NC, not calculable; SD rat, Sprague-Dawley rat; $t_{1/2}$, terminal elimination half-life; $T_{1/2\alpha}$, absorption half-life; $T_{1/2\beta}$, elimination half-life; T_{max}, time of occurrence for maximum (peak) drug concentration.

decades ago as the major components of danshen. They were originally reported to have identical structures except for the configurational assignments of two stereocenters, recently through chemical correlation, they were shown to be the same compound[14].

Currently, MLB is used as a quality-control ingredient and active marker for danshen products by the National Pharmacopoeia Council of China[15]. As the major component (content >85%) of *S miltiorrhiza* depside salt, the pharmacological actions of MLB have been extensively investigated.

Attenuation of atherosclerosis
A large body of evidence has demonstrated that MLB is capable of preventing the development of atherosclerosis *in vivo* and *in vitro*. The *in vivo* evidence for the anti-atherosclerotic effects of MLB is compiled in Table 2. Intimal hyperplasia results from the proliferation and migration of vascular smooth muscle cells (VSMCs) after endothelial injury and excessive oxidative stress, which were significantly reduced by MLB treatment. It has been found that PDGF-BB, SDF-1α, and high glucose could induce VSMC proliferation and migration, which were suppressed by MLB through the following signaling pathways: those induced by PDGF-BB was mediated via inhibiting the phosphorylation of PI3K/Akt and ERK[16], those induced by SDF-1α via suppressing the expression levels of CXCR4 receptor and downstream molecules of SDF-1α/CXCR4 axis[17], and those induced by high glucose via inducing the nuclear factor erythroid 2-related factor-2 (Nrf2)-antioxidant responsive element (ARE)-NAD(P)H:quinone oxidoreductase-1 (NQO1) (Nrf2-ARE-NQO1) pathway[18]. Furthermore, MLB was able to induce VSMC apoptosis by up-regulating p53[19]. Most recently, Cho *et al* elucidated the mechanisms by which MLB regulates the cellular proliferation in VSMCs. Using fluorescein isothiocyanate (FITC)-conjugated MLB to track its cellular localization, these authors found that MLB bound to the non-muscle myosin heavy chain (NMHC-IIA), thereby allowing MLB to suppress the PDGF-induced proliferation of VSMCs[20]. In addition to inhibiting the proliferation and migration of VSMCs, subsequently preventing neointimal hyperplasia, many other effects are involved in the anti-atherogenic effects of MLB, including the scavenging of ROS/free radicals, attenuation of injury of the vascular endothelium, inhibition of inflammatory reactions, avoidance of lipid deposition, and modulation of the immune response.

Table 2. Anti-atherosclerotic effects of magnesium lithospermate B.

Animal models	Mechanisms	References
Cholesterol-fed rabbits	↓ Intimal thickening ↑ Apoptosis in neointimal restenotic lesions ↑ p53 in neointimal restenotic lesions	Hung *et al*[19]
Cholesterol-fed rabbits	↑ LDL resistant to Cu²⁺-induced oxidation ↑ Vitamin E content in LDL ↓ Severity of atherosclerosis ↓ Plasma cholesterol ↓ Endothelial damage	Wu *et al*[21]
ApoE⁻/⁻ mice	↓ Iintimal thickening ↓ MMP-2 and MMP-9 expression and activity ↓ LPS-induced HASMCMMP-2 and MMP-9 expression and activity ↓ ERK and JNK phosphorylation	Lin *et al*[22]
ApoE⁻/⁻ mice	↓ Intimal thickening ↓ COX-2 expression ↓ LPS-induced HASMC NADPH oxidase activity ↓ LPS-induced HASMC PGE₂ production, ICAM-1 expression ↓ LPS-induced HASMC ERK and JNK phosphorylation	Chen *et al*[23]
Rat model of carotid artery balloon injury	↓ Neointimal formation ↓ ROS ↓ PDGF-BB stimulated VSMC proliferation and migration ↓ PDGF-BB stimulated VSMC PI3K/Akt and ERK phosphorylation	Hur *et al*[16]
Rat model of carotid artery balloon injury	↓ Neointimal hyperplasia ↓ SDF-1α-stimulated cell proliferation and migration ↓ CXCR4 receptor ↓ Promoter activity of NF-κB ↓ Raf-1, MEK, ERK1/2, phospho-ERK1/2, FAK, and phospho-FAK	Pan *et al*[17]
Cholesterol-fed rabbits	↓ Cu²⁺-induced LDL oxidation *in vitro* ↓ HAECs-mediated LDL oxidation ↓ oxLDL-induced cytotoxicity and ROS production in HAECs ↓ Lipid deposition in the thoracic aorta ↓ Intimal thickness of the aortic arch and thoracic aorta ↓ Neointimal formation in the abdominal aorta	Yang *et al*[24]
Carotid artery balloon injury in STZ-induced diabetic rats	↓ Diabetes-related neointimal hyperplasia ↓ Hyperglycemia-accelerated proliferation and migration of VSMCs ↑ Nrf2-ARE-NQO1 pathway	Hur *et al*[18]
ApoE⁻/⁻ mice	↓ CD36 gene expression ↓ Lipid uptake in macrophages ↓ Modified LDL (mLDL) uptake in PMA-stimulated THP-1 and RAW 264.7 cells	Bao *et al*[25]

COX-2, cyclooxygenase-2; CXCR4 receptor, cysteine-x-cysteine chemokine receptor 4; HAECs, human aortic endothelial cells; LDL, low-density lipoprotein; HASMC, human vascular smooth muscle cell; ICAM-1, intercellular adhesion molecule 1; LPS, lipopolysaccharide; MMP, matrix metalloproteinase; Nrf2-ARE-NQO1, nuclear factor erythroid 2-related factor-2 (Nrf2)-antioxidant responsive element (ARE)-NAD(P)H:quinone oxidoreductase-1 (NQO1); oxLDL, oxidized LDL; PDGF, platelet-derived growth factor; PMA, phorbol-12-myristate-13-acetate; ROS, reactive oxygen species; VSMC, vascular smooth muscle cell; STZ, streptozotocin.

Free radical scavenging and anti-oxidant activity

MLB exhibited iron chelating and scavenging activities against free hydroxyl radicals (HO·), superoxide anion radicals (O_2^-), 1,1-diphenyl-2-picryl-hydrazyl (DPPH) radicals, 2-azino-bis(3-ethylbenzthiazoline-6-sulfonic acid (ABTS) radicals and hydrogen peroxide (H_2O_2)[26], as well as xanthine oxidase inhibitory activity[27]. Intracellular and extracellular oxidative stress can induce oxidative modification of low-density lipoprotein (LDL) to oxLDL, one of the important substances that drive intimal immune cell infiltration. Inhibiting the formation of oxLDL is beneficial in preventing the development of atherosclerosis[28]. It was found that MLB inhibited serum LDL oxidation[24], and MLB-treated LDL exhibited vitamin E-binding ability and was resistant to Cu^{2+}-induced oxidation[21]. These studies suggest that MLB can attenuate pathological increases in the peroxidation of lipids, thus suppressing the development and progression of atherosclerosis. Consistent with this line of evidence, our previous study showed that MLB prevented auto-oxidation and Fe^{2+}/VitC induced lipid peroxidation in rat serum, liver, kidney, heart, and brain homogenates *in vitro* and exerted similar effects in an *ex vivo* experiment with the exception of brain homogenate[29]. In addition to preventing lipid oxidation, the scavenging of ROS contributes to the effects of MLB on preventing injury-induced neointimal formation in rats and in cholesterol-fed rabbits, inhibiting VSMC proliferation and migration, and preventing human aortic endothelial cells from oxidative injury-mediated cell death[16, 24].

It has been shown that MLB suppresses NADPH oxidase activity, subsequently reducing ROS generation in response to TNF-α, H_2O_2, and Ang-II in human aortic smooth muscle cells (HASMCs)[30]; MLB has also been shown to directly reduce excessive ROS generated by high glucose through the enhancement of high glucose-induced Nrf2 action and the subsequent heme oxygenase-1 expression in HEK293T cells[31]. Moreover, the entire Nrf2-ARE signaling pathway has been found to be involved in the antioxidative effects of MLB. In that study, MLB acted at least in part by activating the Nrf2-ARE-NQO1 pathway and also restored redox balance during hyperglycemia-induced chronic oxidative stress[18]. Thus, we believe that the prevention of oxidative stress and related vascular complications by MLB contributes to its anti-atherosclerotic effects.

Preventing endothelial dysfunction

The death or injury of endothelial cells (ECs) may contribute to the initial endothelial pathophysiological processes, such as angiogenesis, atherosclerosis, and thrombosis. MLB was found to attenuate the endothelial damage in cholesterol-fed rabbits[21] and to protect human endothelial cells from oxidative stress-induced damage via inducing the expression of glucose-regulated protein 78 (GRP78)[32], thus suggesting that MLB could maintain the integrity of the initial endothelium. Endothelial injury leads to a significant increase in LDL permeability, which plays a role in the formation and development of atherosclerosis. MLB inhibited the VEGF-induced LDL permeability of ECs[33] and reduced the TNF-α-induced permeability and disorganization of vascular endothelial-cadherin in ECs by decreasing VEGF protein expression via modulation of the ERK pathway[34]. Loss of the cell-cell adherence junction also increases endothelial permeability. MLB could attenuate TNF-α-induced tyrosine phosphorylation of junctional proteins, including vascular endothelial cadherin and β-catenin. An immunoprecipitation study showed that MLB prevented β-catenin disassociation from the cytoskeleton in TNF-α-treated HUVECs[35]. In addition to reducing the endothelial permeability, MLB also modulated the hemostatic properties of ECs. MLB increased the fibrinolytic and anticoagulant potential of cultured HUVECs by up-regulating the expression of tissue-type plasminogen activator (t-PA) and thrombomodulin (TM) and down-regulating the expression of plasminogen activator inhibitor type 1 (PAI-1)[36]. The NF-κB and ERK-AP-1 pathways were considered possible targets of MLB in the attenuation of the PAI-1 production response to TNF-α in HUVECs[37].

Atherogenic recruitment of leukocytes involves a sequence of rolling, firm adhesion, lateral migration and transendothelial diapedesis and is controlled by chemokines. During atherosclerosis, circulating monocytes and lymphocytes may interact with adhesion molecules, such as vascular adhesion molecule-1 (VCAM-1), intercellular adhesion molecule-1 (ICAM-1) and E-selectin on ECs, to establish firm adhesion, which may be an early event in atherogenesis. MLB pretreatment notably attenuated TNF-α-induced expression of VCAM-1 and ICAM-1 and the binding of monocytes to HAECs, which was associated with its anti-inflammatory property through inhibition of the NF-κB pathway[38, 39]. In IFN-γ-treated ECs, MLB inhibited IFNγ-induced JAK-STAT signaling pathways and consequently suppressed IFN-γ-induced expression of chemokines (including IP-10, Mig, and I-TAC), IP-10 promoter activity, IP-10 protein release, and monocyte adhesion to ECs[40]. These studies support the potential clinical application of MLB in vascular inflammatory diseases, including atherosclerosis.

MLB regulates vascular homeostasis by exerting a number of vasoprotective effects, including the stimulation of vasodilation, suppression of VSMC proliferation, and inhibition of inflammatory responses. Many of these effects are mediated by the most potent endogenous vasodilator, NO. Endothelial cell-derived NO acts as an important mediator in the cardiovascular, nervous, and immune systems[41]. Our previous studies showed that MLB could inhibit Ca^{2+} influx and stimulate NO production in ECs treated with hypoxia/reoxygenation, which in turn could attenuate cell injury[42]. MLB could also inhibit Ca^{2+} influx and decrease NO release in ECs exposed to hypoxia and attenuate cell injury in ECs[43]. In HUVECs, MLB enhanced NO production via the AMPK/PI3K/Akt pathway[44]. MLB was also found to produce endothelium-dependent vasodilation by regulating NO production through the modulation of heme oxygenase-1 and arginase activities[41].

Taking all these data together, we conclude that MLB dimin-

ishes endothelial dysfunction through up-regulating anti-inflammatory responses and promoting vasodilation, which may contribute to the prevention and treatment of various cardiovascular disorders, including atherosclerosis.

Anti-inflammatory effects and regulation of matrix metalloproteinases expression and activity

The inflammatory response is involved in the pathogenesis of atherosclerosis, and the initial degradation of the extracellular matrix (ECM) is an inevitable step for vascular cell hypertrophy, proliferation, and migration, which in turn plays an important role in vascular remodeling and contributes to the vulnerability of atherosclerotic plaques to rupture. Vascular cells, including SMCs, can secrete matrix metalloproteinases (MMPs), the enzymes that selectively digest the individual components of the ECM. MLB treatment effectively attenuated MMP-2, MMP-9[22], and COX-2[23] protein expression in cholesterol-fed *ApoE*$^{-/-}$ mice, which was related to the reduced thickness of the intima and protection of these mice against atherosclerosis. In HASMCs, MLB reduced the LPS-induced MMP-2 and MMP-9 expression via downregulating the JNK and ERK signaling pathways[22] and inhibited the LPS-induced COX-2 expression via reducing PGE_2 production, ICAM-1 expression and NADPH oxidase activity[23]. Furthermore, MLB also inhibited MMP-2 expression and activity in response to TNF-α, Ang II, and H_2O_2 in HASMCs via reducing NADPH oxidase-dependent ROS generation[30]. Moreover, MLB downregulated the SDF-1α-stimulated up-regulation of CXCR4 (total and cell-surface levels), Raf-1, FAK, and phospho-FAK, as well as the promoter activity of NF-κB, which provided a beneficial effect against the counteracting effects of inflammation on VSMCs[17]. These studies demonstrate that MLB can stabilize arterial atherosclerotic plaques and reduce the risk of coronary heart disease.

Modulation of lipid profiles

In cholesterol-fed rabbits, MLB treatment attenuated the increase in plasma cholesterol predominantly in β-VLDL[21]. MLB treatment was also found to decrease the atherosclerotic area, cholesterol deposition[21, 24] and lipid levels of aortic vessels[25]. However, MLB does not exert obvious lipid-lowering effects. The relationship between lipid lowering and the atheroprotective effects of MLB is still unclear. Because dyslipidemia is one of the main risk factors that lead to atherosclerosis, further investigations are required to explore the effects of MLB on cholesterol metabolism.

Potential immunomodulators

The activation of T lymphocytes plays a promoting role in the inflammatory processes of atherosclerotic diseases, and functional, immune-stimulating dendritic cells (DCs) have recently been detected in the aortic intima, the site of origin for atherosclerosis. Immunosuppressive methotrexate for treatment of atherosclerosis is currently under investigation[28]. One study found that MLB effectively suppressed maturation of human monocyte-derived dendritic cells (h-monDC) induced by ox-

LDL through activation of PPARγ[45] and inhibition of IL-2, IL-4, TNF-α, and IFN-γ production from activated T cells[46]; MLB also effectively reduced the expression of T cell activation markers CD25 and CD69[46]. With molecular modeling, MLB was found to act as an inhibitor of protein-protein interactions between the SH2 domains of the Src-family kinases, Src and Lck. The potency of MLB binding to Src and Lck was higher than RA, a natural compound known as the Lck SH2 domain inhibitor[47]. Because Lck is a T cell-restricted Src family protein tyrosine kinase, and inhibition of the Lck SH2 domain has been suggested as a possible mechanism underlying the immunosuppressant activity of RA, it appears that MLB may act as an immunosuppressive agent[48].

CD36, a member of the class B scavenger receptors, is a high-affinity receptor for oxidatively modified low-density lipoprotein (oxLDL) and has been implicated in the pathogenesis of a variety of vascular inflammatory diseases. MLB was found to be antagonistic against CD36-oxLDL binding, which was further validated by its inhibition of oxLDL uptake in RAW 264.7 cells[49]. Yi *et al* confirmed the specificity and efficacy of MLB in inhibition of CD36-mediated lipid uptake *in vitro* and *in vivo* and demonstrated that MLB was an effective CD36 antagonist[25]. These results support a role for MLB as an immune modulator with cardioprotective effects, which would increase its therapeutic potential in atherosclerotic pathologies.

Protecting against myocardial ischemia and reperfusion (I/R) injury

Cardiac glycosides are drugs that are clinically used to relieve the symptoms of congestive heart failure via their reversible inhibition on Na^+/K^+-ATPase located in human myocardium. However, narrow safety margins and severe side effects make administration of these drugs difficult. MLB is a non-steroid compound possessing inhibitory activity against Na^+/K^+-ATPase with potency comparable to that of cardiac glycosides but without the apparent adverse effects. Therefore, MLB has great potential in the treatment of congestive heart failure, provided that it undergoes the necessary clinical trials[50]. MLB has been found to exert protective effects on the heart in various animal models. In a porcine model of myocardial I/R, MLB increased capillary density and decreased infarct size[51]. In C57 mice, MLB was found to inhibit cardiac hypertrophy and infarction and to improve cardiac function at 4 weeks after induction of the infarction[44]. In rats with left anterior descending coronary artery ligation, MLB treatment effectively improved left ventricle (LV) function and the appearance of the myocardium as compared with a group with acute myocardial infarction (AMI)[52, 53]; MLB treatment also prevented myocardial remodeling, a deleterious consequence of myocardial infarction (MI), by significantly down-regulating the mRNA expression level and activity of MMP-9[52]. MLB was found to bind to MMP-9 at the catalytic domain and to function as a competitive inhibitor of MMP-9[54] and thus could attenuate the enhancing effects of MMP-9 on migration, proliferation, collagen synthesis, cytokine secretion, as well as the association between cardiac fibroblasts and myofibro-

blast transition[55]. Metabolomics offers a new approach to the research of traditional Chinese medicines. Lu *et al*, who analyzed plasma from MI rats and built partial least-squares discriminate analysis (PLS-DA) models, found that MLB was able to regulate 22 identified MI biomarkers in rat plasma[56]; this biomarker pattern was similar to the metabolomic profile of propanolol, indicating that the two drugs might have similar mechanisms. They further demonstrated that MLB exhibited a protective effect on MI mainly by decreasing the concentration of cAMP and Ca^{2+} and inhibiting PKA[57].

The cardioprotection of MLB could benefit from improving myocardial cell function and/or preventing myocardial cell death. MLB seems to have pleiotropic effects and may act on multiple molecular targets to exert its protection effect on cardiomyocytes. We found that MLB reversibly inhibited L-type Ca^{2+} current ($I_{Ca,L}$) without significant effects on the fast-inactivating Na^+ current (I_{Na}), delayed rectifier K^+ current (I_K) and inward rectifier K^+ current (I_{K1}) in single ventricular myocytes of adult guinea pigs, suggesting that the voltage-dependent Ca^{2+} antagonistic effects of MLB work together with its antioxidant action for attenuating heart ischemic injury[58]. Furthermore, it was found that MLB administration significantly decreased myocardiocyte apoptosis during I/R via interactions with multiple targets, including elevating superoxide dismutase activity, thioredoxin activity and glutathione concentration; reducing malondialdehyde concentration[51]; direct/indirect inhibiting stress-activated protein (SAP) kinase activity and nuclear translocation of the active kinase[59]; inhibiting the poly (ADP-ribose) polymerase-1 pathway and improving the integrity of mitochondria and nuclei of heart tissue[53]. It was also reported that MLB prevented LPS-induced neonatal cardiomyocyte injury through inhibition of the TLR4-NF-κB-TNF-α pathway[60] and protected against cardiotoxicity of doxorubicin in mice through blockade of oxidative stress[61]. More recently, MLB was found to protect starving cardiomyocytes by blocking the early stage of autophagic flux and inhibiting the apoptosis that occurred during autophagy[62].

In addition to exerting direct benefit effects on a heart undergoing I/R, MLB can protect the heart from I/R injury through indirect effects, as described below.

First, MLB attenuates the risk of I/R via anti-atherosclerotic properties (see the section "Attenuation of atherosclerosis").

Second, MLB produces vasodilator and vasorelaxant effects. Studies from our group and those of others have demonstrated that these effects result from attenuating intracellular Ca^{2+} concentrations ($[Ca^{2+}]_i$) in VSMCs[63], inhibiting Ca^{2+} channels in the VSMCs with a minor component mediated by the opening of K^+ channels[64], decreasing $[Ca^{2+}]_i$ by inhibiting K^+ currents and depolarizing membrane potential in ECs[65], activating large-conductance Ca^{2+}-activated K^+ (BK_{Ca}) currents in smooth muscle cells[66, 67], and inhibiting K_V currents channels in smooth muscle cells and increasing NO release from endothelium[44, 67].

Third, MLB produces antiplatelet, anticoagulant and antithrombotic effects. In myocardial ischemic rabbits, MLB significantly reduced whole-blood and plasma viscosity,

improved hemorheology, prevented angiospasm and platelet aggregation, and reduced oxidative injury[68]. MLB was also found to delay thrombus-initiation time and damp photochemical reaction–inducedmast cell degranulation in rat mesentery[69]. Our previous study showed that MLB decreased the thrombin-activated release of 5-HT and aggregation in rabbit platelets, probably by attenuating $[Ca^{2+}]_i$[70]. MLB also inhibited platelet aggregation induced by high shear stress[71]. Wu *et al* attributed the antiplatelet effect of MLB to a specific interaction with the platelet collagen receptor α2β1[72]. Ma *et al* further demonstrated that the binding of MLB to integrin α2β1 caused changes in $[Ca^{2+}]_i$, the levels of cytoskeleton-related proteins such as coronin-1B and the cytoskeletal structure of platelets, and therefore concluded that integrin α2β1 might be one of the direct target proteins of MLB in platelets[73].

Fourth, MLB improved myocardial microperfusion[74], myocardial microvascular reflow[51], as well as coronary blood flow[68]. MLB also possessed antihypertensive effects partly due to inhibiting angiotensin converting enzyme activity[75].

Finally, MLB protected bone marrow stem cells from apoptosis[76] and synergized with vitamin C in inducing embryonic stem cell differentiation into matured and functional cardiomyocytes[77].

Other pharmacological actions
In addition to its effects on the cardiovascular system, MLB has other pharmacological actions as discussed below.

Preventing cerebral ischemia-reperfusion injury and neurodegeneration
Cerebral ischemia-reperfusion (I/R) injury is the main reason for the loss of neurons in ischemic cerebrovascular disease. In focal cerebral I/R rats, MLB treatment protected the brain against I/R injury by reducing lipid peroxides, scavenging free radicals and improving energy metabolism[78]. MLB exerted neuroprotection against ischemic stroke by inhibiting the Na^+/K^+-ATPase via binding to the extracellular pocket of the Na^+/K^+-ATPase α subunit and then promoting blood circulation[79]. The anti-apoptotic effect of MLB on rheologically induced endothelial injury probably also contributes to its effectiveness in the treatment of cerebrovascular diseases[80].

Alzheimer's disease (AD) and Parkinson's disease (PD) are common degenerative brain disorders. One of the major pathological features of AD is the appearance of senile plaques characterized by extracellular aggregation of amyloid β-peptide (Aβ) fibrils. Inhibition of Aβ fibril aggregation is therefore regarded as one possible method to halt the progression of AD. MLB was found to inhibit fibril aggregation as well as to destabilize the preformed Aβ fibrils. Moreover, preincubation with MLB significantly reduced the cytotoxic effect of $Aβ_{1-42}$ on human neuroblastoma SH-SY5Y cells[81]. Interestingly, MLB was found to alleviate the memory impairments induced by cholinergic dysfunction or $Aβ_{25-35}$ peptide owing to its antagonism of $GABA_A$ receptors[82]. MLB was also found to protect rat cerebral microvascular endothelial cells (rCMECs) against H_2O_2-induced apoptosis through the PI3K/

Akt/Raf/MEK/ERK pathway, which may partly contribute to its beneficial effects on AD[83], given that rCMECs apoptosis is considered partially responsible for the pathogenesis of AD.

PD is associated with mitochondrial dysfunction, oxidative stress, and activation of the apoptotic cascade. MLB was found to exert protective effects on MPP+-induced apoptosis in SH-SY5Y cells (a classic *in vitro* model for PD) by relieving oxidative stress[84]. These observations suggest that MLB has therapeutic potential for the treatment of neurodegenerative diseases.

Inhibitory effects on liver fibrosis
In a double-blind trial consisting of 60 patients, MLB was found to effectively reverse liver fibrosis in chronic hepatitis B, and it was more effective than the control drug, IFN-γ, in the reduction of serum HA content, overall decrease of 4 serum fibrotic markers, and decrease of ultrasound imaging score without side effects or toxicity[85]. Hepatic fibrosis is characterized by hepatic stellate cell (HSC) activation. It was reported that MLB inhibited HSC proliferation and collagen production, decreased the cells' TGF-β1 autocrine levels, ameliorated oxidative damage and eliminated ROS accumulation in hepatocytes[86]. MLB was also found to significantly attenuate liver fibrosis and activation of HSCs in thioacetamide-induced hepatic fibrosis in rats[87, 88]. Taken together, these results suggest that MLB may be used as an effective anti-fibrotic agent in the treatment of hepatic fibrosis.

Improving renal function and preventing diabetic nephropathy
Tubular epithelial cells can undergo an epithelial-to-mesenchymal transition (EMT), which plays an important role in the pathogenesis of renal interstitial fibrosis (RIF). MLB not only prevented and reversed EMT in HK-2 cells[89, 90] but also prevented tubular EMT in HgCl₂-induced fibrosis in kidneys[91]. Our data showed that MLB ameliorated renal cortical microcirculation[92] and inhibited mesangial cell proliferation[93], which may be related to the drug's renoprotective effects.

Diabetic nephropathy, a common cause of renal disease, accounts for significant morbidity and mortality in patients with diabetes. In *in vitro* studies, MLB was found to inhibit the high glucose-induced proliferation of mesangial cells and extracellular matrix production, partially through suppressing the cell-cycle process, and also inhibited the activities of MMP-2 and MMP-9 via the NF-κB-dependent pathway[94]. MLB also inhibited glucose-induced ROS generation and subsequent PKC inactivation and TGF-β1 and fibronectin downregulation in mesangial cells[95]. In *in vivo* studies, MLB treatment effectively inhibited diabetes-associated TGF-β1, fibronectin and collagen upregulation in the renal cortex and significantly suppressed the progression of renal injury in streptozotocin-induced diabetic rats (STZR)[95]. Similar effects were found in Otsuka Long-Evans-Tokushima Fatty (OLETF) rats with type 2 diabetes[96]. The results of these studies suggest that MLB may be a promising therapeutic agent for preventing and treating diabetic nephropathy.

Pharmacological actions of rosmarinic acid (RA)
Both *in vitro* and *in vivo* studies show that RA possesses antioxidant activity as well as anti-inflammatory activities[97, 98], which results in the multiple pharmacological actions of RA; this multi-target mechanism is similar to that described previously for MLB.

Pharmacological properties of RA on the cardiovascular system
First, RA can prevent cardiomyocyte dysfunction. It has been reported that RA could inhibit adriamycin-induced apoptosis in H9c2 cardiac muscle cells by inhibiting ROS generation and JNK and ERK activation[99]. RA also prevented cardiopathology and lowered blood pressure in fructose-fed hypertensive rats as a result of inhibition of p22phox NADPH oxidase[100]. Second, our results showed that RA possessed a potential vasolilator effect due to decreasing $[Ca^{2+}]_i$ in VSMCs. Moreover, RA did not affect the basal level of $[Ca^{2+}]_i$ but instead attenuated ATP-stimulated $[Ca^{2+}]_i$ increases in the absence of external Ca^{2+} and reduced KCl-induced $[Ca^{2+}]_i$ increases in the presence of external $Ca^{2+[63]}$. Third, RA was found to reduce the risk of MI via its anti-atherosclerotic properties, and it could penetrate membranes to inhibit lipid peroxidation *in situ* without causing any noticeable alteration of the membrane structure[101]. The immunoregulatory activities of RA may also contribute to its anti-atherosclerotic effects. RA was found to induce apoptosis of activated T-cell subsets from rheumatoid arthritis patients via a mitochondrial pathway[102], to inhibit TCR-induced T-cell activation and proliferation[48], and to suppress IFN-γ-mediated induction of indoleamine 2,3-dioxygenase transcription via down-regulation of STAT1 activation in IFN-γ-stimulated murine bone marrow-derived dendritic cells[103].

Other pharmacological findings
In addition to the benefits to the cardiovascular system, RA has other pharmacological effects. (1) Due to its scavenging of peroxynitrite (ONOO⁻), daily consumption of RA exhibited protective effects against the memory impairments caused by the neurotoxicity of $A\beta_{25-35}$[104]. In addition, it has been reported that RA could protect MES23.5 dopaminergic cells against 6-OHDA-[105] or MPP+[106]-induced neurotoxicity *in vitro* and achieve neurorescue effects in 6-ODHA-lesioned rat model of PD *in vivo*[107]. (2) RA has an early renal protective role in nephritic damage. RA was found to be potent in the treatment of diabetic nephropathy. It reduced expression of renal connective-tissue growth factor (CTGF) in STZ-induced rat animal models and in high glucose-stimulated HK-2 cells[108]. (3) RA treatment in mice with existing cholestatic liver fibrosis inhibited HSC activation and progression of liver fibrosis via PPARγ derepression mediated by suppression of canonical Wnt signaling in HSCs[109].

Pharmacological actions of lithospermic acid (LA)
LA is a competitive inhibitor of xanthine oxidase that is able to directly scavenge superoxide and inhibit superoxide pro-

duction *in vitro* and thus exhibits hypouricemic and anti-inflammatory actions *in vivo*[110]. Our group reported that LA exerted vasodilator action by modulating Ca^{2+} homeostasis in VSMCs[63] and prevented atherosclerosis by inhibiting VSMC proliferation and migration[111].

Summary and perspectives

S miltiorrhiza depside salt has been widely prescribed for years. Further investigations to elucidate the mechanisms underlying the protective actions of *S miltiorrhiza* depside salt and its effects on cardiovascular diseases (CVDs) are under way in our laboratory. The drug comprises three safe and effective components with multiple pharmacological actions, accounting for its pleiotropic pharmacological effects, and it may act at multiple molecular targets, mainly because of its anti-inflammatory and anti-oxidative activities. Currently, *S miltiorrhiza* depside salt is used primarily for treating CVDs and other circulatory disturbance-related diseases.

Combining *S miltiorrhiza* depside salt with drugs used to treat hepatic fibrosis (*ie*, malotilate) may enhance their therapeutic effects. Combining *S miltiorrhiza* depside salt with antidiabetic drugs reduces the severity of complications of diabetes, such as diabetic nephropathy and diabetic atherosclerosis. However, the possibility that such combinations may result in adverse drug interactions must be taken into account. Targeting cellular functions as a system rather than at the single-target level significantly increases therapeutic potency. Further research is warranted to address the mechanisms of the multitarget actions of *S miltiorrhiza* depside salt and to translate this knowledge into clinical practice.

Acknowledgements

References

1   Li LN. Biologically active components from traditional Chinese medicines. Pure Appl Chem 1998; 70: 547–54.

2   Zhou CX, Luo HW, Niwa M. Studies on isolation and identification of water-soluble constituents of *Salvia miltiorrhiza*. J Chin Pharm Univ 1999; 30: 411–6.

3   Sun J, Huang SH, Tan BK, Whiteman M, Zhu YC, Wu YJ, *et al*. Effects of purified herbal extract of *Salvia miltiorrhiza* on ischemic rat myocardium after acute myocardial infarction. Life Sci 2005; 76: 2849–60.

4   Zhang Q, Liu AD, Huang YS. Clinical non-inferiority trial on treatment of coronary heart disease angina pectoris of Xin-blood stasis syndrome type with lyophilized Salvia salt of lithospermic acid powder for injection. Chin J Integr Med 2006; 12: 12–8.

5   Li X, Yu C, Lu Y, Gu Y, Lu J, Xu W, *et al*. Pharmacokinetics, tissue distribution, metabolism, and excretion of depside salts from *Salvia miltiorrhiza* in rats. Drug Metab Dispos 2007; 35: 234–9.

6   Li X, Yu C, Sun W, Liu G, Jia J, Wang Y. Simultaneous determination of magnesium lithospermate B, rosmarinic acid, and lithospermic acid in beagle dog serum by liquid chromatography/tandem mass spectrometry. Rapid Commun Mass Spectrom 2004; 18: 2878–82.

7   Jia JY, Lu YL, Li XC, Liu GY, Li SJ, Liu Y, *et al*. Pharmacokinetics of depside salts from *Salvia miltiorrhiza* in healthy Chinese volunteers: A randomized, open-label, single-dose study. Curr Ther Res 2010; 71: 260–71.

8   Gao DY, Han LM, Zhang LH, Fang XL, Wang JX. Bioavailability of salvianolic acid B and effect on blood viscosities after oral administration of salvianolic acids in beagle dogs. Arch Pharm Res 2009; 32: 773–9.

9   Zhang Y, Akao T, Nakamura N, Duan CL, Hattori M, Yang XW, *et al*. Extremely low bioavailability of magnesium lithospermate B, an active component from *Salvia miltiorrhiza*, in rat. Planta Med 2004; 70: 138–42.

10 Kim HH, Kim J, Ji HY, Kim YC, Sohn DH, Lee BM, *et al*. Pharmacokinetics of lithospermic acid B isolated from *Salvia miltiorrhiza* in rats. J Toxicol Environ Health A 2005; 68: 2239–47.

11 Qiu F, Zhang R, Sun J, Jiye A, Hao H, Peng Y, *et al*. Inhibitory effects of seven components of danshen extract on catalytic activity of cytochrome P450 enzyme in human liver microsomes. Drug Metab Dispos 2008; 36: 1308–14.

12 Wang QL, Wu Q, Tao YY, Liu CH, El-Nezami H. Salvianolic acid B modulates the expression of drug-metabolizing enzymes in HepG2 cells. Hepatobiliary Pancreat Dis Int 2011; 10: 502–8.

13 Liu YH, Mo SL, Bi HC, Hu BF, Li CG, Wang YT, *et al*. Regulation of human pregnane X receptor and its target gene cytochrome P450 3A4 by Chinese herbal compounds and a molecular docking study. Xenobiotica 2011; 41: 259–80.

14 Watzke A, O'Malley SJ, Bergman RG, Ellman JA. Reassignment of the configuration of salvianolic acid B and establishment of its identity with lithospermic acid B. J Nat Prod 2006; 69: 1231–3.

15 Zhao Y, Hao Y, Ji H, Fang Y, Guo Y, Sha W, *et al*. Combination effects of salvianolic acid B with low-dose celecoxib on inhibition of head and neck squamous cell carcinoma growth *in vitro* and *in vivo*. Cancer Prev Res (Phila) 2010; 3: 787–96.

16 Hur KY, Seo HJ, Kang ES, Kim SH, Song S, Kim EH, *et al*. Therapeutic effect of magnesium lithospermate B on neointimal formation after balloon-induced vascular injury. Eur J Pharmacol 2008; 586: 226–33.

17 Pan CH, Chen CW, Sheu MJ, Wu CH. Salvianolic acid B inhibits SDF-1alpha-stimulated cell proliferation and migration of vascular smooth muscle cells by suppressing CXCR4 receptor. Vascul Pharmacol 2012; 56: 98–105.

18 Hur KY, Kim SH, Choi MA, Williams DR, Lee YH, Kang SW, *et al*. Protective effects of magnesium lithospermate B against diabetic atherosclerosis via Nrf2-ARE-NQO1 transcriptional pathway. Atherosclerosis 2010; 211: 69–76.

19 Hung HH, Chen YL, Lin SJ, Yang SP, Shih CC, Shiao MS, *et al*. A salvianolic acid B-rich fraction of *Salvia miltiorrhiza* induces neointimal cell apoptosis in rabbit angioplasty model. Histol Histopathol 2001; 16: 175–83.

20 Cho YH, Lim EY, Kim JM, Jung M, Lee HC, Seo M, *et al*. Nonmuscle myosin heavy chain and histone H3 are intracellular binding partners of lithospermic acid B and mediate its antiproliferative effect on VSMCs. Curr Med Chem 2012; 19: 1731–7.

21 Wu YJ, Hong CY, Lin SJ, Wu P, Shiao MS. Increase of Vitamin E Content in LDL and reduction of atherosclerosis in cholesterol-fed rabbits by a water-soluble antioxidant-rich fraction of *Salvia miltiorrhiza*. Arterioscler Thromb Vasc Biol 1998; 18: 481–6.

22 Lin SJ, Lee IT, Chen YH, Lin FY, Sheu LM, Ku HH, *et al*. Salvianolic acid B attenuates MMP-2 and MMP-9 expression *in vivo* in apolipoprotein-E-deficient mouse aorta and *in vitro* in LPS-treated human

aortic smooth muscle cells. J Cell Biochem 2007; 100: 372–84.

23 Chen YL, Hu CS, Lin FY, Chen YH, Sheu LM, Ku HH, *et al*. Salvianolic acid B attenuates cyclooxygenase-2 expression *in vitro* in LPS-treated human aortic smooth muscle cells and *in vivo* in the apolipoprotein-E-deficient mouse aorta. J Cell Biochem 2006; 98: 618–31.

24 Yang TL, Lin FY, Chen YH, Chiu JJ, Shiao MS, Tsai CS, *et al*. Salvianolic acid B inhibits low-density lipoprotein oxidation and neointimal hyperplasia in endothelium-denuded hypercholesterolaemic rabbits. J Sci Food Agric 2011; 91: 134–41.

25 Bao Y, Wang L, Xu Y, Yang Y, Wang L, Si S, *et al*. Salvianolic acid B inhibits macrophage uptake of modified low density lipoprotein (mLDL) in a scavenger receptor CD36-dependent manner. Atherosclerosis 2012; 223: 152–9.

26 Zhao GR, Zhang HM, Ye TX, Xiang ZJ, Yuan YJ, Guo ZX, *et al*. Characterization of the radical scavenging and antioxidant activities of danshensu and salvianolic acid B. Food Chem Toxicol 2008; 46: 73–81.

27 Liu X, Chen R, Shang Y, Jiao B, Huang C. Superoxide radicals scavenging and xanthine oxidase inhibitory activity of magnesium lithospermate B from *Salvia miltiorrhiza*. J Enzyme Inhib Med Chem 2009; 24: 663–8.

28 Weber C, Noels H. Atherosclerosis: current pathogenesis and therapeutic options. Nat Med 2011; 17: 1410–22.

29 Wu XJ, Wang YP, Wang W, Sun WK, Xu YM, Xuan LJ. Free radical scavenging and inhibition of lipid peroxidation by magnesium lithospermate B. Acta Pharmacol Sin 2000; 21: 855–8.

30 Zhang HS, Wang SQ. Salvianolic acid B from *Salvia miltiorrhiza* inhibits tumor necrosis factor-alpha (TNF-alpha)-induced MMP-2 upregulation in human aortic smooth muscle cells via suppression of NAD(P)H oxidase-derived reactive oxygen species. J Mol Cell Cardiol 2006; 41: 138–48.

31 Qu J, Ren X, Hou RY, Dai XP, Zhao YC, Xu XJ, *et al*. The protective effect of magnesium lithospermate B against glucose-induced intracellular oxidative damage. Biochem Biophys Res Commun 2011; 411: 32–9.

32 Wu HL, Li YH, Lin YH, Wang R, Li YB, Tie L, *et al*. Salvianolic acid B protects human endothelial cells from oxidative stress damage: a possible protective role of glucose-regulated protein 78 induction. Cardiovasc Res 2009; 81: 148–58.

33 Qui Y, Rui YC, Zhang L, Li TJ, Zhang WD. VEGF induced hyper-permeability in bovine aortic endothelial cell and inhibitory effect of salvianolic acid B. Acta Pharmacol Sin 2001; 22: 117–20.

34 Ding M, Ye TX, Zhao GR, Yuan YJ, Guo ZX. Aqueous extract of *Salvia miltiorrhiza* attenuates increased endothelial permeability induced by tumor necrosis factor-alpha. Int Immunopharmacol 2005; 5: 1641–51.

35 Ding M, Yuan YJ. Study on the mechanisms of an extract of *Salvia miltiorrhiza* on the regulation of permeability of endothelial cells exposed to tumour necrosis factor-alpha. J Pharm Pharmacol 2007; 59: 1027–33.

36 Shi CS, Huang HC, Wu HL, Kuo CH, Chang BI, Shiao MS, *et al*. Salvianolic acid B modulates hemostasis properties of human umbilical vein endothelial cells. Thromb Res 2007; 119: 769–75.

37 Zhou Z, Liu Y, Miao AD, Wang SQ. Salvianolic acid B attenuates plasminogen activator inhibitor type 1 production in TNF-alpha treated human umbilical vein endothelial cells. J Cell Biochem 2005; 96: 109–16.

38 Chen YH, Lin SJ, Ku HH, Shiao MS, Lin FY, Chen JW, *et al*. Salvianolic acid B attenuates VCAM-1 and ICAM-1 expression in TNF-alpha-treated human aortic endothelial cells. J Cell Biochem 2001; 82: 512–21.

39 Xie LX, Durairajan SS, Lu JH, Liu CL, Kum WF, Wang Y, *et al*. The effect of salvianolic acid B combined with laminar shear stress on TNF-alpha-stimulated adhesion molecule expression in human aortic endothelial cells. Clin Hemorheol Microcirc 2010; 44: 245–58.

40 Chen SC, Lin YL, Huang B, Wang DL, Cheng JJ. Salvianolic acid B suppresses IFN-gamma-induced JAK/STAT1 activation in endothelial cells. Thromb Res 2011; 128: 560–4.

41 Joe Y, Zheng M, Kim HJ, Kim S, Uddin MJ, Park C, *et al*. Salvianolic acid B exerts vasoprotective effects through the modulation of heme Oxygenase-1 and arginase activities. J Pharmacol Exp Ther 2012; 341: 850–8.

42 Luo WB, Dong L, Wang YP. Effect of magnesium lithospermate B on calcium and nitric oxide in endothelial cells upon hypoxia/reoxygenation. Acta Pharmacol Sin 2002; 23: 930–6.

43 Luo WB, Wang YP. Magnesium lithospermate B inhibits hypoxia-induced calcium influx and nitric oxide release in endothelial cells. Acta Pharmacol Sin 2001; 22: 1135–42.

44 Pan C, Lou L, Huo Y, Singh G, Chen M, Zhang D, *et al*. Salvianolic acid B and tanshinone IIA attenuate myocardial ischemia injury in mice by NO production through multiple pathways. Ther Adv Cardiovasc Dis 2011; 5: 99–111.

45 Sun A, Liu H, Wang S, Shi D, Xu L, Cheng Y, *et al*. Salvianolic acid B suppresses maturation of human monocyte-derived dendritic cells by activating PPARgamma. Br J Pharmacol 2011; 164: 2042–53.

46 Cheng CC, Yang SP, Lin WS, Ho LJ, Lai JH, Cheng SM, *et al*. Magnesium lithospermate B mediates anti-inflammation targeting activator protein-1 and nuclear factor-kappa B signaling pathways in human peripheral T lymphocytes. Int Immunopharmacol 2012; 13: 354–61.

47 Sperl B, Seifert MH, Berg T. Natural product inhibitors of protein-protein interactions mediated by Src-family SH2 domains. Bioorg Med Chem Lett 2009; 19: 3305–9.

48 Won J, Hur YG, Hur EM, Park SH, Kang MA, Choi Y, *et al*. Rosmarinic acid inhibits TCR-induced T cell activation and proliferation in an Lck-dependent manner. Eur J Immunol 2003; 33: 870–9.

49 Wang L, Bao Y, Yang Y, Wu Y, Chen X, Si S, *et al*. Discovery of antagonists for human scavenger receptor CD36 via an ELISA-like high-throughput screening assay. J Biomol Screen 2010; 15: 239–50.

50 Chen RJ, Jinn TR, Chen YC, Chung TY, Yang WH, Tzen JT. Active ingredients in Chinese medicines promoting blood circulation as Na⁺/K⁺-ATPase inhibitors. Acta Pharmacol Sin 2011; 32: 141–51.

51 Han B, Zhang X, Zhang Q, Zhao G, Wei J, Ma S, *et al*. Protective effects of salvianolate on microvascular flow in a porcine model of myocardial ischaemia and reperfusion. Arch Cardiovasc Dis 2011; 104: 313–24.

52 Jiang B, Wu W, Li M, Xu L, Sun K, Yang M, *et al*. Cardioprotection and matrix metalloproteinase-9 regulation of salvianolic acids on myocardial infarction in rats. Planta Med 2009; 75: 1286–92.

53 Xu L, Deng Y, Feng L, Li D, Chen X, Ma C, *et al*. Cardio-protection of salvianolic acid B through inhibition of apoptosis network. PLoS One 2011; 6: e24036.

54 Jiang B, Chen J, Xu L, Gao Z, Deng Y, Wang Y, *et al*. Salvianolic acid B functioned as a competitive inhibitor of matrix metalloproteinase-9 and efficiently prevented cardiac remodeling. BMC Pharmacol 2010; 10: 10.

55 Wang Y, Xu F, Chen J, Shen X, Deng Y, Xu L, *et al*. Matrix metallo-proteinase-9 induces cardiac fibroblast migration, collagen and cytokine secretion: inhibition by salvianolic acid B from *Salvia miltiorrhiza*. Phytomedicine 2011; 19: 13–9.

56 Lu Y, Liu X, Liang X, Xiang L, Zhang W. Metabolomic strategy to study

therapeutic and synergistic effects of tanshinone IIA, salvianolic acid B and ginsenoside Rb1 in myocardial ischemia rats. J Ethnopharmacol 2011; 134: 45–9.

57 Lu Y, Zheng Y, Liu X, Liang X, Ngai S, Li T, *et al*. Metabolomic profiles of myocardial ischemia under treatment with salvianolic acid B. Chin Med 2012; 7: 6.

58 Wang W, Hu GY, Wang YP. Selective modulation of L-type calcium current by magnesium lithospermate B in guinea-pig ventricular myocytes. Life Sci 2006; 78: 2989–97.

59 Au-Yeung KK, Zhu DY, O K, Siow YL. Inhibition of stress-activated protein kinase in the ischemic/reperfused heart: role of magnesium tanshinoate B in preventing apoptosis. Biochem Pharmacol 2001; 62: 483–93.

60 Wang J, Zhang Y, Guo LL, Wu GJ, Liu RH. Salvianolic acid B inhibits the TLR4-NFkappaB-TNFalpha pathway and attenuates neonatal rat cardiomyocyte injury induced by lipopolysaccharide. Chin J Integr Med 2011; 17: 775–9.

61 Jiang B, Zhang L, Li M, Wu W, Yang M, Wang J, *et al*. Salvianolic acids prevent acute doxorubicin cardiotoxicity in mice through suppression of oxidative stress. Food Chem Toxicol 2008; 46: 1510–5.

62 Han X, Liu JX, Li XZ. Salvianolic acid B inhibits autophagy and protects starving cardiac myocytes. Acta Pharmacol Sin 2011; 32: 38–44.

63 Chen L, Xuan LJ, Wang YP. Effects of magnesium lithospermate B and its analogues on Ca^{2+} homeostasis in cultured rat thoracic aorta vascular smooth muscle cells. Planta Med 2009; 75: 1573–9.

64 Lam FF, Yeung JH, Kwan YW, Chan KM, Or PM. Salvianolic acid B, an aqueous component of danshen (*Salvia miltiorrhiza*), relaxes rat coronary artery by inhibition of calcium channels. Eur J Pharmacol 2006; 553: 240–5.

65 Zhang H, Zhang J, Zha R, Hu M, Wang Y. Magnesium lithospermate B decreases $[Ca^{2+}]_i$ in endothelial cells by inhibiting K^+ currents. Eur J Pharmacol 2011; 650: 285–9.

66 Lam FF, Seto SW, Kwan YW, Yeung JH, Chan P. Activation of the iberiotoxin-sensitive BKCa channels by salvianolic acid B of the porcine coronary artery smooth muscle cells. Eur J Pharmacol 2006; 546: 28–35.

67 Zhang HF, Chen XQ, Hu GY, Wang YP. Magnesium lithospermate B dilates mesenteric arteries by activating BKCa currents and contracts arteries by inhibiting K_V currents. Acta Pharmacol Sin 2010; 31: 665–70.

68 Yang Q, Wang S, Xie Y, Wang J, Li H, Zhou X, *et al*. Effect of salvianolic Acid B and paeonol on blood lipid metabolism and hemorrheology in myocardial ischemia rabbits induced by pituitruin. Int J Mol Sci 2010; 11: 3696–704.

69 Wang F, Liu YY, Liu LY, Zeng QJ, Wang CS, Sun K, *et al*. The attenuation effect of 3,4-dihydroxy-phenyl lactic acid and salvianolic acid B on venular thrombosis induced in rat mesentery by photochemical reaction. Clin Hemorheol Microcirc 2009; 42: 7–18.

70 Wang W, Wang YP, Sun WK, Xu YM, Xuan LJ. Effects of magnesium lithospermate B on aggregation and 5-HT release in rabbit washed platelets. Acta Pharmacol Sin 2000; 21: 859–63.

71 Li M, Zhao C, Wong RN, Goto S, Wang Z, Liao F. Inhibition of shear-induced platelet aggregation in rat by tetramethylpyrazine and salvianolic acid B. Clin Hemorheol Microcirc 2004; 31: 97–103.

72 Wu YP, Zhao XM, Pan SD, Guo de A, Wei R, Han JJ, *et al*. Salvianolic acid B inhibits platelet adhesion under conditions of flow by a mechanism involving the collagen receptor alpha2beta1. Thromb Res 2008; 123: 298–305.

73 Ma C, Yao Y, Yue QX, Zhou XW, Yang PY, Wu WY, *et al*. Differential proteomic analysis of platelets suggested possible signal cascades network in platelets treated with salvianolic acid B. PLoS One 2011; 6: e14692.

74 Li XF, Wang YP. Depside salts from *Salvia miltiorrhiza* improve myocardial microperfusion in rats using laser Doppler flowmetry. Acta Pharmacol Sin 2007; 28: 789–95.

75 Kang DG, Oh H, Chung HT, Lee HS. Inhibition of angiotensin converting enzyme by lithospermic acid B isolated from radix *Salviae miltiorrhiza* Bunge. Phytother Res 2003; 17: 917–20.

76 Lu B, Ye Z, Deng Y, Wu H, Feng J. MEK/ERK pathway mediates cytoprotection of salvianolic acid B against oxidative stress-induced apoptosis in rat bone marrow stem cells. Cell Biol Int 2010; 34: 1063–8.

77 Chan SS, Chen JH, Hwang SM, Wang IJ, Li HJ, Lee RT, *et al*. Salvianolic acid B-vitamin C synergy in cardiac differentiation from embryonic stem cells. Biochem Biophys Res Commun 2009; 387: 723–8.

78 Chen YH, Du GH, Zhang JT. Salvianolic acid B protects brain against injuries caused by ischemia-reperfusion in rats. Acta Pharmacol Sin 2000; 21: 463–6.

79 Tzen JT, Jinn TR, Chen YC, Li FY, Cheng FC, Shi LS, *et al*. Magnesium lithospermate B possesses inhibitory activity on Na^+,K^+-ATPase and neuroprotective effects against ischemic stroke. Acta Pharmacol Sin 2007; 28: 609–15.

80 Li M, Zhao MQ, Kumar Durairajan SS, Xie LX, Zhang HX, Kum WF, *et al*. Protective effect of tetramethylpyrazine and salvianolic acid B on apoptosis of rat cerebral microvascular endothelial cell under high shear stress. Clin Hemorheol Microcirc 2008; 38: 177–87.

81 Durairajan SS, Yuan Q, Xie L, Chan WS, Kum WF, Koo I, *et al*. Salvianolic acid B inhibits Abeta fibril formation and disaggregates preformed fibrils and protects against Abeta-induced cytotoxicty. Neurochem Int 2008; 52: 741–50.

82 Kim DH, Park SJ, Kim JM, Jeon SJ, Cho YW, Son KH, *et al*. Cognitive dysfunctions induced by a cholinergic blockade and Abeta 25–35 peptide are attenuated by salvianolic acid B. Neuropharmacology 2011; 61: 1432–40.

83 Liu CL, Xie LX, Li M, Durairajan SS, Goto S, Huang JD. Salvianolic acid B inhibits hydrogen peroxide-induced endothelial cell apoptosis through regulating PI3K/Akt signaling. PLoS One 2007; 2: e1321.

84 Zeng G, Tang T, Wu HJ, You WH, Luo JK, Lin Y, *et al*. Salvianolic acid B protects SH-SY5Y neuroblastoma cells from 1-methyl-4-phenylpyridinium-induced apoptosis. Biol Pharm Bull 2010; 33: 1337–42.

85 Liu P, Hu YY, Liu C, Zhu DY, Xue HM, Xu ZQ, *et al*. Clinical observation of salvianolic acid B in treatment of liver fibrosis in chronic hepatitis B. World J Gastroenterol 2002; 8: 679–85.

86 Lin YL, Wu CH, Luo MH, Huang YJ, Wang CN, Shiao MS, *et al*. *In vitro* protective effects of salvianolic acid B on primary hepatocytes and hepatic stellate cells. J Ethnopharmacol 2006; 105: 215–22.

87 Paik YH, Yoon YJ, Lee HC, Jung MK, Kang SH, Chung SI, *et al*. Antifibrotic effects of magnesium lithospermate B on hepatic stellate cells and thioacetamide-induced cirrhotic rats. Exp Mol Med 2011; 43: 341–9.

88 Tsai MK, Lin YL, Huang YT. Effects of salvianolic acids on oxidative stress and hepatic fibrosis in rats. Toxicol Appl Pharmacol 2010; 242: 155–64.

89 Yao G, Xu L, Wu X, Yang J, Chen H. Preventive effects of salvianolic acid B on transforming growth factor-beta1-induced epithelial-to-mesenchymal transition of human kidney cells. Biol Pharm Bull 2009; 32: 882–6.

90 Pan RH, Xie FY, Chen HM, Xu LZ, Wu XC, Xu LL, *et al*. Salvianolic acid B reverses the epithelial-to-mesenchymal transition of HK-2 cells

that is induced by transforming growth factor-beta. Arch Pharm Res 2011; 34: 477–83.

91 Wang QL, Tao YY, Yuan JL, Shen L, Liu CH. Salvianolic acid B prevents epithelial-to-mesenchymal transition through the TGF-beta1 signal transduction pathway *in vivo* and *in vitro*. BMC Cell Biol 2010; 11: 31.

92 Chen CG, Wang YP. Magnesium lithospermate B ameliorates renal cortical microperfusion in rats. Acta Pharmacol Sin 2006; 27: 217–22.

93 Xu M, Wang YP, Luo WB, Xuan LJ. Salvianolate inhibits proliferation and endothelin release in cultured rat mesangial cells. Acta Pharmacol Sin 2001; 22: 629–33.

94 Luo P, Tan Z, Zhang Z, Li H, Mo Z. Inhibitory effects of salvianolic acid B on the high glucose-induced mesangial proliferation via NF-kappaB-dependent pathway. Biol Pharm Bull 2008; 31: 1381–6.

95 Lee GT. Delayed treatment with lithospermate B attenuates experimental diabetic renal injury. J Am Soc Nephrol 2003; 14: 709–20.

96 Kang ES, Lee GT, Kim BS, Kim CH, Seo GH, Han SJ, *et al*. Lithospermic acid B ameliorates the development of diabetic nephropathy in OLETF rats. Eur J Pharmacol 2008; 579: 418–25.

97 Bulgakov VP, Inyushkina YV, Fedoreyev SA. Rosmarinic acid and its derivatives: biotechnology and applications. Crit Rev Biotechnol 2012; 32: 203–17.

98 Chu X, Ci X, He J, Jiang L, Wei M, Cao Q, *et al*. Effects of a natural prolyl oligopeptidase inhibitor, rosmarinic acid, on lipopolysaccharide-induced acute lung injury in mice. Molecules 2012; 17: 3586–98.

99 Kim DS, Kim HR, Woo ER, Hong ST, Chae HJ, Chae SW. Inhibitory effects of rosmarinic acid on adriamycin-induced apoptosis in H9c2 cardiac muscle cells by inhibiting reactive oxygen species and the activations of c-Jun N-terminal kinase and extracellular signal-regulated kinase. Biochem Pharmacol 2005; 70: 1066–78.

100 Karthik D, Viswanathan P, Anuradha CV. Administration of rosmarinic acid reduces cardiopathology and blood pressure through inhibition of p22phox NADPH oxidase in fructose-fed hypertensive rats. J Cardiovasc Pharmacol 2011; 58: 514–21.

101 Fadel O, El Kirat K, Morandat S. The natural antioxidant rosmarinic acid spontaneously penetrates membranes to inhibit lipid peroxidation *in situ*. Biochim Biophys Acta 2011; 1808: 2973–80.

102 Hur YG, Suh CH, Kim S, Won J. Rosmarinic acid induces apoptosis of activated T cells from rheumatoid arthritis patients via mitochondrial pathway. J Clin Immunol 2007; 27: 36–45.

103 Lee HJ, Jeong YI, Lee TH, Jung ID, Lee JS, Lee CM, *et al*. Rosmarinic acid inhibits indoleamine 2,3-dioxygenase expression in murine dendritic cells. Biochem Pharmacol 2007; 73: 1412–21.

104 Alkam T, Nitta A, Mizoguchi H, Itoh A, Nabeshima T. A natural scavenger of peroxynitrites, rosmarinic acid, protects against impairment of memory induced by Abeta(25–35). Behav Brain Res 2007; 180: 139–45.

105 Jiang H, Song N, Xu H, Zhang S, Wang J, Xie J. Up-regulation of divalent metal transporter 1 in 6-hydroxydopamine intoxication is IRE/IRP dependent. Cell Res 2010; 20: 345–56.

106 Du T, Li L, Song N, Xie J, Jiang H. Rosmarinic acid antagonized 1-methyl-4-phenylpyridinium (MPP$^+$)-induced neurotoxicity in MES23.5 dopaminergic cells. Int J Toxicol 2010; 29: 625–33.

107 Wang J, Xu H, Jiang H, Du X, Sun P, Xie J. Neurorescue effect of rosmarinic acid on 6-hydroxydopamine-lesioned nigral dopamine neurons in rat model of Parkinson's disease. J Mol Neurosci 2012; 47: 113–9.

108 Jiang WL, Xu Y, Zhang SP, Hou J, Zhu HB. Effect of rosmarinic acid on experimental diabetic nephropathy. Basic Clin Pharmacol Toxicol 2012; 110: 390–5.

109 Yang MD, Chiang YM, Higashiyama R, Asahina K, Mann DA, Mann J, *et al*. Rosmarinic acid and baicalin epigenetically derepress peroxisomal proliferator-activated receptor gamma in hepatic stellate cells for their antifibrotic effect. Hepatology 2012; 55: 1271–81.

110 Liu X, Chen R, Shang Y, Jiao B, Huang C. Lithospermic acid as a novel xanthine oxidase inhibitor has anti-inflammatory and hypouricemic effects in rats. Chem Biol Interact 2008; 176: 137–42.

111 Chen L, Wang WY, Wang YP. Inhibitory effects of lithospermic acid on proliferation and migration of rat vascular smooth muscle cells. Acta Pharmacol Sin 2009; 30: 1245–52.

npg

Review

Computational drug discovery

Si-sheng OU-YANG, Jun-yan LU, Xiang-qian KONG, Zhong-jie LIANG, Cheng LUO, Hualiang JIANG[*]

Drug Discovery and Design Center, State Key Laboratory of Drug Research, Shanghai Institute of Materia Medica, Chinese Academy of Sciences, Shanghai 201203, China

Computational drug discovery is an effective strategy for accelerating and economizing drug discovery and development process. Because of the dramatic increase in the availability of biological macromolecule and small molecule information, the applicability of computational drug discovery has been extended and broadly applied to nearly every stage in the drug discovery and development workflow, including target identification and validation, lead discovery and optimization and preclinical tests. Over the past decades, computational drug discovery methods such as molecular docking, pharmacophore modeling and mapping, *de novo* design, molecular similarity calculation and sequence-based virtual screening have been greatly improved. In this review, we present an overview of these important computational methods, platforms and successful applications in this field.

Introduction

The process of novel drug discovery and development is generally recognized to be time-consuming, risky and costly. The typical drug discovery and development cycle, from concept to market, takes approximately 14 years[1], and the cost ranges from 0.8 to 1.0 billion USD[2]. Rapid developments in combinatorial chemistry and high-throughput screening technologies have provided an environment to expedite the drug discovery process by enabling huge libraries of compounds to be screened and synthesized in short time[3, 4]. Although the investment in new drug development has grown significantly in the past decades, the output is not positively proportional to the investment because of the low efficiency and high failure rate in drug discovery[5]. Consequently, various approaches have been developed to shorten the research cycle and reduce the expense and risk of failure for drug discovery. Computer-aided drug design (CADD) is one of the most effective methods for reaching these goals.

CADD is a widely used term that represents computational tools and sources for the storage, management, analysis and modeling of compounds. It covers many aspects of drug discovery, including computer programs for designing compounds, tools for systematically assessing potential lead candidates and the development of digital repositories for studying

chemical interactions[6]. In the post-genomic era, benefiting from the dramatic increase in biomacromolecule and small molecule information, computational tools can be applied to most aspects of the drug discovery and development process, from target identification and validation to lead discovery and optimization; the tools can even be applied to preclinical trials[5, 7–9], which greatly alters the pipeline for drug discovery and development. Figure 1 shows a flowchart for the tasks that computational approaches have been applied to and the computational methods used at each stage. The use of computational tools could reduce the cost of drug development by up to 50%[10].

The commonly used computational drug discovery approaches can be categorized into structure-based drug design (SBDD), ligand-based drug design (LBDD) and sequence-based approaches. SBDD methods, such as molecular docking and *de novo* drug design, rely on the knowledge of the structure of the target macromolecule, which are mainly obtained from crystal structures, NMR data and homology models[11]. In the absence of three-dimensional (3D) structures of potential targets, LBDD tools, including quantitative structure-activity relationship (QSAR), pharmacophore modeling, molecular field analysis and 2D or 3D similarity assessment, can provide crucial insights into the nature of the interactions between drug targets and ligands, which allows predictive models that are suitable for lead discovery and optimization to be constructed[12]. In recent years, to deal with situations that neither the target structure nor the ligand information is
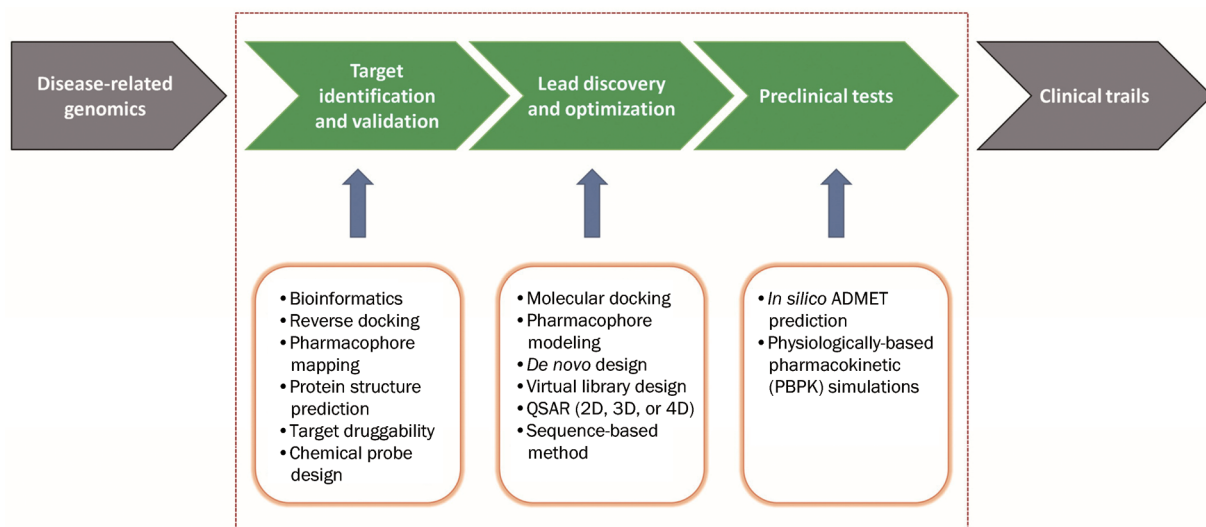
Figure 1. Multiple computational drug discovery approaches that have been applied in various stages of the drug discovery and development pipeline, including target identification and validation, lead discovery and optimization, and preclinical tests.

available, sequence-based approaches that use bioinformatic methods to analyze and compare multiple sequences have been developed to identify potential targets from scratch and to conduct lead discovery[13, 14]. Currently, all single methods are unable to fulfill the practical needs of drug discovery and development. Therefore, combinational and hierarchical strategies that employ multiple computational approaches have been frequently and successfully used.

The efficiency, accuracy and speed of these computational methods largely depend on several technical aspects, including conformation generation and sampling, scoring functions, optimization algorithms, and molecular similarity calculations[7, 11, 15]. In this paper, we focus on these topics and the widely used computational tools in the fields of target identification and lead discovery and address some of the most recent methodologies, platforms and applications.

Methodologies and platforms

Some remarkable methodologies and platforms focused on computational drug discovery and development have been developed and constructed. In this section, several methodologies and platforms that involve target identification, docking-based virtual screening, conformation sampling, scoring functions, molecular similarity calculation, virtual library design and sequence-based drug design are summarized. These aspects are intimately linked, and improvements in any aspect could benefit the others (Figure 2).

Target identification

As the first stage in the drug discovery pipeline, the identification of drug targets from large quantities of candidate macromolecules is both important and challenging[16]. The current major tools for target identification are genomic and proteomic approaches, which are laborious and time-consuming[17]. Therefore, to complement the experimental methods, compu-

tational tools and platforms, including reverse docking and pharmacophore mapping, have been developed.

TarFisDock is a web server that identifies drug targets using a reverse docking strategy to seek all possible binding proteins for a given small molecule[18]. The development of TarFisDock was based on the widely used docking program, DOCK (version 4.0)[19, 20]. This platform consists of a front-end web interface written in PHP and HTML with MySQL as database system. DOCK is used as a back-end tool for reverse docking. The advantage of TarFisDock is obvious; it could be a valuable tool for identifying potential targets for a compound with known biological activity, a newly isolated natural product or an existing drug whose pharmacological mechanism is unclear. In addition, this platform is also able to find potential targets that could be responsible for the toxicity and side effects of a drug, which could allow for the prediction of the off-target effects of a drug candidate. Indeed, studies have shown that off-target effects have been largely responsible for the high attrition rate in drug development[21]. Furthermore, TarFisDock could provide valuable information for constructing drug target networks in order to study the drug-target interaction in a more systematic way. The reliability of this methodology has been tested on vitamin E and 4H-tamoxifen by identifying their putative binding proteins. The results indicated that TarFisDock could predict 50% of the reported corresponding targets. However, this method still has certain limitations: (1) the protein entries are not sufficient to cover all the protein information of disease related genomes; (2) the flexibility of the proteins is not considered during the docking procedure; and (3) the scoring function, which was intended to evaluate small molecules, may not be accurate enough for evaluating reverse docking[18].

A web-accessible potential drug target database (PDTD) was constructed for TarFisDock. This database currently contains more than 1100 protein entries with 3D structures
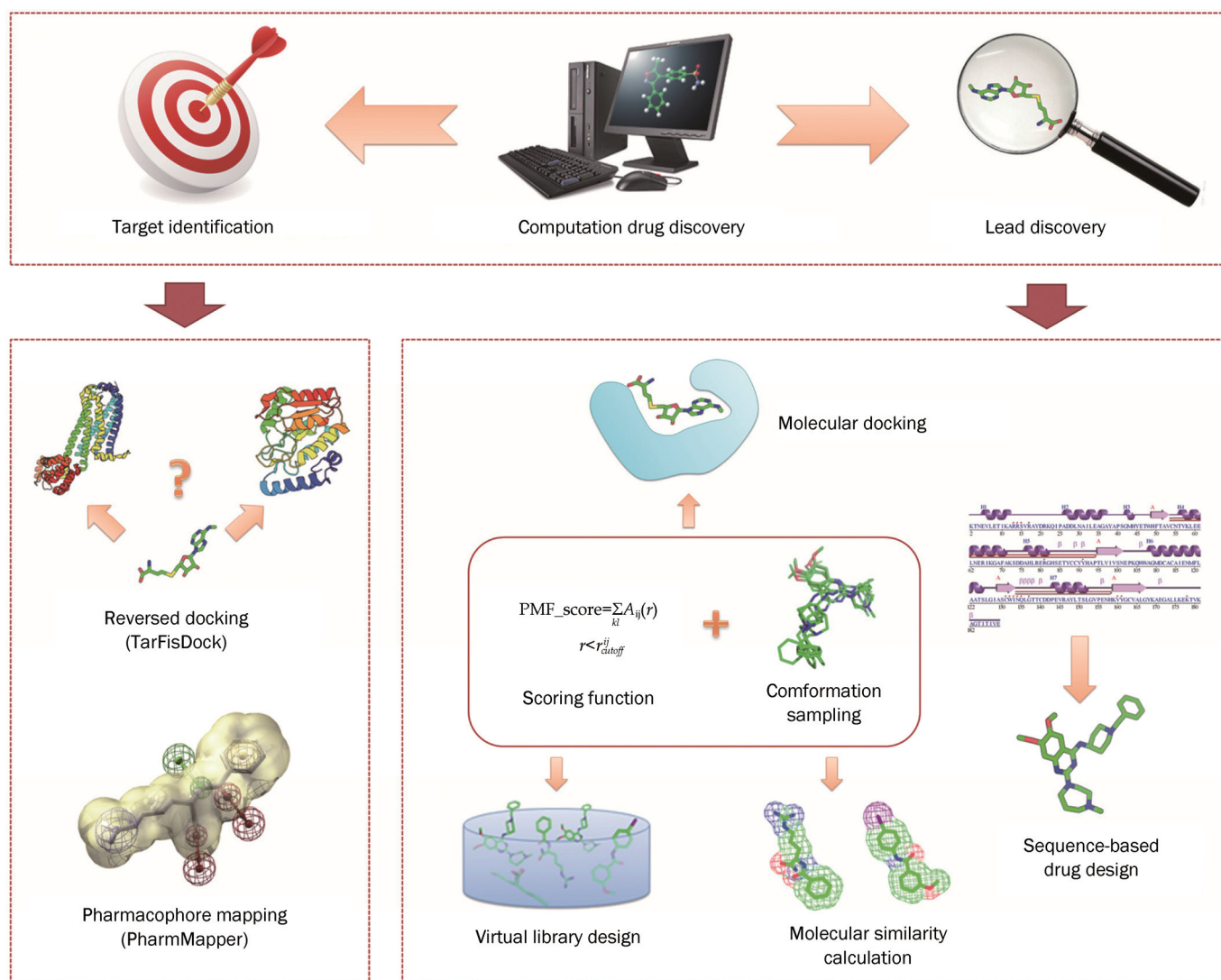
Figure 2. Important methodologies and platforms in the computational drug discovery field introduced and discussed in this article, with a focus on target identification and lead discovery fields.

obtained from the Protein Data Bank. The general information for these proteins was extracted from the literature and several online databases, such as TTD[22], DrugBank[23], and Thomson Pharma. This database contains diverse information on more than 830 potential drug targets, and each drug target has structures in both the PDB and MOL2 formats. Information on related diseases, biological functions and associated signaling pathways has also been collected. All of the targets were classified according to their function and their related diseases. PDTD has a keyword search function for parameters such as the PDB ID, the target name and the disease name[24]. As a comprehensive and unique repository of drug targets, it could be used for *in silico* drug target identification, virtual screening, and the discovery of secondary effects for existing drugs.

Another important issue in target identification is finding the best interaction mode between the potential target can-

didates and the small molecule probes. In addition to the reverse docking method, pharmacophore modeling and mapping can be used to identify the optimal interaction mode. A pharmacophore model is the spatial arrangement of features essential for a molecule to interact with a specific target receptor. PharmMapper is the first web-based tool to use a 'reverse' pharmacophore mapping approach to predict potential drug targets against any given small molecule[25]. However, the PharmMapper server requires a sufficient number of available pharmacophore models that describe the binding modes of known ligands at the binding sites. Thus, a large, in-house database of pharmacophore models annotated with their target information was constructed (PharmTargetDB). The target protein structures in complex with small molecules were carefully extracted from the DrugBank[26], BindingDB[27], PDBBind[28], and PDTD[24] databases, and over 7000 pharmacophore models (covering information for over 1500 drug

targets) based on the complex structures were generated. A sequential combination of triangle hashing (TriHash) and genetic algorithm (GA) optimization was adopted to identify the pharmacophore that best fit the task. Benefiting from the highly efficient and robust triangle hash mapping method, PharmMapper is computationally efficient and has the ability to carry out high throughput screens. The algorithm is highly automated, and the interface is user friendly. For experienced users, optional parameters controlling speed and accuracy and the candidate targets subset can be freely customized. The major limitation of the program is that the pharmacophore database only includes drug targets that have PDB structures with a co-crystallized ligand. However, PharmTargetDB is updated periodically as the number of structures deposited in PDB grows[25].

Docking-based virtual screening

Virtual screening based on molecular docking has become one of the most widely used methods of SBDD. The primary criteria for any docking method are docking accuracy, scoring accuracy, and computational efficiency, which are all strongly influenced by the conformational searching method[29, 30]. Molecular docking is a typical optimization problem; therefore, it is difficult to obtain the global optimum solution. Most conformational optimization methods in docking programs can only deal with a single objective, such as the binding energy, shape complementarity, or chemical complementarity. This type of method is not effective for solving real-world problems, which normally involve multiple objectives[31]. Therefore, an optimization algorithm that comprises several objectives and results in more reasonable and robust binding modes between ligands and macromolecules is urgently needed.

A newly developed docking methodology, GAsDock, uses an entropy-based multi-population GA to optimize the binding poses between small molecules and macromolecule receptors[32]. Information entropy was employed in the GA for optimization, and contracted space was used as the convergence criterion, ensuring that GAsDock can converge rapidly and steadily. A validation test docking known inhibitors into the binding pockets of thymidine kinase (TK) and HIV-1 reverse RT indicated that GAsDock is more accurate than other docking programs, such as GOLD[33], FlexX[33], DOCK[33], Surflex[30], and Glide[29]. To increase the accuracy and speed of the process, an improved adaptive genetic algorithm has been developed that supports a flexible docking method. Some advanced techniques, such as multi-population genetic strategy, entropy-based searching technique with self-adaption and quasi-exact penalty, were introduced into this algorithm. A new iteration scheme was also employed in conjunction with these techniques to speed up the optimization and convergence processes, making this method significantly faster than the old method[34]. In addition, two sets of multi-objective optimization (MO) methods, denoted MOSFOM (Multi-Objective Scoring Function Optimization Methodology), that simultaneously consider both the energy score and the contact score were developed. MOSFOM primarily emphasizes a new strategy to obtain the most reasonable binding conformation and increase the hit rates rather than to accurately predicting the binding free energy[31].

Conformation sampling

One of the imperative aspects of drug design and development is to perceive the bioactive conformations of the small molecules that determine the physical and biological properties of the molecules. Many of the drug discovery methods, such as molecular docking, pharmacophore construction and matching, 3D database searching, 3D-QSAR, and molecular similarity analysis, involve a conformational sampling procedure to generate conformations of small molecules in the binding pocket and a scoring phase to rank these conformations. A practical conformation ensemble should guarantee that the conformers are energy reasonable and span the conformational space in an appropriate amount of time. Other sophisticated criteria, such as pharmacophore and binding pocket mapping, have also been implemented to sample the conformers, making the conformation generation process a multi-objective optimization process[35].

A highly efficient conformational generation method named Cyndi, which is based on the multi-objective evolution algorithm (MOEA), has been developed. Using multiple objectives to control energy accessibility as well as geometric diversity, Cyndi is capable of searching the conformational space in nearly constant time and of sampling the *Pareto* frontier at which both the energy and diversity features are favored. The conformers are encoded into GA individuals with information on the dihedral torsions of the rotatable bonds; the VDW and the torsional energy terms are two distinctive objectives for separating the generated conformers in energy space using the Tripos force field[36]. Cyndi ensures that the generated conformation ensemble simultaneously meets multiple criteria, such as low energy and geometric diversity, instead of concentrating on just one criteria[35]. Recently, Cyndi was updated to incorporate the MMFF94 force field to more rationally assess the conformational energy. A comparison between Cyndi and MacroModel integrated in Maestro V7.5 (Schrodinger Inc), focusing on the balance between the sampling depth of the conformational space and the conformational costs with respect to the algorithm method used has been performed. MacroModel was shown to have comparable performance to Cyndi in terms of retrieving the bioactive conformations, while Cyndi performed better at discovering bioactive conformations in the shortest amount of time with regard to the efficiency of the conformation sampling[37].

Scoring function

The scoring function is an essential component in virtual screening. One major scoring method is the knowledge-based scoring method, which typically extracts structural information from experimentally determined protein-ligand complexes and employs the Boltzmann law to transform the atom pair preferences into distance-dependent pairwise

potentials[38–41]. The potential of mean force (PMF) scoring function can convert structural information into free energy without any knowledge of the binding affinities and is therefore expected to be more applicable. This method implicitly balances many opposing contributions to binding, such as solvation effects, conformational entropy and interaction enthalpy[40]. Several remarkable methodologies focused on these fields are introduced below.

A kinase family-specific PMF scoring function named kinase-PMF was developed with a kinase data set of 872 complexes from the PDB database to assess the binding of ATP-competitive kinase inhibitors[42]. This scoring function inherits the functional form and atom type of PMF04[43]. Compared to eight other commonly used scoring methods, kinase-PMF had the highest success rate in identifying not only positive compounds from decoys but also crystal conformations. Thus, this method could allow researchers to screen and optimize hit compounds in kinase inhibitor development[42].

An improved PMF scoring function named KScore, which is based on several diverse training sets and a newly defined atom-typing scheme using 23 redefined ligand atom types, 17 protein atom types and 28 newly introduced atom types for nucleic acids, has been developed. In comparison with the existing PMF potentials, such as PMF99 and PMF04, the pairwise potentials for different atom types used in KScore have been significantly improved, particularly in the field of reflecting experimental phenomena, including the interaction distances and the strengths of hydrogen bonding, electrostatic interactions, VDW interactions, cation-π interactions and aromatic stacking. KScore is a powerful tool for distinguishing strong binders from a series of compounds and can be applied to large-scale virtual screening. In addition, further improvements should be possible by modifying the atom-typing scheme and diverse training sets[44]. KScore has been integrated into the previously mentioned molecular docking program GAsDock[32].

On the basis of the concept and formalism of PMF and a novel iteration method, a knowledge-based scoring function named IPMF was developed. This scoring function integrates additional experimental binding affinity information into the knowledge base as complementary data to the generally used structural information. The employed iteration method is to extract the 3D structural information and the binding affinity information in order to yield an "enriched" knowledge-based model. The performance of IPMF was evaluated by scoring a diverse set of 219 protein-ligand complexes and comparing the results to seven commonly used scoring functions. As a result, the IPMF score performs best in the activity prediction test. In addition, when re-ranking binding poses, IPMF also demonstrated marginal improvements over the other evaluated knowledge-based scoring functions. These results suggest that the additional binding affinity information can be used not only for developing scoring functions but also for improving their ability to predict binding affinities. The IPMF approach provides a well-defined scheme to introduce binding information into typical statistical potentials, which may

be applicable to other knowledge-based scoring functions[45].

Molecular similarity methods

As the cornerstone of structure-activity relationship (SAR) and structural clustering analysis, molecular similarity is a pivotal concept in LBDD. Similarity-based virtual screening and candidate ranking are considered to be one of the most powerful tools in medicinal chemistry[46, 47] and have been successfully applied in a number of cases. Similarity searching programs can generally be categorized into 2D and 3D similarity according to whether 3D conformation information is considered. 2D similarity methods are efficient for quickly profiling neighboring compounds. However, it may to some extent provide different hits for the same queries as different 2D similarity definitions target different aspects of the information. This method also tends to discover close structural analogues instead of novel scaffold hits[48]. However, 3D similarity methods typically consider multiple aspects of the 3D conformation, including pharmacophores, molecular shapes, and molecular fields. 3D methods can be conveniently used to accomplish scaffold hopping to identify novel compounds.

Based on the pharmacophore matching approach, which was used as the engine of the previously mentioned Pharm-Mapper Server[25], a method named SHAFTS (SHApe-FeaTure Similarity) has been developed for rapid 3D molecular similarity calculation. This method adopts hybrid similarity metrics of molecular shape and colored (or labeled) chemistry groups annotated by pharmacophore features for 3D calculation and ranking in order to integrate the strength of both pharmacophore matching and volumetric similarity approaches. The triplet hashing method is used to enumerate fast molecular alignment poses. The hybrid similarity consists of shape-densities overlaps and pharmacophore feature fit values and is used to score and rank alignment modes. SHAFTS achieved superior performance in terms of both overall and early stage enrichments of known actives and chemotypes compared to other ligand-based methods[48]. SHAFTS has been integrated into ChemMapper Server (unpublished result).

Spherical harmonic (SH) is a set of orthogonal spherical functions that can easily represent the shape of a closed curve surface, such as a molecular surface. SH expansion theory has been successfully applied in virtual screening, protein-ligand recognition, binding pocket modeling, molecular fragment similarity, and so forth. SHeMS is a novel molecular shape similarity comparison method derived from SH expansion. In this method, the SH expansion coefficients are weighted to calculate similarity, leading to a distinct contribution of overall and detailed features to the final score. In addition, the reference set for optimization can be configured by the user, which allows for system-specific and customized comparisons. A retrospective VS experiment on the directory of useful decoys (DUD) database and principal component analysis (PCA) reveals that SHeMS provides dramatically improved performance over the original SH (OSH) and ultra-fast shape recognition (USR) methods[49].

Virtual library construction

De novo drug design aims to chemically fill the binding sites of target macromolecules. One of the critical challenges of this process is to select fragment sets that have the best potential to be parts of new drug leads for a given target. Virtual library construction including focused library, targeted library and primary screening library has been suggested as one way to overcome this challenge[50]. Another challenge is to set up proper criteria for product judgement. To solve this problem, drug-likeness and structural diversity have been introduced into library design to reduce the size and increase the screening efficiency of the constructed libraries.

Focused libraries concentrate on one particular target and are built on the basis of a lead compound or pharmacophore, while targeted libraries are designed to seek drug leads against specific targets[14]. A new efficient approach that adopts the advantages of both focused and targeted libraries and integrates technologies from docking-based virtual screening and drug-like analysis was established to build, optimize and assess focused libraries. A software package named LD1.0 was successfully developed using the new approach[51]. Building blocks are selected from given fragment databases to create a series of virtual libraries. The virtual libraries are then optimized by library-based GA and evaluated on the basis of specified criteria such as docking energy, molecular diversity and drug-likeness. GA retains libraries with higher scores and creates new libraries to form the next generation of focused libraries. Once the termination condition is satisfied, GA optimization ends[51].

Sequence-based drug design

The 3D structures of most proteins have not previously been determined, and many of the proteins do not even have a known ligand. In this situation, neither structure-based methods nor ligand-based methods can be employed to conduct drug discovery and development research. Therefore, a method to predict ligand-protein interactions (LPIs) in the absence of 3D or ligand information is urgently needed. Recently, a sequence-based drug design model for LPI was constructed solely on the basis of the primary sequence of proteins and the structural features of small molecules using the support vector machine (SVM) approach[13]. This model was trained using 15000 LPIs between 626 proteins and over 10000 active compounds collected from the Binding Database[52]. In the validation test of this model, nine novel active compounds against four pharmacologically important targets were found using only the sequence of the target. This is the first example of a successful sequence-based drug design campaign[13].

Applications

The newly developed computational drug discovery approaches have been successfully applied in several cases, which suggests that these methods may further emphasize the role of computational drug discovery in the drug R&D workflow.

Application of computational methods to target identification

The combinational strategy of the reverse docking tools Tar-FisDock and the PDTD database have been successfully used to identify the targets for several bioactive compounds whose *in vivo* targets are unknown. Colonization of the human stomach by the pathogenic bacterium *Helicobacter pylori* is a major cause of gastrointestinal illnesses. However, because of the lack of mature protein targets, discovering anti-*H pylori* agents is a daunting task. Using the active natural product discovered by anti-*H pylori* screening as a probe, potential binding proteins were screened from PDTD using the reverse docking tool TarFisDock. A subsequent homology search indicated that among the 15 candidates discovered by reverse docking, only diaminopimelate decarboxylase (DC) and peptide deformylase (PDF) had homologous proteins in the *H pylori* genome. Enzymatic assays demonstrated that the natural product and one of its analogs are potent inhibitors against *H pylori* PDF (*Hp*PDF), with IC$_{50}$ values of 10.8 and 1.25 μmol/L, respectively. The X-ray crystal structures of *apo-Hp*PDF and inhibitor-*Hp*PDF complexes were determined, demonstrating at the atomic level that *Hp*PDF is a potential target for screening new anti-*H pylori* agents[53].

A natural component of ginger, [6]-gingerol, has been reported to exhibit anti-inflammatory and antioxidant properties and exert substantial anticarcinogenic and antimutagenic activities[54]. Despite its potential efficacy in cancer, the mechanism by which it exerts its chemopreventive effects was elusive. By using TarFisDock, [6]-gingerol was docked to each target in PDTD to identify its potential *in vivo* targets. The top 2% of protein hits from the ranked list were considered to be potential target candidates. Subsequent experimental data revealed that [6]-gingerol can effectively suppress tumor growth in nude mice by inhibiting leukotriene A$_4$ hydrolase (LTA$_4$H). These findings indicated a crucial role for LTA$_4$H in cancer and supported the anticancer role of [6]-gingerol in targeting LTA$_4$H to prevent colorectal cancer[55].

Sphingosine-1-phosphate (S1P) is a sphingolipid metabolite that regulates many cellular and physiological processes, including cell growth, survival, movement, angiogenesis, vascular maturation, immunity and lymphocyte trafficking[56-58]. Although S1P could exert its biological function by binding to five S1P receptors on the cytomembrane, considerable evidence has suggested that S1P has direct intracellular targets. Using an *in silico* target identification approach, S1P was discovered to specifically bind to the histone deacetylases HDAC1 and HDAC2 to regulate histone acetylation[59]. S1P was also found to be a missing cofactor for the E3 ubiquitin ligase TRAF2[60]. These achievements illustrate the pivotal role of S1P in the "inflammation-cancer" chain-related TNFα signaling pathway and in the regulation of gene expression and transcription.

Applications of computational methods in lead discovery

RhoA, one of the most characterized member of the Rho GTPase family, is essential for multiple cellular processes,

including cytoskeletal rearrangement, gene expression, membrane trafficking as well as cell adhesion, migration, differentiation, proliferation and apoptosis[61–63]. This protein is a promising target for treating cardiovascular diseases. Using a docking-based virtual screening strategy in conjunction with chemical synthesis and bioassays, a series of first-in-class small molecular RhoA inhibitors were discovered from the SPECS database. A hierarchical docking strategy was adopted: DOCK4.0[19] was used for the initial screening, and the standard DOCK score was used to rank the resulting list; the top 3000 candidates were further docked and ranked by their new scores with Glide in standard precision (SP) mode[29, 64]. In the end, eight compounds showed high RhoA inhibition activities, and two of them showed significant inhibitory effects against PE-induced contraction in thoracic aorta artery rings[65].

Insulin-like growth factor-1 receptor (IGF-1R), a receptor tyrosine kinase, plays a pivotal role in signaling pathways involved in cell growth, proliferation and apoptosis[66]. IGF-1R has been shown to be overexpressed in many human cancers, which suggests it might be a promising target for cancer therapy[67]. Pharmacophore-based virtual screening combined with molecular docking was applied hierarchically to discover IGF-1R inhibitors. Beginning with the complex crystal structure of IGF-1R and its inhibitor, pyridine-2-one, the key interactions between the protein and the ligand at the ATP-binding site were used to construct a pharmacophore model. The SPECS database was screened using this model. The top ranked hits were then docked to the ATP-binding site using Glide[29, 64]. This strategy led to the identification of a series of novel thiazolidine-2,4-dione analogues as potential IGF-1R inhibitors; the molecules demonstrate favorable inhibitory potency and selectivity against IGF-1R over insulin resistance (IR)[68].

A prospective application of the LBDD program SHAFTS is the discovery of novel inhibitors for p90 ribosomal S6 protein kinase 2 (RSK2). Overexpression and aberrant activation of RSK2 have been linked to many human diseases, such as breast cancer, prostate cancer, and human head and neck squamous cell carcinoma[69]. Using the putative 3D conformations of two weakly binding RSK2 inhibitors with moderate activity as the query templates, 16 compounds with IC_{50} lower than 20 μmol/L, which would be missed by conventional 2D methods, were identified via chemotype switching directed by the SHAFTS calculation. The most potent hits show low micromolar inhibitory activities specifically for RSK2, and one compound also exhibits potent anti-migration activity in MDA-MB-231 tumor cells[70].

In another study, a series of novel small molecule inhibitors of cyclophilin A (CypA) were identified using a *de novo* drug design approach. CypA plays an essential role in many biological processes, including enhancing the rate of protein folding/unfolding[71, 72], inhibiting the serine/threonine phosphatase activity of calcineurin[73, 74], facilitating viral replication and infection[75, 76], and inducing neuroprotective/neurotrophic effects[77, 78]. In addition, CypA has been reported to be overexpressed exclusively in cancer cells, particularly in solid tumors, suggesting that CypA is an important regulator of carcinogenesis[79]. The identification of potent, structurally novel small molecule CypA inhibitors is urgently needed, as the most currently available CypA inhibitors are primarily natural products and peptide analogs that may face pharmacokinetic problems. Using the fragment structures of previously discovered CypA inhibitors[80] as building blocks, a focused combinatorial library containing 255 molecules was designed using the LD1.0[51] program. By applying a docking-based virtual screening strategy that targets the binding pocket of CypA, 16 compounds were selected for synthesis and bioassay. According to the experimental results, these compounds all showed high CypA inhibitory activities. The binding affinity and inhibitory activity of the most potent compound among the identified novel CypA inhibitors are approximately 10 times more potent than the best previously known inhibitor[81].

Outlook

Great progress has been made in methodology development and the application of computational drug discovery, resulting in a paradigm change in both industry and academics. Taking advantage of computational methods, potent hits can be obtained in a matter of weeks[82]. Searching for new chemical entities has led to the construction of high quality datasets and libraries that can be optimized for either molecular diversity or similarity. In addition, distributed computing has become more popular in large-scale virtual screening, in part because of increasingly powerful technology[6].

Although it is apparent that computational drug discovery methods have great potential, one should not rely on computational techniques in a black box manner and should beware of the Garbage In-Garbage Out (GIGO) phenomenon. The *in silico* components in research must still be coupled with experiment resources, and computational discovery tools are not substitutions for the more important *in cerebro* component[9, 83, 84]. In the future, in addition to increasing the accuracy and effectiveness of existing technologies, the most important tendency in computational drug discovery field will be the integration of computational chemistry and biology together with chemoinformatics and bioinformatics, which will result in a new field known as pharmacoinformatics[14, 85]. Inspired by the completion of the human genome and numerous pathogen genomes, great efforts will be made to understand the role of gene products in order to exploit their functions, which could be of great help for discovering new drug targets[86]. Computational methods involving target identification will become more attention-getting[87, 88], and designed small molecules will also be extensively used as probes for functional research[89, 90].

Acknowledgements

Technology Research and Development Program of China (2012AA020302).

References

1 Myers S, Baker A. Drug discovery - an operating model for a new era. Nat Biotechnol 2001; 19: 727–30.

2 Moses H 3rd, Dorsey ER, Matheson DH, Thier SO. Financial anatomy of biomedical research. JAMA 2005; 294: 1333–42.

3 Lahana R. How many leads from HTS? Drug Discov Today 1999; 4: 447–8.

4 Lobanov V. Using artificial neural networks to drive virtual screening of combinatorial libraries. Drug Discov Today Biosilico 2004; 2: 149–56.

5 Shekhar C. *In silico* pharmacology: computer-aided methods could transform drug development. Chem Biol 2008; 15: 413–4.

6 Song CM, Lim SJ, Tong JC. Recent advances in computer-aided drug design. Brief Bioinform 2009; 10: 579–91.

7 Jorgensen WL. The many roles of computation in drug discovery. Science 2004; 303: 1813–8.

8 Xiang M, Cao Y, Fan W, Chen L, Mo Y. Computer-aided drug design: lead discovery and optimization. Comb Chem High Throughput Screen 2012; 15: 328–37.

9 Zhang S. Computer-aided drug discovery and development. Methods Mol Biol 2011; 716: 23–38.

10 Tan JJ, Cong XJ, Hu LM, Wang CX, Jia L, Liang XJ. Therapeutic strategies underpinning the development of novel techniques for the treatment of HIV infection. Drug Discov Today 2010; 15: 186–97.

11 Chen L, Morrow JK, Tran HT, Phatak SS, Du-Cuny L, Zhang S. From laptop to benchtop to bedside: structure-based drug design on protein targets. Curr Pharm Des 2012; 18: 1217–39.

12 Acharya C, Coop A, Polli JE, Mackerell AD Jr. Recent advances in ligand-based drug design: relevance and utility of the conformationally sampled pharmacophore approach. Curr Comput Aided Drug Des 2011; 7: 10–22.

13 Wang F, Liu DX, Wang HY, Luo C, Zheng MY, Liu H, *et al*. Computational screening for active compounds targeting protein sequences: methodology and experimental validation. J Chem Inf Model 2011; 51: 2821–8.

14 Tang Y, Zhu WL, Chen KX, Jiang HL. New technologies in computer-aided drug design: Toward target identification and new chemical entity discovery. Drug Discov Today Technol 2006; 3: 307–13.

15 Jorgensen WL. Efficient drug lead discovery and optimization. Acc Chem Res 2009; 42: 724–33.

16 Hajduk PJ, Huth JR, Tse C. Predicting protein druggability. Drug Discov Today 2005; 10: 1675–82.

17 Huan CM, Elmets CA, Tan DC, Li F, Yusuf N. Proteomics reveals that proteins expressed during the early stage of *Bacillus anthracis* infection are potential targets for the development of vaccines and drugs. Genomics Proteomics Bioinformatics 2004; 2: 143–51.

18 Li HL, Gao ZT, Kang L, Zhang HL, Yang K, Yu KQ, *et al*. TarFisDock: a web server for identifying drug targets with docking approach. Nucleic Acids Res 2006; 34: W219–24.

19 Ewing TJ, Makino S, Skillman AG, Kuntz ID. DOCK 4.0: Search strategies for automated molecular docking of flexible molecule databases. J Comput Aided Mol Des 2001; 15: 411–28.

20 Kuntz ID, Blaney JM, Oatley SJ, Langridge R, Ferrin TE. A geometric approach to macromolecule-ligand interactions. J Mol Biol 1982; 161: 269–88.

21 Paul SM, Mytelka DS, Dunwiddie CT, Persinger CC, Munos BH, Lindborg SR, *et al*. How to improve R&D productivity: the pharmaceutical industry's grand challenge. Nat Rev Drug Discov 2010; 9: 203–14.

22 Chen X, Ji ZL, Chen YZ. TTD: Therapeutic Target Database. Nucleic Acids Res 2002; 30: 412–5.

23 Wishart DS, Knox C, Guo AC, Shrivastava S, Hassanali M, Stothard P, *et al*. DrugBank: a comprehensive resource for *in silico* drug discovery and exploration. Nucleic Acids Res 2006; 34: D668–72.

24 Gao ZT, Li HL, Zhang HL, Liu XF, Kang L, Luo XM, *et al*. PDTD: a web-accessible protein database for drug target identification. BMC Bioinformatics 2008; 9: 104.

25 Liu XF, Ouyang SS, Yu BA, Liu YB, Huang K, Gong JY, *et al*. PharmMapper server: a web server for potential drug target identification using pharmacophore mapping approach. Nucleic Acids Res 2010; 38: W609–14.

26 Wishart DS, Knox C, Guo AC, Cheng D, Shrivastava S, Tzur D, *et al*. DrugBank: a knowledgebase for drugs, drug actions and drug targets. Nucleic Acids Res 2008; 36: D901–6.

27 Liu T, Lin Y, Wen X, Jorissen RN, Gilson MK. BindingDB: a web-accessible database of experimentally determined protein-ligand binding affinities. Nucleic Acids Res 2007; 35: D198–201.

28 Wang R, Fang X, Lu Y, Wang S. The PDBbind database: collection of binding affinities for protein-ligand complexes with known three-dimensional structures. J Med Chem 2004; 47: 2977–80.

29 Friesner RA, Banks JL, Murphy RB, Halgren TA, Klicic JJ, Mainz DT, *et al*. Glide: a new approach for rapid, accurate docking and scoring. 1. Method and assessment of docking accuracy. J Med Chem 2004; 47: 1739–49.

30 Jain AN. Surflex: Fully automatic flexible molecular docking using a molecular similarity-based search engine. J Med Chem 2003; 46: 499–511.

31 Li HL, Zhang HL, Zheng MY, Luo J, Kang L, Liu XF, *et al*. An effective docking strategy for virtual screening based on multi-objective optimization algorithm. BMC Bioinformatics 2009; 10: 58.

32 Li HL, Li CL, Gui CS, Luo XM, Chen KX, Shen JH, *et al*. GAsDock: a new approach for rapid flexible docking based on an improved multi-population genetic algorithm. Bioorg Med Chem Lett 2004; 14: 4671–6.

33 Bissantz C, Folkers G, Rognan D. Protein-based virtual screening of chemical databases. 1. Evaluation of different docking/scoring combinations. J Med Chem 2000; 43: 4759–67.

34 Kang L, Li HL, Jiang HL, Wang XC. An improved adaptive genetic algorithm for protein-ligand docking. J Comput Aided Mol Des 2009; 23: 1–12.

35 Liu XF, Bai F, Ouyang SS, Wang XC, Li HL, Jiang HL. Cyndi: a multi-objective evolution algorithm based method for bioactive molecular conformational generation. BMC Bioinformatics 2009; 10: 101.

36 Shoichet BK, Leach AR, Kuntz ID. Ligand solvation in molecular docking. Proteins 1999; 34: 4–16.

37 Bai F, Liu XF, Li JB, Zhang HY, Jiang HL, Wang XC, *et al*. Bioactive conformational generation of small molecules: a comparative analysis between force-field and multiple empirical criteria based methods. BMC Bioinformatics 2010; 11: 545.

38 Gohlke H, Hendlich M, Klebe G. Knowledge-based scoring function to predict protein-ligand interactions. J Mol Biol 2000; 295: 337–56.

39 Mitchell JBO, Laskowski RA, Alex A, Thornton JM. BLEEP - Potential of mean force describing protein-ligand interactions: I. Generating potential. J Comput Chem 1999; 20: 1165–76.

40 Muegge I, Martin YC. A general and fast scoring function for protein-ligand interactions: a simplified potential approach. J Med Chem 1999; 42: 791–804.

41 Sippl MJ. Boltzmann's principle, knowledge-based mean fields and

protein folding. An approach to the computational determination of protein structures. J Comput Aided Mol Des 1993; 7: 473–501.

42 Xue MZ, Zheng MY, Xiong B, Li YL, Jiang HL, Shen JK. Knowledge-based scoring functions in drug design. 1. Developing a target-specific method for kinase-ligand interactions. J Chem Inf Model 2010; 50: 1378–86.

43 Muegge I. PMF scoring revisited. J Med Chem 2006; 49: 5895–902.

44 Zhao XY, Liu XF, Wang YY, Chen Z, Kang L, Zhang HL, et al. An improved PMF scoring function for universally predicting the interactions of a ligand with protein, DNA, and RNA. J Chem Inf Model 2008; 48: 1438–47.

45 Shen QC, Xiong B, Zheng MY, Luo XM, Luo C, Liu XA, et al. Knowledge-based scoring functions in drug design: 2. Can the knowledge base be enriched? J Chem Inf Model 2011; 51: 386–97.

46 Muchmore SW, Edmunds JJ, Stewart KD, Hajduk PJ. Cheminformatic tools for medicinal chemists. J Med Chem 2010; 53: 4830–41.

47 Maldonado AG, Doucet JP, Petitjean M, Fan BT. Molecular similarity and diversity in chemoinformatics: from theory to applications. Mol Divers 2006; 10: 39–79.

48 Liu XF, Jiang HL, Li HL. SHAFTS: a hybrid approach for 3D molecular similarity calculation. 1. Method and assessment of virtual screening. J Chem Inf Model 2011; 51: 2372–85.

49 Cai CQ, Gong JY, Liu XF, Jiang HL, Gao DQ, Li HL. A novel, customizable and optimizable parameter method using spherical harmonics for molecular shape similarity comparisons. J Mol Model 2012; 18: 1597–610.

50 Drewry DH, Young SS. Approaches to the design of combinatorial libraries. Chemometr Intell Lab Syst 1999; 48: 1–20.

51 Chen G, Zheng SX, Luo XM, Shen JH, Zhu WL, Liu H, et al. Focused combinatorial library design based on structural diversity, druglikeness and binding affinity score. J Comb Chem 2005; 7: 398–406.

52 Liu TQ, Lin YM, Wen X, Jorissen RN, Gilson MK. BindingDB: a web-accessible database of experimentally determined protein-ligand binding affinities. Nucleic Acids Res 2007; 35: D198–201.

53 Cai JH, Han C, Hu TC, Zhang J, Wu DL, Wang FD, et al. Peptide deformylase is a potential target for anti-Helicobacter pylori drugs: Reverse docking, enzymatic assay, and X-ray crystallography validation. Protein Sci 2006; 15: 2071–81.

54 Surh Y. Molecular mechanisms of chemopreventive effects of selected dietary and medicinal phenolic substances. Mutat Res 1999; 428: 305–27.

55 Jeong CH, Bode AM, Pugliese A, Cho YY, Kim HG, Shim JH, et al. [6]-Gingerol suppresses colon cancer growth by targeting leukotriene A4 hydrolase. Cancer Res 2009; 69: 5584–91.

56 Spiegel S, Milstien S. Sphingosine-1-phosphate: An enigmatic signalling lipid. Nat Rev Mol Cell Biol 2003; 4: 397–407.

57 Chun J, Rosen H. Lysophospholipid receptors as potential drug targets in tissue transplantation and autoimmune diseases. Curr Pharm Des 2006; 12: 161–71.

58 Schwab SR, Cyster JG. Finding a way out: lymphocyte egress from lymphoid organs. Nat Immunol 2007; 8: 1295–301.

59 Hait NC, Allegood J, Maceyka M, Strub GM, Harikumar KB, Singh SK, et al. Regulation of histone acetylation in the nucleus by sphingosine-1-phosphate. Science 2009; 325: 1254–7.

60 Alvarez SE, Harikumar KB, Hait NC, Allegood J, Strub GM, Kim EY, et al. Sphingosine-1-phosphate is a missing cofactor for the E3 ubiquitin ligase TRAF2. Nature 2010; 465: 1084–8.

61 Ridley AJ. Rho family proteins: coordinating cell responses. Trends Cell Biol 2001; 11: 471–7.

62 Sander EE, Collard JG. Rho-like GTPases: Their role in epithelial cell-cell adhesion and invasion. Eur J Cancer 1999; 35: 1302–8.

63 Wheeler AP, Ridley AJ. Why three Rho proteins? RhoA, RhoB, RhoC, and cell motility. Exp Cell Res 2004; 301: 43–9.

64 Halgren TA, Murphy RB, Friesner RA, Beard HS, Frye LL, Pollard WT, et al. Glide: A new approach for rapid, accurate docking and scoring. 2. Enrichment factors in database screening. J Med Chem 2004; 47: 1750–9.

65 Deng J, Feng EG, Ma S, Zhang Y, Liu XF, Li HL, et al. Design and synthesis of small molecule RhoA inhibitors: a new promising therapy for cardiovascular diseases? J Med Chem 2011; 54: 4508–22.

66 Randhawa R, Cohen P. The role of the insulin-like growth factor system in prenatal growth. Mol Genet Metab 2005; 86: 84–90.

67 Khandwala HM, McCutcheon IE, Flyvbjerg A, Friend KE. The effects of insulin-like growth factors on tumorigenesis and neoplastic growth. Endocr Rev 2000; 21: 215–44.

68 Liu XF, Xie H, Luo C, Tong LJ, Wang Y, Peng T, et al. Discovery and SAR of thiazolidine-2,4-dione analogues as insulin-like growth factor-1 receptor (IGF-1R) inhibitors via hierarchical virtual screening. J Med Chem 2010; 53: 2661–5.

69 Doehn U, Hauge C, Frank SR, Jensen CJ, Duda K, Nielsen JV, et al. RSK is a principal effector of the RAS-ERK pathway for eliciting a coordinate promotile/invasive gene program and phenotype in epithelial cells. Mol Cell 2009; 35: 511–22.

70 Lu WQ, Liu XF, Cao XW, Xue MZ, Liu KD, Zhao ZJ, et al. SHAFTS: a hybrid approach for 3D molecular similarity calculation. 2. Prospective case study in the discovery of diverse p90 ribosomal S6 protein kinase 2 inhibitors to suppress cell migration. J Med Chem 2011; 54: 3564–74.

71 Dornan J, Taylor P, Walkinshaw MD. Structures of immunophilins and their ligand complexes. Curr Top in Med Chem 2003; 3: 1392–409.

72 Galat A. Peptidylprolyl cis/trans isomerases (immunophilins): biological diversity-targets-functions. Curr Top Med Chem 2003; 3: 1315–47.

73 Liu J, Farmer JD, Lane WS, Friedman J, Weissman I, Schreiber SL. Calcineurin is a common target of cyclophilin-cyclosporin A and FKBP-FK506 complexes. Cell 1991; 66: 807–15.

74 Zuo XJ, Matsumura Y, Prehn J, Saito R, Marchevesky A, Matloff J, et al. Cytokine gene expression in rejecting and tolerant rat lung allograft models: analysis by RT-PCR. Transpl Immunol 1995; 3: 151–61.

75 Luban J, Bossolt KL, Franke EK, Kalpana GV, Goff SP. Human immunodeficiency virus type 1 Gag protein binds to cyclophilins A and B. Cell 1993; 73: 1067–78.

76 Luo C, Luo HB, Zheng SX, Gui CS, Yue LD, Yu CY, et al. Nucleocapsid protein of SARS coronavirus tightly binds to human cyclophilin A. Biochem Biophys Res Commun 2004; 321: 557–65.

77 Curtis M, Nikolopoulos SN, Turner CE. Actopaxin is phosphorylated during mitosis and is a substrate for cyclin B1/cdc2 kinase. Biochem J 2002; 363: 233–42.

78 Dawson TM, Steiner JP, Lyons WE, Fotuhi M, Blue M, Snyder SH. The immunophilins, FK506 binding protein and cyclophilin, are discretely localized in the brain: relationship to calcineurin. Neuroscience 1994; 62: 569–80.

79 Choi KJ, Piao YJ, Lim MJ, Kim JH, Ha J, Choe W, et al. Overexpressed cyclophilin A in cancer cells renders resistance to hypoxia- and cisplatin-induced cell death. Cancer Res 2007; 67: 3654–62.

80 Li J, Chen J, Gui CS, Zhang L, Qin Y, Xu Q, et al. Discovering novel chemical inhibitors of human cyclophilin A: virtual screening, synthesis, and bioassay. Bioorg Med Chem 2006; 14: 2209–24.

81 Li J, Zhang J, Chen J, Luo XM, Zhu WL, Shen JH, et al. Strategy for discovering chemical inhibitors of human cyclophilin a: focused library design, virtual screening, chemical synthesis and bioassay. J Comb Chem 2006; 8: 326–37.

82 Singh S, Malik BK, Sharma DK. Molecular drug targets and structure based drug design: A holistic approach. Bioinformation 2006; 1: 314–20.

83 Kumar N, Hendriks BS, Janes KA, de Graaf D, Lauffenburger DA. Applying computational modeling to drug discovery and development. Drug Discov Today 2006; 11: 806–11.

84 Kubinyi H. Drug research: myths, hype and reality. Nat Rev Drug Discov 2003; 2: 665–8.

85 Schuffenhauer A, Jacoby E. Annotating and mining the ligand-target chemogenomics knowledge space. Drug Discov Today Biosilico 2004; 2: 190–200.

86 Kopec KK, Bozyczko-Coyne D, Williams M. Target identification and validation in drug discovery: the role of proteomics. Biochem

Pharmacol 2005; 69: 1133–9.

87 Paul N, Kellenberger E, Bret G, Muller P, Rognan D. Recovering the true targets of specific ligands by virtual screening of the protein data bank. Proteins 2004; 54: 671–80.

88 Chen YZ, Ung CY. Prediction of potential toxicity and side effect protein targets of a small molecule by a ligand-protein inverse docking approach. J Mol Graph Model 2001; 20: 199–218.

89 Shen JH, Xu XY, Cheng F, Liu H, Luo XM, Shen JK, *et al*. Virtual screening on natural products for discovering active compounds and target information. Curr Med Chem 2003; 10: 2327–42.

90 Stockwell BR. Exploring biology with small organic molecules. Nature 2004; 432: 846–54.

npg

Review

Qinghaosu (artemisinin): Chemistry and pharmacology

Ying LI*

Shanghai Institute of Materia Medica, Chinese Academy of Sciences, Shanghai 201203, China

Qinghaosu and its derivatives are widely used in the world as a new generation of antimalarial drug. Up to now, some important progresses of Qinghaosu research have been made, including synthesis of new Qinghaosu derivatives and analogs, investigation on their bioactivities and mode of actions. The present review briefly describes these efforts made by researchers in China, particularly in this Institute.

Keywords: Qinghaosu; artemisinin; structure modification; antimalarial activity; anticancer activity; immunosuppressive activity; mode of action

On 23rd May 1967, China established National Steering Group on antimalarial drug research, more than 60 institutes and 500 researchers joined in this project. After screening of over 5000 traditional Chinese medicines, Qinghaosu (QHS), an antimalarial principle, was isolated from *Artemisia annua* L in 1972[1, 2]. At the end of 1975, its unique chemical structure was elucidated, as a sesquiterpene lactone bearing a peroxy group, quite different from that of all known antimalarial drugs[3].

Early pharmacological and clinic studies showed QHS have rapid onset of action, low toxicity and high effect on both drug-resistant and drug-sensitive malaria. However, its shortcomings (poor solubility in water or oil; high rate of parasite recrudescence) needed to be overcome. In 1976, our Institute was charged with this important mission, and a research in relationship between chemical structure and activity immediately started.

First of all, the function of peroxy group for antimalarial activity was examined. The negative result of deoxyqinghaosu (Scheme 1) against *P berghei* in mice demonstrated that the peroxy group was essential. Soon afterwards, it was found that some other simple peroxides including monoterpene ascaridol had no antimalarial activity. These experimental results proved peroxy group to be an essential but not a sufficient factor. At that time, we noted the molecule contained a rare segment -O-C-O-C-O-C=O, and realized that whole molecular

* To whom correspondence should be addressed.
E-mail yli@mail.shcnc.ac.cn
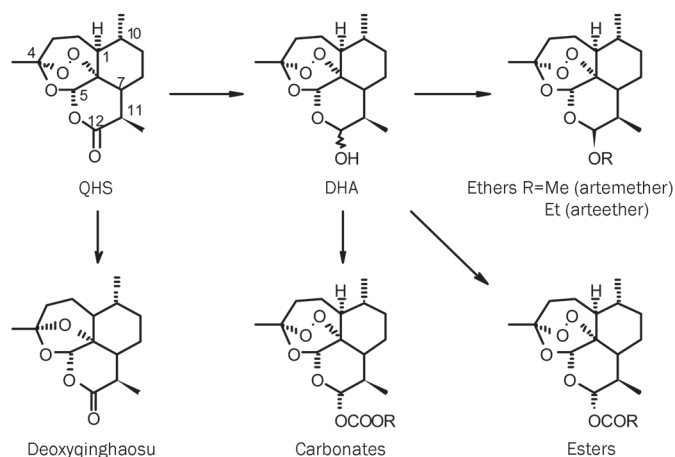
Scheme 1. Synthesis of Qinghaosu derivatives.

skeleton might play an important role for antimalarial activity.

When dihydroartemisinin (DHA) was found to be more active than QHS, but was still with poor solubility and lower stability (as a lactol) than QHS, we decided to prepare its derivatives. In 1976–1977, over 50 derivatives of DHA were synthesized (Scheme 1) and evaluated[4, 5].

The first 25 compounds (in oil solution) were tested in mice infected chloroquine-resistant *P berghei* though intramuscular injection[6]. Most of these derivatives showed higher activity than QHS (SD_{50} 6.20 mg/kg) and DHA (SD_{50} 3.65 mg/kg). In the ether series, SM 224 (R=CH_3, SD_{50} 1.02 mg/kg) is more

active than SM 227 (R=C_2H_5, SD_{50} 1.95 mg/kg) and others. Then, SM 224, SM 108 (ester, R=C_2H_5, SD_{50} 0.66 mg/kg) and SM 242 (carbonate, R=n-C_3H_7, SD_{50} 0.50 mg/kg) were compared with regard to activity, stability, toxicity and cost. Because SM 224 was highly soluble in oil and more stable than others, it was selected as candidate and named as artemether.

At the same period, water-soluble sodium artesunate (ester, R=$COCH_2CH_2COONa$) was developed by the Guilin Pharmaceutical Factory[7]. QHS suppository in 1986; artemether oil injection and sodium artesunate aqueous injection in 1987 were approved as new antimalarial drugs. Since then, other new antimalarial drugs such as dihydroartemisinin, coartem (artemether and benflumetol), co-naphthoquine (naphthoquine phosphate and QHS), compound-dihydroartemisinin were successively developed in China[1, 2].

Since 1980s, millions malaria patients in the world (mainly in China, Southeast Asia and Africa) were saved by administration of QHS, QHS derivatives and their combinations. Artemether, artesunate and coartem have been enrolled in WHO's "List of Essential Medicines" .

Artemisinins can kill drug-resistant *P falciparum*, its antimalarial mechanism must be different from that of the previously-used antimalarial drugs. Elucidation of its mode of action is really an interesting project. Up to now, many research papers have been published[8–14]. Chinese researchers first reported in 1979 that artemisinin drugs had a direct parasiticidal action against *P falciparum* in the erythrocytic stage both *in vitro* and *in vivo,* and observed their morphologic changes under the electron microscope[15, 16]. The main pathological ultrastructural changes caused by QHS were quick damage of the membrane system of the asexual forms of parasites, the swelling and spiral deformation of the membrane of food vacuoles, limiting membrane and the membrane of mitochondria, followed by swelling of the nuclear membrane and endoplasmic reticulum. Among the latter results made in China[17–21], a series of reaction of artemisinins and Fe^{2+}, which involes the intermediate of oxygen-centered or carbon-centered free radicals, is noteworthly.

For exploring the mode of action, reaction of QHS and Fe^{2+} was carefully studied by Chinese chemists[22, 23]. The major products tetrahydrofuran **3** and 3-hydroxy deoxyqinghaosu **4** were proposed to be derived from primary C-centered free radical **1** and secondary C-centered free radical **2,** respectively, as shown in Scheme 2. In addition, the electron spin resonance (ESR) signals of the C-centered free radicals were detected[23, 24].

It is worthy to note that compound **3** and **4** are also the major metabolites of QHS *in vivo* or in human[25, 26].

With the clarification on the C-centered free radicals participation mechanism, it is then interested whether this free radical mechanism is related to its antimalarial activity. Thus, the stable and UV-detectable C-12 aromatic substituted derivatives of QHS were synthezied[27]. Using the usual Lewis acid as the catalyst, the Friedel-Crafts alkylation gave the desired product 2′,4′-dimethoxyphenyl deoxoartemisinin **5** and also 11α-methyl epimer **6** as the by-product (Scheme 3). These
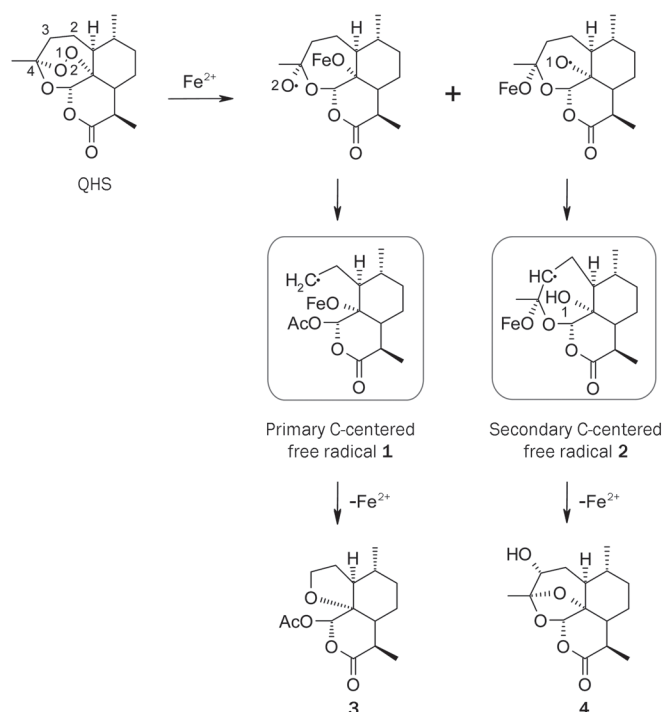
Scheme 2. Formation of Carbon-centered free radicals.
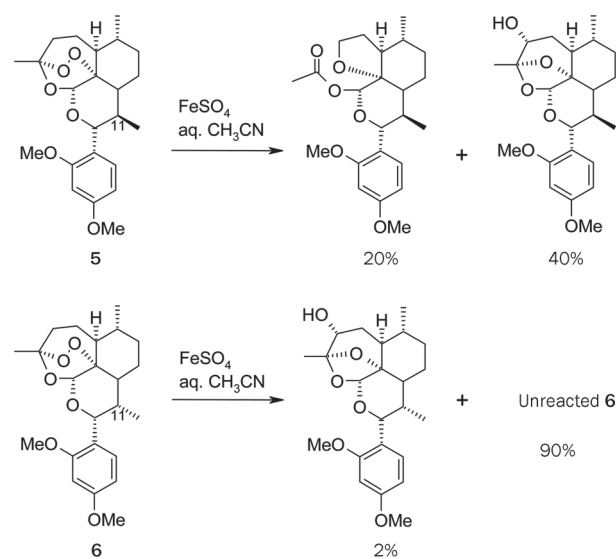
**Scheme 3.** Reaction of QHS derivatives and $FeSO_4$.

products were separated and subjected to both bioassay and chemical reaction with ferrous ion. It is interesting to find that the derivative with normal configuration at C-11 showed higher antimalarial activity and also higher chemical reactivity in the reaction with ferrous ion. On the contrary, the 11α-methyl epimer **6** was obviously less active and almost inert to the reaction with ferrous ion (Scheme 3, Table 1).

In the case of 11α and 11β-epimers of α-hydroxy naphthyl deoxoqinghaosu, similar result was also obtained[28]. Their

Table 1. The ED_{50}- and ED_{90}-values against *P berghei* K173 strain (administered orally to mice as suspensions in Tween 80).

Compound	ED_{50} (mg/kg)	ED_{90} (mg/kg)
Artemether	1	3.1
5	1.27	5.27
6	4.18	76.27

lower activity may be attributed to the steric hindrance around O-1 atom in 11α-epimer, which blocks the way for Fe^{2+} to attack O-1 (Figure 1).
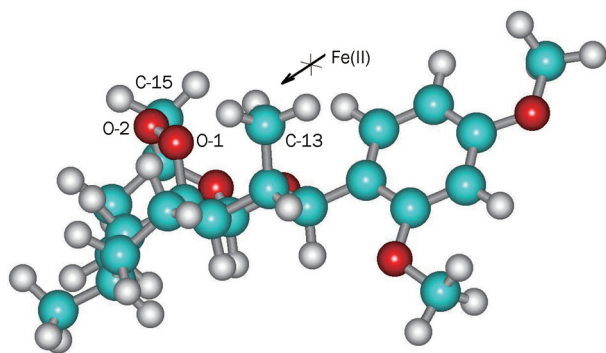

Figure 1. 11α-methyl group blocks the attack of Fe^{2+} on O-1.

The close relationship between antimalarial activity and the primary C-centered free radicals strongly suggests that the Fe^{2+}-induced cleavage of peroxide bond in artemisinins leads to C-centered free radicals, a highly potent alkylating species. Then, what targets would be alkylated? Up to now, a growing list shows that heme, heme-containing protein, translationally controlled tumor-associated protein (TCTP), sarcoendoplasmic reticulum Ca^{2+} ATPase (SERCA)-type protein encoded by PfATP6 might be the targets[14]. Recently, Chinese researchers reported that artemisinins are distributed to malarial mitochondria and directly impair their functions[29].

As for process of alkylation of targets, there was another interesting topic. Considering that malaria-parasite-infected red blood cells have a high concentration of the reducing glutathione (GSH) and excess GSH might be responsible for protecting the parasite from the toxicity of heme, Chinese chemists have performed some reactions, such as artemisinins reacted with cysteine or GSH in the present of a catalytic amount of ferrous ion[27, 30–33]. Successful isolation and identification of the cysteine-artemisinins or GSH-artemisinins adducts proved the formation of covalent bond in these adducts. It is instructive that the C-centered radicals derived from QHS and their derivatives could attack free cysteine and cysteine rasidue not only in peptide but also probably in protein.

The outstanding characteristics of QHS, including high antimalarial action , less significant side effects and less clinical

resistance, impelled researchers to extend its medical application. As a result, hundreds of artemisinin derivatives and analogs were synthesized and widely assayed in China. So far, the successful examples are artemether and artesunate, which were found to be effective in the treatment of Schistosomiasis[34, 35]. From 1993, artemether and artesunate were studied in randomized, double-blind, placebo-controlled trials in China, and approved as the prophylactic drugs for schistosomiasis japonica in 1996[2]. Afterwards, they were found to have similar activity against *S mansoni* and *S haematobium* in other countries[36].

Since 1992, when this Institute first reported that some components of *Artemisia annua* L (such as artemisinic acid, artemisinin B) have antitumor activity *in vitro*[37, 38], hundreds of papers have described the cytotoxicity of QHS and related compounds against tumor cells. Artesunate and DHA are most favorable molecules. In 2001 Efferth *et al* reported that artesunate showed antitumor activity against 55 tumor cell lines, and it was most active against leukemia and colon cancer cell lines. It is notable that none of CEM leukemia sublines, resistant to doxorubicin, vincristin, methotrexate or hydroxyurea showed cross-resistance to artesunate[39]. Since then, more new artemisinin derivatives and analogs were synthesized and tested against human cancer cells. Some compounds showed high activity at the nano- to micromolar range[40]. For example, this Institute in collaboration with French cooperator found that a dihydroartemisinin ether containing cyanoarylmethyl group **7** (Figure 2) was very active against P388 and A549 cell lines, as comparable to VCR, whereas its deoxy-analog **8** (Figure 2) was inactive. Thus peroxy group was proved to be essential for antitumor activity, like for antimalarial activity[41, 42]. In addition, the type of derivative was proved to target G_1 phase of the cell cycle[41]. Thus far, antitumor activity of artemisinins and the underlying mechanisms have been
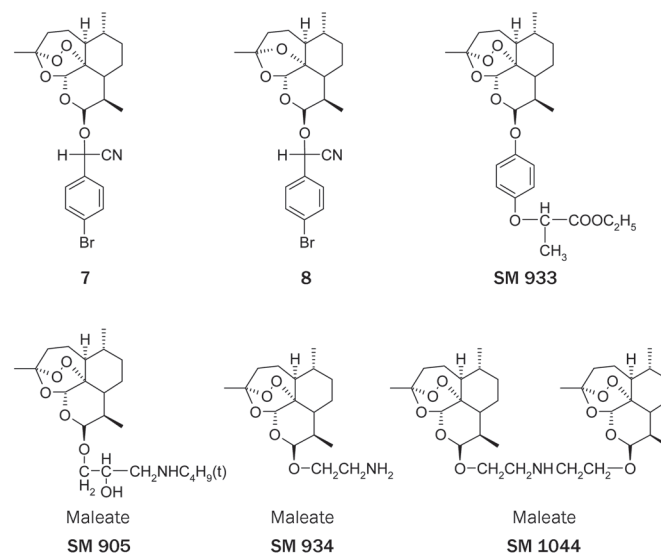
Figure 2. Some compounds with anticancer or immunosuppressive activity.

widely studied[43–49], however, few clinical trials were reported.

Antimalarial chloroquine was used as immunosuppressive agent. Therefore, the research on immunological activity of QHS and its derivatives became an attractive program in China in the 1980'. At the begining, mainly new antimalarial drugs (QHS, artemether and artesunate) were studied in laboratories in China. Afterwards, the clinical trials of artesunate for the treatment of DLE, SLE, rheumatoid arthritis, polymorphous light eruption and chronic actinic dermatitis were conducted. Some clinical data were promising, for example, 56 patients with lupus erythematosus (DLE 16, SCLE 10, and SLE 30) were treated by sodium artesunate (iv 60 mg, once a day, 15 d a course, 2–4 courses), with effective rate at 94%, 90%, and 80%, respectively[50]. To search for highly potent, low toxic immunosuppressive agents, more artemisinin derivatives were synthesized and screened in this Institute since 2001[51–54]. Compounds with various structures were tested in respect to their cytotoxicity to lymphocyte, inhibition activity on ConA-induced T cell proliferation and LPS-induced B cell proliferation, in comparison with QHS, artesunate, artemether and cyclosporin A (CsA). At last, SM 735, SM 905, SM 933, and SM 934 (Figure 2) were selected and tested in the animal models for 2,4-dinitrofluorobenzene (DNFB)-induced delayed-type hypersensitivity (DTH) reaction, sheep red blood cell (SRBC)-induced antibody production, and experimental autoimmune encephalomyelitis (EAE). Up to date, a number of papers related their immuno-suppressive activity and possible mechanisms have been published mainly from this Institute[55–64]. The preclinical research of SM 934 is in progress.

During the latter period of the program of the relationship between chemical structure and activity of artemisinins, SM 1044 was isolated as a by-product during the preparation of SM 934, and interestingly showed excellent antileukemia activity *in vitro* and *in vivo* in the Ruijin Hospital, Shanghai Jiao Tong University School of Medicine[65–69]. These alkaline artemisinins may be a new kind of promising candidates. I sincerely hope they will be successfully developed for treatment of cancer, auto-immune or other diseases, like artemether as antimalarial drug 30 years ago.

References

1 Zhang JF. A detailed chronological record of project 523 and the discovery and development of Qinghaosu (Artemisinin). Guangzhou: Yangcheng Evening News Publisher; 2006. Chinese.

2 Li Y, Wu YL. A golden phoenix arising from the herbal net — A review and reflection on the study of antimalarial drug qinghaosu. Front Chem China 2010; 5: 357–422.

3 Liu JM, Ni MY, Fan JF, Tu YY, Wu ZH, Wu YL, *et al*. Structure and reactions of arteannuin. Acta Chim Sin 1979; 37: 129–43. Chinese.

4 Li Y, Yu PL, Chen YX, Li LQ, Gai YZ, Wang DS, *et al*. Synthesis of some derivatives of artemisinin. Ke Xue Tong Bao 1979; 24: 667–9. Chinese.

5 Li Y, Yu PL, Chen YX, Li LQ, Gai YZ, Wang DS, *et al*. Studies on analogs of artemisinin I. The synthesis of ethers, carboxylic esters and carbonates of dihydroartemisinine. Yao Xue Xue Bao 1981; 16: 429–39. Chinese.

6 Gu HM, Lu BF, Qu ZX. Antimalarial activities of 25 derivatives of artemisinine against chloroquine-resistant *Plasmodium berghei.* Acta Pharmacol Sin 1980; 1: 48–50. Chinese.

7 Liu X. Study on artemisinin derivatives. Yao Xue Tong Bao 1980; 15: 183. Chinese.

8 Meshnick SR, Tsang TW, Lin FB, Pan HZ, Chang CN, Kuypers F, *et al*. Activated oxygen mediates the antimalarial activity of qinghaosu. Prog Clin Biol Res 1989; 313: 95–104.

9 Meshnick SR, Tomas A, Ranz A, Xu CM, Pan HZ. Artemisinin (qinghaosu): the role of intracellular hemin in its mechanism of antimalarial action. Mol Biochem Parasitol 1991; 49: 181–9.

10 Posner GH, Oh CH. A regiospecifically oxygen-18 labeled 1,2,4-trioxane: a simple chemical mode system to probe the mechanism(s) for the antimalarial activity of artemisinin (qinghaosu). J Am Chem Soc 1992; 114: 8328–9.

11 Jefford CW. Why artemisinin and certain synthetic peroxides are potent antimalarials. Implications for the mode of action. Curr Med Chem 2001; 8: 1803–26.

12 Olliaro PL, Haynes RK, Meunier B, Yuthavong Y. Possible modes of action of the artemisinin-type compounds. Trends Parasitol 2001; 17: 122–6.

13 Posner GH, O'Neill PM. Knowledge of the proposed chemical mechanism of action and cytochrome P 450 metabolism of antimalarial trioxanes like artemisinin allows rational design of new antimalarial peroxides. Acc Chem Res 2004; 37: 394–404.

14 O'Neill PM, Barton VE, Ward SA. The molecular mechanism of action of artemisinin — the debate continues. Molecules 2010; 15: 1705–21.

15 Qinghaosu antimaraia coordinating research group: Antimararia studies on qinghaosu. Chin Med J 1979; 92: 811–6.

16 Antimararial efficacy and mode of action of qinghaosu and its derivatives in experimental models. China Cooperative Research Group on qinghaosu and its derivatives as antimalarials. J Tradit Chin Med 1982; 2: 17–24.

17 Jin YG, Teng XH, Sun CP. Free radicals and mechanism of toxicity of sodium artesunate. Chin J Pharmacol Toxicol 1989; 2: 60–5. Chinese.

18 Wang JY, Yuan LZ, Wang MD. Inhibition of sodium artesunate on rat erythrocyte membrane Na$^+$-K$^+$-exchanging ATPase *in vitro*. Yao Xue Xue Bao 1995; 16: 524–6. Chinese.

19 Shi XC, Zhang QL, Wu K, Wang S, Sun CP, Wang ZQ. Hemopoietotoxicity in pregnant mice and their embryos induced by free radicals derived from sodium artesunate. Chin J Pharmacol Toxicol 1997; 11: 226–8. Chinese.

20 Chen Y, Zhu SM, Chen HY, Li Y. Artesunate interaction with heme. Bioelectrochem Bioenerg 1988; 44: 295–300.

21 Cheng F, Shen JH, Luo XM, Zhu WL, Gu JD, JI RY, *et al*. Molecular docking and 3-D-QSAR studies on the possible antimalarial mechanism of artemisinin analogues. Bioorg Med Chem 2002; 10: 2883–91.

22 Wu WM, Yao ZJ, Wu YL, Jiang K, Wang YF, Chen HB, *et al*. Ferrous ion induced cleavage of the peroxy bond in qinghaosu and its derivatives and the DNA damage associated with this process. Chem Commun 1996; 18: 2213–4.

23 Wu WM, Wu YK, Wu YL, Yao ZJ, Zhou CM, Li Y, *et al*. A unified mechanism framework for the Fe(II)-induced cleavage of qinghaosu and derivatives/analogs. The first spin-trapping evidence for the earlier postulated secondary C-4 radical. J Am Chem Soc 1998; 120: 3316–25.

24 Butler AR, Gilbert BC, Hulme P, Irvine LR, Renton L, Whitwood AC. EPR evidence for the involvement of free radicals in the iron-catalysed decomposition of qinghaosu (artemisinin) and some derivatives:

Antimalarial action of some polycyclic endoperoxides. Free Rad Res 1998; 28: 471–6.

25 Zhu DY, Huang BS, Chen ZL, Yin ML, Yang YM, Dai ML, et al. Isolation and identification of the metabolite of artemisinin in human. Yao Xue Xue Bao 1983; 4: 194–7. Chinese.

26 Lee IS, Hufford CD. Metabolism of antimalarial sesquiterpene lactones. Pharmacol Ther 1990; 48: 345–55.

27 Wang DY, Wu YL, Wu YK, Liang J, Li Y. Further evidence for the participation of primary carbon-centered free-radicals in the antimalarial action of the the qinghaosu (artemisinin) series of compounds. ChemInform 2001; 32: 605–9.

28 Wang DY, Wu YK, Wu YL, Li Y, Shan F. Synthesis, iron(II)-induced cleavage and in vivo antimalarial efficacy of 10-(2-hydroxy-1-naphthyl)-dexoxqinghaosu (-deoxoartemisinin). J Chem Soc Perkin Trans 1. 1999; 1827–31.

29 Wang J, Huang L, Li J, Fan Q, Long Y, Li Y, et al. Artemisinin directly targets malaria mitochondria through its specific mitochondrial activation. PLoS One 2010; 5: e9582.

30 Wu YL, Chen HB, Jiang K, Li Y, Shan F, Wang DY, et al. Interaction of biomolecules with qinghaosu (artemisinin) and its derivatives in the presence of ferrous ion — an exploration of antimalarial mechanism. Pure Appl Chem 1999; 71: 1139–42.

31 Wang DY, Wu YL. A possible antimalarial action mode of qinghaosu (artemisinin) series compounds. Alkylation of reduced glutathione by C-centered primary radicals produced from antimalarial compound qinghaosu and 12-(2,4-dimethoxyphenyl)-12-deoxoqinghaosu. Chem Commun 2000; 22: 2193–4.

32 Wu YK, Yue ZY, Wu YL. Interaction of qinghaosu (artemisinin) with cysteine sulfhydryl mediated by traces of non-heme iron. Angew Chem Int Ed 1999; 38: 2580–2.

33 Wu WM, Chen YL, Zhai ZL, Xiao SH, Wu YL. Study on the mechanism of action of artemether against schistosomes — The identification of cysteine adducts of both carbon-centered free-radicals derived from artemether. Bioorg Med Chem Lett 2003; 13: 1645–7.

34 Chen DJ, Fu LF, Shao PP, Wu FZ, Fan CZ, Shu Y, et al. The experimental studies of artemisinin against Schistosoma japonicum in animals. Zhonghua Yi Xue Za Zhi 1980; 60: 422–5. Chinese.

35 Le WJ, Wang GF, You JQ, Xie RR, Mei JY. The experimental studies of artemisinin derivatives against Schistosoma japonicum in animals. Yao Xue Tong Bao 1980; 15: 182. Chinese.

36 Xiao SH, Tanner M, N'Goran EK, Utzinger J, Chollet J, Bergquist R, et al. Recent investigations of artemether, a novel agent for the prevention of Schistosomiasis japonica, mansoni and haematobia. Acta Trop 2002; 82: 175–81.

37 Sun WC, Han JX, Yang WY, Deng DA, Yue XF. Antitumor activities of 4 derivatives of artemisinic acid and artemisinin B, in vitro. Acta Pharmacol Sin 1992; 13: 541–3. Chinese.

38 Deng DA, Xu CH, Cai JC. Derivatives of arteannuin B with antileukemia activity. Yao Xue Xue Bao 1992; 27: 317–20. Chinese.

39 Efferth T, Dunstan H, Sauerbrey A, Miyachi H, Chitambar CR. The antimalarial artesunate is also active ahainst cancer. Int J Oncol 2001; 18: 767–73.

40 Crespo-Ortiz MP, Wei MQ. Antitumor activity of artemisinin and its derivatives: from a well-known antimalarial agent to a potential anticancer drug. J Biomed Biotech 2012; 2012: 247597.

41 Li Y, Shan F, Wu JM, Wu GS, Ding J, Xiao D, et al. Novel antitumor artemisinin derivatives targeting G_1 phase of the cell cycle. Bioorg Med Chem Lett 2001; 11: 5–8.

42 Wu JM, Shan F, Wu GS, Li Y, Ding J, Xiao D, et al. Synthesis and cytotoxicity of artemisinin derivatives containing cyanoarylmethyl group. Eur J Med Chem 2001; 36: 240–5

43 Efforth T. Willmar Schwabe Award 2006: Antiplasmodial and anti-tumor activity of artemisinin from bench to bedside. Planta Med 2007; 73: 299–309.

44 Liu Y, Lok CN, Ko BCB, Shum TYT, Wong MK, Che CM. Subcellular localization of a fluorescent artemisinin derivative to endoplasmic reticulum. Org Lett 2010; 12: 1420–3.

45 Morrissey C, Gallis B, Solazzi JW, Kim BJ, Gulati R, Vakar-Lopez F, et al. Effect of artemisinin derivatives on apoptosis and cell cycle in prostate cancer cells. Anticancer Drug 2010; 21: 423–32.

46 Lu JJ, Meng LH, Cai YJ, Chen Q, Tong LJ, Lin LP, et al. Dihydroartemisinin induces apoptosis in HL-60 leukemia cells dependent of iron and p38 mitogen-activated protein kinase activation but independent of reactive oxygen species. Cancer Biol Ther 2008; 7: 1017–23.

47 Lu JJ, Meng LH, Shankavaram UT, Zhua CH, Tong LJ, Chen G, et al. Dihydroartemisinin accelerates c-MYC oncoprotein degradation and induces apoptosis in c-MYC-overexpressing tumor cells. Biochem Pharmacol 2010; 80: 22–30.

48 Lu JJ, Chen SM, Zhang XW, Ding J, Meng LH. The anti-cancer activity of dihydroartemisinin is associated with induction of iron-dependent endoplasmic reticulum stress in colorectal carcinoma HCT116 cells. Invest New Drugs 2011; 29: 1276–83.

49 Lu JJ, Chen SM, Ding J, Meng LH. Characterization of dihydro-artemisinin-resistant colon carcinoma HCT116/R cell line. Mol Cell Biochem 2012; 360: 329–37.

50 Yu QB, Gao YX. 56 cases of lupus erythematosus treated with artesunate. Zhonghua Pi Fu Ke Za Zhi 1997, 30: 51–2. Chinese.

51 Yang ZS, Zhou WL, Sui Y, Wang JX, Wu JM, Zhou Y, et al. Synthesis and immunosuppressive activity of new artemisinin derivatives. Part I. [12 (β or α)-Dihydroartemisininoxy] phen(ox)yl aliphatic acids/esters. J Med Chem 2005; 48: 4608–17.

52 Yang ZS, Wang JX, Zhou Y, Zuo JP, Li Y. Synthesis and immuno-suppressive activity of new artemisinin derivatives. Part 2: 2-[12(β or α)-Dihydro-artemisininoxymethyl- (or 1′-ethyl) phenoxyl propionic acids and esters. Bioorg Med Chem 2006; 14: 8043–9.

53 Zhang JX, Wang JX, Zhang Y, Zuo JP, Wu JM, Sui Y, et al. Synthesis and immunosuppressive activity of new artemisinin derivatives containing polyethylene glycol group. Yao Xue Xue Bao 2006; 41: 65–70. Chinese.

54 Li Y, Zhu YM, Jiang HJ, Pan JP, Wu GS, Wu JM, et al. Synthesis and antimalarial activity of artemisinin derivatives containing an amino group. J Med Chem 2000; 43: 1635–40.

55 Zhou WL, Wu JM, Wu QL, Wang JX, Zhou Y, Zhou R, et al. A novel artemisinin derivative, 3-(12-beta-artemisininoxy) phenoxyl succinic acid (SM735), mediates immunosuppressive effects in vitro and in vivo. Acta Pharmacol Sin 2005; 26: 1352–8.

56 Wang JX, Tang W, Shi LP, Wan J, Zhou R, Ni J, et al. Investigation of the immunosuppressive activity of artemether on T cell activation and proliferation. Br J Pharmacol 2007; 150: 652–61.

57 Wang Z, Qiu J, Guo TB, Liu A, Wang Y, Li Y, et al. Anti-inflammatory properties and regulatory mechanism of a novel derivative of artemisinin in experimental autoimmune encephalomyelitis. J Immunol 2007; 179: 5958–65.

58 Wang JX, Tang W, Shi LP, Wan J, Zhou R, Ni J, et al. Investigation of the immunosuppressive activity of artemether on T-cell activation and proliferation. Br J Pharmacol 2007; 150: 652–61.

59 Wang JX, Tang W, Yang ZS, Wan J, Shi LP, Zhang Y, et al. Suppressive effect of a novel water-soluble artemisinin derivative SM 905 on T cell activation and proliferation in vitro and in vivo. Eur J Pharmacol 2007; 564: 211–8.

60 Wang JX, Tang W, Zhou R, Wan J, Shi LP, Zhang Y, et al. The new water-soluble artemisinin derivative SM 905 ameliorates collagen-

induced arthritis by suppression of inflammatory and Th17 responses. Br J Pharmacol 2008, 153: 1303–10.

61 Wang JX, Hou LF, Yang Y, Tang W, Li Y, Zuo JP. SM 905, a novel artemisinin derivative, inhibition of NO and pro-inflammatory cytokine production by suppressing MAPK and NF-kappa B pathways in RAW 264.7 macrophages. Acta Pharmacol Sin 2009; 30: 1428–35.

62 Hou LF, He SJ, Wang JX, Yang Y, Zhu FH, Zhou Y, et al. SM 934, a water-soluble derivative of artemisinin, exerts immunosuppressive functions in vitro and in vivo. Int Immunopharmacol 2009; 9: 1509–17.

63 Hou LF, He SJ, Li X, Yang Y, He PL, Zhou Y, et al. Oral administration of artemisinin analog SM934 ameliorates lupus syndromes in MRL/lpr mice by inhibiting Th1 and Th17 cell responses. Arthritis Rheum 2011; 63: 2445–55.

64 Hou LF, He SJ, Li X, Wan CP, Yang Y, Zhang XH, et al. SM934 treated lupus-prone NZB×NZW F1 mice by enhancing macrophage interleukin-10 production and suppressing pathogenic T cell development. PLoS One 2012; 7: e32424.

65 Li Y, Zhu Y, Zhang Y, Zhou JY, Cai L, Xie SW, inventors; Qinghaosu dimer containing nitrogen atom(s), its preparation and use. Shanghai Institute of Materia Medica, Chinese Academy of Sciences and Shanghai Institute of Planned Parenthood Research. Chinese Patent 201110034154.9, 2011 Jan 31.

66 Mi JQ, Li Y, Liu JJ, Zhang Y, Cai X, Wang ZY, inventors; Use of a qinghaosu dimer. Ruijin Hospital, Shanghai Jiao Tong University School of Medicine and Shanghai Institute of Materia Medica, Chinese Academy of Sciences. Chinese Patent 201110034201.X, 2011 Jan 31.

67 Mi JQ, Li Y, Ni RM, Zhang Y, Wang J, Cai X, Wang ZY, inventors; Qinghaosu derivative and its salt, a new type of agent for treatment of acute leukemia. Ruijin Hospital, Shanghai Jiao Tong University School of Medicine and Shanghai Institute of Materia Medica, Chinese Academy of Sciences. Chinese Patent 201210011774.5, 2012 Jan 16.

68 Mi JQ, Li Y, Ni RM, Zhang Y, Wang J, Cai X, Wang ZY, inventors; Qinghaosu derivative and its salt, a new type of agent for treatment of leukemia. Ruijin Hospital, Shanghai Jiao Tong University School of Medicine and Shanghai Institute of Materia Medica, Chinese Academy of Sciences. Chinese Patent 201210012386.9, 2012 Jan 16.

69 Mi JQ, Li Y, Peng Y, Zhang Y, Wang J, Cai X, Wang ZY, inventors; Qinghaosu derivative and its salt, a new type of agent for treatment of acute myelocytie leukemia. Ruijin Hospital, Shanghai Jiao Tong University School of Medicine and Shanghai Institute of Materia Medica, Chinese Academy of Sciences. Chinese Patent 201210012204.8, 2012 Jan 16.

npg

Review

Discovery of structurally diverse and bioactive compounds from plant resources in China

Sheng-ping YANG, Jian-min YUE*

State Key Laboratory of Drug Research, Shanghai Institute of Materia Medica, Chinese Academy of Sciences, Shanghai 201203, China

This review describes the major discoveries of structurally diverse and/or biologically significant compounds from plant resources in China, mainly from the traditional Chinese medicines (TCMs) since the establishment of our research group in 1999. In the past decade, a large array of biologically significant and novel structures has been identified from plant resources (or TCM) in our laboratory. The structural modification of several biologically important compounds led to more than 400 derivatives, some of which exhibited significantly improved activities and provided opportunities to elucidate the structure-activity relationship of the related compound class. These findings are important for drug discovery and help us understand the biological basis for the traditional applications of these plants in TCM.

Keywords: natural products; plant resources; traditional Chinese medicine; bioactive compounds; structural modification; structure-activity relationship

Introduction

Natural products have long been used by humans, especially in the healthcare industry, providing us products from food supplements to chemical therapeutics to biological probes and beyond. Natural products from both plants and microbes have had great success in past drug discovery programs[1, 2]. Structural novelty and biological significance are the two major innovative elements of natural products chemistry and are also key issues for drug development. The identification of natural compounds with novel structures and important biological activities, especially those possessing new carbon skeletons, has been the main challenge in the fields of natural products, organic synthesis and pharmacology. Traditional Chinese medicines (TCM) medications are proven reservoirs of novel lead structures, including the well-known examples of artemisinin (an antimalarial)[3] and huperzine A (for AD treatment)[4, 5]. China has rich medicinal plant resources, and approximately 11 000 species have been documented, only approximately 30% of which have been chemically studied. We therefore view TCM plants as a promising resource for lead structures that deserve further investigation. In depth chemical and pharmacological studies of TCM plants will also provide starting points for TCM development and standardization.

In the past decade, chemical studies conducted in our research group have led to the isolation more than 2700 structurally diverse compounds from 125 plants (most with applications in TCM or folk medicine), of which 650 compounds were new structures, and 63 compounds featured unprecedented carbon skeletons or possessed unique structural motifs. The biosynthetic origins of most of these compounds with new carbon skeletons or unique structural motifs were proposed. Biological tests on these isolates via collaboration with the pharmacological research groups both in our institute and in outside organizations revealed that 182 compounds were active in the tested assays, and a number of them showed significant bioactivities associated with fatal human diseases. The structural modification of a few of the most promising bioactive compounds or drug leads produced more than 400 derivatives, 58 of which showed obviously improved activity. These studies also demonstrated the structure-activity relationship of the related compound classes. The major research findings are summarized here.

Structurally diverse and novel alkaloids

Daphniphyllum alkaloids (Figure 1): The genus *Daphniphyllum* is mainly distributed in the southern Asia, with 10 species growing in China. Some of these species have long been used

* To whom correspondence should be addressed.
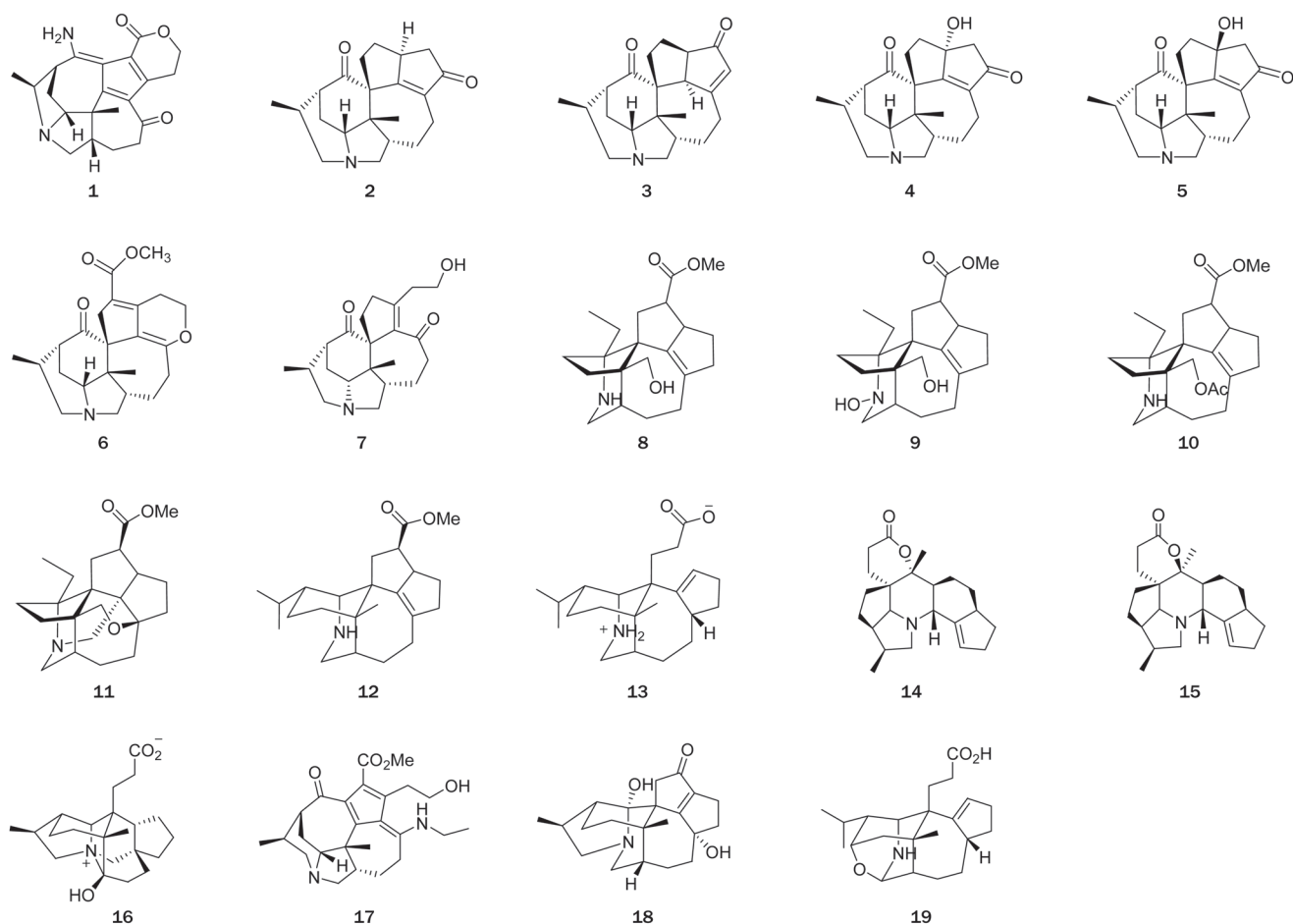E-mail jmyue@mail.shcnc.ac.cn

Figure 1. Alkaloids isolated from *Daphniphyllum* genus.

in TCM for the treatment of various disorders. *Daphniphyllum* alkaloids possessing highly complex and polycyclic features have been a challenging topic in natural products and organic synthesis. Since we published the first chemical studies on *D subverticillatum* in 2003, a total of 194 structurally complex alkaloids have been isolated from 9 species of *Daphniphyllum* in our research group, 72 of which were novel structures. Among the novel compounds, 14 of them had new skeletons or possessed rearranged carbon frameworks[6–21]. Some alkaloids showed strong cytotoxic activity[16].

Daphnipaxinin (**1**)[8], the first diamino *Daphniphyllum* alkaloid, was isolated from *D paxianum*. The structure of **1** was determined by spectroscopic methods, and its absolute configuration was assigned by CD spectrum. A series of structurally related *Daphniphyllum* alkaloids with an unusual degraded skeleton of C-22-noryuzurimine-type (**2–5**)[15, 16] were identified from *D longeracemosum* and *D yunnanense*. Compound **4** showed strong cytotoxic activities, with IC$_{50}$ values of 3.0 and 0.6 µmol/L against the tumor cell lines P388 and A549, respectively[16]. The discovery of daphnilongeranin A (**6**)[15], the first *seco*-10,17-longistylumphlline alkaloid from *D longeracemosum*, suggested that the hypothetical biosynthetic route proposed for daphnicyclidine A should be reconsidered. The

chemical investigation of *D yunnanense* also afforded the first C22-*nor*,10,17-*seco*-yuzurimine-type alkaloid, daphniyunnine B (**7**)[16], which represents the most degraded compound in the *Daphniphyllum* alkaloid class.

A series of *Daphniphyllum* alkaloids possessing cage-like skeletons were isolated from the seeds of *D paxianum*[11] and *D macropodum*[18]. Compounds **8–11** are the representatives of these cage-like *Daphniphyllum* alkaloids; in particular, paxdaphnine A (**11**) is the first identified 1,19-bisnor-*Daphniphyllum* alkaloid with a highly caged skeleton and a constrained Ring-A by the formation of C2–C8 and C1–C9 bonds, whose absolute configuration was determined by X-ray diffraction of its iodide derivative. Two structurally relevant alkaloids, paxdaphnidine A (**12**), bearing a unique pentacyclic framework, and paxdaphnidine B (**13**), possessing an uncommon tetracyclic skeleton, were isolated from the twigs and leaves of *D paxianum*[9]. Deoxycalyciphylline B (**14**) and deoxyisocalyciphylline B (**15**) were the major alkaloids with a unique fused hexacyclic skeleton from the stem of *D subverticillatum*[8]. Their structures were assigned based on spectroscopic methods and chemical evidence, and that of **14** was confirmed by a single crystal X-ray diffraction determination.

Recently, angustimine (**16**), featuring an unprecedented

skeleton, and angustifolimine (**17**), a rare diamino *Daphniphyllum* alkaloid, were isolated from *D angustifolium*[6]. Calycinumines A (**18**) and B (**19**) were isolated from *D calycinum*[7]. Compound **18** is the first example of C-22-nor yuzurimine-type alkaloid, whose structure was confirmed by a single crystal X-ray diffraction study, and calycinumine B (**19**) features an unprecedented heteroatom-containing adamantane-like motif.

C,C-linked dimeric indolizidine alkaloids (Figure 2): *Flueggea virosa* Roxb ex Willd (Euphorbiaceae) is a TCM that has been used to treat rheumatism, pruritus, cephalic eczema, leucorrhea, and injuries. Previous chemical studies on this plant identified a number of indolizidine-type alkaloids known as *Securinega* alkaloids. In our recent study of this plant, two unprecedented C,C-linked dimeric indolizidine alkaloids, flueggenines A (**20**) and B (**21**), along with their precursor (–)-norsecurinine, were isolated from the roots of *F virosa*[22]. Their structures and absolute configurations were elucidated by extensive spectroscopic analyses. The biogenetic origin of these two compounds could be traced back to the coexisting major alkaloid (–)-norsecurinine via a self-catalyzed Baylis-Hillman reaction as the key step to achieve the dimerization.

Other structural classes of alkaloids (Figure 2): Alkaloids are a class of structurally interesting and biologically important natural products. In the past years, we examined the chemical components of eight other plant species in the families Loganiaceae, Apocynaceae, and Lycopodiaceae, and a total of 142 structurally diversified alkaloids were isolated from the genera *Gelsemium*[23, 24], *Ervatamia*[25, 26], *Stephania*[27, 28], *Winchia*[29], and *Lycopodium*[30], of which 42 were new compounds and 5 had novel skeletons. Some alkaloids showed strong cytotoxic activities. For example, gelseganines A–D (**22–25**), a new class of monoterpenoid indole alkaloids that bear an N_4-iridoid unit, together with three new analogs (**26–29**)[23, 24] were isolated from the stems and leaves of *Gelsemium elegans*, a well-known toxic plant in Southeast Asia. The structures of **22–29** were determined by spectroscopic analysis, single-crystal X-ray diffraction, and chemical evidence. A plausible biogenetic pathway for alkaloids **22–25** was also postulated.

Complex and novel terpenoids

Triterpenoids (limonoids) from Meliaceae plants (Figure 3): China has a rich diversity of Meliaceae. To date, 62 species and 12 varieties of 15 genera in the Meliaceae family have been documented, and these are mainly distributed in the provinces south of the Yangtze River. Plants of this family are known to metabolize abundant nortriterpenoids (limonoids) with diverse and complex structures that have been demonstrated to have a variety of important biological activities, such as antifeeding, antibacterial, anticancer and antimalarial activities.

In the past several years, our research group made tremendous efforts to explore biologically significant chemical components from the plants in the Meliaceae family, which has led to the isolation of more than 600 structurally diverse compounds from 30 plant species. Among these, 406 were new structures, and 32 possessed previously unknown skeletons.
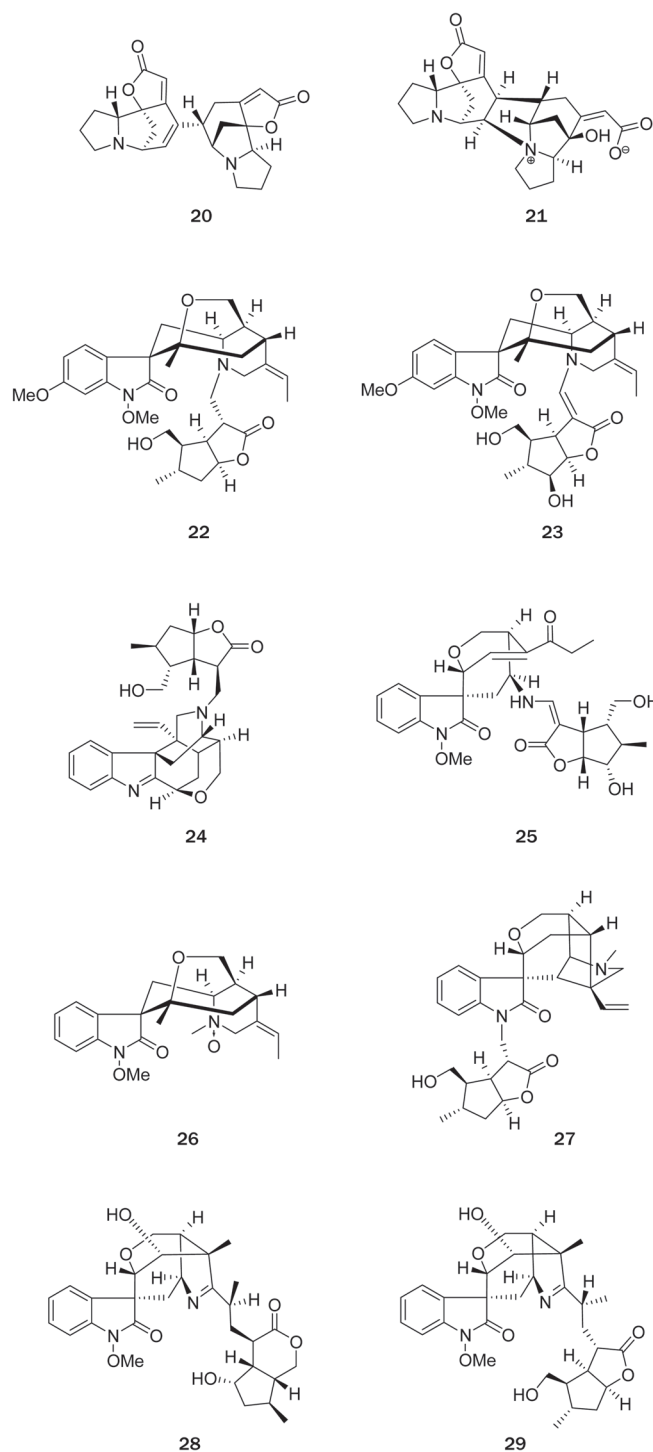

Figure 2. Dimeric indolizidine alkaloids and monoterpenoid indole alkaloids.

A variety of assays revealed that 50 additional compounds had important biological activities[31–71]. Our research results supported the traditional medical applications of several plants in the Meliaceae family. This is by far the most systematic and leading chemical study on the plants of the Meliaceae family worldwide. Several representative examples are summarized
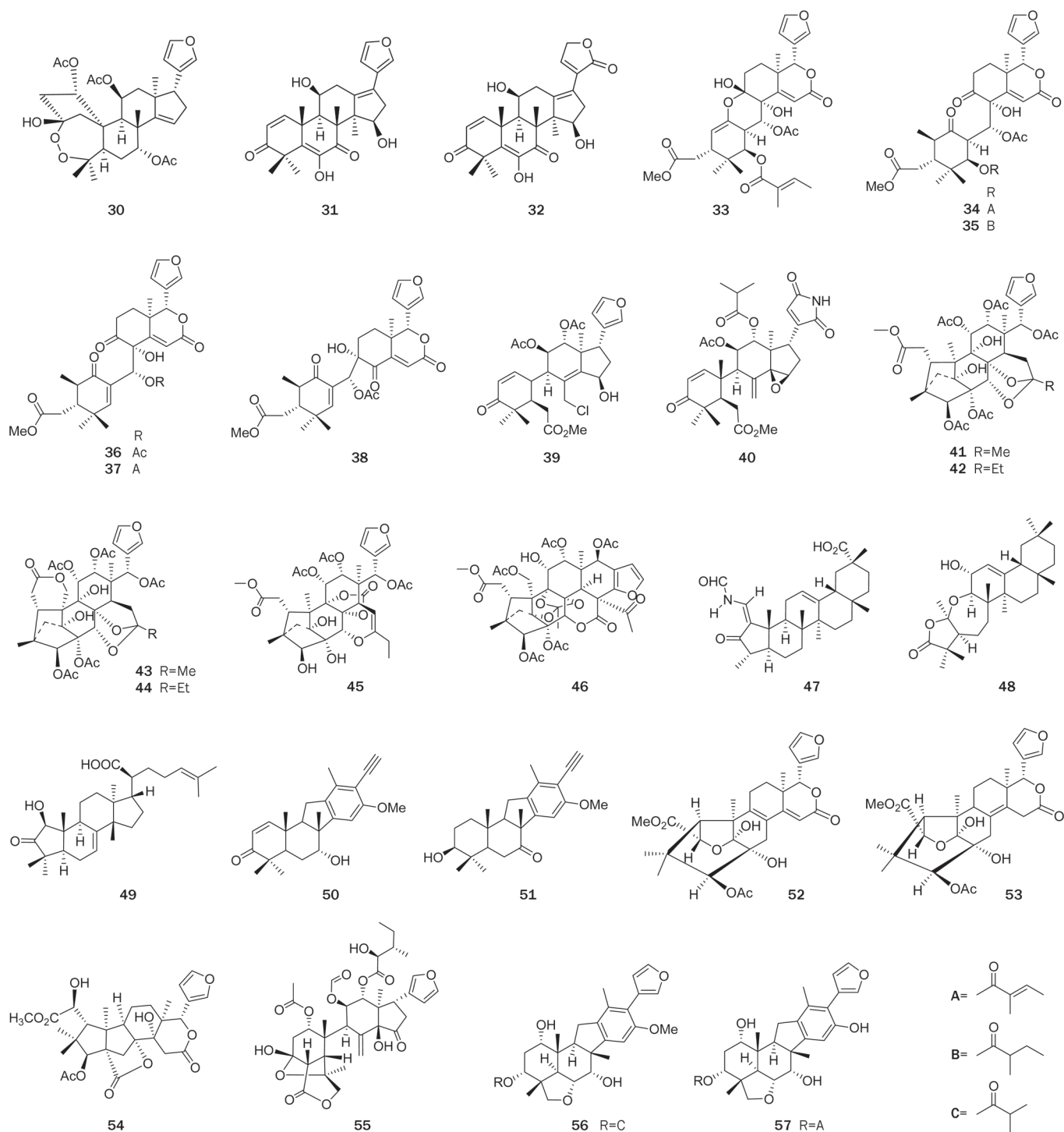
Figure 3. Triterpenoids (limonoids) isolated from Meliaceae plants.

below.

Walsuronoid A (30)[39], a limonoid featuring an unprecedented 3,4-peroxide-bridged A-*seco* skeleton, together with walsuronoids B (31) and C (32), possessing a rare 18(13→14)-abeo-limonoid skeleton, was isolated from *Walsura robusta*. Their structures were elucidated by spectroscopic analysis and chemical correlation, and that of 30 was con-

firmed by single-crystal X-ray diffraction. Compounds 31 and 32 showed antimalarial activities, which well matched the traditional application of this plant as a treatment for malaria.

Compounds 33–38 are 9,10-seco-tetranortriterpenoids that were discovered in the seeds of the Chinese marine mangrove plant *Xylocarpus granatum*[42, 63]. Xylogranatin A (33) featured a unique 1,9-oxygen bridge, whose structure was confirmed by
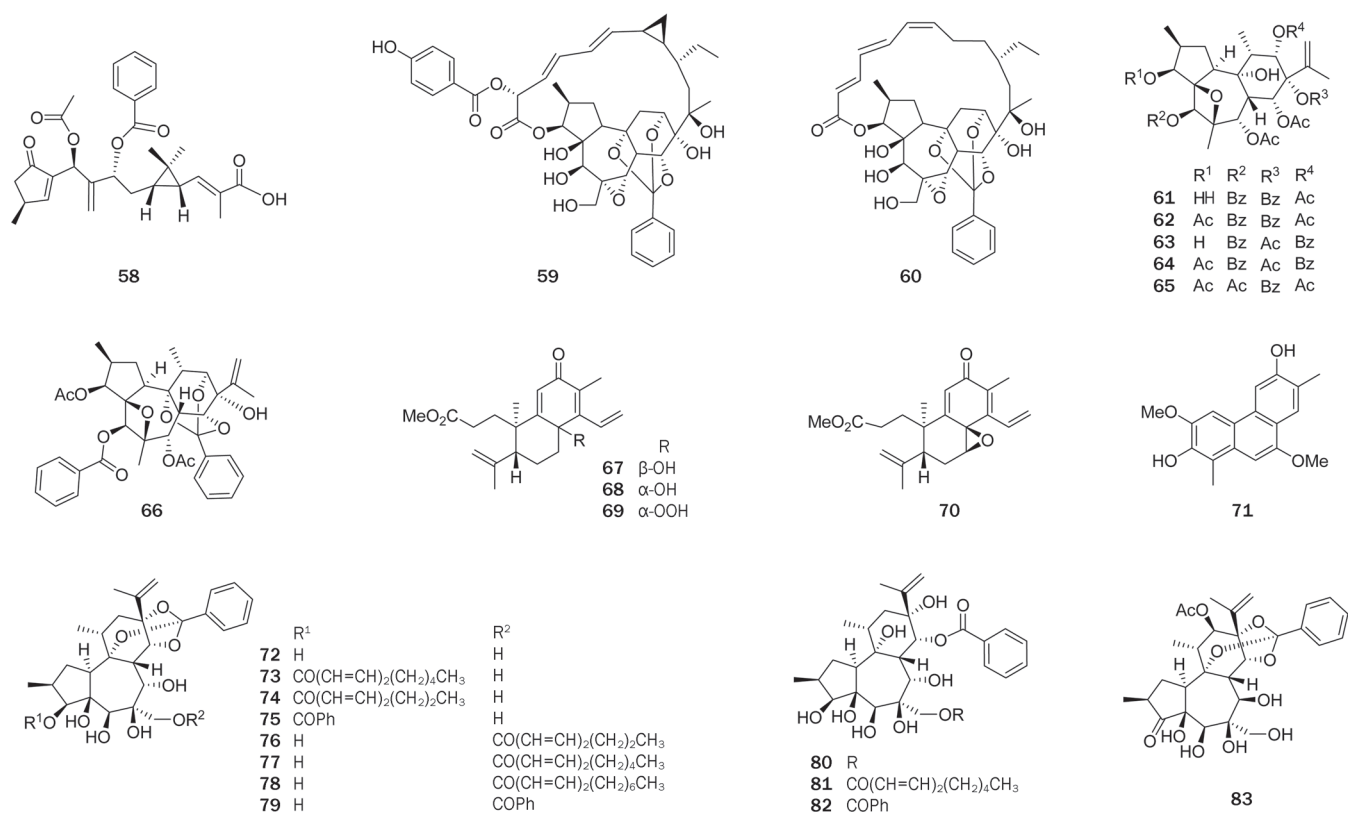
Figure 4. Structurally interesting and biologically important diterpenoids.

single-crystal X-ray diffraction, and xylogranatin D (**38**) furnished a novel skeleton via C-30–C-9 linkage that was postulated to arise from **36** via an γ-hydroxyl ketone rearrangement, and this pathway was chemically mimicked. Compounds **33–38** were cytotoxic to the tumor cell lines P388 and A549, with IC$_{50}$ values ranging from 6.3 to 15.7 μmol/L.

Turrapubesins A (**39**) and B (**40**)[41], two tetranortriterpenoids representing the first examples of halogenated and maleimide-bearing limonoids, respectively, were isolated from the twigs and leaves of *Turraea pubescens*. Their absolute configurations were determined by X-ray crystallography (**39**) and by CD analysis of a dihydrogenated derivative (**40**).

Four 16-norphragmalin-type limonoids, chuktabularins A-D (**41–44**)[40], featuring unprecedented carbon skeletons of a biosynthetically extended C2 or C3 unit at C-15 forming a unique 2,7-dioxabicyclo[2.2.1]heptane moiety, and two limonoids, chuktabrin A (**45**), with the unique 1,3-dioxolan-2-one and 3,4-dihydro-2*H*-pyran motifs, and chuktabrin B (**46**)[37] possessing an unprecedented polycyclic skeleton, were isolated from *Chukrasia tabularis*. Their structures were elucidated by spectroscopic analyses and single crystal X-ray diffraction.

The chemical investigations of *Dysoxylum hainanense* revealed a series of ring A modified triterpenoids among which dysoxyhainanin A (**47**)[38] possessed a unique 1,3-cyclo-2,3-*seco* A ring with a formamido-containing appendage, dysoxyhainanin B (**48**)[38] featured an unprecedented 1,2-dinor-3,10:9,10-*bisseco* skeleton, and dysoxyhainic acid A (**49**)[52] had

an unprecedented 2-nor-1,3-cyclotirucallane skeleton. Four compounds, dysoxyhainanin A (**47**) and dysoxyhainic acids B–C, showed significant activities against four gram-positive bacteria, *Staphylococcus aureus* ATCC 25923, *S epidermidis* ATCC 12228, *Micrococcus luteus* ATCC 9341, and *Bacillus subtilis* CMCC 63501, with MICs in the range of 6.25–50 μg/mL.

Walsucochins A (**50**) and B (**51**), with a novel carbon skeleton, were isolated from *Walsura cochinchinensis*[36]. Their structures, including absolute configuration, were elucidated by spectral methods. Both compounds significantly attenuated H$_2$O$_2$-induced damage in PC12 cells in a dose-dependent manner at dosages of 1, 5, and 10 μmol/L.

A chemical study of the stems of *Khaya senegalensis* led to the isolation of two limonoids, namely khayalenoids A (**52**) and B (**53**)[35], with an unprecedented 8-oxa-tricyclo[4.3.2.0²,⁷]unde-cane motif in the nortriterpenoid core. Their structures, with absolute configuration, were determined by spectroscopy, X-ray crystallography, and CD analysis. Recently, another limonoid with an unprecedented carbon skeleton, grandifotane A (**54**), was isolated from the stem bark of *K grandifoliola*[34]. The absolute configuration of **54** was determined by spectroscopy, X-ray crystallography, and ECD calculations. A biogenetic route for grandifotane A (**54**) synthesis from a mexicanolide-type limonoid precursor, involving an enzymatic Baeyer-Villiger oxidation as the key step, was proposed.

Aphanamolide A (**55**)[33], featuring an unprecedented carbon skeleton with a C-3–C-6 bond, was isolated from the seeds of

Aphanamixis polystachya. Its structure was established using spectroscopic methods.

Walsucochinoids A (**56**) and B (**57**)[32], two rearranged limonoids possessing an unprecedented carbon framework, were isolated from *Walsura cochinchinensis*. Their absolute configurations were assigned based on a detailed examination of spectroscopic data, single crystal X-ray diffraction analysis, and CD experiments.

Diterpenoids (Figure 4): Diterpenoids are a class of structurally interesting and biologically important natural products that are found in many TCM plants, and some were even proven to be the active ingredients in their respective plants. More than 260 diterpenoids were obtained by our research group in the past years from the *Euphorbia*[72], *Trigonostemon*[73–79], *Daphne*[80], *Pseudolarix*[81, 82], *Siegesbeckia*[83], *Sapium*[84], and *Larix*[85] genera. Among them, 122 were new compounds, and 4 possessed novel carbon scaffolds. Biological tests demonstrated that 49 compounds exhibited important biological activities in a variety of bioassays, some of which demonstrated the biological basis of the traditional applications of those plants in TCM medication.

Diterpenoids from the Euphorbiaceae family: Lathyranoic acid A (**58**)[72], the first *seco*-lathyrane diterpenoid with a new skeleton was isolated from the seeds of *Euphorbia lathyris*. Its structure was elucidated by spectroscopic analysis and chemical transformation. Lathyranoic acid A was proposed to be biosynthetically produced from the co-existing diterpenoid *Euphorbia* factor L11 with an enzymatic Baeyer-Villiger oxidation as the key and the committed step, and its chemical synthesis was achieved (Scheme 1).
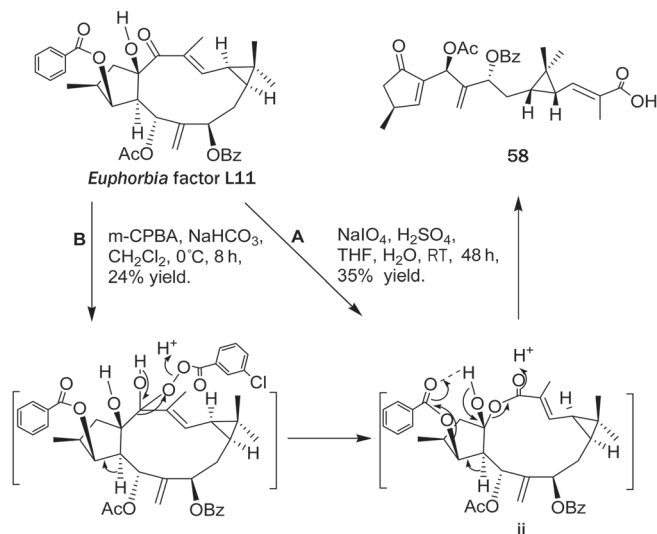
Scheme 1. Chemical transformations from *Euphorbia* factor **L11** to **58**.

Two highly modified daphnane-type diterpenoids, trigochilides A (**59**) and B (**60**), together with six highly oxygenated diterpenes, trigochinins A-I (**61–66**)[73–75], were isolated

from the twigs and leaves of *Trigonostemon chinensis* Merr collected from Yunnan Province. Trigochilides A (**59**) and B (**60**) contain 12-carbon-containing polyketide appendages, which are linked to the diterpenoid core at C-16 by a C-bond and form a macrolactone between C-1′ and C-3, while trigochinins A–I (**61–66**) share a rare 4,6-oxetane moiety. Their structures were elucidated by spectroscopic analysis, X-ray crystallography, and CD analysis. Compounds **64** and **65** showed potent cytotoxic activities against HL-60 tumor cell lines with IC$_{50}$ values of 8.1 and 6.4 µmol/L, respectively. Compound **66** significantly inhibited MET tyrosine kinase activity (IC$_{50}$=1.95 µmol/L). Trigonochinenes A–E (**66–71**)[79], five antibacterial diterpenoids, were isolated from the aerial parts of this plant collected from Hainan Province. Compounds **67–70** possess a rare 3,4-*seco*cleistanthanic skeleton, and compound **71** is a highly aromatized tetranorditerpene. Compounds **67–71** were tested for antimicrobial activity against 11 microorganisms *in vitro*. All compounds tested were active against *Helicobacter pylori*-SS1, with MICs of 12.5–25 µg/mL, and compounds **67–70** also significantly inhibited the growth of the drug (metronidazole)-resistant strain *H pylori*-ATCC 43504, with MICs of *ca* 50 µg/mL. Compounds **69** and **71** also exhibited selective activities against the gram-positive bacteria *Staphylococcus aureus* ATCC 25923, *Staphylococcus epidermidis* ATCC 12228, and *Micrococcus luteus* ATCC 9341 with MICs in the range of 6.25–50 µg/mL.

Twelve new highly oxygenated daphnane-type diterpenoids, genkwanines A–L (**72–83**)[80], were isolated from the bud of *Daphne genkwa*, a well-known TCM. These compounds showed very potent cytotoxic activities against two tumor cell lines, P388 and A549, with IC$_{50}$ levels of 0.15–8.40 µmol/L. Most interestingly, three of the compounds, **75**, **78**, and **81,** and two known compounds, yuanhuacine and yuanhuadine, strongly inhibited the endothelial cell line HMEC at the IC$_{50}$ levels of 2.90–15.0 µmol/L.

Sesquiterpenoids: Sesquiterpenoids are the major components of many TCM plants, and they have a broad spectrum of biological activities including antiinflammatory, antiparasitic, antitumor, and anti-HIV properties. More than 18 TCM plants in the families of Chloranthaceae (four genera, *Chloranthus*, *Sarcandra*, and *Hedyosmum*)[86–95] and Compositae (five genera, *Eupatorium*[96, 97], *Vernonia*[98], *Siegesbeckia*, *Saussurea*, and *Parasenecio*)[96–101], and a fungus (*Lactarius piperatus*)[102], have been investigated in our laboratory, which led to the identification more than 280 compounds. Among them, 126 were new compounds, and 8 possessed new carbon skeletons. Biological activity screening revealed that 28 isolates showed important biological activities in a number of tested bioassays, and some of the results were consistent with the traditional applications of these plants in TCM.

Mono- and dimeric sesquiterpenoids (Figure 5): The Chloranthaceae family has 16 species and 5 variants belonging to three genera, *Chloranthus*, *Sarcandra* and *Hedyosmum*, in China. Most plants in this family have been applied in TCM and/or Chinese folk medicine for a variety of indications. Chemical studies of seven species in the Chloranthaceae family con-
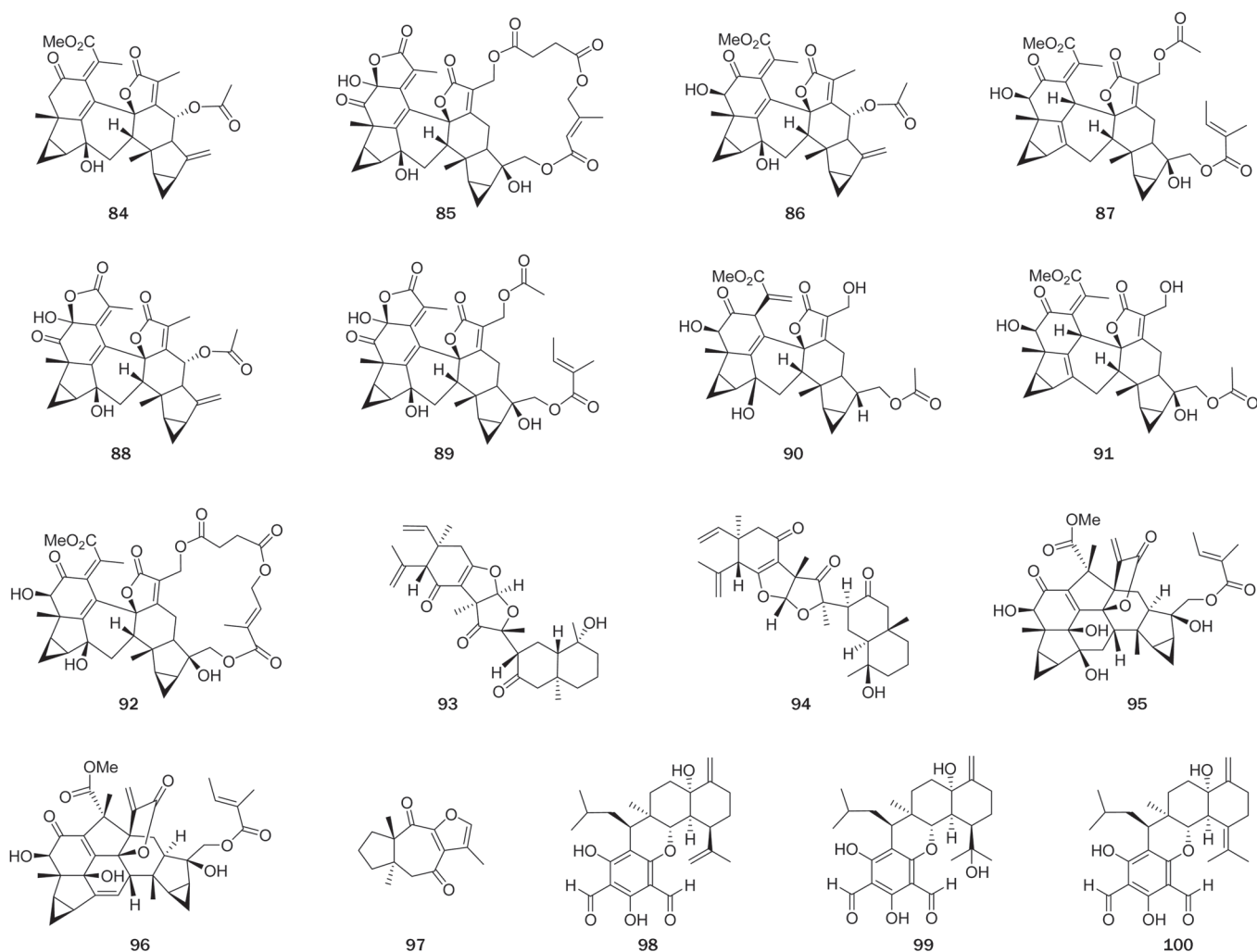
Figure 5. Structurally complex sesquiterpenoids.

ducted in our research group identified 42 new mono- and dimeric sesquiterpenoids, of which the sesquiterpenoid dimers are particularly interesting, especially 4 of these dimers, which possessed unprecedented carbon skeletons.

Chlorahololides A–F (**84–89**)[87, 88], six highly complex sesquiterpenoid dimers, were isolated from whole *C holostegius*. Their structures and absolute configurations were established by spectroscopy, X-ray crystallography and CD analysis. Chlorahololides A–F (**84–89**) exhibited potent and selective inhibition of the delayed rectifier (I_K) K$^+$ current, with IC$_{50}$ values of 10.9±12.3, 18.6±2.5, 3.6±10.1, 2.7±0.3, 27.5±5.1, and 57.5±6.1 μmol/L, respectively. It is noteworthy that the activities of chlorahololides A–F (**84–89**) are 18- to 388-fold more potent than the positive control tetraethylammonium chloride (IC$_{50}$=1.05±0.21 mmol/L), a classical blocker of the delayed rectifier K$^+$ current. Three more sesquiterpenoid dimers, multistalides A–B and chloramultilide A (**90–92**), were isolated from whole *C multistachys*[90, 91]. Serratustones A (**93**) and B (**94**), which share an unprecedented carbon skeleton representing a novel dimerization of an elemane and a eudesmane

sesquiterpenoid, were isolated from *C serratus*[86]. Two novel lindenane-type sesquiterpenoid dimers, sarcanolides A (**95**) and B (**96**), featuring an unprecedented carbon framework via the formation of C-11–C-7' bond, were isolated from whole *S hainanensis*[92]. The structures of compounds **93–96,** including the absolute configuration were fully determined by spectroscopy, X-ray crystallography, and CD analysis in combination with ECD calculation. A number of novel sesquiterpenoids were also isolated from plants in the Chloranthaceae family; *eg,* hlorantene A (**97**) isolated from *C serratus* possessed a unique C-4 to C-10 linkage[89].

Phloroglucinol-coupled sesquiterpenoids (Figure 5): *Eucalyptus globulus* Labill, a tall timber tree, grows widely in the southern part of China. Its fruits and leaves have been used as a Chinese folk medicine to treat flu, dysentery, eczema, and scald. A large number of phloroglucinol-coupled sesquiterpenoids and other classes of phloroglucinol-coupled compounds were isolated from *E globulus* and other species in the *Eucalyptus* genus. Of these, eucalyptals A–C (**98–100**)[94], with a novel 3,5-diformyl-isopentyl phloroglucinol-coupled cadinane

carbon framework, were isolated from the fruits of *E globulus*. Their structures were elucidated by spectroscopic analysis, and that of **98** was confirmed by single-crystal X-ray diffraction. Compounds **98–100** showed selective activity against HL-60, with IC$_{50}$ values of 1.7, 6.8, and 17 µmol/L, respectively.

Miscellaneous

In addition to our particular interests in natural alkaloids and terpenoids (tri, di, and sesquiterpenoids), we isolated more than 300 phenolics and prenylated polyketides from approximately 20 TCM or herb plants. Among them, approximately 60 were new compounds, and 6 had new carbon skeletons (Figure 6). In particular, 48 of these compounds showed significant biological activities in a variety of bioassays and provided a scientific foundation for the use of a number of traditional Chinese herbs[103–114].

A series of phenolic compounds were isolated from the ethanolic extract of whole *Sarcostemma acidum*. Sacidumlignan D (**101**)[108] was found to have an unprecedented rearranged tetrahydrofuran lignan skeleton. Psoracorylifols A–E (**102–106**)[105] represented five novel compounds from buguzhi, a well-known TCM made from the seeds of *Psoralea corylifolia*. The structure of **102** was confirmed by single-crystal X-ray diffraction. Psoracorylifols D and E (**105** and **106**) exhibit an unprecedented carbon skeleton. A plausible biogenetic origin of psoracorylifols A–E (**102–106**) was also postulated. Psoracorylifols A–E (**102–106**) showed significant inhibition against two strains of *H pylori* (SS1 and ATCC 43504), with

MICs of 12.5–25 µg/mL, respectively. Notably, the activity of psoracorylifols A–E (**102–106**) are 5–10 times stronger than that of metronidazole against *H pylori* ATCC 43504, a drug (metronidazole)-resistant strain; metronidazole is a critical ingredient in combination therapies of *H pylori* infection. The chemical investigation of the seeds of *Psoralea corylifolia* also revealed a number of prenylflavonoids, among which the two new compounds, corylifols A and B (**107** and **108**)[107], significantly inhibited two hospital pathogenic gram-positive bacteria, *S aureus* ATCC 25923 (MICs: 0.147 and 0.037 mmol/L) and *S epidermidis* ATCC 12228 (MICs: 0.147 and 0.037 mmol/L) *in vitro*. Cinnacassides A–E (**109–113**)[103] are five novel glycosides with a unique geranylphenylacetate aglycone carbon skeleton from a common TCM (Rougui) based on the stem bark of *Cinnamomum cassia*. Each of the cinnacassides A–D (**109–113**) possessed one of the four stereoisomers of the aglycone. Their structures were established by extensive spectroscopic analysis and chemical and chiroptical methods. Plausible biosynthetic routes for **109–113** were also proposed.

Harrisotones A–E (**114–118**), five novel prenylated polyketides with a rare spirocyclic hydroperoxypolyketide-derived skeleton, along with the new hydroperoxypolyketide harrisonol A (**119**), were isolated from *Harrisonia perforate*[104]. Their structures were extensively elucidated through spectroscopic analysis and CD spectra. The origins of compounds **114–118** could be traced back to harrisonol A (**119**). Harrisotone A and C and harrisonol A (**114**, **116**, and **119**) exhibited significant cytotoxic activity against P388 tumor cells, with IC$_{50}$ values of 1.56, 2.35, and 0.27 µmol/L, respectively. Har-
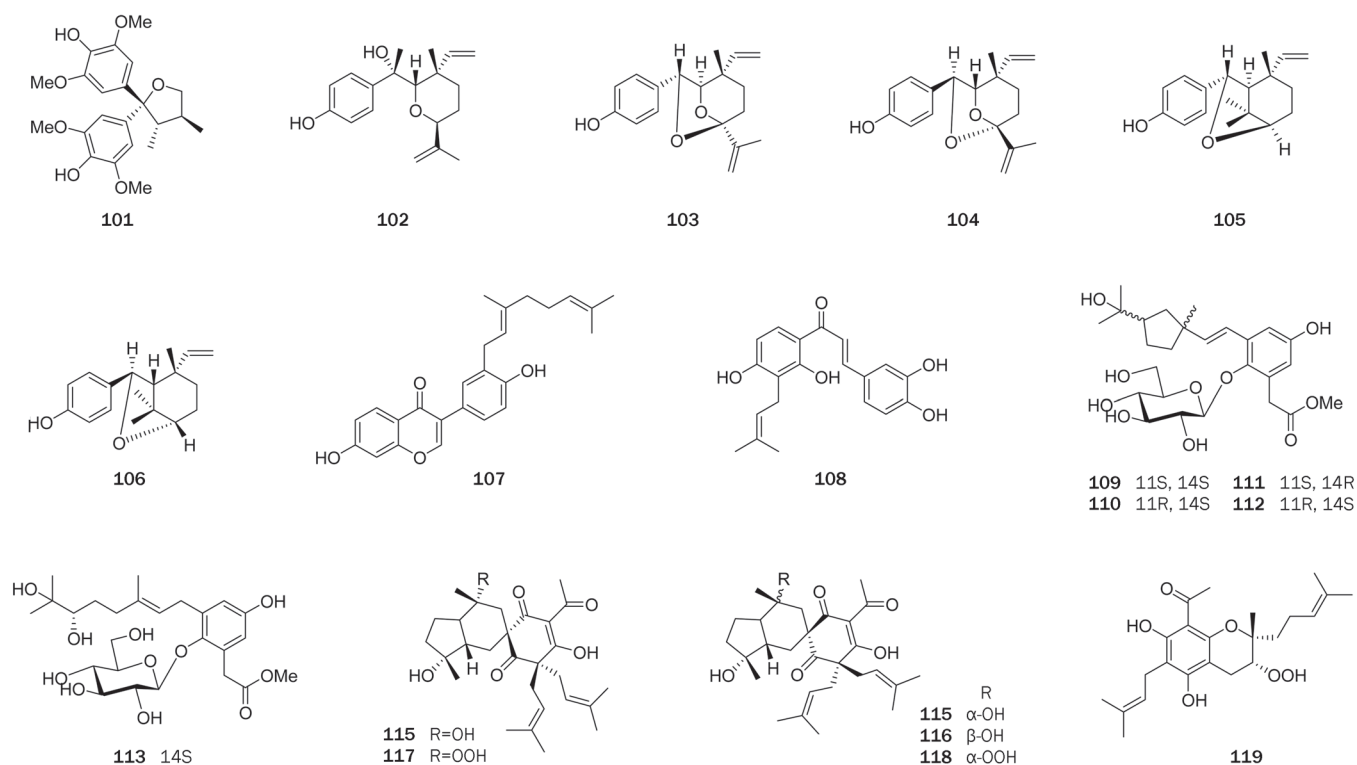

Figure 6. Phenolics and prenylated polyketides.

risotone A (**114**) and harrisonol A (**119**) also showed moderate activity against A549 tumor cells, with IC_{50} values of 24.5 and 26.6 μmol/L, respectively.

Structural modifications and structure-activity relationship studies

In our search for bioactive natural products[13, 16, 22, 24, 25, 29, 33, 36, 38, 39, 41, 42, 44–46, 51–53, 58, 63, 68, 70, 73–81, 85, 87–88, 93, 95–98, 103–109, 115–120], a large number of compounds were found to exhibit a variety of biological activities, and 11 compounds with particularly promising potential were selected for structure optimization and structure-activity relationship studies. As a result, over 400 new derivatives were obtained. Among these derivatives, 58 showed significantly improved activities, which provided opportunities to explore the structure-activity relationship of the related compound class[121–125]. As an example, we will discuss the structure optimization and structure-activity relationship study of the antiangiogenesis pseudolaric acid B (PAB)[121]. PAB is the major active component of a well-known TCM (Tujinpi), the root bark of *Pseudolarix kaempferi*, which has traditional applications as an antifungal and abortifacient for use in the early stage of pregnancy. PAB also showed strong cytotoxic activity. In our collaboration study, this compound was found for the first time to have strong antiangiogenic activity with a unique mode of antitumor action[118–120]. A structural modification of PAB was thus conducted, and more than 40 derivatives were prepared in the first round. Antitumor assays showed that nine derivatives in the series **120a–120n** showed significantly improved activities, while those in the **121a–121d** and **122a–122g** series were inactive.

Observation of the structures of PAB and its derivatives revealed a clear antitumor structure activity relationship (Scheme 2)[121]: (1) All of the active PAB compounds tested in our study (**120a–120n**) have amphipathic properties and possess a hydrophobic domain of a constrained-rings system and a hydrophilic domain consisting of a side chain possessing an conjugated double bond and a terminal carboxylic acid. (2) A hydrophobic group R^1 at C-7 and a Δ^7 double bond are necessary for the anticancer activity, and the bulk and steric factor of R^1 also seem relevant to the activity. (3) The chain length and/or the conjugated double bonds in the side chain are essential for the anticancer activity. (4) Any structural changes in the seven-membered ring, *eg*, Δ^7 double bond migration and oxygenation at C-7 or C-8, will render the analogs inactive. (5) The C-4 acetoxyl group is crucial for the activity and its removal or replacement with a bulk acyloxy group significantly attenuated the activity. (6) The free carboxylic acid group in the terminus of the side chain is necessary for the anticancer activity, while acylation or amidation of this group with either a hydrophilic or a hydrophobic group is detrimental to the activity.

PAB is also a strong antifungal agent. The anticancer SAR of the aforementioned PAB analogs is very similar to the antifungal SAR reported by our group[81], except for the difference in the modification of the R^1 group. The modification of the R^1 group of PAB showed a particularly exciting result with respect to anticancer activity. Meanwhile, in an antifungal assay, all of the structurally modified PAB analogs showed attenuated activities or were completely inactive[81]. Our studies suggest that PAB is very promising as an anticancer drug
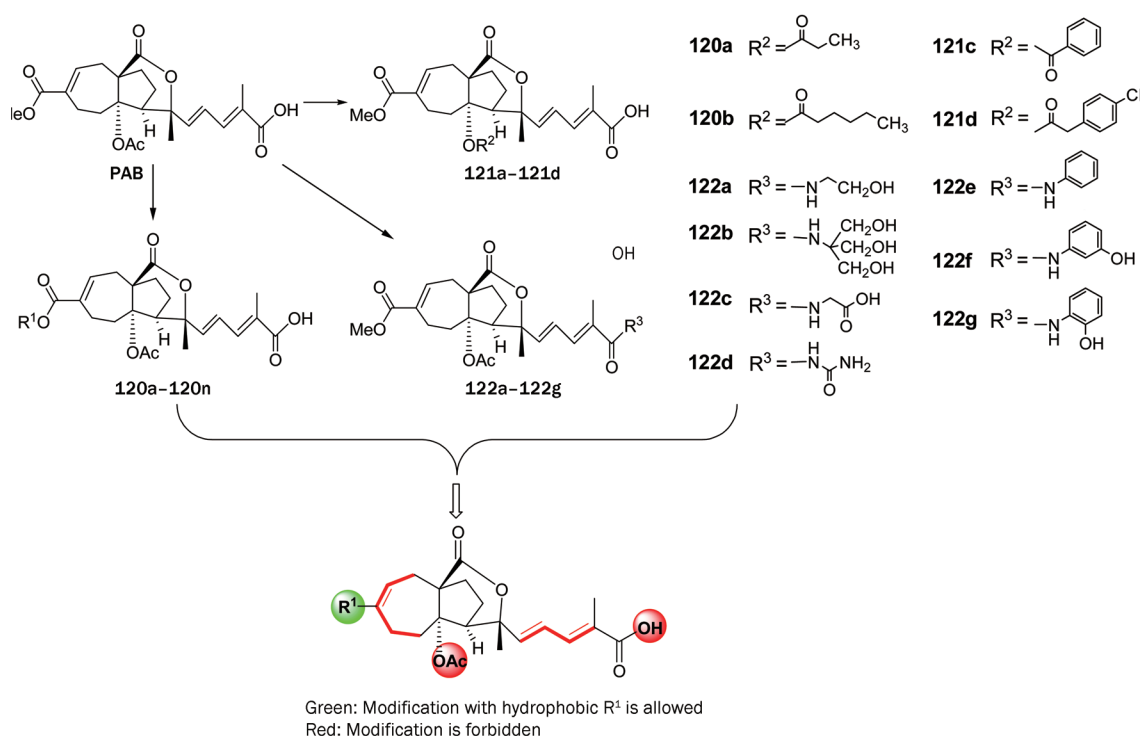
Scheme 2. Preparation of PAB derivatives and structure activity relationship study.

lead but limited as an antifungal lead due to its loss of activity upon modification and strong cytotoxic side effects.

References

1   Newman DJ, Cragg GM. Natural products as sources of new drugs over the last 25 years. J Nat Prod 2007; 70: 461–77.

2   Newman DJ, Cragg GM, Snader KM. Natural products as sources of new drugs over the period 1981–2002. J Nat Prod 2003; 66: 1022–37.

3   Li Y, Wu YL. Advances in medicinal chemistry and pharmacology of artemisinin and its derivatives; Chapter 11. In: Bai DL, Chen KX, editors. Progress in chemistry series advances in medicinal chemistry. Beijing: Chemical Industry Press; 2004. p 433–503.

4   Liu JS, Zhu YL, Yu CM, Zhou YZ, Han YY, Wu FW, *et al*. The structures of huperzine A and B, two new alkaloids exhibiting marked anticholinesterase activity. Can J Chem 1986; 64: 837–9.

5   Xu ZL, Chu BM, Luan XH, Wu WZ, Cai DG. The structural identification of fordine. Med J Chin PLA 1985; 10: 263–4.

6   Zhang CR, Fan CQ, Dong SH, Liu HB, Zhou WB, Wu Y, *et al*. Angustimine and angustifolimine: two new alkaloids from *Daphniphyllum angustifolium*. Org Lett 2011; 13: 2440–3.

7   Zhang CR, Liu HB, Dong SH, Zhu JY, Wu Y, Yue JM. Calycinumines A and B, two novel alkaloids from *Daphniphyllum calycinum*. Org Lett 2009; 11: 4692–5.

8   Yang SP, Yue JM. First diamino *Daphniphyllum* alkaloid, daphnipaxinin, with an unprecedented heterohexacyclic skeleton from *Daphniphyllum paxianum*. Org Lett 2004; 6: 1401–4.

9   Zhan ZJ, Yang SP, Yue JM. Paxdaphnidines A and B, novel penta- and tetracyclic alkaloids from *Daphniphyllum paxianum*. J Org Chem 2004; 69: 1726–9.

10   Yang SP, Yue JM. Two novel alkaloids with a unique fused hexacyclic skeleton from *Daphniphyllum subverticillatum*. J Org Chem 2003; 68: 7961–6.

11   Fan CQ, Yin S, Xue JJ, Yue JM. Novel alkaloids, paxdaphnines A and B with unprecedented skeletons from the seeds of *Daphniphyllum paxianum*. Tetrahedron 2007; 63: 115–9.

12   Zhan ZJ, Zhang CR, Yue JM. Caldaphnidines A–F, six new *Daphniphyllum* alkaloids from *Daphniphyllum calycinum*. Tetrahedron 2005; 61: 11038–45.

13   Zhang CR, Liu HB, Feng T, Zhu JY, Geng MY, Yue JM. Alkaloids from the leaves of *Daphniphyllum subverticillatum*. J Nat Prod 2009; 72: 1669–72.

14   Zhang CR, Yang SP, Yue JM. Alkaloids from the twigs of *Daphniphyllum calycinum*. J Nat Prod 2008; 71: 1663–8.

15   Yang SP, Zhang H, Zhang CR, Chen HD, Yue JM. Alkaloids from *Daphniphyllum longeracemosum*. J Nat Prod 2006; 69: 79–82.

16   Zhang H, Yang SP, Fan CQ, Ding J, Yue JM. Daphniyunnines A–E, alkaloids from *Daphniphyllum yunnanense*. J Nat Prod 2006; 69: 553–7.

17   Gan LS, Wang XN, Fan CQ, Wu Y, Yue JM. Alkaloids from fruits of *Daphniphyllum oldhamii*. Helv Chim Acta 2007; 90: 2395–400.

18   Wang XN, Gan LS, Fan CQ, Yin S, Yue JM. Alkaloids from the fruits of *Daphniphyllum macropodum*. Helv Chim Acta 2007; 90: 2156–62.

19   Yang SP, Yue JM. Alkaloids from *Daphniphyllum longeracemosum*. Helv Chim Acta 2006; 89: 2783–8.

20   Chen X, Zhan ZJ, Yue JM. Longistylumphyllines A-C, three new alkaloids from *Daphniphyllum longistylum*. Helv Chim Acta 2005; 88: 854–60.

21   Chen X, Zhan ZJ, Yue JM. Oldhamiphylline A: a novel hexacyclic alkaloid from *Daphniphyllum oldhami*. Chem Biodivers 2004; 1: 1513–8.

22   Gan LS, Fan CQ, Yang SP, Wu Y, Lin LP, Ding J, *et al*. Flueggenines A and B, two novel C,C-linked dimeric indolizidine alkaloids from *Flueggea virosa*. Org Lett 2006; 8: 2285–8.

23   Yin S, He XF, Wu Y, Yue JM. Monoterpenoid indole alkaloids bearing an N_4-iridoid from *Gelsemium elegans*. Chem Asian J 2008; 3: 1824–9.

24   Xu YK, Yang SP, Liao SG, Zhang H, Lin LP, Ding J, *et al*. Alkaloids from *Gelsemium elegans*. J Nat Prod 2006; 69: 1347–50.

25   Zhang H, Wang XN, Lin LP, Ding J, Yue JM. Indole alkaloids from three species of the *Ervatamia* genus: *E officinalis*, *E divaricata*, and *E divaricata* Gouyahua. J Nat Prod 2007; 70: 54–9.

26   Zhang H, Yue JM. Indole alkaloids from the whole plants of *Ervatamia officinalis*. Helv Chim Acta 2005; 88: 2537–42.

27   Zhang H, Yue JM. Hasubanan type alkaloids from *Stephania longa*. J Nat Prod 2005; 68: 1201–7.

28   Zhang H, Yue JM. New stephaoxocane alkaloids from *Stephania longa*. Helv Chim Acta 2006; 89: 1105–9.

29   Gan LS, Yang SP, Wu Y, Ding J, Yue JM. Terpenoid indole alkaloids from *Winchia calophylla*. J Nat Prod 2006; 69: 18–22.

30   Yin S, Fan CQ, Wang XN, Yue JM. Lycodine-type alkaloids from *Lycopodium casuarinoides*. Helv Chim Acta 2006; 89: 138–43.

31   Liao SG, Chen HD, Yue JM. Plant orthoesters. Chem Rev 2009; 109: 1092–140.

32   Han ML, Zhang H, Yang SP, Yue JM. Walsucochinoids A and B: new rearranged limonoids from *Walsura cochinchinensis*. Org Lett 2012; 14: 486–9.

33   Yang SP, Chen HD, Liao SG, Xie BJ, Miao ZH, Yue JM. Aphanamolide A, a new limonoid from *Aphanamixis polystachya*. Org Lett 2011; 13: 150–3.

34   Yuan T, Zhu RX, Zhang H, Odeku OA, Yang SP, Liao SG, *et al*. Structure determination of grandifotane a from *Khaya grandifoliola* by NMR, X-ray diffraction, and ECD calculation. Org Lett 2010; 12: 252–5.

35   Yuan T, Yang SP, Zhang CR, Zhang S, Yue JM. Two limonoids, khayalenoids A and B with an unprecedented 8-oxa-tricyclo[4.3.2.0^{2,7}] undecane motif from *Khaya senegalensis*. Org Lett 2009; 11: 617–20.

36   Zhou ZW, Yin S, Zhang HY, Fu Y, Yang SP, Wang XN, *et al*. Walsucochins A and B with an unprecedented skeleton isolated from *Walsura cochinchinensis*. Org Lett 2008; 10: 465–8.

37   Zhang CR, Fan CQ, Zhang L, Yang SP, Wu Y, Lu Y, *et al*. Chuktabrins A and B, two novel limonoids from the twigs and leaves of *Chukrasia tabularis*. Org Lett 2008; 10: 3183–6.

38   He XF, Wang XN, Gan LS, Yin S, Dong L, Yue JM. Two novel triterpenoids from *Dysoxylum hainanense*. Org Lett 2008; 10: 4327–30.

39   Yin S, Wang XN, Fan CQ, Liao SG, Yue JM. The first limonoid peroxide in the meliaceae family: walsuronoid a from *Walsura robusta*. Org Lett 2007; 9: 2353–6.

40   Zhang CR, Yang SP, Liao SG, Fan CQ, Wu Y, Yue JM. Chuktabularins A-D, four new limonoids with unprecedented carbon skeletons from the stem bark of *Chukrasia tabularis*. Org Lett 2007; 9: 3383–6.

41   Wang XN, Yin S, Fan CQ, Wang FD, Lin LP, Ding J, *et al*. Turrapubesins

A and B, first examples of halogenated and maleimide-bearing limonoids in nature from *Turraea pubescens*. Org Lett 2006; 8: 3845–8.

42 Yin S, Fan CQ, Wang XN, Lin LP, Ding J, Yue JM. Xylogranatins A–D: novel tetranortriterpenoids with an unusual 9,10-*seco* scaffold from marine mangrove *Xylocarpus granatum*. Org Lett 2006; 8: 4935–8.

43 Fan CQ, Wang XN, Yin S, Zhang CR, Wang FD, Yue JM. Tabularisins A–D, phragmalin *ortho* esters with new skeleton isolated from the seeds of *Chukrasia tabularis*. Tetrahedron 2007; 63: 6741–7.

44 Wang XN, Yin S, Fan CQ, Lin LP, Ding J, Yue JM. Eight new limonoids from *Turraea pubescens*. Tetrahedron 2007; 63: 8234–41.

45 Liu J, Yang SP, Su ZS, Lin BD, Wu Y, Yue JM. Limonoids from the stems of *Toona ciliata* var *henryi* (Meliaceae). Phytochemistry 2011; 72: 2189–96.

46 Lin BD, Chen HD, Liu J, Zhang S, Wu Y, Dong L, *et al*. Mulavanins A–E: limonoids from *Munronia delavayi*. Phytochemistry 2010; 71: 1596–601.

47 Zhang B, Yang SP, Yin S, Zhang CR, Wu Y, Yue JM. Limonoids from *Khaya ivorensis*. Phytochemistry 2009; 70: 1305–8.

48 Xie BJ, Yang SP, Yue JM. Terpenoids from *Dysoxylum densiflorum*. Phytochemistry 2008; 69: 2993–7.

49 Zhang H, Odeku QA, Wang XN, Yue JM. Limonoids from the stem bark of *Khaya grandifoliola*. Phytochemistry 2008; 69: 271–5.

50 Wang XN, Fan CQ, Yin S, Gan LS, Yue JM. Structural elucidation of limonoids and steroids from *Trichilia connaroides*. Phytochemistry 2008; 69: 1319–27.

51 Liu HB, Zhang H, Li P, Wu Y, Gao ZB, Yue JM. Kv1.2 potassium channel inhibitors from *Chukrasia tabularis*. Org Biomol Chem 2012, 10: 1448–58.

52 He XF, Wang XN, Ying S, Dong L, Yue JM. Ring A modified novel triterpenoids from *Dysoxylum hainanense*. Eur J Org Chem 2009; 28: 4818–24.

53 Dong SH, Zhang CR, Dong L, Wu Y, Yue JM. Onoceranoid-type triterpenoids from *Lansium domesticum*. J Nat Prod 2011; 74: 1042–8.

54 Yuan T, Zhang CR, Yang SP, Yue JM. Limonoids and triterpenoids from *Khaya senegalensis*. J Nat Prod 2010; 73: 669–74.

55 Dong SH, Zhang CR, He XF, Liu HB, Wu Y, Yue JM. Mesendanins A-J, limonoids from the leaves and twigs of *Melia toosendan*. J Nat Prod 2010; 73: 1344–9.

56 Lin BD, Zhang CR, Yang SP, Zhang S, Wu Y, Yue JM. D-ring-opened phragmalin-type limonoid orthoesters from the twigs of *Swietenia macrophylla*. J Nat Prod 2009; 72: 1305–13.

57 Lin BD, Yuan T, Zhang CR, Dong L, Zhang B, Wu Y, *et al*. Structurally diverse limonoids from the fruits of *Swietenia mahagoni*. J Nat Prod 2009; 72: 2084–90.

58 Chen HD, Yang SP, Wu Y, Dong L, Yue JM. Terpenoids from *Toona ciliata*. J Nat Prod 2009; 72: 685–9.

59 Chen HD, Yang SP, Liao SG, Zhang B, Wu Y, Yue JM. Limonoids and sesquiterpenoids from *Amoora tsangii*. J Nat Prod 2008; 71: 93–7.

60 Xie BJ, Yang SP, Chen HD, Yue JM. Agladupols A–E, triterpenoids from *Aglaia duperreana*. J Nat Prod 2007; 70: 1532–5.

61 Zhang CR, Yang SP, Zhu Q, Liao SG, Wu Y, Yue JM. Nortriterpenoids from *Chukrasia tabularis* var. *velutina*. J Nat Prod 2007; 70: 1616–9.

62 Liao SG, Yang SP, Yuan T, Zhang CR, Chen HD, Wu Y, *et al*. Limonoids from the leaves and stems of *Toona ciliate*. J Nat Prod 2007; 70: 1268–73.

63 Yin S, Wang XN, Fan CQ, Lin LP, Ding J, Yue JM. Limonoids from the seeds of the marine mangrove *Xylocarpus granatum*. J Nat Prod 2007; 70: 682–5.

64 Gan LS, Wang XN, Wu Y, Yue JM. Tetranortriterpenoids from *Cipadessa baccifera*. J Nat Prod 2007; 70: 1344–7.

65 Chen YY, Wang XN, Fan CQ, Yin S, Yue JM. Swiemahogins A and B, two novel limonoids from *Swietenia mahogany*. Tetrahedron Lett 2007; 48: 7480–4.

66 Wang XN, Fan CQ, Yue JM. New pregnane steroids from *Turraea pubescens*. Steroids 2006; 71: 720–4.

67 He XF, Wang XN, Ying S, Dong L, Yue JM. Ring A-*seco* triterpenoids with antibacterial activity from *Dysoxylum hainanense*. Bioorg Med Chem Lett 2011; 21: 125–9.

68 Zhang F, Liao SG, Zhang CR, He XF, Chen WS, Yue JM. Limonoids and diterpenoids from *Toona ciliata* Roem var *yuunanensis*. Planta Med 2011; 77: 1617–22.

69 Lin BD, Zhang CR, Yang SP, Wu Y, Yue JM. Phragmalin-type linomoid orthoesters from the twigs of *Swietenia macrophylla*. Chem Pharm Bull 2011; 59: 458–65.

70 Zhang CR, Yang SP, Chen XQ, Wu Y, Zhen XC, Yue JM. Limonoids from the twigs and leaves of *Chukrasia tabularis*. Helv Chim Acta 2008; 91: 2338–50.

71 Wang XN, Fan CQ, Yin S, Lin LP, Ding J, Yue JM. Cytotoxic terpenoids from *Turraea pubescens*. Helv Chim Acta 2008; 91: 510–9.

72 Liao SG, Zhan ZJ, Yang SP, Yue JM. Lathyranoic acid A: first secolathyrane diterpenoid in nature from *Euphorbia lathyris*. Org Lett 2005; 7: 1379–82.

73 Chen HD, He XF, Ai J, Geng MY, Yue JM. Trigochilides A and B, two highly modified daphnane-type diterpenoids from *Trigonostemon chinensis*. Org Lett 2009; 11: 4080–3.

74 Chen HD, Yang SP, He XF, Ai J, Liu Z, Liu HB, *et al*. Trigochinins A–C: three new daphnane-type diterpenes from *Trigonostemon chinensis*. Org Lett 2010; 12: 1168–71.

75 Chen HD, Yang SP, He XF, Liu HB, Ding J, Yue JM. Trigochinins D-I: six new daphnane-type diterpenoids from *Trigonostemon chinensis*. Tetrahedron 2010; 66: 5065–70.

76 Dong SH, Liu HB, Xu CH, Ding J, Yue JM. Constituents of *Trigonostemon heterophyllus*. J Nat Prod 2011; 74: 2576–81.

77 Dong SH, Zhang CR, Xu CH, Ding J, Yue JM. Daphnane-type triterpenoids from *Trigonostemon howii*. J Nat Prod 2011; 74: 1255–61.

78 Lin BD, Han ML, Ji YC, Chen HD, Yang SP, Zhang S, *et al*. Trigoxyphins A–G: diterpenes from *Trigonostemon xyphophylloides*. J Nat Prod 2010; 73: 1301–5.

79 Yin S, Su ZS, Zhou ZW, Dong L, Yue JM. Antimicrobial diterpenes from *Trigonostemon chinensis*. J Nat Prod 2008; 71: 1414–7.

80 Zhan ZJ, Fan CQ, Ding J, Yue JM. Novel diterpenoids with potent inhibitory activity against endothelium cell HMEC and cytotoxic activities from a well-known TCM plant *Daphne genkwa*. Bioorg Med Chem 2005; 13: 645–55.

81 Yang SP, Dong L, Wang Y, Wu Y, Yue JM. Antifungal diterpenoids of *Pseudolarix kaempferi*, and their structure-activity relationship study. Bioorg Med Chem 2003; 11: 4577–84.

82 Yang SP, Wu Y, Yue JM. Five new diterpenoids from *Pseudolarix kaempferi*. J Nat Prod 2002; 65: 1041–4.

83 Xiang Y, Zhang H, Fan CQ, Yue JM. Novel diterpenoids and diterpenoid glycosides from *Siegesbeckia orientalis*. J Nat Prod 2004; 67: 1517–21.

84 Liu HB, Zhang H, Yu JH, Xu CH, Ding J, Yue JM. Cytotoxic diterpenoids from *Sapium insigne*. J Nat Prod 2012; 75: 722–7.

85 Xue JJ, Fan CQ, Dong L, Yang SP, Yue JM. Novel antibacterial diterpenoids from *Larix chinensis* Beissn. Chem Biodivers 2004; 1: 1702–7.

86 Yuan T, Zhu RX, Yang SP, Zhang H, Zhang CR, Yue JM. Serratustones A and B representing a new dimerization pattern of two types of sesquiterpenoids from *Chloranthus serratus*. Org Lett 2012; 14:

3198–201.

87 Yang SP, Gao ZB, Wang FD, Liao SG, Chen HD, Zhang CR, *et al*. Chlorahololides A and B, two potent and selective blockers of the potassium channel isolated from *Chloranthus holostegius*. Org Lett 2007; 9: 903–6.

88 Yang SP, Gao ZB, Wu Y, Hu GY, Yue JM. Chlorahololides C–F: a new class of potent and selective potassium channel blockers from *Chloranthus holostegius*. Tetrahedron 2008; 64: 2027–34.

89 Yuan T, Zhang CR, Yang SP, Yin S, Wu WB, Dong L, *et al*. Sesquiterpenoids and phenylpropanoids from *Chloranthus serratus*. J Nat Prod 2008; 71: 2021–5.

90 Zhang S, Yang SP, Yuan T, Lin BD, Wu Y, Yue JM. Multistalides A and B, two novel sesquiterpenoid dimers from *Chloranthus multistachys*. Tetrahedron Lett 2010; 51: 764–6.

91 Yang SP, Yue JM. Chloramultilide A, a highly complex sesquiterpenoid dimmer from C*hloranthus multistachys*. Tetrahedron Lett 2006; 47: 1129–32.

92 He XF, Zhang S, Zhu RX, Yang SP, Yuan T, Yue JM. Sarcanolides A and B: two sesquiterpenoid dimers with a nonacyclic scaffold from *Sarcandra hainanensis*. Tetrahedron 2011; 67: 3170–4.

93 He XF, Yin S, Ji YC, Su ZS, Geng MY, Yue JM. Sesquiterpenes and dimeric sesquiterpenoids from *Sarcandra glabra*. J Nat Prod 2010; 73: 45–50.

94 Yin S, Xue JJ, Fan CQ, Miao ZH, Ding J, Yue JM. Eucalyptals A–C with a new skeleton isolated from *Eucalyptus globules*. Org Lett 2007; 9: 5549–52.

95 Su ZS, Yin S, Zhou ZW, Wu Y, Ding J, Yue JM. Sesquiterpenoids from *Hedyosmum orientale*. J Nat Prod 2008; 71: 1410–3.

96 Yang SP, Huo J, Wang Y, Lou LG, Yue JM. Cytotoxic sesquiterpenoids from *Eupatorium chinense*. J Nat Prod 2004; 67: 638–43.

97 Huo J, Yang SP, Ding J, Yue JM. Cytotoxic sesquiterpene lactones from *Eupatorium lindleyanum*. J Nat Prod 2004; 67: 1470–5.

98 Chen X, Zhan ZJ, Zhang XW, Ding J, Yue JM. Sesquiterpene lactones with potent cytotoxic activites from *Vernonia chinensis*. Planta Med 2005; 71: 949–54.

99 Xiang Y, Fan CQ, Yue JM. Novel sesquiterpenoids from *Siegesbeckia orientali*s. Helv Chim Acta 2005; 88: 160–70.

100 Fan CQ, Zhan ZJ, Li H, Yue JM. Eudesmane-type sesquiterpene derivatives from *Saussurea conica*. Helv Chim Acta 2004; 87: 1446–51.

101 Zhang H, Liao ZX, Yue JM. Five new sesquiterpenoids from *Parasenecio petasitoide*s. Helv Chim Acta 2004; 87: 976–82.

102 Wang Y, Yang SP, Yue JM. Novel sesquiterpenes from the fungus *Lactarius piperatus*. Helv Chim Acta 2003; 86: 2424–33.

103 Liao SG, Yuan T, Zhang C, Yang SP, Wu Y, Yue JM. Cinnacassides A–E, five geranylphenylacetate glycosides from *Cinnamomum cassia*. Tetrahedron 2009; 65: 883–7.

104 Yin S, Chen X, Su ZS, Yang SP, Fan CQ, Ding J, *et al*. Harrisotones A–E, five novel prenylated polyketides with a rare spirocyclic skeleton from *Harrisonia perforate*. Tetrahedron 2009, 65: 1147–52.

105 Yin S, Fan CQ, Dong L, Yue JM. Psoracorylifols A–E, five novel compounds with activity against *Helicobacter pylori* from seeds of *Psoralea corylifolia*. Tetrahedron 2006; 62: 2569–75.

106 Fan CQ, Yue JM. Biologically active phenols from *Saussurea medusa*. Bioorg Med Chem 2003; 11: 703–8.

107 Yin S, Fan CQ, Wang Y, Dong L, Yue JM. Antibacterial prenylflavone derivatives from *Psoralea corylifolia* and their structure-activity

108 Gan LS, Yang SP, Fan CQ, Yue JM. Lignans and their degraded derivatives from *Sarcostemma acidum*. J Nat Prod 2005; 68: 221–5.

109 Fan CQ, Zhu XZ, Zhan ZJ, Ji XQ, Li H, Yue JM. Lignans from *Saussurea conica* and their NO production suppressing activity. Planta Med 2006; 72: 590–5.

110 Liao SG, Zhang BL, Wu Y, Yue JM. New phenolic components from *Daphne giraldii*. Helv Chim Acta 2005; 88: 2873–8.

111 Zhou ZW, Yin S, Wang XN, Fan CQ, Li H, Yue JM. Two new lignan glycosides from *Saussurea laniceps*. Helv Chim Acta 2007; 90: 951–6.

112 Zhang CR, Yang SP, Liao SG, Wu Y, Yue JM. Polyoxygenated cyclohexene derivatives from *Uvaria rufa*. Helv Chim Acta 2006; 89: 1408–16.

113 Liao SG, Wu Y, Yue JM. Lignans from *Wikstroemia hainanensis*. Helv Chim Acta 2006; 89: 73–80.

114 Yang SP, Yue JM. Five new quassinoids from the bark of *Picrasma quassioides*. Helv Chim Acta 2004; 87: 1591–600.

115 Yang SP, Yue JM. Two novel cytotoxic and antimicrobial triterpenoids from *Pseudolarix kaempferi*. Bioorg Med Chem Lett 2001; 11: 3119–22.

116 Cai JH, Han C, Hu TC, Zhang J, Wang FD, Liu YQ, *et al*. Peptide deformylase is a potential target for anti-*Helicobacter pylori* drugs: reverse docking, enzymatic assay and X-ray crystallography validation. Protein Sci 2006; 15: 2071–81.

117 Liu H, Li Y, Song MK, Tan XJ, Cheng F, Zheng SX, *et al*. Structure-based discovery of potassium channel blockers from natural products-virtual screening and electro-physiological assay testing. Chem Biol 2003; 10: 1103–13.

118 Tong YG, Zhang XW, Geng MY, Yue JM, Xin XL, Tian F, *et al*. Pseudolarix acid B, a new tubulin-binding agent, inhibits angiogenesis by interacting with a novel binding site on tubulin. Mol Pharmacol 2006; 69: 1226–33.

119 Li MH, Miao ZH, Tan WF, Yue JM, Zhang C, Lin LP, *et al*. Pseudolaric acid B inhibits angiogenesis and reduces hypoxia-inducible factor 1α by promoting proteasome-mediated degradation. Clin Cancer Res 2004; 10: 8266–74.

120 Tan WF, Zhang XW, Li MH, Yue JM, Chen Y, Lin LP, *et al*. Pseudolarix acid B inhibits angiogenesis by antagonizing the VEGF-mediated anti-apoptotic effect. Eur J Pharmacol 2004, 499: 219–28.

121 Yang SP, Cai YJ, Zhang BL, Tong LJ, Xie H, Wu Y, *et al*. Structural modification of an angiogenesis inhibitor discovered from traditional Chinese medicine and a structure-activity relationship study. J Med Chem 2008; 51: 77–85.

122 Zhang BL, Fan CQ, Dong L, Wang FD, Yue JM. Structural modification of a specific antimicrobial lead against *Helicobacter pylori* discovered from traditional Chinese medicine and a structure-activity relationship study. Eur J Med Chem 2010; 45: 5258–64.

123 Wang FD, Yue JM. Novel and highly efficient syntheses of (+)-and (−)-dihydrokawain using sonochemical Blaise reaction as the key step. Eur J Org Chem 2005; 2005: 2575–9.

124 Zhang BL, Wang FD, Yue JM. A new efficient method for the total synthesis of linear furocoumarins. ChemInform 2006; 37: 567–70.

125 Wang FD, Yue JM. Total synthesis of *R*-(+)-kavain via (MeCN)$_2$PdCl$_2$-catalyzed isomerization of *cis*-double bond and sonochemical Blaise reaction. SynLett 2005; 13: 2077–9.

npg

Review

Bioactive natural products from Chinese marine flora and fauna

Zhen-fang ZHOU, Yue-wei GUO*

State Key Laboratory of Drug Research, Shanghai Institute of Materia Medica, Chinese Academy of Sciences, Shanghai 201203, China

In recent decades, the pharmaceutical application potential of marine natural products has attracted much interest from both natural product chemists and pharmacologists. Our group has long been engaged in the search for bioactive natural products from Chinese marine flora (such as mangroves and algae) and fauna (including sponges, soft corals, and mollusks), resulting in the isolation and characterization of numerous novel secondary metabolites spanning a wide range of structural classes and various biosynthetic origins. Of particular interest is the fact that many of these compounds show promising biological activities, including cytotoxic, antibacterial, and enzyme inhibitory effects. By describing representative studies, this review presents a comprehensive summary regarding the achievements and progress made by our group in the past decade. Several interesting examples are discussed in detail.

Keywords: marine natural products; biological activity; mangrove; algae; soft coral; sponges; mollusks

Introduction

The unique ocean habitat has caused marine organisms to evolve distinctive metabolic pathways, producing remarkable secondary metabolites that differ from those of terrestrial plants. Because the compounds isolated from marine organisms are structurally and biologically intriguing, research on marine natural products has been attracting the attention of chemists as a challenging research topic. To date, more than 30 000 compounds bearing unusual structures and exhibiting various bioactivities have been isolated from marine plants and invertebrates.

In recent years, the interest in natural products from Chinese marine organisms has increased dramatically, making the annual average number of natural products isolated from marine organisms increase rapidly. As one of the most active research groups in this area, we have been devoted to the investigation of Chinese marine plants and invertebrates since 2000. In the course of our studies, a series of structurally diverse and biologically interesting compounds belonging to various structural classes, such as macrocyclic polydisulfides, spirodioxynaphthalene, and alkaloids, have been isolated and characterized. Through these productive studies, we have made important contributions to the research and develop-

ment of Chinese marine natural products. This review summarizes the progress and achievements made by our group in the study of Chinese marine flora and fauna in the past decade, and several interesting examples are discussed in detail.

Chemical studies on Chinese marine plants
Algae

Microalgae play important roles in marine biological systems. Through their photosynthetic ability, algae are the major producers of biomass and organic compounds in the ocean. More importantly, many algal metabolites present unique structures and are formed via biosynthetic routes that are quite different from those known to produce terrestrial metabolites.

Marine dinoflagellates are flagellated organisms with both photosynthetic and heterotrophic attributes. The lifestyle of these organisms is diverse, and many of them participate in symbiotic relationships. For some time, the study of dinoflagellates has focused on their toxin production and pigment composition, and only a small number of these organisms have been found to produce other secondary metabolites. As part of our ongoing research on the biologically active substances of Chinese marine organisms, three new polyhydroxylpolyene compounds, lingshuiols A and B (**1** and **2**) and lingshuiol (**3**), have been isolated from the Chinese marine dinoflagellate *Amphidinium* sp collected at Lingshui Bay, Hainan Province, China[1, 2] (Figure 1). The structures of these compounds are
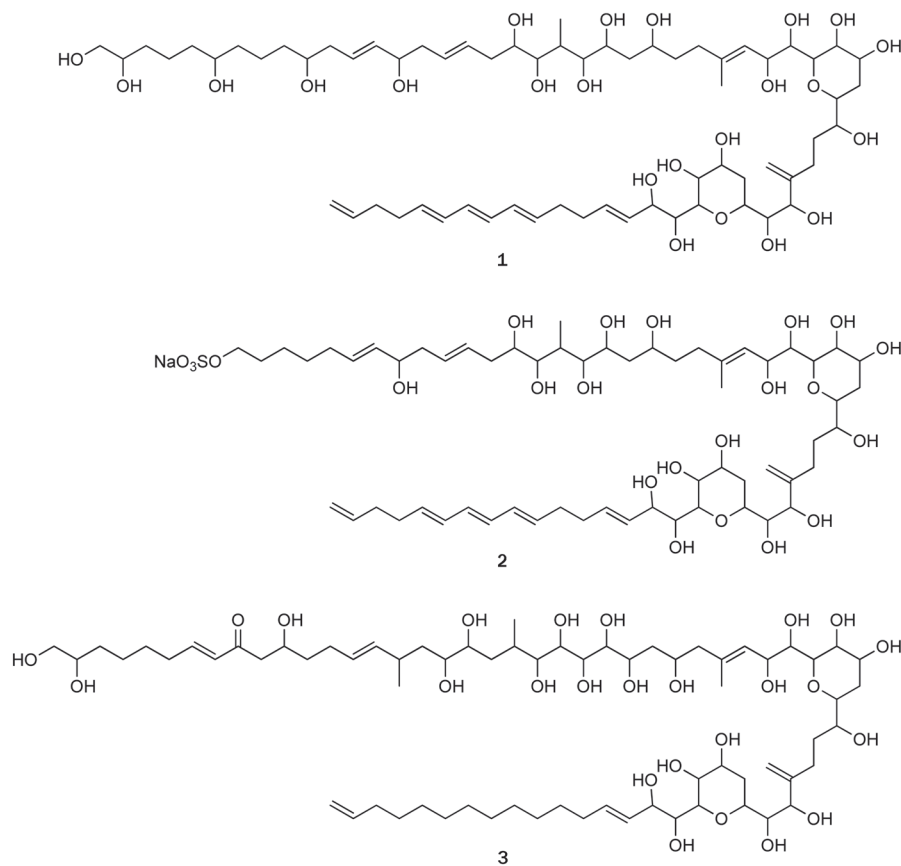
Figure 1. Structures of polyhydroxylpolyene compounds 1–3.

characterized by linear carbon chains, as determined by extensive analyses of 2D NMR spectroscopic data; however, the absolute configurations remain to be determined. In previous studies, polyhydroxylpolyene compounds were found to exhibit antifungal, hemolytic, and antimicrobial activities[3–5]. It was demonstrated that lingshuiol (3) possessed potent *in vitro* cytotoxic activities against A549 and HL-60 cells, with IC$_{50}$ values of 0.21 and 0.23 µmol/L, respectively.

Red algae of the genus *Laurencia* are found throughout the world, mostly in tropical and subtropical regions. Since Irie's pioneering investigations on *Laurencia* over the last four decades[6], a number of cuparene- and laurane-derived sesquiterpenoids have been isolated from this genus. The chemical investigation of the Chinese red alga *Laurencia okamurai* Yamada led to the isolation of a new laurane sesquiterpenoid, 3β-hydroxyaplysin (4), and two novel rearranged sesquiterpenes, laurokamurenes A and B (5 and 6)[7] (Figure 2). Their structures, including their relative stereochemistry, were determined based on a detailed interpretation of 2D NMR spectra and comparisons with related known compounds. To the best of our knowledge, this is also the first report of the isolation of sesquiterpenes containing a 2,2,3-trimethylcyclopentenyl moiety from a natural source. The sesquiterpenoids isolated from the red algae of the genus *Laurencia* in recent years can be classified into more than 20 sesquiterpenoid skeletons[8]. However, in most cases, the three methyl groups in the aliphatic portion are located at either positions 1,2,3
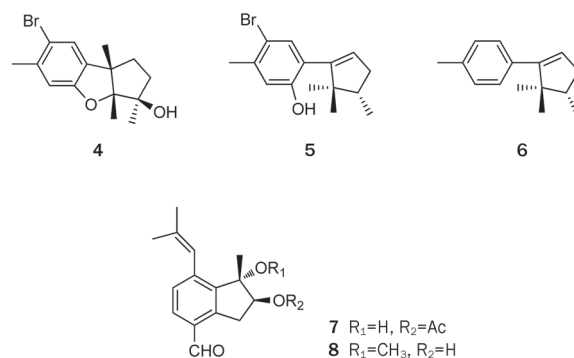

Figure 2. Structures of sesquiterpenes 4–8.

(laurene type) or 1,2,2 (cuparene type), with the exception of laurokamurenes A and B (5 and 6).

Two novel aromatic valerenane-type sesquiterpenes, caulerpals A and B (7 and 8), were isolated from the Chinese green alga *Caulerpa taxifolia*[9] (Figure 2). Compounds 7 and 8 were evaluated for their inhibitory activity against human protein tyrosine phosphatase 1B (PTP1B), a potential drug target for the treatment of type 2 diabetes and obesity, but neither compound exhibited a potent PTP1B inhibitory activity. It is important to note that caulerpals A and B (7 and 8) are the only two known compounds with an aromatic valerenane-type carbon skeleton from a natural source.

Mangroves

Mangroves comprise a large number of various salt-tolerant plants growing in tropical and subtropical intertidal estuarine zones. Mangrove plants are usually categorized into two subgroups, true mangrove and semi-mangrove plants, according to their living environment. True mangrove plants are confined to the typical intertidal mangrove habitats where the seawater salinity is usually 17.0‰–36.4‰. Semi-mangrove plants, however, grow on the landward fringe of the mangrove habitats or in the terrestrial marginal zones that are subjected to irregularly high tides. In general, mangrove plants consist of 84 species globally, belonging to 24 genera and 16 families; 14 are semi-mangrove species[10, 11].

Most of our studies involve plants belonging to the Rhizophoraceae, Sonneratiaceae, Euphorbiaceae, and Meliaceae families. A series of unusual compounds bearing unprecedented structures were identified in these taxa, some of which showed marked biological activities and are currently in preclinical studies.

For instance, an unusual novel macrocyclic polydisulfide gymnorrhizol (9) was isolated from the mangrove plant *Bruguiera gymnorrhiza* (Rhizophoraceae family). Compound 9 possesses an uncommon carbon skeleton that is characteristic of a 15-membered macrocycle composed of 3 repeated 1,3-dimercaptopropan-2-ol units[12] (Figure 3). The structure of compound 9 was established by extensive spectroscopic studies and confirmed using X-ray crystallography[13]. The first total synthesis of gymnorrhizol (9) was completed by our group with a high overall yield[14] (Scheme 1).

Prompted by the unusual structure of gymnorrhizol (9) and its potent inhibitory activity against PTP1B (an IC_{50} value of 14.9 µmol/L), we investigated the same mangrove species collected from different areas, which led to the isolation of two new macrocyclic polydisulfides, 10 and 11[15]. The structures of 10 and 11 were unequivocally determined through single-crystal X-ray diffraction analysis.

A plausible biosynthetic pathway for these cyclic polydisulfides was also proposed in which the 1,3-dimercaptopropan-2-ol unit should be the common building block for the biosynthesis of all of these macrocyclic polydisulfides; the self-cyclization of the 1,3-dim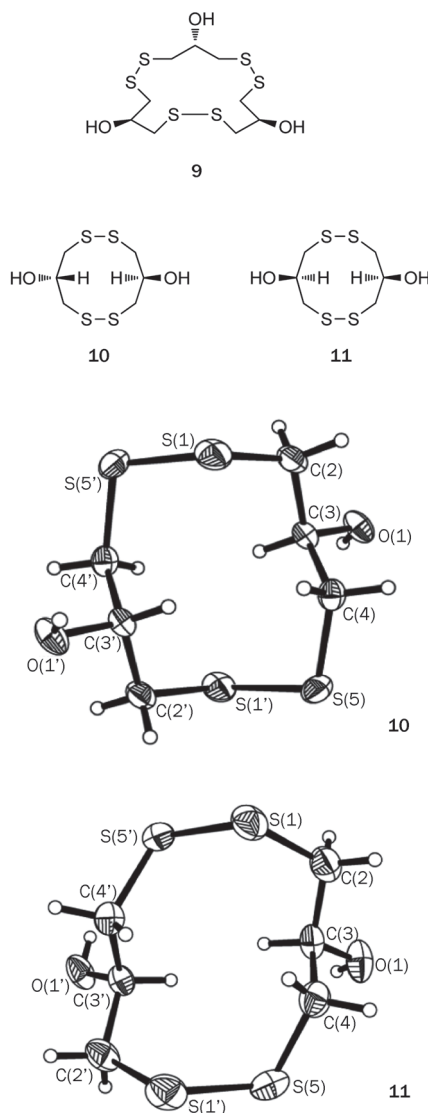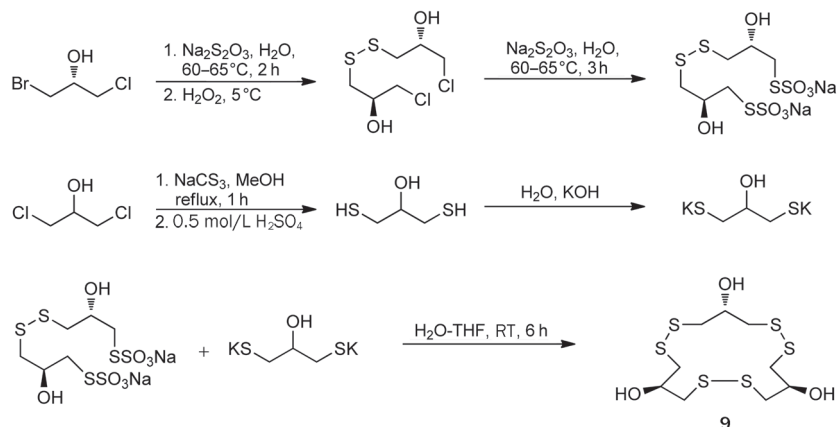ercaptopropan-2-ol unit of different sizes gave rise to macrocyclic polydisulfides ranging from 5-membered to 30-membered polydisulfides or even to larger

Figure 3. Structures of macrocyclic polydisulfides 9–11 and their X-rays.

Scheme 1. Total synthesis of gymnorrhizol (9).

polydisulfides. Marine disulfide- and multisulfide-containing metabolites are a special and important class of natural products. Due to the increasing interest in these compounds, the progress in this area was previously summarized by our group[16], encompassing the literature published between 1971 and 2010.

To obtain sufficient amounts of the polydisulfides for pharmacological research, the mangrove plant *B gymnorrhiza* collected from Zhanjiang, Guangdong Province, was investigated. Unexpectedly, instead of the ubiquitous macrocyclic polydisulfides, seven new spirodioxynaphthalene compounds, named palmarumycins BG1–BG7 (**12–18**) (Figure 4), were found[17]. It is noteworthy that these intriguing compounds were generally considered to be fungal metabolites, even though there were four reports on the isolation of palmarumycins (or preussomerins) from plants[18–21]. The fact that compounds **12–18** were isolated in quite an appreciable quantity indicated that these compounds were produced by *B gymnorrhiza*; however, we could not rule out the possibility that they were the metabolites of an endophytic or epiphytic fungus. The absolute configurations of metabolites **12–18** were determined using time-dependent density functional theory electronic circular dichroism (TDDFTECD) calculations of the solution conformers. It was found that compound **16** displayed an inhibitory activity against the HL-60 and MCF-7 cell lines. Additionally, we published a report summarizing the literature on the isolation, structure elucidation, biological activities, biosynthesis, and chemical synthesis of spirodioxynaphthalenes over the last 20 years[22].

Although the chemical investigation of the plants belonging to the Sonneratiaceae family was not as fruitful as that of the Rhizophoraceae family, a novel α-alkylbutenolide dimer, paracaseolide A (**19**), was isolated from the mangrove plant *Sonneratia paracaseolaris* (Sonneratiaceae family); this compound is characterized by an unusual tetraquinane oxa-cage bislactone skeleton bearing two linear alkyl chains[23] (Figure 5). Moreover, paracaseolide A (**19**) exhibited a potent inhibitory activity against the dual-specificity phosphatase Cdc25B, a key enzyme for cell cycle progression, with an IC$_{50}$ value of 6.44 μmol/L. A retrosynthetic pathway for paracaseolide A (**19**) was proposed in which **19** should be biosynthesized through a Diels-Alder [4+2] cycloaddition, starting from two molecules of **20** (Scheme 2). Paracaseolide A (**19**) represents the first example of an α-alkylbutenolide dimer from a natural source. Upon publication, the article was immediately covered in the
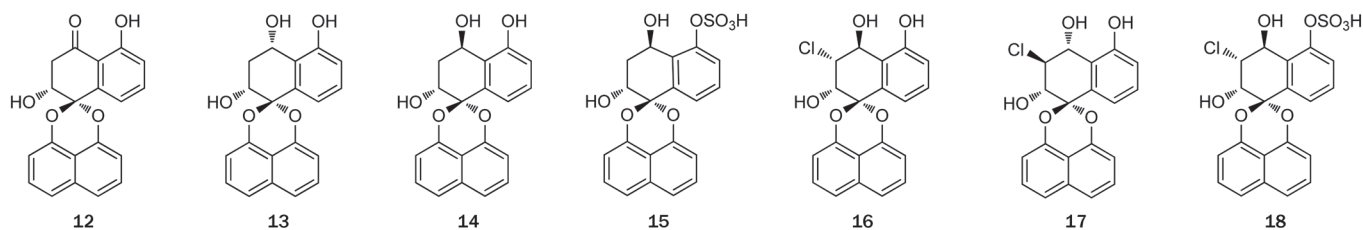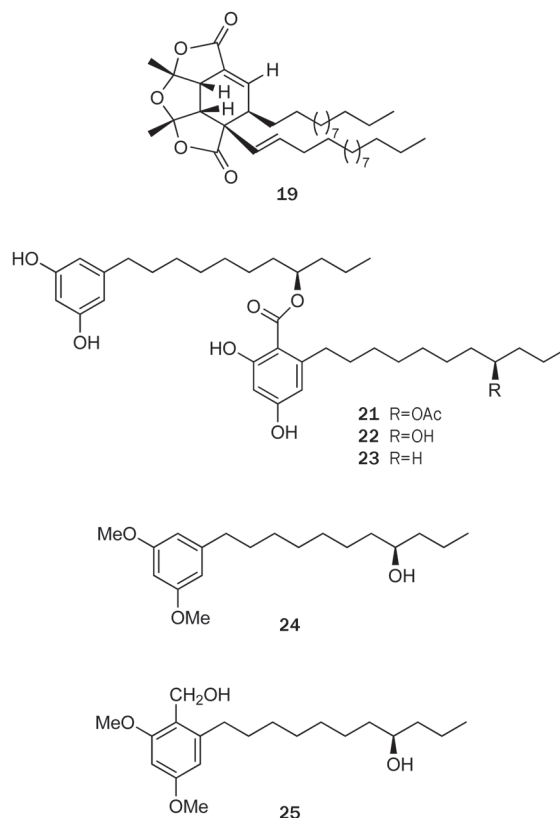

Figure 5. Structures of compounds **19** and **21–25**.

journal of *Natural Product Reports* as "hot off the press"[24].

In addition, three known compounds, integracins A and B (**21** and **22**) and 15-dehydroxy-integracin B (**24**), were isolated for the first time from the Chinese mangrove plant *Sonneratia hainanensis*[25] (Figure 5). Although compounds **21–24** had been reported previously, their absolute configurations were not resolved until their absolute chemistry was determined using Mosher's method, the specific rotation analysis of the alcohols (**24** and **25**) obtained from integracin A (**21**) in two steps, and chemical correlation. Integracin A (**21**) exhibited a cytotoxic effect against the tumor cell lines HepG2 and NCI-H460, both of which were 100% inhibited at 25 mg/mL.

The Euphorbiaceae family is composed of various species that are distributed widely throughout China. Although poisonous, most of the plants in this family are utilized in folk

Figure 4. Structures of spirodioxynaphthalene compounds **12–18**.
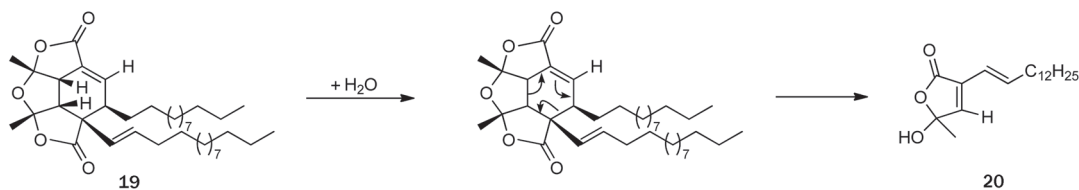
Scheme 2. Plausible retrosynthetic pathway for paracaseolide A (**19**).

medicine. Thus, the substances of the mangrove plant *Excoecaria agallocha* L (Euphorbiaceae family for the first time) were investigated, which led to the isolation of four diterpenes with an unprecedented skeleton, named excoagallochaols A–D (**26–29**)[26] (Figure 6). In addition to these terpenes, a novel octacyclic alkaloid with an unusual scaffold, suffruticosine (**30**), was isolated from *Securinega suffruticosa* (Pall) Rehd in the same family[27] (Figure 6). The absolute configuration of suffruticosine (**30**) was determined on the basis of CD spectral analysis.
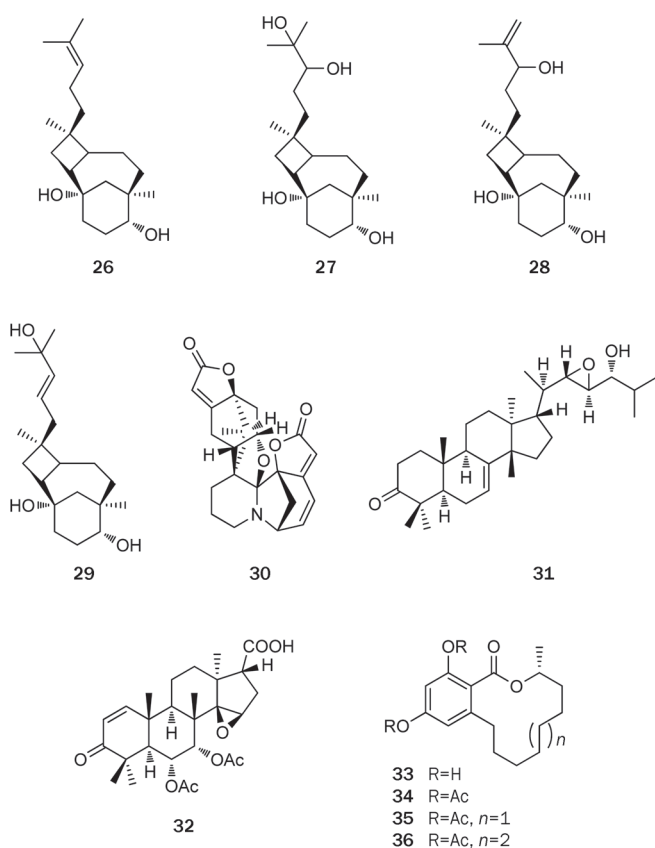
Figure 6. Structures of diterpenoids and the alkaloid **26–36**.

Plants of the Meliaceae family are a rich source of limonoids, which are a structurally diverse group of natural products with highly complex polycyclic skeletons. These unusual structural features have attracted the attention of chemists as

challenging targets for total synthesis, bioactivity evaluation, and biosynthetic studies. Chemical investigation on the stem bark of the plant *Toona ciliata* var *pubescens* resulted in the isolation of nine new compounds, including toonapubesin A (**31**), toonapubesic acid A (**32**), and their derivatives[28] (Figure 6). The proposed structure of **32** was confirmed by the X-ray diffraction analysis of its methyl ester, whereas the absolute configuration was determined by a novel solid-state TDDFT ECD approach on its methyl ester.

More importantly, macrolide (*R*)-de-O-methyllasiodiplodin (**33**), isolated from the semi-mangrove *Cerbera manghas*, was found to be a potent nonsteroidal antagonist of the mineralocorticoid receptor (MR), a drug target for the treatment of hypertension and other cardiovascular diseases, showing an IC$_{50}$ value of 8.93 µmol/L. Due to its low natural yield, further study on its structural derivatization/modification and the structure-activity relationship (SAR) was conducted. Consequently, a series of analogs were synthesized and evaluated for their MR antagonistic activities[29], and compounds **34–36** were found to exhibit a better selectivity and more potent activity against MR than compound **33**, with IC$_{50}$ values ranging from 0.58 to 1.11 µmol/L.

Chemical studies on Chinese invertebrates
Sponges

Sponges are animals of the phylum Porifera, which consists of approximately 5 000–10 000 species that can be classified mainly according to the composition of their skeletons as calcarea, glass sponges, and demosponges. Their chemical variability results from the individual species, particular metabolism and complex environment. In the past half century, a large number of compounds, including terpenoids, alkaloids, and polyacetylenes, were isolated and characterized from various sponges collected from different regions of the world.

For instance, five new sesquiterpenes, lingshuiolides A and B (**37** and **38**), lingshuiperoxide (**39**), isodysetherin (**40**), and spirolingshuidolide (**41**) were isolated from the Hainan sponge *Dysidea septosa*[30] (Figure 7). The absolute configuration of lingshuiolide B (**38**) was established by using a modified Mosher's method. The chemical study on another *Dysidea* sp led to the discovery of a new sesquiterpene quinone (**42**), along with a known related analog dysidine (**43**)[31] (Figure 7). A bioassay showed that dysidine (**43**) had a potent PTP1B inhibitory activity, with an IC$_{50}$ value of 6.70 µmol/L, whereas the new compound **42** exhibited a moderate PTP1B inhibitory activity and cytotoxicity, with IC$_{50}$ values of 39.50 and 19.45
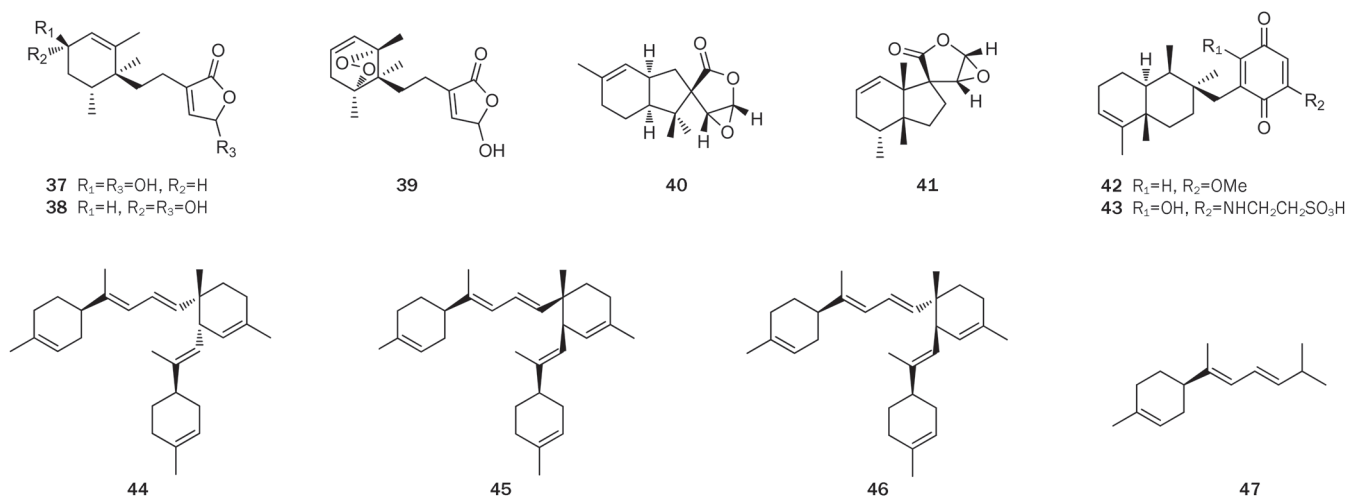
Figure 7. Structures of compounds **37–47**.

μmol/L, respectively[32].

Three unprecedented diastereoisomeric dimers, *cis*-dimers A (**44**) and B (**45**) and *trans*-dimer C (**46**), representing bis-bisabolene skeletons, and their potential precursor dehydrotheonelline (**47**) have been isolated from the South China Sea sponges *Axinyssa variabilis* and *Lipastrotethya ana*[33] (Figure 7). The three diastereoisomers (**44–46**) were possibly biosynthesized through an intermolecular [4+2] Diels-Alder cycloaddition involving two molecules of dehydrotheonelline (**47**). The *trans*- and *cis*-dimers were possibly formed through *exo*- and *endo*-Diels-Alder coupling, respectively (Scheme 3). Furthermore, a mixture of *cis*-dimers **44** and **45** and the pure *trans*-dimer **46** were active at 50 mg/cm² in a feeding-deterrence test against the gold fish *Carassius auratus*, suggesting a possible defensive role for these compounds.

Soft corals

Soft corals from the South China Sea have been extensively studied by Chinese chemists and have yielded a plethora of steroids and terpenoids. It has been suggested that such secondary metabolites produced by soft corals are most likely involved in the defensive mechanisms of the animals; indeed, the animals appear to be relatively free from predation.

As expected, the chemical study of the soft coral *Lobophytum cristatum* Tixier-Durivault led to the isolation of two new prenylgermacrane-type diterpenoids, lobophytumins A and B (**48** and **49**), two new prenyleudesmane-type diterpenoids, lobophytumins C and D (**50** and **51**), and two new spatane-type
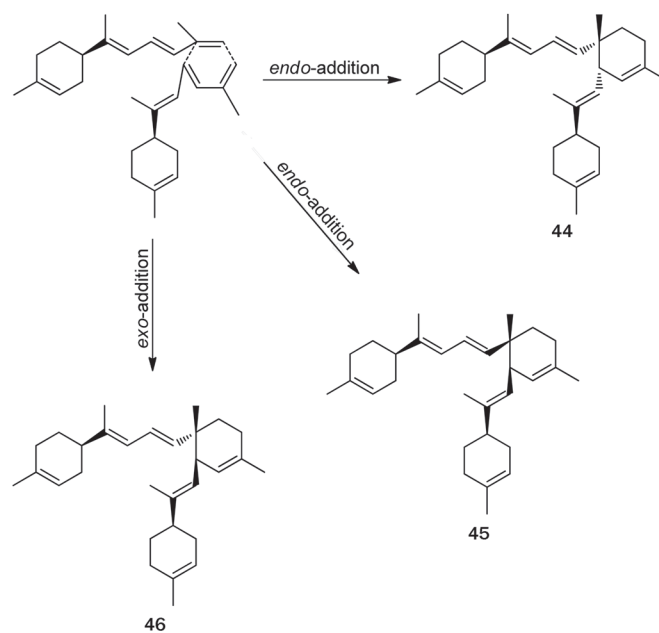
Scheme 3. Possible pathways for compounds **44–46**.

diterpenoids, lobophytumins E and F (**52** and **53**)[34] (Figure 8). Their structures, including the relative configurations, were determined via a detailed analysis of the spectroscopic data and comparison with related known compounds. In addi-
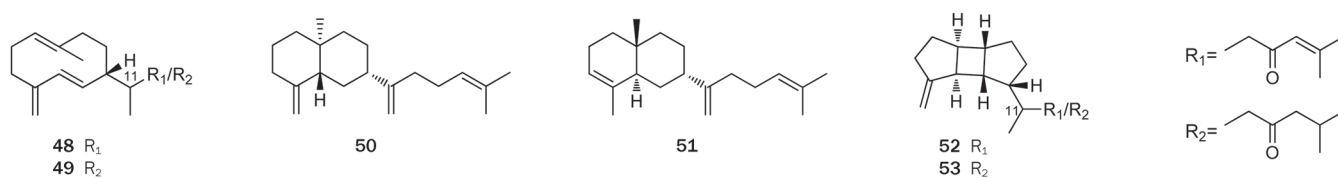

**Figure 8.** Structures of diterpenoids **48–53** from *L cristatum*.

tion, the absolute configuration of lobophytumin C (**50**) was tentatively assigned by comparing its specific rotation with that of the closely related model compound (–)-β-selinene; in contrast, the stereochemistry of C-11 in compounds **48–49** and **52–53** remains undefined. This is the first report of spatane-type diterpenoids from a soft coral source[34], and it supports Faulkner's proposal of prenylgermacrene as the precursor of many diterpenes, including quite different but biogenetically related ones. In a bioactivity evaluation, lobophytumins C and D (**50 and 51**) showed weak *in vitro* cytotoxicities against the tumor cell lines A549 and HCT-116.

Casbane diterpenes are characterized by the presence of a dimethyl-cyclopropyl moiety fused to the 14-membered ring, structures that are extremely rare in nature and marine organisms and previously found only in *Sinularia microclavata*[35]. From the Hainan soft coral *Sinularia depressa*, we isolated nine casbane diterpenes (**54–62**), either *cis* or *trans* ring junctions, including two pairs of epimers: depressin (**54**) and 1-*epi*-depressin (**55**) and 10-hydroxydepressin (**56**) and 1-*epi*-10-hydroxydepressin (**57**)[36] (Figure 9). Compounds **56** and **57** played a key role in the establishment of the absolute stereochemistry, as the *S* configuration at C-10 of both compounds could be easily assigned using Mosher's method. Three further casbanes (**59–61**) displayed identical structures, with the exception of the stereochemistries at the ring junction, which were *cis* in **59** and *trans* in both **60** and **61**. Compound **58** was similar to **57**, except for the oxidization of the hydroxyl; nevertheless, compound **62** had many similarities with 10-hydroxydepressin (**56**), with the exception of an additional oxygen atom. 10-Hydroxydepressin (**56**) showed a cytotoxic activity against the tumor cell lines HepG2 and SW-1990, with IC_{50} values of 61 and 37 μmol/L, respectively, and an antimicrobial activity against *Staphylococcus aureus* and *Escherichia coli* at the concentration of 17 μmol/L.

The genus *Sarcophyton* is a productive source for unusual tetraterpenoids, which are constructed by coupling two cembranoid units through the Diels-Alder reaction. Five novel biscembranoids, ximaolides A–E (**64–68**), together with their proposed biogenetic precursor, methyl tortuosoate (**63**), were isolated from the Hainan soft coral *Sarcophyton tortuosum*[37] (Figure 10). The relative stereochemistries of ximaolides A and E (**64 and 68**) were acquired by X-ray diffraction analysis, whereas the stereochemistries of the other compounds were suggested by both biosynthetic considerations and NOESY experiments. Furthermore, ximaolide D (**67**) is the first example of a biscembranoid possessing a tetrahydrofuran ring

between the A and B rings.

The study of *Sarcophyton lactum* also led to the discovery of two unprecedented biscembranoids, bislatumlides A and B (**69** and **70**), for which the dienophilic double bond belonged to an α,β-conjugated-γ-lactone, along with a new cembranolide diterpene, isosarcophytonolide D (**71**)[38] (Figure 10). Compounds **69** and **70** differ in the configuration of the double bond at C-11: *E* for **69** and *Z* for **70**. However, it was proven that the isomerization of the double bond in **69** readily occurred in the presence of trace amount of acid. Compounds **69** and **70** could be biosynthesized by the Diels-Alder addition of two cembranoid units. Compound **71** and the known compound sarcophytonolide D (**72**) may comprise half of the biosynthetic precursors, as shown in Scheme 4.
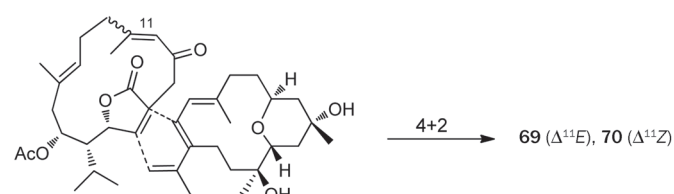
Scheme 4. Plausible Diels–Alder reaction leading to compounds **69** and **70**.

Steroids are a large group of compounds encountered in marine organisms and are reported to display various bioactivities. For instance, a novel steroid with an uncommon 21-oic acid methyl ester moiety, designated methyl spongoate (**73**), was isolated from the Sanya soft coral *Spongodes* sp; this steroid exhibited a potent cytotoxicity against BEL-7402 tumor cells *in vitro*[39]. Later, its stereoselective synthesis was achieved in our laboratory[40]. Owning to its unusual structure and potent cytotoxicity, a number of analogs with different C-20 side chains were synthesized and evaluated for their cytotoxic activities, and some of the analogs were found to be more potent than compound **73** against the A549, HCT-116, HepG2, SW-1990, MCF-7, and NCI-H460 tumor cell lines. The preliminary SAR study suggested that the unsaturated carbonyl moiety, a Michael acceptor in ring A, and the C-20 side chain played important roles in the cytotoxic effect of these derivatives[41] (Figure 10).

Mollusks

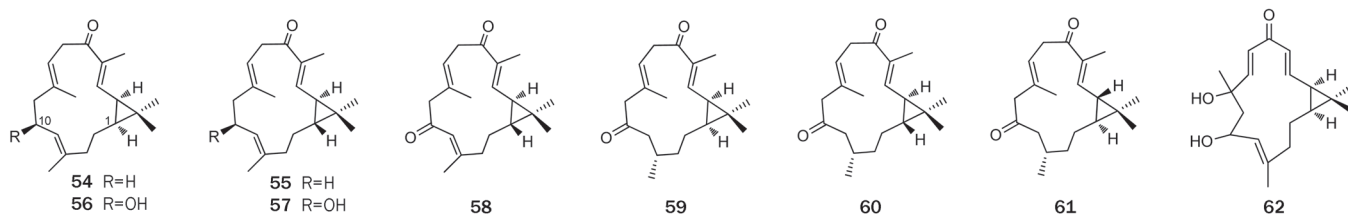Mollusks are a large phylum of invertebrate animals that are

Figure 9. Structures of casbane diterpenes **54–62**.

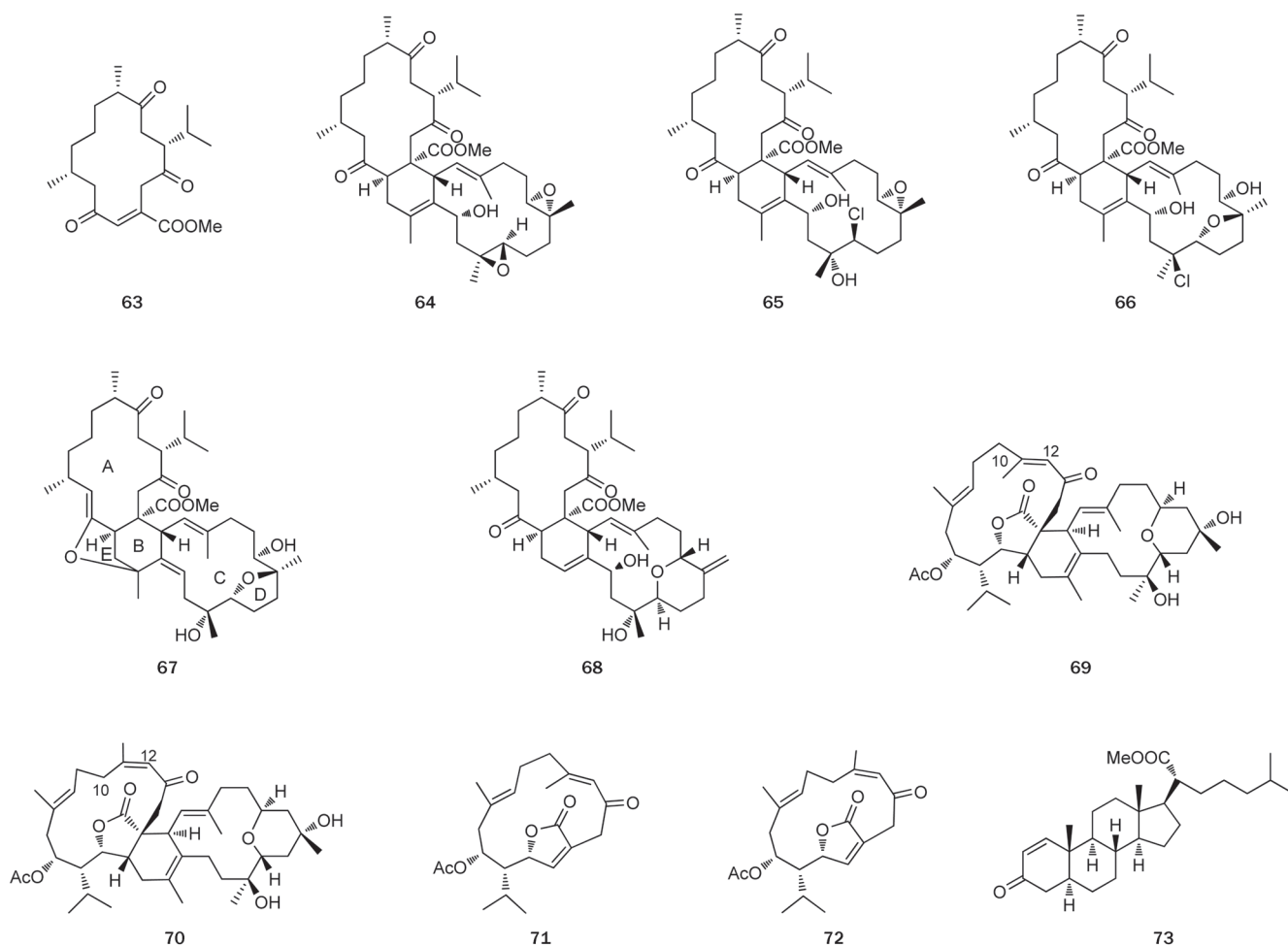54 R=H
56 R=OH

55 R=H
57 R=OH

58

59

60

61

62

Figure 10. Structures of biscembranoids **63–73**.

highly diverse in size and anatomical structure and also in their behavior and habitat. Mollusks show such a variety in body structures that it is difficult to find definite characteristics that apply to all of the classification groups. The two most universal features are a mantle with an important cavity used for breathing and excretion and the structure of the nervous system. However, most of the animals in the Opisthobranchia family lose their mantles and require other defensive system for protection. Thus, these animals usually produce structurally diverse substances to form a chemical defensive system, representing a different source of bioactive compounds from marine organisms. As expected, a series of metabolites with complex structures and intriguing biological activities have been isolated from mollusks.

The study on the South China Sea nudibranch *Tritoniopsis elegans* led to the isolation of four diterpenes, tritoniopsins A-D (**74–77**), which display an unprecedented pyran ring in the cladiellane framework and represent a novel cladiellane-based diterpene family[42] (Figure 11). These compounds were also found in the nudibranch's prey, *Cladiella krempfi*. The structure of tritoniopsin A (**74**) was elucidated by X-ray diffraction

analysis, whereas the *S* configuration of the hydroxyl at C-6 in tritoniopsin C (**76**) was assigned by applying Mosher's method. Both tritoniopsins A and B (**74** and **75**) were discovered from *T elegans* and *C krempfi*, but, surprisingly, the major compound in this mollusk was tritoniopsin A (**74**). Such an uneven metabolite distribution could be explained by the fact that the mollusk either modified dietary tritoniopsin B (**75**) or selectively accumulated compound **74**. The presence of these unique metabolites in both the nudibranch and the soft coral *C krempfi* also confirmed the trophic relationship between the predator and prey.

During the investigation of the nudibranch *Glossodoris rufomarginata* and its unidentified prey sponge from the South China Sea, it was observed that scalaradial (**78**) and its deacetyl derivative (**79**) were the main components of the extract of the dietary sponge, whereas a series of related scalaranes (**80–84**) (Figure 11), most likely derived from dietary scalaradial, were isolated from the mollusk, thus proving the ability of *Glossodoris rufomarginata* to modify dietary molecules[43]. The finding of these molecules (**80**, **81**, and **84**) with a keto functionalization at C-12 is particularly interesting.
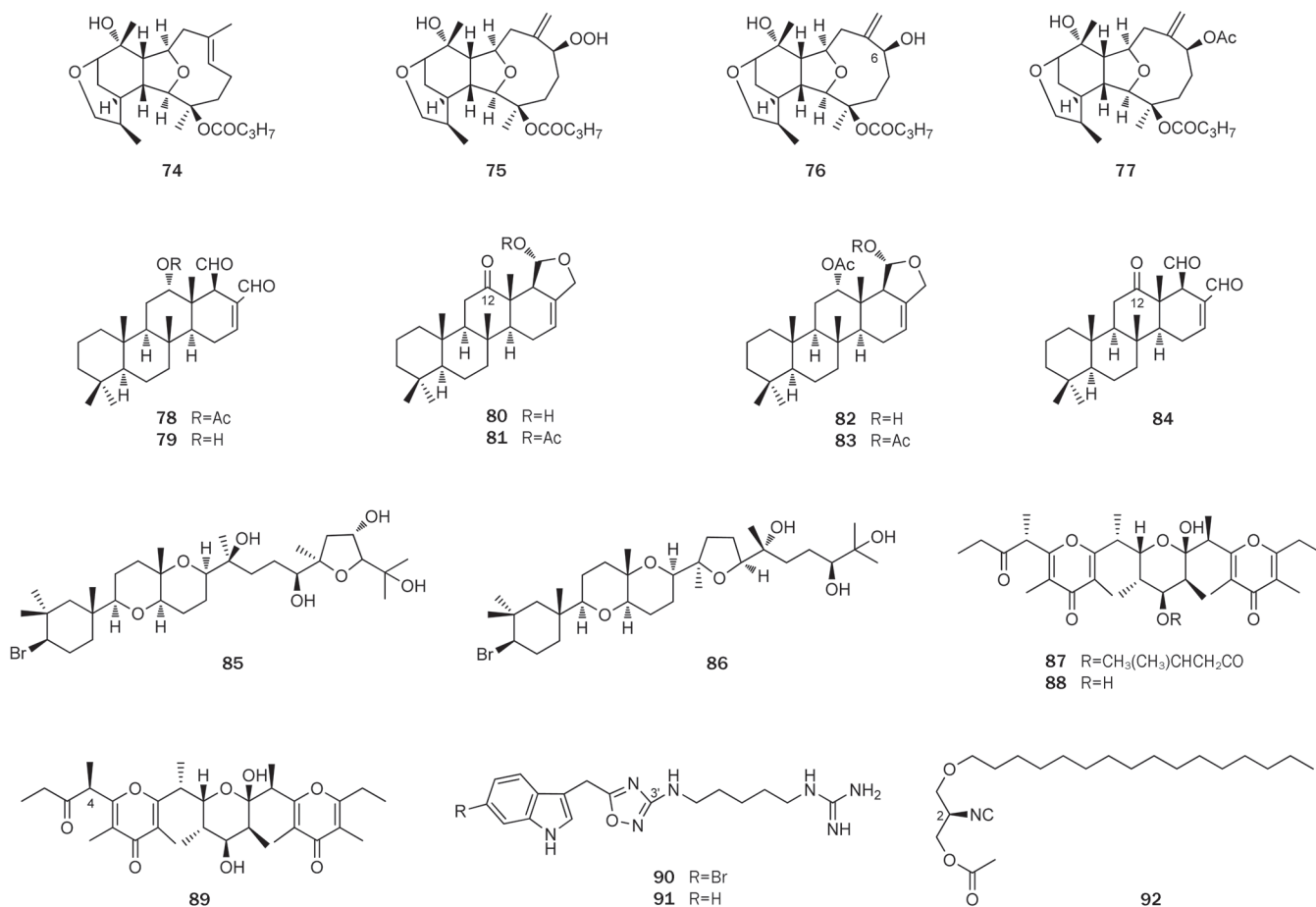
Figure 11. Structures of the compounds **74–92** from mollusks.

This structural feature is quite common in the homoscalarane series but unusual in the scalaranes, and in particular it has been encountered only in nudibranch metabolites. In fact, in addition to 12-deacetoxy-12-oxo-deoxoscalarin (**80**), previously isolated from Indian *Glossodoris atromarginata*[44], only one 12-keto-scalarane, 12-deacetoxy-12-oxo-18-epi-scalaradial, from Pacific nudibranch *Chromodoris youngbleuthi*[45], has been previously reported.

In our research on the sea hare *Aplysia dactylomela*, two novel triterpenes, aplysiols A and B (**85** and **86**), characterized as squalene-derived polyethers, were isolated[46] (Figure 11). The absolute stereochemistry of aplysiol A (**85**) was determined using Mosher's method and biogenetic considerations, whereas the configuration of aplysiol B (**86**) was established by an integrated NMR-QM (quantum mechanical) approach on the basis of ^{13}C NMR chemical shifts and $^{2,3}J_{C-H}$ coupling-constant DFT (density functional theory) calculations.

Marine pulmonata of the Onchidiidae family are shell-less mollusks living on sheltered intertidal shores. Previous chemical studies on distinct species in this family mostly focused on polypropionates. In our study, onchidione (**87**), as the main metabolite, was characterized from the first collection of the Chinese marine pulmonate *Onchidium* sp (Figure 11), which

was present both in the mucus and in the mantle[47]. The structure of the polypropionate was suggested by an analysis of spectral data. In particular, the relative stereochemistry of the central ring was supported by a series of nuclear overhauser enhancement (NOE) experiments, and the complete structure was confirmed by X-ray diffraction analysis. A recent study on the second collection of the mollusk led to the isolation of onchidiol (**88**) and 4-*epi*-onchidiol (**89**), related alcohols of onchidione (**87**)[48] (Figure 11). The absolute configurations of onchidiol (**88**) and 4-*epi*-onchidiol (**89**) were established by TDDFTECD. Moreover, the absolute chemistry of onchidione (**87**) was corroborated by X-ray diffraction analysis, with the final refinement using Cu-$K\alpha$ data.

In the final section of this review, we describe the nitrogen-containing compounds of marine mollusks. The first example consists of phidianidines A and B (**90** and **91**) obtained from *Phidiana militaris*, belonging to the Glaucidae family[49] (Figure 11). The two novel alkaloids were characterized with an unprecedented carbon skeleton featuring the presence of a 1,2,4-oxadiazole ring linking the indole system through a methylene bridge and displaying an aminoalkylguanidine group at C-3'. The 1,2,4-oxadiazole ring is extremely rare in nature. The phidianidines were tested in a panel of tumor

cell lines (C6 rat glioma cells, HeLa human epithelial cervical cancer cells and CaCo-2 human epithelial colorectal adenocarcinoma cells) and non-tumor cell lines (H9c2 rat embryonic cardiac myoblasts and 3T3-L1 murine embryonic fibroblasts) and showed a strong and selective activity against C6 and 3T3-L1 cells by IC$_{50}$ values within the nanomolar range, as shown in Table 1.

Table 1. Cytotoxicity profile of compounds **90** and **91** against tumor and non-tumor cell lines, IC$_{50}$ (μmol/L)[a].

Cell line	Phidianidine A (**90**)	Phidianidine B (**91**)
C6	**0.642±0.2**	**0.98±0.3**
HeLa	1.52±0.3	**0.417±0.4**
CaCo-2	35.5±4	100.2±8.5
3T3-L1	**0.14±0.2**	**0.786±0.3**
H9c2	2.26±0.6	5.42±0.8

[a] IC$_{50}$ values are expressed as mean±SEM (*n*=24) of the three independent experiments. Bold values show IC$_{50}$ of less than 1 μmol/L.

The second example is an unusual molecule, actisonitrile (**92**), found in the mantle of *Actinocyclus papillatus*[50] (Figure 11), belonging to the Actinocyclidae family that is another family of opisthobranch, which was never studied thus far. Despite its structure is quite simple, the determination of the absolute stereochemistry of **92** was a challenging task, yet its absolute configuration was recently solved by a synthetic approach. Thus, both the *S* and *R* enantiomers were synthesized, and the comparison of optical rotation and CD profile of the natural product with those of the pair of the synthetic enantiomers resulted in the assignment of the *R* configuration at the C-2 position of compound **92**.

Conclusions

This review summarizes representative substances from Chinese marine plants and invertebrates found by our group, indicating that marine organisms are an inexhaustible source of new molecules that often display unique structures and sometimes have very interesting pharmacological properties, such as antifungal, antibacterial, enzyme-inhibitory, and other activities. Some of the compounds isolated from marine organisms even show promising activities within the nanomolar range and can be developed as drug candidates or at least lead compounds in the near future. Although our research on marine natural products is limited, it has established the foundation for further studies.

Because our understanding of the biosynthetic origin and the real ecological role of these bioactive compounds remains incomplete, further research to clarify these important issues is necessary.

References

1 Huang XC, Zhao D, Guo YW, Wu HM, Trivellone E, Cimino G. Lingshuiols A and B, two new polyhydroxy compounds from the Chinese marine dinoflagellate *Amphidinium* sp. Tetrahedron Lett 2004; 45: 5501–4.

2 Huang XC, Zhao D, Guo YW, Wu HM, Lin LP, Wang ZH, *et al*. Lingshuiol, a novel polyhydroxyl compound with strongly cytotoxic activity from the marine dinoflagellate *Amphidinium* sp. Bioorg Med Chem Lett 2004; 14: 3117–20.

3 Doi Y, Ishibashi M, Nakamichi H, Kosaka T, Ishikawa T, Kobayashi J. Luteophanol A, a new polyhydroxyl compound from symbiotic marine dinoflagellate *Amphidinium* sp. J Org Chem 1997; 62: 3820–3.

4 Paul GK, Matsumori N, Murata M, Tachibana K. Isolation and chemical structure of amphidinol 2, a potent hemolytic compound from marine dinoflagellate *Amphidinium klebsii*. Tetrahedron Lett 1995; 36: 6279–82.

5 Satake M, Murata M, Yasumoto T, Fujita T, Naoki H. Amphidinol, a polyhydroxy-polyene antifungal agent with an unprecedented structure, from a marine dinoflagellate, *Amphidinium klebsii*. J Am Chem Soc 1991; 113: 9859–61.

6 Irie T, Suzuki M, Masamune T. Laurencin, a constituent from laurencia species. Tetrahedron Lett 1965; 6: 1091–9.

7 Mao SC, Guo YW. A laurane sesquiterpene and rearranged derivatives from the Chinese red alga *Laurencia okamurai* Yamada. J Nat Prod 2006; 69: 1209–11.

8 Mao SC, Guo YW. Sesquiterpenes from algae of the *Genus Larencia*: chemistry and biological activities. Chin Tradit Herb Drugs 2004; 35: 8–18.

9 Mao SC, Guo YW, Shen X. Two novel aromatic valerenane-type sesquiterpenes from the Chinese green alga *Caulerpa taxifolia*. Bioorg Med Chem Lett 2006; 16: 2947–50.

10 Wang BS, Liang SC, Zhang WY, Zan QJ. Mangrove Flora of the world. Acta Bot Sin 2003; 45: 644–53.

11 Li MY, Xiao Q, Pan JY, Wu J. Natural products from semi-mangrove flora: source, chemistry and bioactivities. Nat Prod Rep 2009; 26: 281–98.

12 Sun YQ, Guo YW. Gymnorrhizol, an unusual macrocyclic polydisulfide from the Chinese mangrove *Bruguiera gymnorrhiza*. Tetrahedron Lett 2004; 45: 5533–5.

13 Sun YQ, Guo YW. Crystal structure of 1,2,6,7,11,12-hexathia-cyclopentadecane-4,9,14-triol, C$_9$H$_{18}$O$_3$S$_6$. Z Kristallogr NCS 2004; 219: 121–3.

14 Gong JX, Shen X, Yao LG, Jiang H, Krohn K, Guo YW. Total synthesis of gymnorrhizol, an unprecedented 15-membered macrocyclic polydisulfide from the Chinese mangrove *Bruguiera gymnorrhiza*. Org Lett 2007; 9: 1715–6.

15 Huang XY, Wang Q, Liu HL, Zhang Y, Xin GR, Shen X, *et al*. Diastereoisomeric macrocyclic polydisulfides from the mangrove *Bruguiera*

gymnorrhiza. Phytochemistry 2009; 70: 2096–100.

16 Jiang CS, Muller WE, Schroder HC, Guo YW. Disulfide- and multisulfide-containing metabolites from marine organisms. Chem Rev 2012; 112: 2179–207.

17 Cai YS, Kurtan T, Miao ZH, Mandi A, Komaromi I, Liu HL, *et al*. Palmarumycins BG1-BG7 and preussomerin BG1: establishment of their absolute configurations using theoretical calculations of electronic circular dichroism spectra. J Org Chem 2011; 76: 1821–30.

18 Wang L, Zhang CF, Wang ZT, Zhang M, Xu LS. Five new compounds from *Dendrobium crystallinum*. J Asian Nat Prod Res 2009; 11: 903–11.

19 Prajoubklang A, Sirithunyalug B, Charoenchai P, Suvannakad R, Sriubolmas N, Piyamongkol S, *et al*. Bioactive deoxypreussomerins and dimeric naphthoquinones from *Diospyros ehretioides* fruits: deoxypreussomerins may not be plant metabolites but may be from fungal epiphytes or endophytes. Chem Biodivers 2005; 2: 1358–67.

20 Ravindranath N, Ravinder Reddy M, Mahender G, Ramu R, Ravi Kumar K, Das B. Deoxypreussomerins from *Jatropha curcas*: are they also plant metabolites? Phytochemistry 2004; 65: 2387–90.

21 Kouam TNM, Lavaud C, Massiot G, Nuzillard JM, Connolly JD, Ryeroft DS. Bipendensin, an unusual phenolic acetal from *Afzelia bipendensis*. Nat Prod Lett 1993; 3: 299–303.

22 Cai YS, Guo YW, Krohn K. Structure, bioactivities, biosynthetic relationships and chemical synthesis of the spirodioxynaphthalenes. Nat Prod Rep 2010; 27: 1840–70.

23 Chen XL, Liu HL, Li J, Xin GR, Guo YW. Paracaseolide A, first alpha-alkylbutenolide dimer with an unusual tetraquinane oxa-cage bis-lactone skeleton from Chinese mangrove *Sonneratia paracaseolaris*. Org Lett 2011; 13: 5032–5.

24 Hill RA, Sutherland A. Hot off the press. Nat Prod Rep 2011; 28: 1879–82.

25 Liu HL, Huang XY, Li J, Xin GR, Guo YW. Absolute configurations of integracins A, B, and 15'-dehydroxy-integracin B. Chirality 2012; 24: 459–62.

26 Wang JD, Zhang W, Li ZY, Xiang WS, Guo YW, Krohn K. Elucidation of excogallochaols A–D, four unusual diterpenoids from the Chinese mangrove *Excoecaria agallocha*. Phytochemistry 2007; 68: 2426–31.

27 Qin S, Liang JY, Gu YC, Guo YW. Suffruticosine, a novel octacyclic alkaloid with an unprecedented skeleton from *Securinega suffruticosa* (Pall) Rehd. Tetrahedron Lett 2008; 49: 7066–9.

28 Wang JR, Liu HL, Kurtan T, Mandi A, Antus S, Li J, *et al*. Protolimonoids and norlimonoids from the stem bark of *Toona ciliata* var pubescens. Org Biomol Chem 2011; 9: 7685–96.

29 Jiang CS, Zhou R, Gong JX, Chen LL, Kurtan T, Shen X, *et al*. Synthesis, modification, and evaluation of (*R*)-de-O-methyllasiodiplodin and analogs as nonsteroidal antagonists of mineralocorticoid receptor. Bioorg Med Chem Lett 2011; 21: 1171–5.

30 Huang XC, Li J, Li ZY, Shi L, Guo YW. Sesquiterpenes from the Hainan Sponge *Dysidea septosa*. J Nat Prod 2008; 71: 1399–403.

31 Li Y, Zhang Y, Shen X, Guo YW. A novel sesquiterpene quinone from Hainan sponge *Dysidea villosa*. Bioorg Med Chem Lett 2009; 19: 390–2.

32 Zhang Y, Li Y, Guo YW, Jiang HL, Shen X. A sesquiterpene quinone, dysidine, from the sponge *Dysidea villosa*, activates the insulin pathway through inhibition of PTPases. Acta Pharmacol Sin 2009; 30: 333–45.

33 Mao SC, Manzo E, Guo YW, Gavagnin M, Mollo E, Ciavatta ML, *et al*. New diastereomeric bis-sesquiterpenes from Hainan marine sponges

*Axinyssa variabili*s and *Lipastrotethya ana*. Tetrahedron 2007; 63: 11108–13.

34 Li L, Sheng L, Wang CY, Zhou YB, Huang H, Li XB, *et al*. Diterpenes from the Hainan soft coral *Lobophytum cristatum* Tixier-Durivault. J Nat Prod 2011; 74: 2089–94.

35 Zhang CX, Yan SJ, Zhang GW, Lu WG, Su JY, Zeng LM, *et al*. Cytotoxic diterpenoids from the soft coral *Sinularia microclavata*. J Nat Prod 2005; 68: 1087–9.

36 Li Y, Carbone M, Vitale RM, Amodeo P, Castelluccio F, Sicilia G, *et al*. Rare casbane diterpenoids from the Hainan soft coral *Sinularia depressa*. J Nat Prod 2010; 73: 133–8.

37 Jia R, Guo YW, Chen P, Yang YM, Mollo E, Gavagnin M, *et al*. Biscembranoids and their probable biogenetic precursor from the Hainan soft coral *Sarcophyton tortuosum*. J Nat Prod 2007; 70: 1158–66.

38 Yan XH, Gavagnin M, Cimino G, Guo YW. Two new biscembranes with unprecedented carbon skeleton and their probable biogenetic precursor from the Hainan soft coral *Sarcophyton latum*. Tetrahedron Lett 2007; 48: 5313–6.

39 Yan XH, Lin LP, Ding J, Guo YW. Methyl spongoate, a cytotoxic steroid from the Sanya soft coral *Spongodes* sp. Bioorg Med Chem Lett 2007; 17: 2661–3.

40 Gong JX, Miao ZH, Yao LG, Ding J, Kurtan T, Guo YW. Stereoselective synthesis of methyl spongoate, a new steroid with potent antitumor activities. Synlett 2010; 2010: 480–2.

41 Jiang CS, Huang CG, Feng B, Li J, Gong JX, Kurtan T, *et al*. Synthesis and antitumor evaluation of methyl spongoate analogs. Steroids 2010; 75: 1153–63.

42 Ciavatta ML, Manzo E, Mollo E, Mattia CA, Tedesco C, Irace C, *et al*. Tritoniopsins A–D, cladiellane-based diterpenes from the South China Sea nudibranch *Tritoniopsis elegans* and its prey *Cladiella krempfi*. J Nat Prod 2011; 74: 1902–7.

43 Gavagnin M, Mollo E, Docimo T, Guo YW, Cimino G. Scalarane metabolites of the nudibranch *Glossodoris rufomarginata* and its dietary sponge from the South China Sea. J Nat Prod 2004; 67: 2104–7.

44 Fontana A, Cavaliere P, Ungur N, D'Souza L, Parameswaram PS, Cimino G. New scalaranes from the nudibranch *Glossodoris atromarginata* and its sponge prey. J Nat Prod 1999; 62: 1367–70.

45 Terem B, Scheuer PJ. Scalaradial derivatives from the nudibranch chromodoris youngbleuthi and the sponge spongia oceania. Tetrahedron 1986; 42: 4409–12.

46 Manzo E, Gavagnin M, Bifulco G, Cimino P, Di MS, Ciavatta ML, *et al*. Aplysiols A and B, squalene-derived polyethers from the mantle of the sea hare *Aplysia dactylomela*. Tetrahedron 2007; 63: 9970–8.

47 Carbone M, Gavagnin M, Mattia CA, Lotti C, Castelluccio F, Pagano B, *et al*. Structure of onchidione, a bis-γ-pyrone polypropionate from a marine pulmonate mollusk. Tetrahedron 2009; 65: 4404–9.

48 Wang JR, Carbone M, Gavagnin M, Mandi A, Antus S, Yao LG, *et al*. Assignment of absolute configuration of bis-γ-pyrone polypropionates from marine pulmonate molluscs. Eur J Org Chem 2012; 2012: 1107–11.

49 Carbone M, Li Y, Irace C, Mollo E, Castelluccio F, Di Pascale A, *et al*. Structure and cytotoxicity of phidianidines A and B: first finding of 1,2,4-oxadiazole system in a marine natural product. Org Lett 2011; 13: 2516–9.

50 Manzo E, Carbone M, Mollo E, Irace C, Di Pascale A, Li Y, *et al*. Structure and synthesis of a unique isonitrile lipid isolated from the marine mollusk *Actinocyclus papillatus*. Org Lett 2011; 13: 1897–9.

npg

Perspective

New insights into huperzine A for the treatment of Alzheimer's disease

Hai-yan ZHANG*

State Key Laboratory of Drug Research, Shanghai Institute of Materia Medica, Chinese Academy of Sciences, Shanghai 201203, China

Huperzine A, an active *Lycopodium* alkaloid extracted from traditional Chinese herb, is a potent, selective and reversible acetylcholinesterase (AChE) inhibitor and has been widely used in China for the treatment of Alzheimer's disease (AD). Accordingly, some new mechanisms of action for huperzine A have been discovered over the past decades. In addition to its AChE inhibitory effect, potent multifaceted neuroprotective effect through activating cholinergic system and directly acting on mitochondria have been explored. Moreover, in order to maximize the efficacy and safety of huperzine A therapy, great efforts have been made to optimize drug delivery system. In the present article, an attempt is made to discuss the current progress and future perspective for huperzine A therapy in AD.

Introduction

Alzheimer's disease (AD) is a neurodegenerative disorder characterized by gradually loss of memory and other cognitive functions. Understanding the complexity of AD and its underlying pathophysiological mechanisms of AD provides a potential new paradigm that may help to develop new AD treatment[1]. Among the limited therapeutic approaches, cholinergic replacement therapy especially acetylcholinesterase inhibitors (AChEIs), has been at the forefront of efforts to pharmacologically ameliorate the symptom of AD patients. So far, four AChEIs, tacrine, donepezil, rivastigmine, and galantamine, have been approved by the United States Food and Drug Administration for the treatment of mild or moderate AD.

Huperzine A is a novel *Lycopodium* alkaloid isolated from Chinese herb *Huperzia serrata* (Thunb) Trev (Qian Ceng Ta), which was traditionally used to relieve pain, antidote the poison, as well as alleviate swelling. Huperzine A is widely proved to be a potent, selective and well-tolerated inhibitor of acetylcholinesterase (AChE) (reviewed by[2]). This effect was accidentally discovered in the 1970s while herbal extraction of *Huperzine serrata* was used to treat schizophrenia and found with significant cholinergic side effects. Huperzine A was

approved by State Food and Drug Administration of China for AD therapy in 1994. Since then, large amount of clinical studies have shown that huperzine A administration can significantly improve the memory, cognitive skills, and daily life abilities of AD patients with no severe side effects. Besides being indicated for AD, huperzine A is also used in treating memory impairment in vascular dementia (VaD) patients, schizophrenia patients and sleep disorder in insomniacs (reviewed by[2]).

Suggestions on the multifaceted neuroprotective effects of huperzine A came from its superior preclinical and clinical benefits as compared with other clinically used AChEIs, and also from large numbers of laboratory studies evaluating the mechanisms of this compound (reviewed by[3]). This perspective summarizes the evidences of novel insights of huperzine A to reduce AD risk, the molecular mechanisms involved in the anti-AD effects of huperzine A aside from its traditional AChE inhibition, and the novel delivery system which modified release patterns of this drug.

Multifaceted pharmacological effects of huperzine A: cholinergic-dependent and -independent mechanism

Although we are still at the stage of symptomatic treatments for AD since AChEIs remains the most widely used drugs, we are moving into an age in which disease-modifying agents, particularly, drugs with potent neuroprotective effect are considered to play a significant role in delaying AD development.

Interestingly, recent studies reveal that huperzine A, might be of disease-modifying properties. The classical cholinergic effect and novel potential non-cholinergic actions of huperzine A are discussed as following paragraphs and summarized as Figure 1.

Multiple lines of evidences proved that huperzine A is a mixed-competitive and reversible AChE inhibitor, which shows higher potency and selectivity of AChE inhibition both *in vitro* and *in vivo* as compared with galanthamine, donepezil, tacrine, and rivastigmine (reviewed by[2]). The potent inhibitory effect on AChE could in turn markedly enhance the synaptic ACh release and consequently cholinergic neurotransmission. Beside aforementioned classical effects, more and more beneficial characters of huperzine A are continuously discovered by employing various AD models, mainly from two aspects: expanded effects of cholinergic system in neuroprotection, and novel pharmacological target independent of its AChE inhibitory effect.

Cholinergic system is well established as an important part of the neuronal circuitry that modulates cognition, while, muscarinic and nicotinic ACh receptor antagonists are well known to produce or exacerbate cognitive impairments, respectively[4–7]. Although ACh is generally considered to be a neurotransmitter, it can also function as a cytokine and might participate in various neuroprotective pathways: close association was found between ACh and the neurotrophins nerve growth factor (NGF) and brain-derived neurotrophic factor in the rat hippocampus[8]; activating M1 muscarinic ACh receptor could activate the non-amyloidogenic APP pathway[9, 10]; α7 nicotinic ACh receptor is increasing believed to be a critical link between inflammation and neurodegeneration in AD[11].

In line with this observation, huperzine A administration was found to enhance the expression and secretion of NGF, as well as increase p75NTR mRNA in primary astrocytes[12], enhance the non-amyloidogenic pathway by increasing the levels of sAPPα[13] possibly associated with M1 muscarinic ACh receptor mediated pathway[14–16], and reduce the hypoxia ischemia-triggered inflammatory response through α7 nicotinic ACh receptor[17–19]. Since previous study has proven that huperzine A had no direct effect on the amplitude or kinetics of nAChRs activation[20], above cholinergic system-associated beneficial effects of huperzine A administration may mainly act through the enhancement of synaptic ACh level. These neuroprotective effects are probably potential common performance of cholinergic activation, since similar results are found from other AChEIs[21–23].

As shown in Figure 1, effect of huperzine A on the cholinergic system may simultaneously contribute to symptomatic and disease modifying efficacy in AD. Meanwhile, huperzine A was recently found to exhibit additional benefits that appear to be independent of AChE inhibition, and differentiate the drug from other AChEIs. It is well known that mitochondria are the powerhouse of the cell which participates in a number of physiological functions[24], and the mitochondrial dysfunction is considered as one of the key intracellular lesions associated with the pathogenesis of AD[25]. We recently discovered that huperzine A was able to effectively ameliorate brain mitochondrial malfunction under Aβ[26–28] or ischemia insult[29]. We further elucidated that the ameliorative effects of huperzine A on Aβ-induced mitochondrial dysfunction are associated with the reduced production in reactive oxygen species (ROS) and the increases in the activities of some key components of
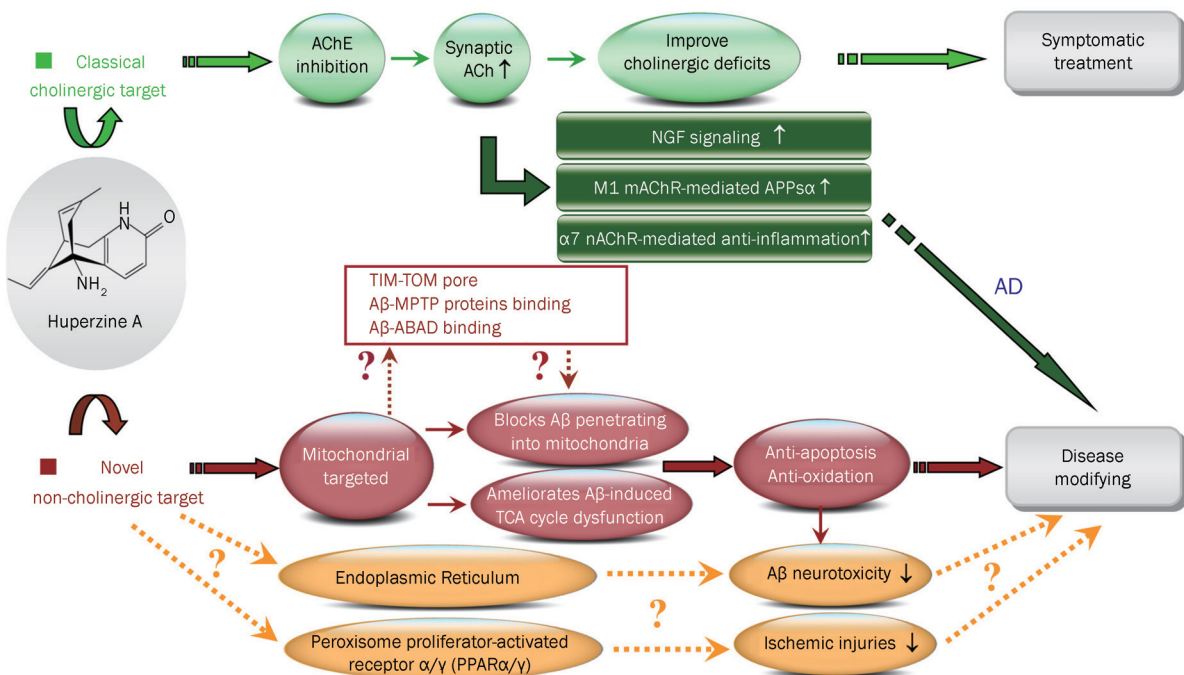

Figure 1. Summary of classical cholinergic and potential non-cholinergic pharmacological targets of huperzine A.

the respiratory chain and key enzymes in tricarboxylic acid (TCA) cycle[26–28]. These findings clearly implicate that mitochondrion appears to be an important target of huperzine A, which is further supported by the findings that huperzine A inhibited the penetration of Aβ into mitochondria and ameliorated Aβ-induced TCA cycle dysfunction in isolated brain cortical mitochondria[28]. The mitochondria-targeted effects of huperzine A are clearly independent of cholinergic system since there is no evidence indicated the existence of cholinergic system in isolated brain mitochondria. As mitochondria participate in a number of physiological functions that include calcium homeostasis, signal transduction, oxidative stress and apoptosis. This potential independent pharmacological target of huperzine A on mitochondria may further interpret the anti-oxidative stress[30–36] and anti-apoptotic effects[30, 31, 37–39] shown by huperzine A administration in various *in vivo* and *in vitro* models (Figure 1). Interestingly, several lines of evidence suggest that Aβ directly interacts with several proteins on and inside mitochondria[40]: Aβ could import into mitochondria through a pore formed by the outer membrane (TOM40) and the inner membrane (TIM22)[41]; Aβ could also interact with mitochondrial proteins from the membrane permeability transition pore (MPTP)[42], which may in turn affect the mitochondrial membrane potential; Aβ was also reported to bind with β-amyloid binding alcohol dehydrogenase (ABAD) upon entering into mitochondria and leading to mitochondrial dysfunction[43, 44]. Although the precise molecular target of huperzine A on Aβ-induced mitochondrial dysfunction remains to be clarified, whether and how huperzine A affects above mentioned Aβ-mitochondrion interactions could be a very promising future project.

Emerging evidence implies that a ligand-activated nuclear transcription factor, peroxisome proliferator-activated receptor (PPAR), could be a potential pharmacological target against inflammation and brain damage after ischemic injury[45–47], and potent dual PPARα/γ agonist exerted anti-inflammatory and neuroprotective effects[48]. Moreover, similar as mitochondrion, endoplasmic reticulum (ER) is a multifunctional organelle that plays a central role in various malignant events in AD (reviewed by[49]). Considerable studies have proved that huperzine A could effectively ameliorate ischemic injuries in various *in vivo* and *in vitro* models[15, 17–19, 29], and our preliminary data also showed that huperzine A could affect Aβ-associated abnormal ER function (unpublished data). In order to further understand the above beneficial effects, it is also worthy to explore whether huperzine A could target on PPAR or ER.

Controlled delivery of huperzine A as a better drug administrtion strategy

Based on multifaceted beneficial profiles and well confirmed memory improvement effects, huperzine A has been proved to be one of the most promising agents for palliative therapy of cognitive deficits in patients with AD. The recommended dose of huperzine A for the clinical practice in China is 150–250 μg b.i.d, and the most-recently published phase II clinical trial

conducted in the United States showed that mild to moderate AD patients treated with huperzine A (400 μg b.i.d.) manifested significant improvement in cognitive function as compared to placebo[50]. Meanwhile, it is also important to assess the side effects and tolerability of huperzine A therapy at the clinically used doses. As a specific AChE inhibitor, it will be easy to predict that adverse effects of huperzine A should relate to the well-known cholinergic activity. In fact, two US Phase I studies have shown that, although rated as mild scale, adverse symptoms included tachycardia, low energy levels, and hypertension at multiple dose ranges; bradycardia, headache, and intense dreams at a dose of 400 μg b.i.d.; muscle cramps at 400 μg b.i.d.; arthralgia at 300–400 μg b.i.d.

Taken together, the efficacy and safety data from clinical trails of huperzine A treatment indicated that larger doses of huperzine A were needed for better clinical effects in AD patients, however, the increasing of dosage may also increase the possibility of emergency of more severe side effects[51]. It will be therefore very interesting to unravel the rational behind above phenomenon and search for proper solution. The pharmacokinetic data indicated that huperzine A had a rapid and nearly complete oral absorption and was extensively distributed into tissues after drug administration in dogs[52]. The concentration of huperzine A in plasma quickly reached its peak at 1.25 h with a steep ratio after oral administration, the oral bioavailability is about 94%[52], and approximately 20% of the huperzine A level in plasma reached the cerebrospinal fluid after both intranasal and intravenous administration[53]. In combination of clinical, pharmacological and pharmacokinetic data, it is suggested that the increased side effect caused by high dosage of huperzine A may attribute to the promptly reached peak plasma drug level after oral administration, while the better efficacy shown by high dosage of huperzine A may due to higher level and longer duration of huperzine A in the plasma at this situation, besides, the high blood-brain-barrier penetration rate allows more huperzine A entering into the brain and maintain at a higher level, which could also enhance the efficacy of huperzine A.

At present, huperzine A is available in the market mainly as tablet or capsule, which has to be given orally 2–3 times per day. The pharmacokinetic parameters of huperzine A determined that it is difficult to optimize both efficacy and safety of the drug with the current two formulations, and it is not convenient for AD patient who suffers memory disorder not to miss scheduled self-medication. Therefore, developing new sustained released drug formulations with long-term efficacy may solve afore-mentioned problems. Currently, several new controlled released formulations are developed, most of them are performed on huperzine A loaded poly (lactic-co-glycolic acid) (PLGA) microspheres using an oil/water emulsion solvent evaporation technique[54–56], and the period of the sustained release could range from one day to six weeks. While which delivery system exerts best efficacy still remain to be explored, it is reported that ACh has been implicated in cortical synaptic plasticity and memory processes, and suggested the existence of a circadian rhythm in central cholinergic trans-

mission, which modulates memory processes, with high ACh levels during wakefulness and reduced levels during slow-wave sleep[57]. Therefore, huperzine A sustained release formulation with long lasting over than 12 h may not be a good choice, based on the evidence that low levels of ACh during slow-wave sleep were critical for the consolidation of declarative memory[58]. Developing novel delivery system with stable and proper plasma concentrations during active cycle (light cycle for human) could be a promising strategy to create better clinical efficacy in AD therapy.

Conclusions and future prospects

AD is a multi-causal progressive neurodegenerative disease with complicated pathogenesis, the major current obstacle of this mysterious syndrome is the lack of effective therapeutic strategy. However, based on the fact that a big gap exists between bench research and clinical application, which is termed as "valley of death"[59], large increases in spending on medical research have not produced corresponding increases in new effective therapeutic strategy. Recently, the concept of "translational medicine" is increasingly used to bridge benchside to bedside, in order to broaden and deepen the understanding of the real fact of AD pathogenesis, and also to shorten the period of drug development. One inneligible aspect is to further understand the beneficial profiles and weakness of an existed effective drug when used in clinical practice, trying to unravel the molecular mechanisms and optimize the medicine performance. This article reflects the research progress made in molecular pharmacology and pharmacological therapy for treating AD with huperzine A, showing that the classical cholinergic and potential non-cholinergic target of huperzine A may shed more light on the successes gained from huperzine A in the AD therapy. Accumulative evidence suggests that single target drug always exert limited clinical effects for AD therapy, while combined therapies or drugs with multi-pharmacological activities would be a promising future therapeutic approach to address the varied pathological aspects of the disease. The multiple neuroprotective effects of huperzine A together with the optimized drug delivery system will give this drug new opportunity to prove its merit, however, further studies still need to be performed to validate its efficacy, especially solid evidence from the bedside.

References

1 Huang Y, Mucke L. Alzheimer mechanisms and therapeutic strategies. Cell 2012; 148: 1204–22.

2 Wang R, Yan H, Tang XC. Progress in studies of huperzine A, a natural cholinesterase inhibitor from Chinese herbal medicine. Acta Pharmacol Sin 2006; 27: 1–26.

3 Zhang HY, Tang XC. Neuroprotective effects of huperzine A: new therapeutic targets for neurodegenerative disease. Trends Pharmacol Sci 2006; 27: 619–25.

4 Domer FR, Schueler FW. Investigations of the amnesic properties of scopolamine and related compounds. Arch Int Pharmacodyn Ther 1960; 127: 449–58.

5 Drachman DA, Leavitt J. Human memory and the cholinergic system. A relationship to aging? Arch Neurol 1974; 30: 113–21.

6 Bartus RT, Dean RL 3rd, Beer B, Lippa AS. The cholinergic hypothesis of geriatric memory dysfunction. Science 1982; 217: 408–14.

7 Sunderland T, Tariot PN, Weingartner H, Murphy DL, Newhouse PA, Mueller EA, et al. Pharmacologic modelling of Alzheimer's disease. Prog Neuropsychopharmacol Biol Psychiatry 1986; 10: 599–610.

8 Knipper M, da Penha Berzaghi M, Blochl A, Breer H, Thoenen H, Lindholm D. Positive feedback between acetylcholine and the neurotrophins nerve growth factor and brain-derived neurotrophic factor in the rat hippocampus. Eur J Neurosci 1994; 6: 668–71.

9 Fisher A, Michaelson DM, Brandeis R, Haring R, Chapman S, Pittel Z. M1 muscarinic agonists as potential disease-modifying agents in Alzheimer's disease. Rationale and perspectives. Ann N Y Acad Sci 2000; 920: 315–20.

10 Rossner S, Ueberham U, Schliebs R, Perez-Polo JR, Bigl V. The regulation of amyloid precursor protein metabolism by cholinergic mechanisms and neurotrophin receptor signaling. Prog Neurobiol 1998; 56: 541–69.

11 Conejero-Goldberg C, Davies P, Ulloa L. Alpha7 nicotinic acetylcholine receptor: a link between inflammation and neurodegeneration. Neurosci Biobehav Rev 2008; 32: 693–706.

12 Tang LL, Wang R, Tang XC. Effects of huperzine A on secretion of nerve growth factor in cultured rat cortical astrocytes and neurite outgrowth in rat PC12 cells. Acta Pharmacol Sin 2005; 26: 673–8.

13 Zhang HY, Yan H, Tang XC. Huperzine A enhances the level of secretory amyloid precursor protein and protein kinase C-alpha in intracerebroventricular beta-amyloid-(1–40) infused rats and human embryonic kidney 293 Swedish mutant cells. Neurosci Lett 2004; 360: 21–4.

14 Tang LL, Wang R, Tang XC. Huperzine A protects SHSY5Y neuroblastoma cells against oxidative stress damage via nerve growth factor production. Eur J Pharmacol 2005; 519: 9–15.

15 Wang ZF, Tang LL, Yan H, Wang YJ, Tang XC. Effects of huperzine A on memory deficits and neurotrophic factors production after transient cerebral ischemia and reperfusion in mice. Pharmacol Biochem Behav 2006; 83: 603–11.

16 Yan H, Zhang HY, Tang XC. Involvement of M1-muscarinic acetylcholine receptors, protein kinase C and mitogen-activated protein kinase in the effect of huperzine A on secretory amyloid precursor protein-alpha. Neuroreport 2007; 18: 689–92.

17 Wang ZF, Tang XC. Huperzine A protects C6 rat glioma cells against oxygen-glucose deprivation-induced injury. FEBS Lett 2007; 581: 596–602.

18 Wang ZF, Wang J, Zhang HY, Tang XC. Huperzine A exhibits anti-inflammatory and neuroprotective effects in a rat model of transient focal cerebral ischemia. J Neurochem 2008; 106: 1594–603.

19 Wang J, Zhang HY, Tang XC. Huperzine A improves chronic inflamma-

tion and cognitive decline in rats with cerebral hypoperfusion. J Neurosci Res 2010; 88: 807–15.

20 Fayuk D, Yakel JL. Regulation of nicotinic acetylcholine receptor channel function by acetylcholinesterase inhibitors in rat hippocampal CA1 interneurons. Mol Pharmacol 2004; 66: 658–66.

21 Shigeta K, Ootaki K, Tatemoto H, Nakanishi T, Inada A, Muto N. Potentiation of nerve growth factor-induced neurite outgrowth in PC12 cells by a *Coptidis Rhizoma* extract and protoberberine alkaloids. Biosci Biotechnol Biochem 2002; 66: 2491–4.

22 Giacobini E, Mori F, Lai CC. The effect of cholinesterase inhibitors on the secretion of APPS from rat brain cortex. Ann N Y Acad Sci 1996; 777: 393–8.

23 Mori F, Lai CC, Fusi F, Giacobini E. Cholinesterase inhibitors increase secretion of APPs in rat brain cortex. Neuroreport 1995; 6: 633–6.

24 Frey TG, Mannella CA. The internal structure of mitochondria. Trends Biochem Sci 2000; 25: 319–24.

25 Silva DF, Esteves AR, Oliveira CR, Cardoso SM. Mitochondria: the common upstream driver of amyloid-beta and tau pathology in Alzheimer's disease. Curr Alzheimer Res 2011; 8: 563–72.

26 Gao X, Tang XC. Huperzine A attenuates mitochondrial dysfunction in beta-amyloid-treated PC12 cells by reducing oxygen free radicals accumulation and improving mitochondrial energy metabolism. J Neurosci Res 2006; 83: 1048–57.

27 Gao X, Zheng CY, Yang L, Tang XC, Zhang HY. Huperzine A protects isolated rat brain mitochondria against beta-amyloid peptide. Free Radic Biol Med 2009; 46: 1454–62.

28 Yang L, Ye CY, Huang XT, Tang XC, Zhang HY. Decreased accumulation of subcellular amyloid-beta with improved mitochondrial function mediates the neuroprotective effect of huperzine A. J Alzheimers Dis 2012; 31: 131–42.

29 Zheng CY, Zhang HY, Tang XC. Huperzine A attenuates mitochondrial dysfunction after middle cerebral artery occlusion in rats. J Neurosci Res 2008; 86: 2432–40.

30 Xiao XQ, Zhang HY, Tang XC. Huperzine A attenuates amyloid beta-peptide fragment 25–35-induced apoptosis in rat cortical neurons via inhibiting reactive oxygen species formation and caspase-3 activation. J Neurosci Res 2002; 67: 30–6.

31 Wang R, Zhang HY, Tang XC. Huperzine A attenuates cognitive dysfunction and neuronal degeneration caused by beta-amyloid protein-(1–40) in rat. Eur J Pharmacol 2001; 421: 149–56.

32 Xiao XQ, Wang R, Han YF, Tang XC. Protective effects of huperzine A on beta-amyloid(25–35) induced oxidative injury in rat pheochromocytoma cells. Neurosci Lett 2000; 286: 155–8.

33 Xiao XQ, Wang R, Tang XC. Huperzine A and tacrine attenuate beta-amyloid peptide-induced oxidative injury. J Neurosci Res 2000; 61: 564–9.

34 Xiao XQ, Yang JW, Tang XC. Huperzine A protects rat pheochromocytoma cells against hydrogen peroxide-induced injury. Neurosci Lett 1999; 275: 73–6.

35 Wang LM, Han YF, Tang XC. Huperzine A improves cognitive deficits caused by chronic cerebral hypoperfusion in rats. Eur J Pharmacol 2000; 398: 65–72.

36 Shang YZ, Ye JW, Tang XC. Improving effects of huperzine A on abnormal lipid peroxidation and superoxide dismutase in aged rats. Zhongguo Yao Li Xue Bao 1999; 20: 824–8.

37 Zhang HY, Tang XC. Huperzine A attenuates the neurotoxic effect of staurosporine in primary rat cortical neurons. Neurosci Lett 2003; 340: 91–4.

38 Zhou J, Tang XC. Huperzine A attenuates apoptosis and mitochondria-dependent caspase-3 in rat cortical neurons. FEBS Lett 2002; 526: 21–5.

39 Wang R, Xiao XQ, Tang XC. Huperzine A attenuates hydrogen peroxide-induced apoptosis by regulating expression of apoptosis-related genes in rat PC12 cells. Neuroreport 2001; 12: 2629–34.

40 Tillement L, Lecanu L, Papadopoulos V. Alzheimer's disease: effects of beta-amyloid on mitochondria. Mitochondrion 2011; 11: 13–21.

41 Hansson Petersen CA, Alikhani N, Behbahani H, Wiehager B, Pavlov PF, Alafuzoff I, et al. The amyloid beta-peptide is imported into mitochondria via the TOM import machinery and localized to mitochondrial cristae. Proc Natl Acad Sci U S A 2008; 105: 13145–50.

42 Singh P, Suman S, Chandna S, Das TK. Possible role of amyloid-beta, adenine nucleotide translocase and cyclophilin-D interaction in mitochondrial dysfunction of Alzheimer's disease. Bioinformation 2009; 3: 440–5.

43 Lustbader JW, Cirilli M, Lin C, Xu HW, Takuma K, Wang N, et al. ABAD directly links Abeta to mitochondrial toxicity in Alzheimer's disease. Science 2004; 304: 448–52.

44 Murakami Y, Ohsawa I, Kasahara T, Ohta S. Cytoprotective role of mitochondrial amyloid beta peptide-binding alcohol dehydrogenase against a cytotoxic aldehyde. Neurobiol Aging 2009; 30: 325–9.

45 Culman J, Zhao Y, Gohlke P, Herdegen T. PPAR-gamma: therapeutic target for ischemic stroke. Trends Pharmacol Sci 2007; 28: 244–9.

46 Fong WH, Tsai HD, Chen YC, Wu JS, Lin TN. Anti-apoptotic actions of PPAR-gamma against ischemic stroke. Mol Neurobiol 2010; 41: 180–6.

47 Zhao X, Strong R, Zhang J, Sun G, Tsien JZ, Cui Z, et al. Neuronal PPARgamma deficiency increases susceptibility to brain damage after cerebral ischemia. J Neurosci 2009; 29: 6186–95.

48 Wang Y, Yang YS, Tang XC, Zhang HY. T33, a novel peroxisome proliferator-activated receptor gamma/alpha agonist, exerts neuroprotective action via its anti-inflammatory activities. Acta Pharmacol Sin 2011; 32: 1100–8.

49 Ferreiro E, Baldeiras I, Ferreira IL, Costa RO, Rego AC, Pereira CF, et al. Mitochondrial- and endoplasmic reticulum-associated oxidative stress in Alzheimer's disease: from pathogenesis to biomarkers. Int J Cell Biol 2012; 2012: 735206.

50 Rafii MS, Walsh S, Little JT, Behan K, Reynolds B, Ward C, et al. A phase II trial of huperzine A in mild to moderate Alzheimer disease. Neurology 2011; 76: 1389–94.

51 Wang BS, Wang H, Wei ZH, Song YY, Zhang L, Chen HZ. Efficacy and safety of natural acetylcholinesterase inhibitor huperzine A in the treatment of Alzheimer's disease: an updated meta-analysis. J Neural Transm 2009; 116: 457–65.

52 Chu D, Liu W, Li Y, Li P, Gu J, Liu K. Pharmacokinetics of huperzine A in dogs following single intravenous and oral administrations. Planta Med 2006; 72: 552–5.

53 Wang Q, Chen G. Pharmacokinetic behavior of huperzine A in plasma and cerebrospinal fluid after intranasal administration in rats. Biopharm Drug Dispos 2009; 30: 551–5.

54 Fu X, Ping Q, Gao Y. Effects of formulation factors on encapsulation efficiency and release behaviour in vitro of huperzine A-PLGA microspheres. J Microencapsul 2005; 22: 705–14.

55 Gao P, Ding P, Xu H, Yuan Z, Chen D, Wei J, et al. In vitro and in vivo characterization of huperzine a loaded microspheres made from end-group uncapped poly(d,l-lactide acid) and poly(d,l-lactide-co-glycolide acid). Chem Pharm Bull (Tokyo) 2006; 54: 89–93.

56 Liu WH, Song JL, Liu K, Chu DF, Li YX. Preparation and in vitro and in vivo release studies of Huperzine A loaded microspheres for the treatment of Alzheimer's disease. J Control Release 2005; 107: 417–27.

57 Nieoullon A, Bentue-Ferrer D, Bordet R, Tsolaki M, Forstl H. Importance of circadian rhythmicity in the cholinergic treatment of Alzheimer's disease: focus on galantamine*. Curr Med Res Opin

2008; 24: 3357–67.

58 Gais S, Born J. Low acetylcholine during slow-wave sleep is critical for declarative memory consolidation. Proc Natl Acad Sci U S A 2004; 101: 2140–4.

59 Roberts SF, Fischhoff MA, Sakowski SA, Feldman EL. Perspective: Transforming science into medicine: how clinician-scientists can build bridges across research's "valley of death". Acad Med 2012; 87: 266–70.

Original Article

Discovery of N-(3,5-bis(1-pyrrolidylmethyl)-4-hydroxy-benzyl)-4-methoxybenzenesulfamide (sulcardine) as a novel anti-arrhythmic agent

Dong-lu BAI[1, *], Wei-zhou CHEN[2], Yun-xin BO[1], Yue-li DONG[2], Ai-li KANG[1], Wei-kang SUN[2], Wei WANG[2], Zhong-liang HU[1], Yi-ping WANG[2, *]

[1]Department of Medicinal Chemistry, [2]Department of Pharmacology, State Key Laboratory of Drug Research, Shanghai Institute of Materia Medica, Chinese Academy of Sciences, Shanghai 201203, China

Aim: To investigate the anti-arrhythmic effects of sulfamide analogues of changrolin and to characterize the sulfate of compound **6f** (sulcardine sulfate, Sul) as a novel anti-arrhythmic agent.
Methods: The anti-arrhythmic effects of compounds were studied against aconitine-induced arrhythmias in rats and ouabain-induced arrhythmias in guinea pigs. The effects of Sul on transmembrane action potentials were investigated in isolated rabbit sinoatrial nodes and guinea-pig papillary muscles using intracellular recording. With a whole-cell recording technique, the effects of Sul on sodium current, calcium current, and potassium currents were examined in isolated single guinea-pig ventricular myocytes.
Results: In aconitine-induced arrhythmias of rats, sulfamide analogues of changrolin (**4**, **5**, and **6a–6p**) exhibited various anti-arrhythmic activities. The sulfate of compound **6f** (Sul) increased the amount of aconitine required to induce arrhythmias in each treated animal. The ED_{50} value of Sul in rats was 196 mg/kg. In ouabain-induced arrhythmias of guinea pigs, 25, 50, and 100 mg/kg doses of Sul increased the dose of ouabain required to induce VP, VT, and VF in a dose-dependent manner. In papillary preparations, Sul produced a concentration-dependent decrease in APA and V_{max}, prolonged APD_{90} and ERP, whereas RP was unaffected. In the spontaneously beating sinus nodes, Sul reduced APA and V_{max} in a concentration-dependent manner. The whole-cell recording studies revealed that Sul produced a reversible reduction in I_{Na} (IC_{50}=26.9 μmol/L) and $I_{Ca,L}$ (IC_{50}=69.2 μmol/L), whereas the inward rectifier (I_{K1}) and the delayed rectifier potassium currents (I_K) were unaffected.
Conclusion: As a multi-ion channel blocker, Sul may have potent efficacy in anti-atrial and ventricular arrhythmias.

Keywords: sulcardine; sulcardine sulfate; changrolin; heart; arrhythmias; aconitine; ouabain; sodium current; L-type calcium current

Introduction

The use of anti-arrhythmic drugs has decreased over the last 20 years because of the side effect of pro-arrhythmia, more serious rhythm disorders induced by some anti-arrhythmic agents. The majority of anti-arrhythmic agents are ion channel blockers. The Cardiac Arrhythmia Suppression Trial (CAST) and subsequent CAST II studies have provided evidence indicating that these drugs primarily act by blocking sodium ion channels and may have the potential to increase mortality in patients with structural heart disease[1]. Since then, the study of anti-arrhythmic agents has shifted away from sodium ion channel blockers and focused on potassium channel blockers,

such as amiodarone and sotalol derivatives, which have been proven to be highly effective agents for treating life-threatening arrhythmias. However, no selective channel blocker has yet been shown to unequivocally reduce the mortality associated with atrial or ventricular arrhythmias. Recent studies have shown that amiodarone, an agent with a broad range of effects, including the blocking of sodium, calcium and delayed rectifier potassium current (I_{kr}) channels and non-competitive β-blockade, can prolong the QT interval but rarely causes pro-arrhythmia. The likely explanation for this paradox is that mixed or multi-ion channel blocking effects decrease the pro-arrhythmia side effect[2]. However, amiodarone therapy has other serious side effects such as pulmonary, skin and thyroid toxicities. Therefore, there is a major need for new drugs that will control arrhythmias more safely and effectively. Based on clinical data, compounds with appropriate mixed channel blocking effects may be a promising route to new anti-arrhyth-

* To whom correspondence should be addressed.
E-mail dlbai@mail.shcnc.ac.cn (Dong-lu BAI);
    ypwang@mail.shcnc.ac.cn (Yi-ping WANG)

mic drugs[3].

Since the 1980s, implantable cardioventer-defibrillators have been an option for treating arrhythmia. However, an adjuvant drug therapy is often required to provide maximum prevention and treatment of life-threatening arrhythmias.

It is well-known that the anti-malarial drug quinine and its optical isomer quinidine have anti-arrhythmic properties. The demonstration of both anti-malarial and anti-arrhythmic activities is not confined to quinine and quinidine. Febrifugine is an alkaloid isolated from *Dichroa febrifuga* that was used against malaria in traditional Chinese medicine. In the 1970s, changrolin (**1**), a compound derived from febrifugine, was found to have anti-arrhythmic properties in malaria patients with arrhythmia and markedly diminished ectopic beats in patients. In subsequent investigations of its anti-arrhythmic effects, changrolin exhibited significant protective and therapeutic effects against arrhythmia, both in animal models and in clinical trials. In animal studies, the anti-arrhythmic potency of changrolin was higher and its toxicity was lower than those of quinidine. Changrolin effectively prevented atrial fibrillation induced by acetylcholine in rats and elevated the threshold of electrically induced ventricular fibrillation in rabbits and dogs. The results of clinical trials on 489 patients with various arrhythmias demonstrated that changrolin was most effective in reducing paroxysmal ventricular tachycardia and ventricular premature beats by 85.7% and 84.3%, respectively[4, 5]. However, changrolin also exhibited some side effects, including skin pigmentation and parasympatholytic activity[4]. Aqueous solutions of changrolin are unstable and turns brownish-yellow after storage at room temperature for one or two days. The chemical structure of changrolin is unlike those of currently marketed anti-arrhythmic drugs, and a number of analogues and derivatives of changrolin have been prepared and tested for anti-arrhythmic activity[6–13].

Structurally, changrolin could be divided into three portions: a quinazoline moiety, a 3,5-bis(1-pyrrolidylmethyl)-4-hydroxy phenyl moiety and a linker between the two moieties. In 1981, Sun *et al* reported that the benzoyl analogue of changrolin, compound **2**, exhibited protective effects against experimental arrhythmia induced by aconitine. Compound **2** was more potent than changrolin in protecting dogs from atrial fibrillation induced by acetylcholine[6, 7]. Subsequently, Stout *et al* reported an amide analogue **3**, which is the amide-reversed form of amide **2**. Compound **3** possessed excellent profiles as

a class 1 anti-arrhythmic[11]. All of the SAR data reported so far regarding the structure-activity relationships of changrolin can be summed as follows:

1) The 3,5-bis(1-pyrrolidylmethyl)-4-hydroxyphenyl moiety is essential for optimal anti-arrhythmic activity; pyrrolidine yields greater activity than other secondary amines.

2) The quinazoline moiety could be replaced by a variety of aromatic or heteroaromatic rings without loss of activity. The position and type of substituents on the rings did not affect activity.

3) The –NH-linker could be replaced with –CH_2O–, –NHCO–, –CONH–, –CONHCH_2–, and –CO–. Some amides were found to be potent anti-arrhythmic agents.

4) The quinazoline moiety and –NH-linker could be simultaneously replaced by –$(CH_2)_n$COOR group without loss of activity (Figure 1).

Based on the reported structure-activity relationship data for changrolin, further structural modifications were performed by our groups. The purpose of this study was to assess the protective and therapeutic effects against arrhythmia of the new analogues of changrolin[14].

Materials and methods
Chemistry
The synthesis of all target compounds (**4**, **5**, **6a–6p**) is straightforward. The preparation of compounds **4** and **5** is depicted in Scheme 1. Chloroquinazoline was coupled with 4-hydroxybenzylamine or N-methyl-4-hydroxyaniline to give compound **7** or **8**. The target compounds **4** and **5** were obtained by Mannich reaction of **7** and **8**, respectively, with formaldehyde and pyrrolidine.

Sulfamides **6a**, **6e**, **6h**, and **6k** were prepared by the reaction of 4-amino-2,6-bis(1-pyrrolidylmethyl)phenol (**9**)[9] with the corresponding 4-substituted benzenesulfonyl chloride (Scheme 2).

Sulfamides **6b**, **6f**, **6i**, and **6m**, the methylene insertion analogues of compounds **6a**, **6e**, **6h**, and **6k**, were obtained by sulfonylation of 4-hydroxybenzylamine with 4-substituted benzenesulfonyl chlorides in the presence of triethylamine, followed by Mannich reaction of the resulting sulfamides **10–13** with formaldehyde and pyrrolidine in ethanol (Scheme 3).

Using N-methyl-4-hydroxy-aniline instead of 4-hydroxybenzylamine, the N-methyl analogues **6c**, **6g**, **6j**, and **6n** were synthesized in the same manner as described in Scheme 4.
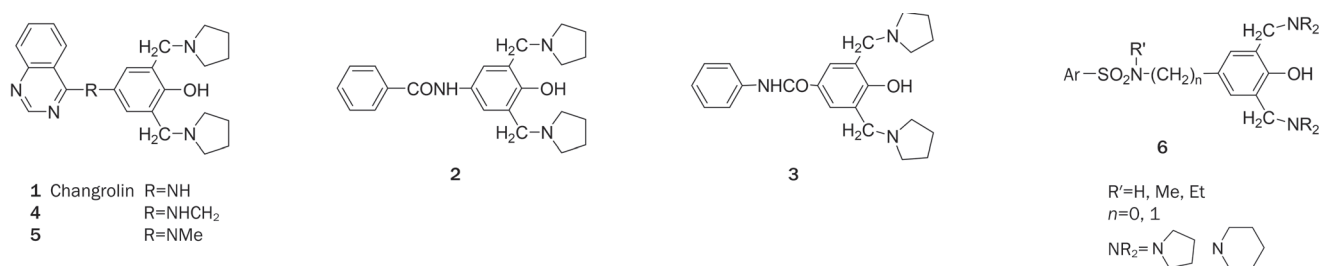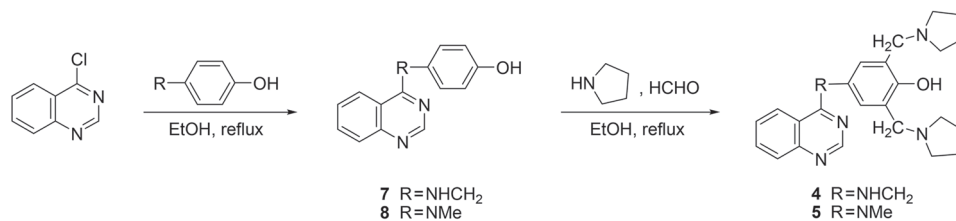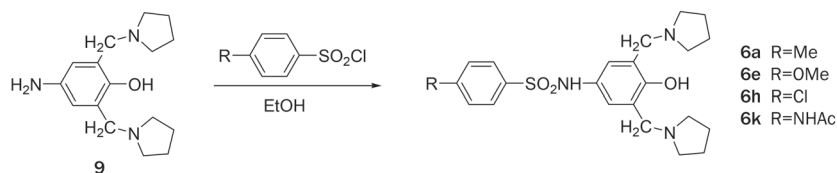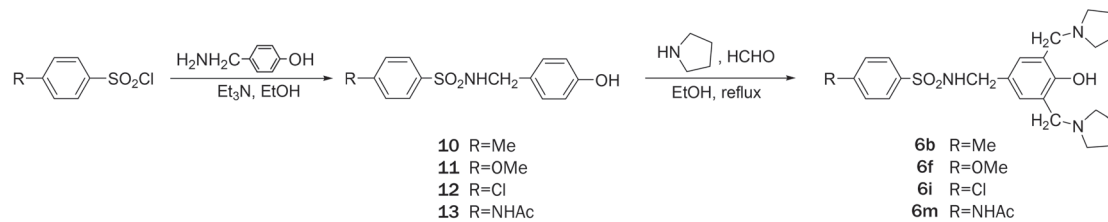

Figure 1. Chemical structures of compound **1**–**6**.

Scheme 1. Synthesis of compounds **4** and **5**.

Scheme 2. Preparation of sulfamides **6a**, **6e**, **6h**, and **6k**.

Scheme 3. Synthesis of the methylene insertion sulfamides **6b**, **6f**, **6i**, and **6m**.

The N-ethyl analogue **6d** was prepared by coupling 4-toluenesulfonyl chloride with 4-ethylamino-2,6-bis(1-pyrrolidylmethyl)phenol (**18**) in the presence of triethylamine in ethanol (Scheme 5).

The two 1-naphthalenesulfamides **6o** and **6p** were yielded via Mannich reaction of N-(4-hydroxyphenyl)-1-naphthalenesulfamide with formaldehyde and pyrrolidine or peperidine, respectively.
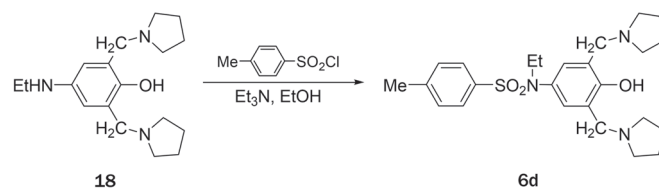
Scheme 5. Synthesis of N-ethylsulfamide **6d**.

Drugs and reagents

Sulfamide analogues of changrolin and sulcardine sulfate (**6f**, a yellowish powder with purity over 98.5%, MW=611.76) were synthesized by the chemists in our groups. Aconitine, ouabain, and collagenase (type I) were purchased from Sigma Chemical Co (St Louis, MO, USA). Other reagents, unless otherwise specified, were commercial products of reagent grade and purchased from Sigma-Aldrich China, Inc (Shanghai, China).
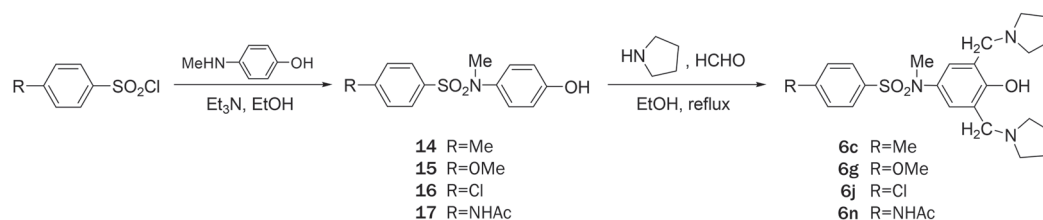
Scheme 4. Synthesis of N-methyl analogues **6c**, **6g**, **6j**, and **6n**.

Animals

Mice, Sprague Dawley rats, and guinea pigs were obtained from the Shanghai Laboratory Animal Center (Shanghai, China). The animals were cared for in accordance with the institutional guidelines of the Animal Care and Use Committee of the Shanghai Institute of Materia Medica, Chinese Academy of Sciences.

Aconitine-induced arrhythmias in rats

Sprague Dawley rats of either sex weighing 220–250 g were used. The animals were anesthetized by intraperitoneal injection of 1.2 g/kg urethane. Aconitine (10 μg/mL) was administered through continuous infusion into the saphenous vein at a rate of 0.08 mL/min, and the electrocardiogram (ECG) in lead II was recorded. The test compound was given orally 2 h prior to aconitine infusion. The time until the onset of the first ventricular premature (VP), ventricular tachycardia (VT), and ventricular fibrillation (VF) was chosen as the endpoint, and the amount of aconitine required to induce the arrhythmias was calculated. The percent increase in the amount of aconitine required to induce arrhythmias in animals treated with each test compound (above the mean value in the appropriate control group) was calculated, and log dose-response curves were constructed by liner regression analysis. ED_{50} values were defined as the dose of test compound required to increase the arrhythmogenic dose of aconitine by 50% relative to that required in control animals.

Ouabain-induced arrhythmias in guinea pigs

Guinea pigs of either sex weighing 250–300 g were anesthetized with 1.2 g/kg urethane intraperitoneally. One jugular vein was catheterized. Ouabain (300 μg/mL) was infused into the jugular vein at a rate of 3 μg/min. The ECG in lead II was recorded with subcutaneous steel-needle electrodes. The time until the onset of the first VP, VT, and VF was chosen as the endpoint, and the amount of ouabain required to induce the arrhythmias was calculated.

Prophylactic index and therapeutic index

The prophylactic index and therapeutic index were obtained by the following procedures: the performance of an acute toxicity test in mice to obtain the medium lethal dose (LD_{50}); the use of an aconitine-induced arrhythmia model in rats to obtain the medium effective dose (ED_{50}) in prophylactic tests and the effective dose (ED) in therapeutic tests; and the calculation of the prophylactic indexes as the ratio $LD_{50}:ED_{50}$ and the therapeutic index as the ratio $LD_{50}:ED$. Both indexes were used to evaluate the compounds for their anti-arrhythmic activities[15, 16].

Action potential recording in isolated guinea-pig papillary muscles

The guinea pig papillary muscle was dissected from the right ventricle and superfused in a 1.5 mL chamber (15 mL/min) with modified Tyrode's solution gassed with 95% O_2/5% CO_2 at 32±0.5 °C[17]. The composition of the modified Tyrode's solution was as follows: 120.3 mmol/L NaCl, 4.0 mmol/L KCl, 1.2 mmol/L $CaCl_2$, 1.3 mmol/L $MgSO_4$, 25.2 mmol/L $NaHCO_3$ and 5.5 mmol/L glucose (pH 7.4). The preparations were allowed to equilibrate for 1 h before recording the control. Action potentials (APs) were recorded using glass microelectrodes filled with 3 mol/L KCl and a tip resistance of 10–20 MΩ. Signals were delivered to a microelectrode amplifier (MEZ-7101, Nihon Kohden, Japan). The maximum upstroke velocity of AP (V_{max}) was measured with a PowerLab System (AD Instruments Pty Ltd, Australia). Both AP and V_{max} were monitored on the PowerLab System. The APs were elicited with rectangular pulses (1 ms, twice the threshold) generated by a stimulator (SEN-7203, Nihon Kohden, Japan) at 1 Hz.

Isolation of ventricular myocytes

The enzymatic dissociation method was described previously[18, 19]. In brief, the excised guinea pig heart was perfused through the aorta retrogradely with a Ca^{2+}-free Tyrode's solution for 10 min at 37 °C, followed by a Tyrode's solution containing 0.2 mg/mL collagenase (type I) for 3–4 min. The composition of the Tyrode's solution was as follows: 135 mmol/L NaCl, 5.4 mmol/L KCl, 1 mmol/L $MgCl_2$, 0.33 mmol/L NaH_2PO_4, 5 mmol/L HEPES and 5 mmol/L glucose (pH 7.4); the solution was oxygenated with 100% O_2. The ventricles were then minced and gently triturated for 10 min in Kraft-Brühe (KB) solution containing the following: 50 mmol/L *L*-glutamic acid, 80 mmol/L KOH, 40 mmol/L KCl, 3 mmol/L $MgSO_4$, 25 mmol/L KH_2PO_4, 10 mmol/L HEPES, 1 mmol/L EGTA, 20 mmol/L taurine, and 10 mmol/L glucose (pH 7.4). Myocytes were harvested with 200 μm nylon mesh and stored in KB solution at 20–24 °C.

Voltage-clamp recording

A cell suspension was placed in a 3 mL chamber mounted on the stage of a microscope (Optiphot-2; Nikon, Japan) and superfused with an external solution via a PBS-8 solution exchange system (ALA Scientific Instruments Inc, USA) at a rate of 3 mL/min. Patch pipettes were pulled with a P-97 microelectrode puller (Shutter Instruments Co, USA), and had a tip resistance of 1–5 MΩ when filled with a pipette solution. Whole-cell voltage-clamp recording was made from single ventricular myocytes with an Axopatch-1D amplifier (Axon Instruments, USA). After a gigaseal formation (seal resistance 1 GΩ), the membrane was ruptured with gentle suction to obtain the whole-cell voltage-clamp configuration. Voltage command protocols were provided by the pClamp 6.0.4 software package (Axon Instruments, USA) via a DigiData-1200 interface (Axon Instruments, USA). Capacitance compensation was routinely optimized, and series resistance was compensated by 40%–80%. Linear leaks were subtracted digitally online. Signals were filtered at 3 kHz, digitized at 10 kHz, and stored in an IBM-compatible computer. Cell capacitance was measured with a short hyperpolarizing ramp pulse (5 mV in 5 ms) from a holding potential of -40 mV. The membrane capacitance of myocytes ranged from 100–150 pF. The Na+ current (I_{Na}), L-type Ca^{2+} current ($I_{Ca,L}$) and inward rectifier K+ current

(I_{K1}) were recorded at 20–24 °C, whereas the delayed rectifier K$^+$ current (I_K) was recorded at 35±1 °C.

The composition of the external solution for recording I_{Na} was as follows: 120 mmol/L tetraethylammonium chloride (TEA-Cl), 30 mmol/L NaCl, 1 mmol/L MgCl$_2$, 1 mmol/L CaCl$_2$, 0.1 mmol/L CdCl$_2$, 10 mmol/L HEPES, and 10 mmol/L glucose (pH 7.4). The external solution used to record $I_{Ca,L}$ contained the following: 120 mmol/L TEA-Cl, 1 mmol/L MgCl$_2$, 10 mmol/L CsCl, 1.8 mmol/L CaCl$_2$, 10 mmol/L HEPES and 10 mmol/L glucose (pH 7.4). The external solution used to record the K$^+$ currents contained the following: 140 mmol/L NaCl, 5.4 mmol/L KCl, 1 mmol/L MgCl$_2$, 0.1 mmol/L CaCl$_2$, 0.1 mmol/L CdCl$_2$, 5 mmol/L HEPES, and 5 mmol/L glucose (pH 7.4). The pipette solution for recording I_{Na} contained the following: 80 mmol/L CsCl, 40 mmol/L CsOH, 10 mmol/L EGTA, 10 mmol/L HEPES, and 5 mmol/L Na$_2$ATP (pH 7.2). The pipette solution for recording $I_{Ca,L}$ contained the following: 80 mmol/L CsCl, 40 mmol/L CsOH, 10 mmol/L EGTA, 10 mmol/L HEPES, and 5 mmol/L MgATP (pH 7.2), while that for recording the K$^+$ currents contained the following: 140 mmol/L KCl, 0.5 mmol/L MgCl$_2$, 10 mmol/L EGTA, 10 mmol/L HEPES, and 5 mmol/L K$_2$ATP (pH 7.2). The myocytes were perfused with external solutions and allowed to equilibrate for about 5 min with ascending concentrations of drug to generate concentration-response relationships.

Statistical analysis

Data are presented as the mean±SD. A two-tailed Student's *t*-test was used for analyses of anti-arrhythmic activity and AP measurements. The patch-clamp data were analyzed using the Clampfit 9.0 (Axon Instruments, USA) and Prism 3.0 software (GraphPad Software, USA). For all tests, $P<0.05$ was considered statistically significant. The concentration of sulcardine sulfate that yielded a 50% inhibitory effect (IC$_{50}$ value) was obtained by fitting the concentration–response relationship to the equation: X=1/{1+([C]/IC$_{50}$)N}, where X is the normalized response, [C] is the concentration of the agent, and N is the Hill coefficient.

Results and discussion

Anti-arrhythmic activity of sulfamide analogues (6a–6p) of changrolin (1)

It was supposed that the aminophenol moiety in changrolin could be oxidized into an iminoquinone unit, resulting in an extended conjugated system with quinazoline *in vivo*, which may be responsible for both the skin pigmentation in patients after long-term administration of changrolin and the darkening of the aqueous solution of changrolin at room temperature *in vitro*. Because both bis(pyrrolidylmethyl)phenol and heteroaromatic or aromatic moieties in the changrolin molecule are essential for anti-arrhythmic activity, two approaches could be adopted to avoid the formation of the extended iminoquinone-containing conjugate chromophore. First, the –NH-linkage of the two aromatic rings in changrolin could be replaced by –NHCH$_2$- or –NMe-, giving compounds 4 and 5, respectively. An alternative approach was the replacement of

the quinazolylamino moiety in changrolin with an arylamido group, such as in compounds 2 and 3, both of which have been reported to show potent anti-arrhythmic activities[6, 7, 11]. Considering that sulfamide is the isostere of amide, we focused on the analogues with a –SO$_2$NH-linkage instead of –CONH- in compound 2 and with an additional –CH$_2$– unit between the sulfamido and bis(1-pyrrolidylmethyl)phenol moiety (Table 1). A new series of aromatic sulfamide analogues of changrolin, 6a–6p, was thus designed and prepared.

Two analogues, 4 and 5, derived from changrolin by inserting a methylene between the amino group and the phenol ring and by methylation of the amino group in changrolin, respectively, were first designed and synthesized. The anti-arrhythmic activities of 4 and 5 were less potent than that of changrolin itself. The pharmacological screening data of sulfamides 6a–6p showed that most of the sulfamides possessed anti-arrhythmic activity (Table 1). Among them, compound 6f (sulcardine) was the best one. Compounds with one carbon extension (6i and 6m) or N-methyl substitution (6j and 6n) did not change the potency markedly relative to 6h and 6k, respectively. When the 1-pyrrolidyl group in 6o was replaced by 1-piperidyl (6p), the anti-arrhythmic activity increased. In the 4-methoxybenzenesulfamides group (6e, 6f, 6g), the insertion of a methylene unit between the sulfamido and phenol ring enhanced the prophylactic index up to 6-fold (6f *vs* 6e). N-Methylation of 6e increased the prophylactic index by 2.3-fold (6g *vs* 6e). In the 4-methylbenzensulfamides group, although all of the compounds tested (6a–6d) exhibited anti-arrhythmic activity, the results were ambiguous. Inserting a methylene unit between the sulfamido and phenol ring in 6a resulted in a slight change in both the prophylactic index and the therapeutic index (6a *vs* 6b). N-Methylation of 6a caused a 3.7-fold increase in the prophylactic index and a 5.5-fold decrease in the therapeutic index (6c *vs* 6a). However, N-ethylation of 6a resulted in a 5-fold decrease in both the prophylactic index and the therapeutic index (6a *vs* 6d).
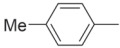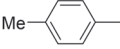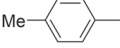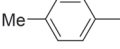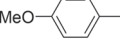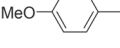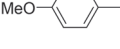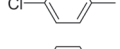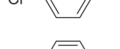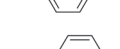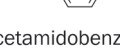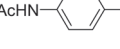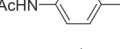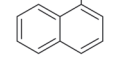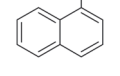
The prophylactic indexes of the naphthylenesulfamides (6o and 6p) were much higher than those of the benzenesulfamides, with the exception of 6f (sulcardine). There was no obvious correlation of anti-arrhythmic activity with electron-donating or electron-withdrawing substituents on the benzene ring (6a, 6e, and 6k *vs* 6h; 6b, 6m *vs* 6i; 6c, 6g, and 6n *vs* 6j). Surprisingly, 6f (sulcardine) had a much higher prophylactic index than 6b. The optimal spectrum of prophylactic index and therapeutic index was given by 6f (sulcardine).

To summarize our findings on the chemical modifications of the structure of changrolin (1), we have found that the quinazoline moiety could be replaced by an aromatic sulfonyl group without loss of activity. The insertion of a methylene unit between the sulfamido and phenol ring and N-methylation of sulfamido resulted in the retention of or an increase in anti-arrhythmic activity.

Effects of compound 6f sulfate (sulcardine sulfate) on experimental arrhythmia models in animals

Compound 6f sulfate was tested in various arrhythmia mod-

Table 1. The anti-arrhythmic activity of sulfamide analogues of changrolin (**6a–6p**).

Compound	Ar	R′	n	NR$_2$	Prophylactic index	Therapeutic index
Changrolin (**1**)					16.2	2.0
6a	Me–C$_6$H$_4$–	H	0	1-pyrrolidyl	5.6	20
6b	Me–C$_6$H$_4$–	H	1	1-pyrrolidyl	3.8	12
6c	Me–C$_6$H$_4$–	Me	0	1-pyrrolidyl	21	3.7
6d	Me–C$_6$H$_4$–	Et	0	1-pyrrolidyl	1.1	4.0
6e	MeO–C$_6$H$_4$–	H	0	1-pyrrolidyl	5.5	–
6f (sulcardine)	MeO–C$_6$H$_4$–	H	1	1-pyrrolidyl	33	18
6g	MeO–C$_6$H$_4$–	Me	0	1-pyrrolidyl	13	6.1
6h	Cl–C$_6$H$_4$–	H	0	1-pyrrolidyl	5.3	–
6i	Cl–C$_6$H$_4$–	H	1	1-pyrrolidyl	5.5	8.6
6j	Cl–C$_6$H$_4$–	Me	0	1-pyrrolidyl	3.9	–
6k	AcHN–C$_6$H$_4$–	H	0	1-pyrrolidyl	1.9	–
6l	4-acetamidobenzene sulfonate of **6k**			1-pyrrolidyl	4.0	–
6m	AcHN–C$_6$H$_4$–	H	1	1-pyrrolidyl	3.2	–
6n	AcHN–C$_6$H$_4$–	Me	0	1-pyrrolidyl	3.0	2.0
6o	naphthyl	H	0	1-pyrrolidyl	20	5.2
6p	naphthyl	H	0	1-piperidyl	34	9.7

els in animals. Against aconitine-induced arrhythmias in rats, **6f** sulfate (100, 150, and 250 µg/kg) significantly increased the amount of aconitine required to induce arrhythmias at each dose tested (Table 2). The ED$_{50}$ value of **6f** sulfate in rats was 196 mg/kg. At 2, 3, 4, and 6 h after administration, **6f** sulfate (at a dose of 1.5-fold ED$_{50}$) significantly raised the arrhythmogenic dose of aconitine to induce VP, VT, and VF in rats. The effects of **6f** sulfate reached a peak at 2–3 h and lasted up to 6 h after administration (Table 3).

Against ouabain-induced arrhythmias in guinea pigs, **6f** sulfate at 25, 50, and 100 mg/kg increased the dose of ouabain required to induce VP from 134±8 µg/kg to 156±9, 176±16, and 187±14 µg/kg, respectively. The amount of ouabain required

to induce VT and VF was also increased as the administered dose of **6f** sulfate increased (Table 4).

Effects of compound 6f sulfate (sulcardine sulfate) on action potentials

Guinea pig papillary muscle cells are characterized by firing fast response action potentials. The application of **6f** sulfate (10, 30, and 100 µmol/L) reduced the action potential amplitude (APA) and the maximum upstroke velocity of the action potential (V_{max}) and prolonged the action potential duration at 90% repolarization (APD$_{90}$) as well as the effective refractory period (ERP) (Table 5). In rabbit sinoatrial nodal dominant pacemaker cells, which are characterized by firing slow

Table 2. Effects of compound **6f** sulfate (sulcardine sulfate) on aconitine-induced arrhythmia in rats (mean±SD, *n*=10). [b]*P*<0.05, [c]*P*<0.01 *vs* control.

Dose (mg/kg, *po*)		Aconitine (µg/kg, iv)			
		VP	VT	VF	Lethal dose
Control		20±2	31± 6	42±7	63±6
Sulcardine	100	21±2[b]	32±6[b]	38±4[b]	67±8[b]
	150	25±2[c]	35±6[b]	45±13[b]	68±15[b]
	200	31±4[c]	45±11[c]	54±13[c]	88±19[c]

Table 3. Time-response effects of compound **6f** sulfate (sulcardine sulfate) on aconitine-induced arrhythmia in rats (mean±SD, *n*=10). [b]*P*<0.05, [c]*P*<0.01 *vs* control.

Time after sulcardine sulfate administration (h)	Aconitine (µg/kg, iv)			
	VP	VT	VF	Lethal dose
Control	22±5	30±6	37±6	66±8
2	44±14[c]	60±10[c]	88±19[c]	124±4[c]
3	42±7[c]	65±23[c]	81±17[c]	122±5[b]
4	34±4[c]	52±2[c]	59±8[c]	105±9[c]
6	32±6[c]	57±6[c]	65±10[c]	108±8[c]

Table 4. Effect of sulcardine on ouabain-induced arrhythmia in guinea pigs (mean±SD, *n*=10–17). [b]*P*<0.05, [c]*P*<0.01 *vs* control.

Dose (mg/kg, *po*)	*n*	Ouabain (µg/kg, iv)		
		VP	VT	VF
Control	17	134±8	175±30[c]	228±42[c]
Sulcardine	25	10	156±9[c]	220±22[b]	276±30
	50	10	176±16[c]	203±19[c]	253±33
	100	10	187±14[c]	215±18[c]	258±30[b]

response action potentials, the application of 6f sulfate (10, 30, and 100 µmol/L) reduced V_{max} and the slope of phase 4 depolarization and decreased APA. At 100 µmol/L, **6f** sulfate also prolonged APD, decreased MRP and SEF. The changes were 5.5%, 11.6%, and 4.7%, respectively (*n*=5, *P*<0.05) (Table 6).

Inhibition of sodium current and L-type calcium current in ventricular myocytes

The above results suggest that **6f** sulfate is a mixed or multi-ion channel blocker against Na^{+}, Ca^{2+}, and K^{+} channels[20]. Thus, the actions of 6f sulfate on cardiac ion channels were studied with the whole-cell patch clamp method in isolated ventricular myocytes. The application of **6f** sulfate caused a reversible reduction in I_{Na} (IC$_{50}$=26.9 µmol/L) and $I_{Ca,L}$ (IC$_{50}$=69.2 µmol/L), whereas the inward rectifier (I_{K1}) and the delayed rectifier potassium currents (I_K) were unaffected. The inhibition of voltage-gated sodium and calcium channels

Table 5. Effects of compound **6f** sulfate (sulcardine sulfate) on the fast response action potentials of guinea-pig papillary muscles (mean±SD, *n*=6). [b]*P*<0.05, [c]*P*<0.01 *vs* control.

Parameters	Control	Sulcardine sulfate (µmol/L)		
		10	30	100
RP (mV)	87.3±2.0	87.3±1.8	88.0±2.1	88.8±2.4
APA (mV)	119.7±1.2	119.0±1.5	116.3±1.8[c]	112.2±2.6[c]
V_{max} (V/s)	248±45	230±45[c]	202±42[c]	176±39[c]
APD$_{50}$ (ms)	148±19	149±18	155±22	159±22
APD$_{90}$ (ms)	172±21	173±18	178±20	191±26[b]
ERP (ms)	174±19	176±18	185±22	204±34[b]
ERP/APD$_{90}$	1.01±0.06	1.02±0.03	1.04±0.02	1.06±0.06

Table 6. Effects of compound **6f** sulfate (sulcardine sulfate) on the fast response action potentials of guinea-pig papillary muscles (mean±SD, *n*=5). [b]*P*<0.05, [c]*P*<0.01 *vs* control.

Parameters	Control	Sulcardine sulfate (µmol/L)		
		10	30	100
APA (mV)	61.6±14.9	58.0±14.9[b]	56.2±13.8[b]	51.4±14.7[b]
APD (ms)	347.6±91.1	346.8±96.6	351.0±95.9	366.8±100.0[b]
V_{max} (V/s)	11.6±6.9	8.9±4.2[b]	7.3±2.4[b]	6.1±1.9[b]
MRP (mV)	55.0±12.1	54.4±11.5	51.8±9.6	48.6±11.4[b]
SDVP4 (V/s)	0.12±0.03	0.09±0.03	0.09±0.03	0.09±0.03
SEF (bpm)	181.6±43.2	183.4±47.4	180.8±46.2	173.0±43.4[c]

induced by **6f** sulfate may contribute to its effect on atrial and ventricular tachyarrhythmias.

An overall preclinical examination of **6f** sulfate demonstrated that this compound possesses a promising profile as an anti-arrhythmic agent. Thus, the phase I clinical trial of this compound is complete, and the data indicate that this compound may be a novel anti-arrhythmic drug with low proarrhythmic side effects.

Conclusion

We have designed and synthesized a series of sulfamide analogues of changrolin (**1**) as potential anti-arrhythmic agents. To avoid the formation of the extended conjugation system from the changrolin molecule *in vivo*, which may be the cause of skin pigmentation, changrolin was chemically modified by two routes. One was the replacement of the quinazoline moiety by aromatic sulfonyl groups; the other was the insertion of a methylene unit between the NH group and phenol ring or N-alkylation of the NH group.

Pharmacological screenings of the target compounds (**4**, **5**, and **6a–6p**) demonstrated that all of the target compounds possessed various anti-arrhythmic activities. A considerable improvement of the anti-arrhythmic potency of these compounds compared to changrolin was observed. Based on both the prophylactic and therapeutic indexes, the target

compounds with better anti-arrhythmic activity are **6a**, **6f**, **6i**, **6o**, and **6p**. Among these compounds, compound **6f** is exceptionally potent and was chosen for considera tion as a drug candidate. The preclinical and phase I clinical studies of **6f** in the sulfate trihydrate form are complete. The compound has been named sulcardine sulfate and is well-tolerated in phase I trials. Sulcardine sulfate is now undergoing phase II trials. The chemical structure of **6f** is different from marketed anti-arrhythmic drugs. As a multi-ion channel blocker, it may have potent efficacy in anti-atrial fibrillation and anti-ventricular tachycardia, which are two particularly important cardiac arrhythmias with important clinical implications.

Experimental section
General methods
The ^{1}H NMR spectra were recorded on Bruker Am-400 and Bruker Ac-100 NMR spectrometers. The data are reported in parts per million relative to TMS and are referenced to the solvent in which they were analyzed. Elemental analyses were obtained on an Elemental Vario EL instrument. Melting points were determined on a Buchi-510 capillary apparatus and are uncorrected. IR spectra were recorded on a Perkin-Elmer-599B spectrometer. The solvent was removed by rotary evaporation under reduced pressure, and flash column chromatography was performed on silica gel (200–300 mesh) from the Qingdao Haiyang Chemical Company. Anhydrous solvents were obtained by redistillation over sodium wire.

4-[3,5-bis(1-pyrrolidylmethyl)-4-hydroxybenzyl]aminoquinazoline (4)
A mixture of 4-chloroquinazoline (1.51 g, 9.12 mmol) and 4-hydroxybenzylamine (2.82 g, 22.9 mmol) in ethanol (6 mL) was refluxed for 3 h. After cooling, the precipitate was collected and washed successively with a saturated solution of NaHCO$_3$ and water. The solid was recrystallized from EtOH-H$_2$O to give 4-(4-hydroxybenzyl)aminoquinazoline 7 (1.30 g, 56%), mp 231–232 °C. ^{1}H NMR (CDCl$_3$) δ 4.58 (s, 2H), 6.58 (d, J=8.4 Hz, 2H), 7.33 (d, J=8.4 Hz, 2H), 7.35 (m, 1H), 7.53 (d, J=8.7 Hz, 1H), 7.61 (m, 1H), 7.97 (d, J=8.8 Hz, 1H), 8.27 (s, 1H). Anal. (C$_{15}$H$_{13}$N$_3$O·H$_2$O) C, H, N.

A mixture of 7 (1.30 g, 5.2 mmol), pyrrolidine (1.1 mL, 13.2 mmol) and a 36%–38% solution of formaldehyde (1.1 mL, 15 mmol) in ethanol (10 mL) was refluxed for 3 h. The solvent was removed under reduced pressure to give an oil that became crystalline upon standing. Recrystallization from EtOH-H$_2$O yielded 4 (1.35 g, 63%), mp 155–156 °C . ^{1}H NMR (CDCl$_3$) δ 1.60–1.90 (m, 8H), 2.50–2.80 (m, 8H), 3.72 (s, 4H), 4.75 (s, 2H), 7.00–7.80 (m, 6H), 8.60 (s, 1H). Anal. (C$_{25}$H$_{31}$N$_5$O) C, H, N.

4-N-[3,5-bis(1-pyrrolidylmethyl)-4-hydroxyphenyl]-N-methyl-aminoquinazoline (5)
In the same manner as in the preparation of **7** and **4**, 4-N-methyl-(4-hydroxyphenyl)aminoquinazoline (**8**) was obtained from 4-chloroquinazoline and N-methylaminophenol in 65% yield, mp 258–260 °C (DMF-EtOH). ^{1}H NMR (CDCl$_3$)

δ 3.25 (s, 3H), 7.03 (d, J=8.5 Hz, 2H), 7.40 (d, J=8.5 Hz, 2H), 8.00–8.60 (m, 4H), 8.78 (s, 1H). Anal. (C$_{15}$H$_{13}$N$_3$O) C, H, N.

Mannich reaction of **8** gave **5** in 51% yield. The crude product was first purified by column chromatography (silica gel, EtOH:25% NH$_4$OH=10:0.25), and recrystallized from EtOH-H$_2$O, mp 129–130 °C. ^{1}H NMR (CDCl$_3$) δ 1.55–1.80 (m, 8H), 2.30–2.60 (m, 8H), 3.45 (s, 3H), 3.62 (s, 4H), 6.90–7.80 (m, 6H), 8.50 (s, 1H). Anal. (C$_{25}$H$_{31}$N$_5$O) C, H, N.

N-[3,5-bis(1-pyrrolidylmethyl)-4-hydroxyphenyl]-4-chlorobenzene-sulfamide (6h)
To a solution of 2,6-bis-(1-pyrrolidiylmethyl)-4-aminophenol (1.3 g, 4.8 mmol) in tetrahydrofuran (5 mL) was added dropwise a solution of 4-chlorobenzenesulfonyl chloride (1.0 g, 4.8 mmol) in tetrahydrofuran (5 mL). The mixture was stirred at room temperature for 4 h. The solvent was removed in vacuo, and the residue was dissolved in water. After neutralization with 2 mol/L KOH solution, the mixture was extracted with ethyl acetate. The organic layer was successively washed with water and brine and dried over anhydrous Na$_2$SO$_4$. After removing the solvent in vacuo, the residue was purified by column chromatography (silica gel, CH$_3$COOEt:CH$_3$OH:25% NH$_4$OH=9:1:0.05). The resultant solid was recrystallized from ethyl acetate to give the product 6h (1.3 g, 60%), mp 187–188 °C. ^{1}H NMR (CDCl$_3$) δ 1.72–2.08 (m, 8H), 2.56–2.88 (m, 8H), 3.88 (s, 4H), 6.90 (s, 2H), 7.36 (d, J=8.7 Hz, 2H), 7.64 (d, J=8.7 Hz, 2H). Anal. (C$_{22}$H$_{28}$N$_3$ClO$_3$S) C, H, N, Cl.

Compounds **6a**, **6e**, and **6k** were prepared in the same manner as **6h**.

N-[3,5-bis(1-pyrrolidylmethyl)-4-hydroxyphenyl]-4-methylbenzene-sulfamide (6a)
Yield: 47%, mp 160–161 °C (EtOH-H$_2$O). ^{1}H NMR (CDCl$_3$) δ 1.76–2.12 (m, 8H), 2.38 (s, 3H), 2.72-3.08 (m, 8H), 3.96 (s, 4H), 6.99 (s, 2H), 7.18 (d, J=8.6 Hz, 2H), 7.56 (d, J=8.6 Hz, 2H). Anal. (C$_{23}$H$_{31}$N$_3$O$_3$S) C, H, N.

N-[3,5-bis(1-pyrrolidylmethyl)-4-hydroxyphenyl]-4-methoxy-benzenesulfamide (6e)
Yield: 79%, white crystals, mp 143–144 °C (CH$_3$COOEt). ^{1}H NMR (CDCl$_3$) δ 1.64–1.94 (m, 8H), 2.35–2.65 (m, 8H), 3.65 (s, 3H), 3.81 (s, 4H), 6.75 (s, 2H), 6.85 (d, J=8.7 Hz, 2H), 7.58 (d, J=8.7 Hz, 2H). Anal. (C$_{23}$H$_{31}$N$_3$O$_4$S) C, H, N.

N-[3,5-bis(1-pyrrolidylmethyl)-4-hydroxyphenyl]-4-acetamido-benzenesulfamide (6k)
Yield: 85%, mp 186–187 °C (CH$_3$COOEt). ^{1}H NMR (CDCl$_3$) δ 1.82–2.06 (m, 8H), 2.17 (s, 3H), 2.83–3.07 (m, 8H), 3.76 (s, 4H), 7.09 (s, 2H), 7.54 (d, J=8.6 Hz, 2H), 7.65 (d, J=8.7 Hz, 2H), 9.50 (s, 1H). Anal. (C$_{24}$H$_{32}$N$_4$O$_4$S) C, H, N.

N-[3,5-bis(1-pyrrolidylmethyl)-4-hydroxybenzyl]-4-methoxy-benzenesulfamide (sulcardine, 6f) and the sulfate (sulcardine sulfate)
(1) To a suspension of 4-hydroxybenzylamine (133 g, 1.08 mol) in DMF (500 mL) was added dropwise 4-methoxybenzensul-

fonyl chloride (206 g, 1.00 mol) in DMF (320 mL) over a period of 30 min at 0–10 °C with stirring, followed by the addition of triethylamine (158 mL, 1.12 mol) over 30 min at the same temperature. The stirring was continued for an additional 1.5 h at room temperature. The reaction mixture was poured into ice-water (5 L). After stirring for 10 min, the suspension was allowed to stand for 2 h. The solid was filtered, washed with water (300 mL×3), and dried in a desiccator over anhydrous calcium chloride, yielding N-(4-hydroxybenzyl)-4-methoxybenzenesulfamide (**11**) (248 g, 85%) as a white solid, mp 160–162 °C. The authentic sample was obtained by recrystallization from ethyl acetate, mp 161–162 °C. ^{1}H NMR (CD$_3$OD) δ 3.70 (s, 3H), 3.76 (s, 2H), 6.48 (d, J=8.4 Hz, 2H), 6.82(d, J=8.4 Hz, 2H), 6.86 (d, J=8.7 Hz, 2H), 7.56 (d, J=8.7 Hz, 2H). EIMS (*m/z*): 293 (M$^+$), 254, 195, 185, 171, 155, 149, 122 (100), 107, 99, 77, 65. Anal. (C$_{14}$H$_{15}$NO$_4$S) C, H, N.

(2) A mixture of **11** (230 g, 0.78 mmol), pyrrolidine (200 mL, 2.44 mol) and 36% aqueous formaldehyde (250 mL, 3.30 mol) in ethanol (800 mL) was stirred under reflux for 8 h. The reaction mixture was concentrated under vacuum to dryness. The resulting oil residue was dissolved in chloroform (350 mL), and the solution was washed with water (300 mL×3). Under stirring, the organic layer was mixed with water (300 mL), and then concentrated hydrochloric acid (approximately 165 mL) was added portionwise at 0-10 °C to adjust the pH of the aqueous phase to ~2. The aqueous phase was washed with chloroform (200 mL) and then mixed with additional chloroform (300 mL). Under stirring, the two-phase mixture was treated portionwise with 25%–28% aqueous ammonia (~300 mL) to adjust the pH of the aqueous phase to **9–10**. The organic layer was separated, and the aqueous layer was further extracted with chloroform (200 mL×2). The combined organic layer was dried over anhydrous sodium sulfate and concentrated under vacuum to dryness. The oily residue was treated with acetone (45 mL) and isopropyl ether (290 mL), and the mixture was heated under reflux until the suspension became a solution. The solution was cooled to room temperature, seeded with an authentic sample, and allowed to stand at 0 °C overnight. The solid was filtered and dried under vacuum, yielding product **6f** (290 g, 81%) as a yellowish solid, mp 96–98 °C. The authentic sample was obtained by preparative TLC or column chromatography (silica gel; CHCl$_3$:MeOH:25% NH$_4$OH=92:7:1). The compound could be recrystallized from ethanol-water, mp 101–102 °C. ^{1}H NMR (CDCl$_3$) δ 1.77–1.86 (m, 8H), 2.53–2.63 (m, 8H), 3.68 (s, 4H), 3.86 (s, 3H), 3.97 (s, 2H), 6.86 (s, 2H), 6.95 (d, J=8.7 Hz, 2H), 7.78 (d, J=8.6 Hz 2H). EIMS (*m/z*): 459 (M$^+$), 390, 388, 202, 171, 148, 107, 84, 70 (100). Anal. (C$_{24}$H$_{33}$N$_3$O$_4$S) C, H, N.

(3) Under stirring, the Mannich base **6f** (150.5 g, 0.327 mol) was mixed with 2 mol/L H$_2$SO$_4$ (172 mL, 0.344 mol), and the mixture was heated at 80 °C until the solid dissolved. The solution was cooled to room temperature, seeded with an authentic sample, and the sulfate of **6f** was formed as crystals. To the stirred mixture was added anhydrous ethanol (520 mL), and the mixture was allowed to stand at 0 °C for 24 h. The solid was filtered, washed with ethanol, and recrystal-

lized with 80% ethanol (250 mL). The sulfate was dried over concentrated sulfuric acid in a desiccator, giving the sulfate of **6f** (143 g, 71%) as a trihydrate, mp 125–140 °C. ^{1}H NMR (D$_2$O) δ 2.00–2.13 (m, 4H), 2.14–2.25 (m, 4H), 3.12–3.22 (m, 4H), 3.45–3.55 (m, 4H), 3.90 (s, 3H), 4.20 (s, 2H), 4.33 (s, 4H), 7.06 (d, J=8.7 Hz, 2H), 7.28 (s, 2H), 7.66 (d, J=8.9 Hz, 2H). ^{13}C NMR (D$_2$O) δ 24.7, 47.6, 55.7, 56.1, 58.1, 116.6, 122.5, 131.3, 132.3, 133.3, 136.0, 155.8, 164.8. EIMS (*m/z*): 459, 390, 388, 202, 171, 148, 107, 84, 70 (100). Anal. (C$_{24}$H$_{33}$N$_3$O$_4$S·H$_2$SO$_4$·3H$_2$O) C, H, N, S.

Compounds **10**, **12**, **13**, **6b**, **6i**, and **6m** were also prepared by the above-mentioned procedures for **11** and **6f**.

N-[3,5-bis(1-pyrrolidylmethyl)-4-hydroxybenzyl]-4-methylbenzenesulfamide (6b)

N-(4-hydroxybenzyl)-4-methylbenzenesulfamide (**10**) was obtained in 73% yield, mp 183–184 °C (EtOH). ^{1}H NMR (CDCl$_3$) δ 2.45 (s, 3H), 3.96 (s, 2H), 6.70 (d, J=8.6 Hz, 2H), 7.03 (d, J=8.5 Hz, 2H), 7.31 (d, J=8.7 Hz, 2H), 7.72 (d, J=8.8 Hz, 2H). Anal. (C$_{14}$H$_{15}$NO$_3$S) C, H, N.

Mannich reaction of **10** afforded the crude product **6b**. It was purified by column chromatography (silica gel, AcOEt:MeOH:25% NH$_4$OH=1:1:0.1) and recrystallized from EtOH-H$_2$O to give **6b** in 80% yield, mp 129–130 °C. ^{1}H NMR (CDCl$_3$) δ 1.68–1.88 (m, 8H), 2.41 (s, 3H), 2.44–2.64 (m, 8H), 3.63 (s, 4H), 3.70 (s, 2H), 6.84 (s, 2H), 7.28 (d, J=8.7 Hz, 2H), 7.72 (d, J=8.8 Hz, 2H). Anal. (C$_{24}$H$_{33}$N$_3$O$_3$S) C, H, N.

N-[3,5-bis(1-pyrrolidylmethyl)-4-hydroxybenzyl]-4-chlorobenzenesulfamide (6i)

N-(4-hydroxybenzyl)-4-chlorobenzenesulfamide (**12**) was obtained in 73% yield, mp 187–189 °C (EtOH). ^{1}H NMR (CDCl$_3$) δ 3.14 (s, 2H), 6.76 (d, J=8.7 Hz, 2H), 6.95 (d, J=8.7 Hz, 2H), 7.51 (m, 4H). Anal. (C$_{13}$H$_{12}$NO$_3$SCl) C, H, N, Cl.

Mannich reaction of **12** gave product **6i** in 77% yield, mp 112–113 °C (EtOH). ^{1}H NMR (CDCl$_3$) δ 1.67–1.87 (m, 8H), 2.43–2.63 (m, 8H), 3.63 (s, 4H), 3.97 (s, 2H), 6.81 (s, 2H), 7.42 (d, J=8.6 Hz, 2H), 7.75 (d, J=8.7 Hz, 2H). Anal. (C$_{23}$H$_{30}$N$_3$O$_3$SCl) C, H, N, Cl.

N-[3,5-bis(1-pyrrolidylmethyl)-4-hydroxybenzyl]-4-acetamidobenzenesulfamide (6m)

N-(4-hydroxybenzyl)-4-acetamidobenzenesulfamide (**13**) was obtained in 81% yield, mp 185–186 °C (EtOH). ^{1}H NMR (CDCl$_3$) δ 2.12 (s, 3H), 3.97 (s, 2H), 6.72 (d, J=8.7 Hz, 2H), 7.08 (d, J=8.7 Hz, 2H), 7.78 (m, 4H). Anal. (C$_{15}$H$_{16}$N$_2$O$_4$S) C, H, N.

Mannich reaction of **13** gave product **6m** in 93% yield, mp 105–107 °C (EtOH-H$_2$O). ^{1}H NMR (CDCl$_3$) δ 1.68–1.88 (m, 8H), 2.16 (s, 3H), 2.48–2.68 (m, 8H), 3.65 (s, 4H), 3.94 (s, 2H), 6.83 (s, 2H), 7.60 (d, J=8.8 Hz, 2H), 7.69 (d, J=8.8 Hz, 2H), 8.37 (s, 1H). Anal. (C$_{25}$H$_{34}$N$_4$O$_4$S·H$_2$O) C, H, N.

N-[3,5-bis(1-pyrrolidylmethyl)-4-hydroxyphenyl]-N-methyl-4-methyl-benzenesulfamide (6c)

A mixture of 4-methylaminophenol sulfate (0.34 g, 2.0 mmol), triethylamine (0.56 mL, 4.0 mmol) and 4-toluenesulfonyl chloride (0.37 g, 2.0 mmol) in ethanol (5 mL) was stirred at room

temperature overnight. The solvent was removed under reduced pressure, and the residue was treated with ether. The ether layer was successively washed with 2 N hydrochloric acid, a saturated solution of NaHCO$_3$ and water. The organic layer was dried over anhydrous Na$_2$SO$_4$. After removal of the solvent, the residue was recrystallized from EtOH to give 0.43 g (77%) of N-(4-hydroxyphenyl)-N-methyl-4-methyl-benzenesulfamide (**14**), mp 136–137 °C. ^{1}H NMR (CDCl$_3$) δ 2.35 (s, 3H), 3.04 (s, 3H), 6.64 (d, J=8.4 Hz, 2H), 6.82 (d, J=8.4 Hz, 2H), 7.14 (d, J=8.7 Hz, 2H), 7.36 (d, J=8.7 Hz, 2H). Anal. (C$_{14}$H$_{15}$NO$_3$S) C, H, N.

A mixture of **14** (0.33 g, 1.2 mmol), pyrrolidine (0.33 mL, 4.0 mmol) and a 36%–38% solution of formaldehyde (0.33 mL, 4.4 mmol) in EtOH (3 mL) was refluxed for 4 h. The solvent was removed on a rotary evaporator, and the crude product was purified by column chromatography (silica gel, AcOEt:MeOH:25% NH$_4$OH=9:1:0.05) to give an oil that crystallized upon standing. Recrystallization from EtOH-H$_2$O gave 0.41 g (78%) of 6c, mp 78–79 °C. ^{1}H NMR (CDCl$_3$) δ 1.68–1.88 (m, 8H), 2.38 (s, 3H), 2.43–2.63 (m, 8H), 3.10 (s, 3H), 3.66 (s, 4H), 6.74 (s, 2H), 7.17 (d, J=8.8 Hz, 2H), 7.40 (d, J=8.8 Hz, 2H). Anal. (C$_{24}$H$_{33}$N$_3$O$_3$S) C, H, N.

N-[3,5-bis(1-pyrrolidylmethyl)-4-hydroxyphenyl]-N-methyl-4-methoxy-benzenesulfamide (6g)

In the same manner as for the preparation of **14** and **6c**, N-(4-hydroxyphenyl)-N-methyl-4-methoxybenzenesulfamide (**15**) was obtained in 95% yield, mp 89–90 °C (EtOH). ^{1}H NMR (CDCl$_3$) δ 3.04 (s, 3H), 3.80 (s, 3H), 6.65 (d, J=8.4 Hz, 2H), 6.72–6.89 (m, 4H), 7.41 (d, J=8.7 Hz, 2H). Anal. (C$_{14}$H$_{15}$NO$_4$S) C, H, N.

Mannich reaction of **15** gave the product **6g** in 78% yield, mp 125–127 °C (EtOH-H$_2$O). ^{1}H NMR (CDCl$_3$) δ 1.69–1.89 (m, 8H), 2.46–2.66 (m, 8H), 3.10 (s, 3H), 3.68 (s, 4H), 3.83 (s, 3H), 6.77 (s, 2H), 6.86 (d, J=8.7 Hz, 2H), 7.46 (d, J=8.7 Hz, 2H). Anal. (C$_{24}$H$_{33}$N$_3$O$_4$S) C, H, N.

N-[3,5-bis(1-pyrrolidylmethyl)-4-hydroxyphenyl]-N-methyl-4-chloro-benzenesulfamide (6j)

In the same manner as for the preparation of **14** and **6c**, N-(4-hydroxyphenyl)-N-methyl-4-chlorobenzenesulfamide (**16**) was obtained in 80% yield, mp 162–163 °C (Et$_2$O). ^{1}H NMR (CDCl$_3$) δ 3.16 (s, 3H), 6.73 (d, J=8.6 Hz, 2H), 6.89 (d, J=8.6 Hz, 2H), 7.55 (m, 4H). Anal. (C$_{13}$H$_{12}$NO$_3$SCl) C, H, N, Cl.

Mannich reaction of **16** gave the product **6j** in 78% yield, mp 87–88 °C (EtOH-H$_2$O). ^{1}H NMR (CDCl$_3$) δ 1.69–1.89 (m, 8H), 2.42–2.62 (m, 8H), 3.12 (s, 3H), 3.65 (s, 4H), 6.73 (s, 2H), 7.37 (d, J=8.7 Hz, 2H), 7.46 (d, J=8.7 Hz, 2H). Anal. (C$_{23}$H$_{30}$N$_3$O$_3$SCl) C, H, N, Cl.

N-[3,5-bis(1-pyrrolidylmethyl)-4-hydroxyphenyl]-N-methyl-4-acetamido-benzenesulfamide (6n)

In the same manner as for the preparation of **14** and **6c**, N-(4-hydroxyphenyl)-N-methyl-4-acetamidobenzenesulfamide (**17**) was obtained in 77% yield, mp 202–203 °C (EtOH). ^{1}H NMR (CDCl$_3$) δ 2.07 (s, 3H), 3.03 (s, 3H), 6.64 (d, J=8.4 Hz, 2H), 6.82 (d, J=8.4 Hz, 2H), 7.36 (d, J=8.8 Hz, 2H), 7.70 (d, J=8.8 Hz, 2H). Anal. (C$_{15}$H$_{16}$N$_2$O$_4$S) C, H, N.

Mannich reaction of **17** gave the product **6n** in 81% yield, mp 96–97 °C (EtOH-H$_2$O). ^{1}H NMR (CDCl$_3$) δ 1.67–1.87 (m, 8H), 2.17 (s, 3H), 2.44-2.64 (m, 8H), 3.09 (s, 3H), 3.64 (s, 4H), 6.73 (s, 2H), 7.43 (d, J=9.0 Hz, 2H), 7.57 (d, J=9.0 Hz, 2H), 8.20 (brs, 1H). Anal. (C$_{25}$H$_{34}$N$_4$O$_4$S ·0.5H$_2$O) C, H, N.

N-[3,5-bis(1-pyrrolidylmethyl)-4-hydroxyphenyl]-N-ethyl-4-methyl-benzenesulfamide (6d)

Using the same procedure as for the preparation of **6a**, compound **6d** was prepared from 4-ethylamino-2,6-bis(1-pyrrolidyl methyl)phenol and 4-toluenesulfonyl chloride in 48% yield, mp 119–120 °C (AcOEt). ^{1}H NMR (CDCl$_3$) δ 1.21 (t, J=7.0 Hz, 3H), 1.60–2.12 (m, 8H), 2.51 (s, 3H), 2.68–3.20 (m, 10H), 3.85 (s, 4H), 6.92 (s, 2H), 7.40 (d, J=8.7 Hz, 2H), 7.77 (d, J=8.7 Hz, 2H). Anal. (C$_{25}$H$_{35}$N$_3$O$_3$S) C, H, N.

N-[3,5-bis(1-piperidylmethyl)-4-hydroxyphenyl]-1-naphthalene-sulfamide (6p)

A mixture of N-(4-hydroxyphenyl)-1-naphthalenesulfonamide (2.0 g, 6.7 mmol), 37% aqueous formaldehyde (4.5 g, 56 mmol) and piperidine (5.6 g, 66 mmol) in ethanol (100 mL) was heated to reflux for 12 h. The ethanol was removed by evaporation under vacuum, and chloroform was added to the residue. The organic layer was washed with water and dried over anhydrous Na$_2$SO$_4$. The chloroform was then removed in vacuo, and the residue was triturated in water to give a solid, which was recrystallized from ethanol to give the title product **6p** (1.4 g, 42%), mp 197–198 °C. ^{1}H NMR (CDCl$_3$) δ 1.35–1.50 (m, 12H), 2.10–2.21 (m, 8H), 3.28 (s, 4H), 6.45 (s, 2H), 7.24–8.04 (m, 6H), 8.56 (m, 1H). Anal. (C$_{28}$H$_{35}$N$_3$O$_3$S) C, H, N.

N-[3,5-bis(1-pyrroliylmethyl)-4-hydroxyphenyl]-1-naphthalene-sulfamide (6o)

Compound **6o** was prepared by the same procedure as that used for **6p** in 34% yield, mp 181–182 °C (EtOH). ^{1}H NMR (CDCl$_3$) δ 1.52–1.80 (m, 8H), 2.10–2.20 (m, 8H), 3.42 (s, 4H), 6.45 (s, 2H), 7.25–8.00 (m, 6H), 8.55 (m, 1H). Anal. (C$_{26}$H$_{31}$N$_3$O$_3$S) C, H, N.

Author contribution

Dong-lu BAI, Wei-zhou CHEN, and Yi-ping WANG designed and supervised the research project; Yun-xin BO, Zhong-liang HU, and Ai-li KANG performed the chemical synthesis; Yue-li DONG, Wei-kang SUN, and Yi-ping WANG performed the animal assays; Wei WANG and Yi-ping WANG performed

the assays *in vitro;* Dong-lu BAI and Yi-ping WANG analyzed the data and wrote the manuscript.

Supplementary information

Supplementary information (IR spectra and elemental analysis data for all new compounds) are available at website of Acta Pharmacologica Sinica on NPG.

References

1 Echt DS, Liebson PR, Mitchell LB, Peters RW, Obias-Manno D, Barker AH, *et al*. Mortality and morbidity in patients receiving encainide, flecainide, or placebo. The Cardiac Arrhythmia Suppression Trial. N Engl J Med 1991; 324: 781–8.

2 Nattel S, Carlsson L. Innovative approaches to anti-arrhythmic drug therapy. Nat Rev Drug Discov 2006; 5: 1034–49.

3 Walker MJA, So PPS. Anti-arrhythmics, In: Comprehensive Medicinal Chemistry II, Vol. 6 (Williams, M Ed). Amsterdam: Elsevier; 2007. p 729–62.

4 Li LQ, Qu ZX, Wang ZM, Zeng YL, Ding GS, Hu GJ, *et al*. Studies on a new antiarrhythmic drug changrolin — 4-(3′, 5′- bis(N-pyrrolidinylmethyl)-4′-hydroyanilino)quinazoline. Sci Sin 1979; 22: 1220–8.

5 Changrolin Coordination Research Group. Clinical observation on changrolin, an antiarrhythmic drug. Nat Med J Chin 1978; 58: 84–6.

6 Sun CJ, Zhang XY, Yang XZ, Wang PP, Shen J, Shu Y, *et al*. Studies on drugs for coronary diseases II. Synthesis of compounds related to changrolin as potential antiarrhythmic drugs. Yao Xue Xue Bao 1981; 16: 564–70.

7 Kang AL, Sun CJ. Studies on drugs for coronary diseases III. Synthesis of some Mannich lases of substituted aminophenols. Yao Xue Xue Bao 1986; 21: 892–8.

8 Chen WZ, Dong YL, Ding GS. Cardiovascular effect of a new antiarrhythmic drug — changrolin. Yao Xue Xue Bao 1979; 14: 710–4.

9 Stout DM, Matier WL, Barcelon-Yang C, Reynolds RD, Brown BS. Synthesis and antiarrhythmic and parasympatholytic properties of substituted phenols. 1. Heteroarylamine derivatives. J Med Chem 1983; 26: 808-13.

10 Stout DM, Matier WL, Barcelon-Yang C, Reynolds RD, Brown BS. Synthesis and antiarrhythmic and parasympatholytic properties of substituted phenols. 2. Amides. J Med Chem 1984; 27: 1347–50.

11 Stout DM, Matier WL, Barcelon-Yang C, Reynolds RD, Brown BS. Synthesis and antiarrhythmic and parasympatholytic properties of substituted phenols. 3. Modification of the linkage region. J Med Chem 1985; 28: 295–8.

12 Stout DM, Black LA, Barcelon-Yang C, Matier WL, Brown BS, Quon CY, *et al*. Ester derivatives of 2,6-bis(1-pyrrolidinylmethyl)-4-benzamidophenol as short-acting antiarrhythmic agents 1. J Med Chem 1989; 32: 1910–3.

13 Chorvat RJ, Black LA, Ranade VV, Barcelon-Yang C, Stout DM, Brown BS, *et al*. Mono- and bis(aminomethyl)phenylacetic acid esters as short-acting antiarrhythmic agents 2. J Med Chem 1993; 36: 2494–8.

14 Bo YX. The preparation of changrolin analogs [dissertation]. Shanghai Institute of Materia Medica, Chinese Academy of Sciences; 1991.

15 Chen WZ, Dong YL, Zhang YF, Ding GS. Antiarrhythmic effects of guan-fu base A. Zhongguo Yao Li Xue Bao 1983; 4: 247–50.

16 Dong YL, Chen WZ. Effects of guan-fu base A on experimental cardiac arrhythmia and myocardial contractility. Yao Xue Xue Bao 1995; 30: 577–82.

17 Kuang Y, Liu TP. Rate-dependent depression of maximal rate of depolarization in guinea pig papillary muscle action potentials by changrolin. Zhongguo Yao Li Xue Bao 1990; 11: 225–9.

18 Farmer BB, Mancina M, Williams ES, Watanabe AM. Isolation of calcium tolerant myocytes from adult rat heart: review of the literature and description of a method. Life Sci 1983; 33: 1–18.

19 Wang W, Hu GY, Wang YP. Selective modulation of L-type calcium current by magnesium lithospermate B in guinea-pig ventricular myocytes. Life Sci 2006; 78: 2989–97.

20 Wang W. Electrophysiological characterization of new cardiovascularly active compounds and cholinesterase inhibitors in guinea-pig heart [dissertation]. Shanghai Institute of Materia Medica, Chinese Academy of Sciences; 2005.

npg

Original Article

LLDT-67 attenuates MPTP-induced neurotoxicity in mice by up-regulating NGF expression

Dong-dong WU[1], Li HUANG[1], Lei ZHANG[1], Le-yu WU[1], Yuan-chao LI[2], Linyin FENG[1, *]

[1]State Key Laboratory of Drug Research, [2]Department of Medicinal Chemistry, Shanghai Institute of Materia Medica, Chinese Academy of Sciences, Shanghai 201203, China

Aim: To investigate the neuroprotective effects of LLDT-67, a novel derivative of triptolide, in MPTP-induced mouse Parkinson's disease (PD) models and in primary cultured astrocytes, and to elucidate the mechanisms of the action.
Methods: In order to induce PD, C57BL/6 mice were injected MPTP (30 mg/kg, ip) daily from d 2 to d 6. MPTP-induced behavioral changes in the mice were examined using pole test, swimming test and open field test. The mice were administered LLDT-67 (1, 2, or 4 mg/kg, *po*) daily from d 1 to d 11. On d 12, the mice were decapitated and brains were collected for immunohistochemistry study and measuring monoamine levels in the striatum. Primary cultured astrocytes from the cortices of neonatal C57BL/6 mouse pups were prepared for *in vitro* study.
Results: In MPTP-treated mice, administration of LLDT-67 significantly reduced the loss of tyrosine hydroxylase-positive neurons in the substantia nigra, and ameliorated the behavioral changes. LLDT-67 (4 mg/kg) significantly increased the expression of NGF in astrocytes in the substantia nigra and striatum of the mice. Furthermore, administration of LLDT-67 caused approximately 2-fold increases in the phosphorylation of TrkA at tyrosine 751, and marked increases in the phosphorylation of AKT at serine 473 as compared with the mice model group. In the cultured astrocytes, LLDT-67 (1 and 10 nmol/L) increased the NGF levels in the culture medium by 179% and 160%, respectively.
Conclusion: The neuroprotective effect of LLDT-67 can be mostly attributed to its ability to enhance NGF synthesis in astrocytes in the midbrain and to rescue dopaminergic neurons indirectly through TrkA activation.

Keywords: LLDT-67; triptolide; Parkinson's disease; MPTP; neuroprotection; dopaminergic neurons; substantia nigra; striatum; NGF; TrkA

Introduction

Parkinson's disease (PD) is the second most common neurodegenerative disease and is characterized by bradykinesia, resting tremor, gait disturbance and postural instability. PD is caused by the progressive degeneration of dopaminergic neurons in the substantia nigra, which results in the depletion of the neurotransmitter dopamine in the striatum. It has been proposed that parkinsonian clinical signs appear at the point when dopaminergic neuronal cell loss exceeds a critical threshold: 70%–80% of striatal nerve terminals and 50%–60% of the substantia nigra par compacta perikaryons[1, 2]. L-dopa is the most widely used drug for the treatment of PD, but long-term treatment can produce several adverse side effects. Therefore, the search for novel drugs for the treatment of PD

is an important endeavor. Triptolide is one of the major active components of the Chinese herb *Tripterygium wilfordii* Hook F. It is well known that triptolide has anti-inflammatory, immunosuppressive, contraceptive and antitumor properties[3–5]. Some studies indicate that PD is a chronic neuroinflammatory process, and triptolide has been found to possess antiparkinsonian effects[6]. However, triptolide's severe toxicity limits its clinical applications. LLDT-67, which is characterized by strong biological activity and low toxicity, is a novel derivative of triptolide.

Materials and methods
Reagents
(5*R*)-5a-hydroxytriptolide (T8) and LLDT-67 (Figure 1) were synthesized by Prof Yuan-chao LI of the Department of Medicinal Chemistry of Shanghai Institute of Materia Medica. 1-Methyl-4-phenyl-1,2,3,6-tetrahydropyridine (MPTP) and *L*-dopa were purchased from Sigma Chemical Co (St Louis,
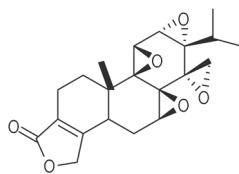
Figure 1. Structure of LLDT-67.

MO, USA) and dissolved in saline. Anti-tyrosine hydroxylase (TH) antibodies and anti-glial fibrillary acidic protein (GFAP) were purchased from Chemicon International (Temecula, CA, USA). Anti-NGF was purchased from Sigma Chemical Co (St Louis, MO, USA). Anti-phospho-ERK1/2 and anti-phospho-AKT (473) antibodies were purchased from Cell Signaling Technology, Inc (Boston, USA); the anti-p-TrkA (490) antibody was purchased from Abcam Ltd (Hongkang, China); and the anti-phospho-TrkA (751) antibody was purchased from Invitrogen Inc (Carlsbad, CA, USA). All DyLight™488- and DyLight™59-labeled secondary antibodies were purchased from Jackson ImmunoResearch Laboratories, Inc (West Grove, PA, USA). Biotinylated secondary antibodies and avidin-biotin peroxidase complexes were purchased from Vector Laboratories (Burlingame, CA, USA). Dopamine (DA) and its metabolites, 3,4-dihydroxyphenylacetic acid (DOPAC), homo-vanillic acid (HVA) and 3,4-dihydroxybenzylamine (DHBA), were purchased from Fluka Chemicals (Switzerland). The ChemiKine NGF Immunoassay system and the SuperSignal West Dura Extended Duration Substrate were purchased from Chemicon (Temecula, CA, USA) and Pierce (Rockford, IL, USA), respectively.

Animals

Male C57BL/6 mice, weighing 20–22 g, were used in the present study. The animals had free access to solid food and water under standard conditions of temperature, humidity and lighting. The study was performed in compliance with the National Research Council's guidelines and was approved by the Animal Care and Use Committee of the Shanghai Institute of Materia Medica, Chinese Academy of Sciences.

1-Methyl-4-phenyl-1,2,3,6-tetrahydropyridine (MPTP) induced PD in mice at a dose of 30 mg/kg. MPTP was administered intraperitoneally for five consecutive days starting from d 2[7, 8]. Three doses of LLDT-67 were administered intra-gastrically for 11 consecutive days starting from d 1. On d 12, the animals were anesthetized and brain tissue was collected.

Behavioral studies
Pole test

The pole test was used to evaluate bradykinesia, a typical symptom of parkinsonism[9, 10]. The mice were placed head up near the top of a vertical rough-surfaced pole (8 mm in diameter and 55 cm in length). The time it took the mice to turn around completely and face the floor (time to turn; T-turn) and the time it took the mice to climb down the pole and place all four feet on the floor (locomotion activity time; T-LA) were

recorded with a cutoff limit of 30 s. The test was performed five times on each mouse.

Swimming test

The mice were forced to swim in an acrylic glass cylinder filled with water and from which they could not escape. The test lasted 90 s, and the time that the mice spent swimming was measured. If the time that mice swimming is over 90 s, then the measure is stopped and the time is recorded as 90 s.

Open-field test

The open field test is a simple assessment used to determine general activity levels, gross locomotor activity and exploration habits in mice[11]. The assessment was conducted on the 7th d in one of two square arenas (40 cm×40 cm) enclosed by a 30-cm wall. Each arena was divided into 16 smaller equal-sized squares (10 cm×10 cm). Each mouse was placed in the center of the open-field arena and allowed to move about freely for 5 min. Four parameters were measured in this experiment: line crossing (the number of lines crossed), cleaning (the number of times the mouse cleaned its fur), hind limb standing (the number of times the mouse stood on its hind legs), and inactive sitting (the duration of inactivity measured in sitting). At the conclusion of each trial, the surface of the arena was cleaned with 90% ethanol. The evaluation was conducted by an investigator who was unaware of the information of grouping and drug administration.

Immunohistochemistry

On d 12, after anesthetization with 10% chloral hydrate, the mice were perfused with PBS via the intracardiac route, followed by 4% paraformaldehyde in PBS. The mice were then decapitated, and the brains were removed and immersed for 24 h in 4% paraformaldehyde for fixation. Midbrain coronal sections were then prepared using a cryostat. For DAB staining, the sections were first rinsed with PBS containing 0.1% Triton-X and then immersed in a solution of 0.5% H_2O_2 for 30 min. After incubating overnight with anti-TH (1:1000) in PBS-T containing 10% goat serum at 4 °C, the sections were washed three times with PBS-T and incubated with a biotinylated secondary antibody in PBS-T for 2 h at room temperature. The sections were then incubated with an avidin-biotin peroxidase complex for 1 h. A final incubation with DAB was performed for visualization. The sections were then washed with PBS, mounted on aminopropyltriethoxysilane-coated slides, dried, dehydrated in a graded series of ethanol, cleared in xylene, and coverslipped. For immunofluorescence staining, the sections were immersed in a 1% SDS solution and incubated for 5 min at room temperature. The sections were then incubated in a serum blocking solution for 1 h. After incubating overnight with mouse monoclonal anti-GFAP (1:1000) and anti-NGF (1:1000) in PBS-T containing 10% goat serum at 4 °C, the sections were washed three times with PBS-T, incubated with DyLight™488- and DyLight™59-labeled secondary antibodies (1:800) and then examined using laser scanning confocal microscopy (Olympus FV300, IX70).

HPLC analysis of monoamine neurotransmitter levels in the striatum

On completion of the study, the mice were deeply anesthetized by administering 10% chloral hydrate and rapidly decapitated. Striata were dissected and homogenized by sonication in an ice-cold processing solution (0.2 mol/L perchloric acid, 0.2 mmol/L sodium pyrosulfite, and 0.01% EDTA-2Na). The homogenate was centrifuged at 17 000×g for 15 min at 4 °C. The supernatant was analyzed for dopamine and its metabolites, DOPAC and HVA, using reverse-phase HPLC coupled to an electrochemical detector (EC). The mobile phase consisted of 40 mmol/L sodium acetate, 15 mmol/L citric acid, 0.25 mmol/L sodium octanesulfonate, 0.2 mmol/L EDTA-2Na, and 16% methanol (pH 4.3). The filtered supernatant was introduced into the autosampler carrousel (Agilent 1100) with a flow rate of 1 mL/min using a C18 column (DIKMA). The concentrations of DA and its metabolites were quantified using a standard curve, generated by determining the ratio between the known concentration of amines and the concentration of an internal standard of DHBA, and expressed in units of μg/g of wet weight.

Primary astrocyte culture

Astrocytes were prepared from the brains of 1- to 2-d-old neonatal C57BL/6 mouse pups, as described previously by Menet *et al*[12]. Briefly, brain tissues were trypsinized for 15 min, dissociated by gentle trituration, and plated at a density of 5×10^7 cells per 75-cm^2 flask (Corning, USA) in Dulbecco's modified Eagle's medium (DMEM) containing 10% heat-inactivated FBS. Cells were maintained in a complete culture medium for 7 d. Between the 8th and 12th d, the cultures were shaken to remove the top layer of cells sitting on top of the astroglial monolayer to yield mainly type-1 astrocytes with a flat morphology. Before experimental treatments, the cultures of astrocytes were passaged twice. Cells were allowed to reach 90% confluence. To investigate the effects of LLDT-67 on NGF expression, astrocytes were maintained in serum-free DMEM and treated with various concentrations of LLDT-67 for the indicated incubation times. Untreated cells were used as controls.

Enzyme-linked immunosorbent assay (ELISA) for measuring NGF

NGF was detected with the ChemiKine NGF Immunoassay system (Chemicon) according to the manufacturer's instructions. Brain tissue was homogenized in an ice cold homogenization buffer consisting of 100 mmol/L Tris/HCl, pH 7.0, 1 mol/L NaCl, 4 mmol/L EDTA-2Na, 2% Triton X-100, 0.1% sodium azide and protease inhibitors (Sigma) at the following concentrations: 5 μg/mL aprotinin, 0.5 μg/mL antipain, 157 μg/mL benzamidine, 0.1 μg/mL pepstatin A and 17 μg/mL phenylmethylsulphonyl fluoride. The homogenate was centrifuged at 14 000×g for 30 min. The resulting supernatant and mouse astrocyte primary culture medium were used in the NGF assay. Protein concentrations in the supernatant were measured using the mini-Bradford Coomassie Blue colorimetric assay (Bio-Rad). In using the NGF ELISA kit, sheep poly-

clonal antibodies generated against mouse NGF were coated onto a microplate and used to capture NGF from the sample. The sample was incubated overnight at 4 °C. After washing the microplate with wash buffer, NGF-specific mouse monoclonal antibodies were added and incubated at room temperature for 2 h. After washing the plate a second time, mouse-specific donkey polyclonal antibodies were added, labeled with peroxidase, and incubated at room temperature for 2 h. After the addition of the substrate and the stop solution, the optical density was measured at 450 nm using a plate reader.

Western blot analysis

The substantia nigra of decapitated mice were lysed in RIPA lysis buffer and loaded onto a 12% SDS–polyacrylamide gel for electrophoresis. The proteins were transferred onto a polyvinylidene difluoride (PVDF) membrane and incubated with the primary antibodies p-ERK1/2 (1:1000), p-AKT (473) (1:1000), p-TrkA (490) (1:500), and p-TrkA (751) (1:1000, Invitrogen). After washing, the blot was incubated with peroxidase-conjugated secondary antibodies and developed with a SuperSignal West Dura Extended Duration Substrate (Pierce). The bands were digitized, and the optical densities were analyzed using Image-J 1.38.

Statistical analysis

The data are presented as the mean±SEM. Significant differences were determined by paired Student's t-test or one-way analysis of variance (ANOVA) followed by Dunnett's *post hoc* comparison. In all cases, the differences were considered statistically significant if $P<0.05$.

Results

Effect of LLDT-67 on MPTP-induced motor deficits

To ascertain the effect of LLDT-67 on MPTP mouse models, subacute MPTP PD models were used for evaluating the efficacy of LLDT-67. LLDT-67 was administered to C57BL/6 mice (1, 2, and 4 mg/kg, *po*) for 11 d, and the mice were injected with MPTP every day from d 2 until d 6. MPTP injections resulted in significant motor deficits as evaluated by the pole test. Administration of MPTP caused a 33.8-fold increase in the time to turn (T-turn) and a 3.9-fold increase in the locomotion activity time (T-LA), compared with untreated controls. The results were statistically significant ($P<0.01$). Treatment with LLDT-67 significantly reduced the T-turn, but it did not have a significant effect on the T-LA (Figure 2A). We also used the swimming test to evaluate the efficacy of LLDT-67. Swimming time was reduced by 42.6% in MPTP-treated mice, compared with untreated controls ($P<0.01$). LLDT-67 (1 and 4 mg/kg) increased the swimming time significantly (Figure 2B). As for the open-field test, MPTP noticeably reduced the frequency of line crossing and increased the time of inactive sitting, compared with untreated controls ($P<0.001$ and $P<0.01$, respectively). Treatment with LLDT-67 greatly reduced the magnitude of the MPTP-induced changes in locomotor activity (Figure 2C).
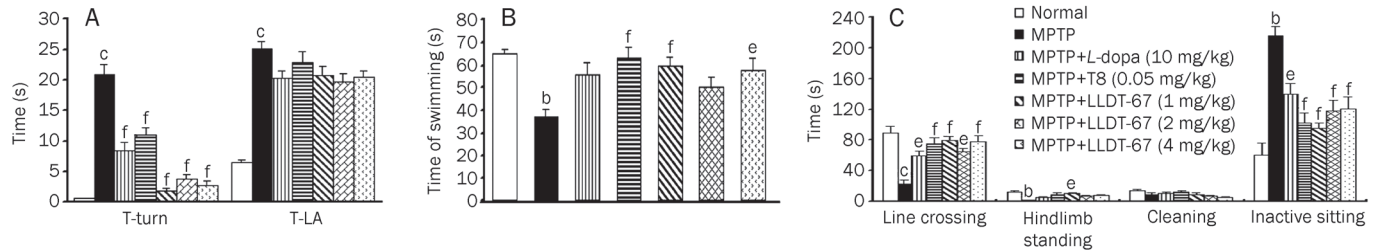
Figure 2. Effect of LLDT-67 on MPTP-induced behavioral changes in mice. (A) Pole test results. (B) Swimming test results. (C) Open-field test results. Each column represents the mean±SEM of the results from 12 mice. $^bP<0.05$, $^cP<0.01$ compared with the control group. $^bP<0.05$, $^cP<0.01$ compared with the model group (one-way ANOVA followed by Dunnett's *post hoc* comparison).

Effect of LLDT-67 on MPTP-induced dopaminergic neuro-degeneration

To elucidate the effect of LLDT-67 on MPTP-induced mouse dopaminergic neurodegeneration, sections of substantia nigra and striatum were stained with anti-TH antibody as a dopaminergic neuron-specific marker. MPTP was administered intraperitoneally for five consecutive days, and dopaminergic neurons in the substantia nigra compacta zone (SNc) were largely lost (Figure 3B). Treatment with LLDT-67 significantly reduced the loss of dopaminergic neurons in the SNc (Figure 3E–3G). These results indicate that LLDT-67 has a neuroprotective effect when administered to mice with MPTP-induced PD.

LLDT-67 increases dopamine content in the striatum

The supernatants of homogenates of the striata of mice in each experimental group were analyzed for dopamine and
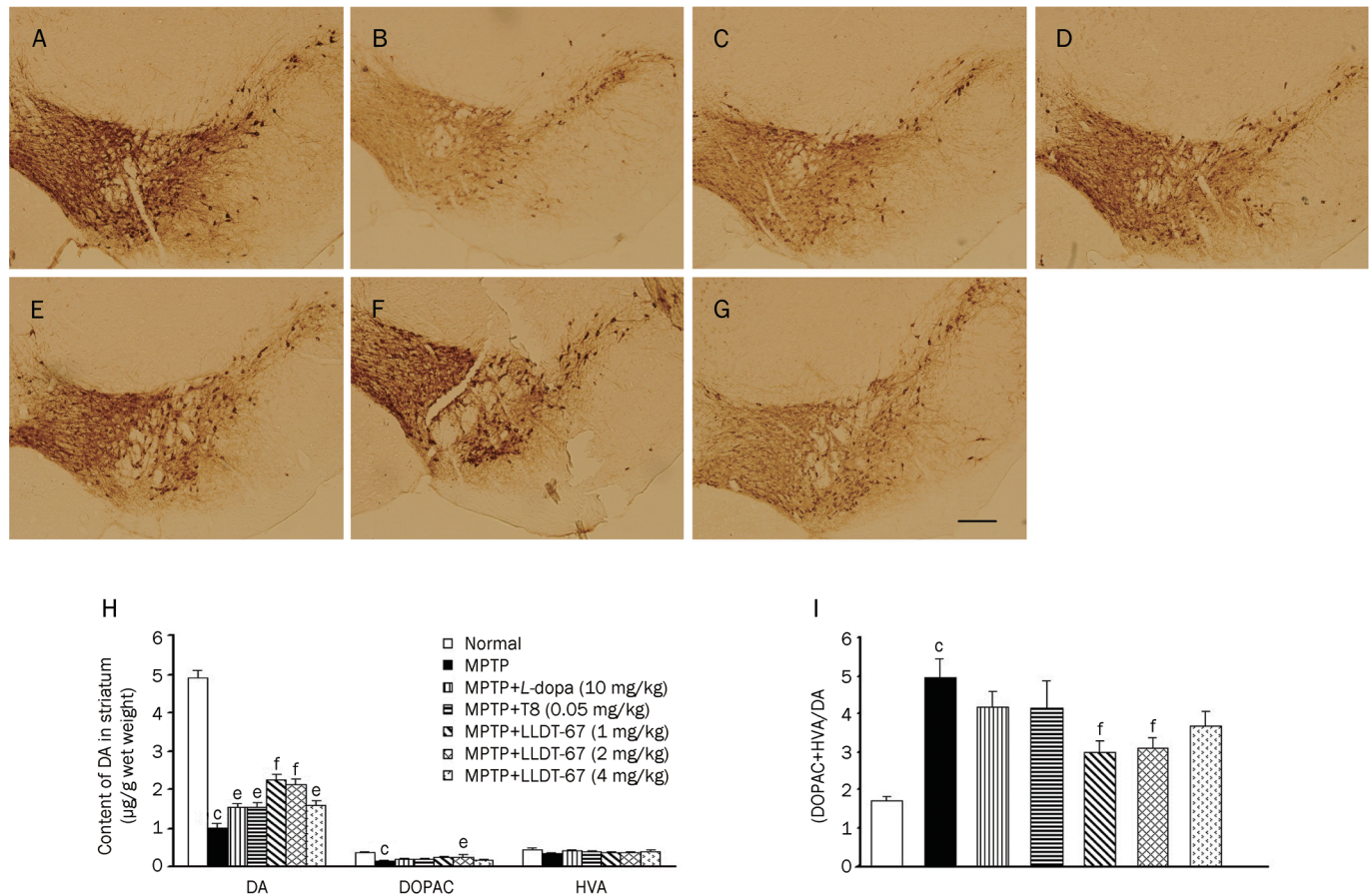

Figure 3. Effect of LLDT-67 on MPTP-induced dopaminergic neuronal loss in the SNc and dopamine-content reduction in the striatum. (A–G) Results of TH histoimmunochemistry, bar=200 μmol/L. ×100. (A) Normal; (B) MPTP; (C) MPTP+*L*-dopa (10 mg/kg); (D) MPTP+T8 (0.05 mg/kg); (E) MPTP+LLDT-67 (1 mg/kg); (F) MPTP+LLDT-67 (2 mg/kg); (G) MPTP+LLDT-67 (4 mg/kg); (H, I) Results of HPLC analysis of the DA content in the striatum. Each column represents the mean±SEM of the results from six mice. $^bP<0.05$, $^cP<0.01$ compared with the control group; $^eP<0.05$, $^fP<0.01$ compared with the model group (one-way ANOVA followed by Dunnett's *post hoc* comparison).

its metabolites, DOPAC and HVA. The samples were analyzed using reverse-phase HPLC coupled to an electrochemical detector (EC). The results indicate that MPTP decreased the dopamine content of the striatum by approximately 80%, whereas LLDT-67 significantly increased the striatal dopamine content compared with the model group. The increased ratio of DOPAC+HVA to DA is indicative of an increase in the DA metabolic rate, which is commonly associated with partial neuronal damage. This result indicates that LLDT-67 can slow down the DA metabolic rate in injured neurons and exert a neuroprotective effect (Figure 3H, 3I).

LLDT-67 increases NGF expression in astrocytes of the SNc of MPTP-treated mice

To understand the mechanisms underlying the neuroprotective effect of LLDT-67 on mice with MPTP-induced PD, we used fluorescent immunohistochemistry to measure NGF expression in MPTP-treated mice. The results indicate that NGF and GFAP colocalized in astrocytes, and LLDT-67 increased NGF expression in astrocytes of the SNc as shown in Figure 4. In the SNc, 2 mg/kg of LLDT-67 significantly increased the expression of NGF in astrocytes, whereas doses of 1 mg/kg and 4 mg/kg only caused a small increase in NGF expression.

LLDT-67 increases the NGF content in the SN and striatum of MPTP-treated mice

We measured NGF concentrations in the SN and the striatum of MPTP-treated mice by performing an ELISA assay. We found that LLDT-67 markedly increased the NGF content in the SN and the striatum of MPTP-treated mice. As shown in Figure 5A and 5B, treatment with a low or moderate dose of LLDT-67 significantly increased NGF concentrations. Interestingly, T8 and L-dopa were ineffective in promoting NGF expression (Figure 5A and 5B).

Effect of LLDT-67 on NGF secretion by mouse astrocytes

To confirm the effect of LLDT-67 on NGF secretion in astrocytes, we purified astrocytes from the brains of newborn C57BL/6 mice and cultured the astrocytes in the presence of LLDT-67 (1×10^{-11}–1×10^{-7} mol/L) for 48 h. NGF levels in the culture medium were measured using an ELISA assay. LLDT-67 treatment increased the NGF levels to some extent in a dose-dependent manner. Notably, 1×10^{-8} and 1×10^{-9} mol/L LLDT-67 increased the NGF levels in the culture medium by approximately 160% and 179%, respectively, compared with controls (Figure 5C).

Effect of LLDT-67 on the phosphorylation of the TrkA tyrosine 751 site and AKT in the SN

To study the mechanism of action of LLDT-67 in promoting neuronal survival, we examined several proteins of the NGF signaling pathway. The results indicate that LLDT-67 can activate TrkA in the SN of mice. Therefore, we set out to determine whether TrkA signaling could be activated by three different doses of LLDT-67 in the mouse brain. Phosphorylation

of TrkA on the 751 site was observed. The results indicate that LLDT-67 increased the phosphorylation of the tyrosine 751 site of TrkA in a dose-dependent manner (Figure 6A). Phosphorylation of AKT (Ser473) paralleled that of the TrkA receptors as shown in Figure 6B. We have demonstrated that LLDT-67 indirectly activates NGF-signaling pathways leading to PI3-kinase activation by directly increasing NGF expression. No changes were observed in the phosphorylation of TrkA-490 and its downstream protein, ERK1/2 (data not shown).

Discussion

To date, triptolide's mechanism of action has remained largely elusive. Recently, Liu *et al*[13] reported that triptolide covalently binds to human XPB (also known as ERCC3), a subunit of the transcription factor TFIIH, and inhibits its DNA-dependent ATPase activity, which leads to the inhibition of RNA polymerase II-mediated transcription and likely nucleotide excision repair. Yu *et al*[14] also found that triptolide inhibits global transcription in cancer cells by induction of phosphorylation and subsequent proteasome-dependent degradation of RNA polymerase II (Rpb1), resulting in global gene transcription. Meanwhile triptolide's anti-proliferative and pro-apoptotic effects have been reported as being caused by the inhibition of nuclear factor-kappaB (NF-κB) and nuclear factor of activated T-cells-mediated (NFAT-mediated) transcription and the suppression of HSP70 expression[15–17].

In this report, we demonstrate for the first time that LLDT-67, a novel derivative of triptolide, has a potent and specific effect on the expression of NGF in astrocytes in vitro and in vivo, which suggests that LLDT-67 can potentially serve as a neuroprotective agent in the treatment of neurodegenerative diseases. NGF is critical for the survival and maintenance of sympathetic and sensory neurons. Without it, these neurons undergo apoptosis[18]. NGF causes axonal growth. Studies have shown that it stimulates axonal branching and elongation[19]. NGF binds to the high-affinity tyrosine kinase receptor TrkA. TrkA is then phosphorylated, and this leads to the activation of the phosphatidylinositol-3 kinase (PI3K) and PLC signaling pathways. One major pathway leads to the activation of AKT. This pathway begins with the Trk receptor complex recruitment of a second adaptor protein called growth factor-receptor bound protein-2 (Grb2) along with a docking protein called Grb2-associated Binder-1 (GAB1). Subsequently, PI3K is activated, which leads to AKT kinase activation[20]. Some studies have shown that inhibiting PI3K or AKT activity results in the death of sympathetic neurons in cultures, regardless of NGF presence[21].

Preclinical and clinical findings suggest that neurotrophins are a promising treatment for peripheral neuropathies[22] and neurodegenerative diseases, such as Alzheimer's[23] and Parkinson's disease[24]. However, neurotrophins do not make good drug candidates because of their poor pharmacokinetic properties and poor bioavailability at desired targets. One of the major hurdles for neurotrophin therapy is the inability of peptide hormones to cross the blood-brain barrier[25, 26]. Peripheral administration of peptide hormones only leads to a
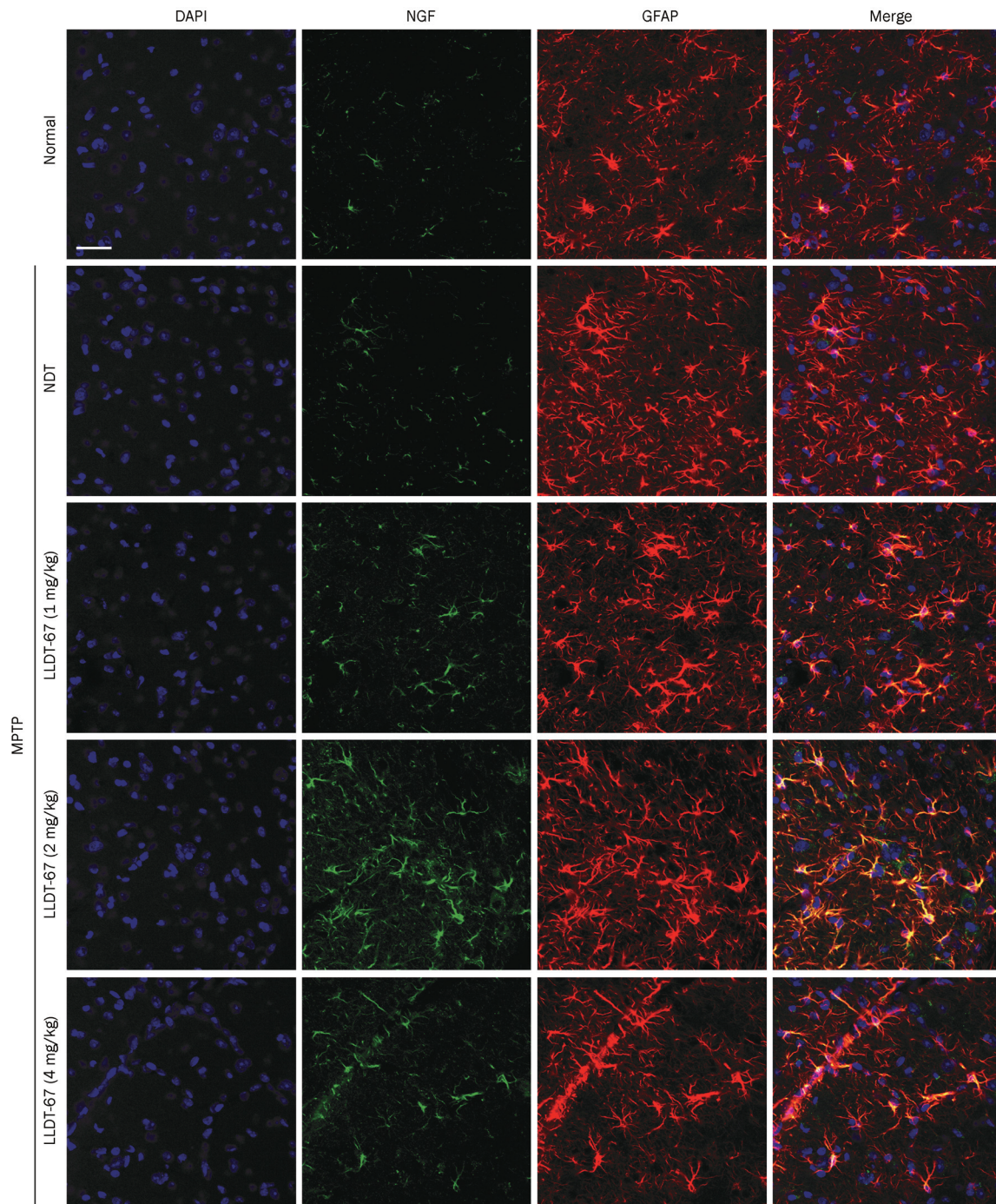
Figure 4. Effect of LLDT-67 on NGF expression in astrocytes of the SNc of MPTP-treated mice. bar=30 μm. ×400.

small increase in their intracerebral concentration. Therefore, much effort has been devoted to the search for complicated methods of delivery[27, 28] and the development of nonpeptidyl small molecule neurotrophin mimics that can elicit the desired neuroregenerative responses[29].

Our data show that LLDT-67 can up-regulate NGF expression in astrocytes and that PI3K signaling downstream of TrkA contributes to the neuroprotective effects of NGF. The PI3-kinase signaling pathway plays a greater role than the MAPK pathway in neuronal survival[24, 30–32]. The MAPK pathway, however, is essential for NGF-induced neurogenesis[33]. This fact may explain why LLDT-67 is more effective in promoting survival than it is in stimulating differentiation because LLDT-67 is a potent activator of AKT but a weak activator of ERK. A low dose of LLDT-67 (1–2 mg/kg) is more effective at activating AKT than a higher dose (4 mg/kg). This result may partially explain the ability of LLDT-67 to attenuate the neurodegeneration induced by MPTP.
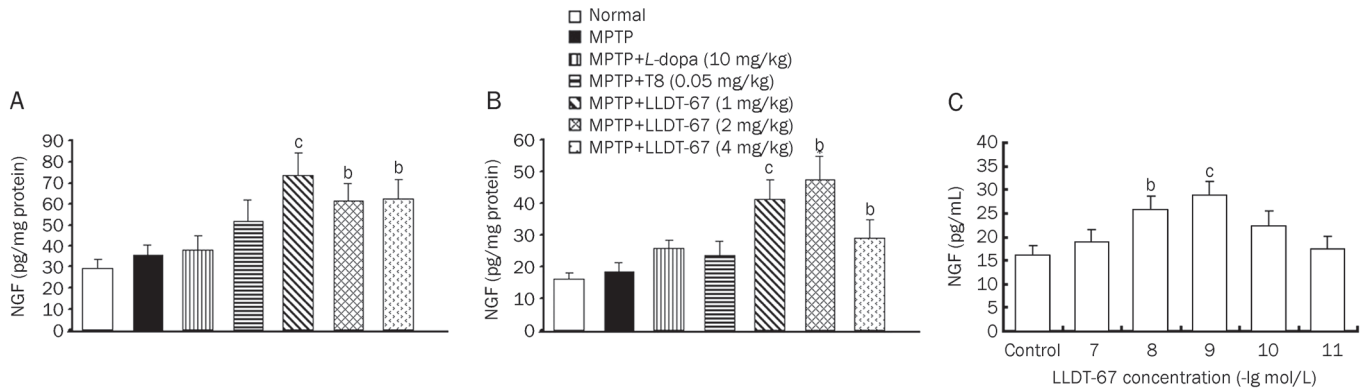
Figure 5. Effect of LLDT-67 on the NGF content in the SN and striatum of MPTP-treated mice and NGF secretion from primary astrocytes. (A) Results of the ELISA assay measuring the NGF content in the SN. (B) Results of the ELISA assay measuring the NGF content in the striatum. Each column represents the mean±SEM of the results from 6 mice. $^{b}P<0.05$, $^{c}P<0.01$ compared with MPTP-treated mice. (C) Results of the ELISA assay measuring NGF secretion from primary astrocytes. Each column represents the mean±SEM of six measurements. $^{b}P<0.05$, $^{c}P<0.01$ compared with control (one-way ANOVA followed by Dunnett's *post hoc* comparison).
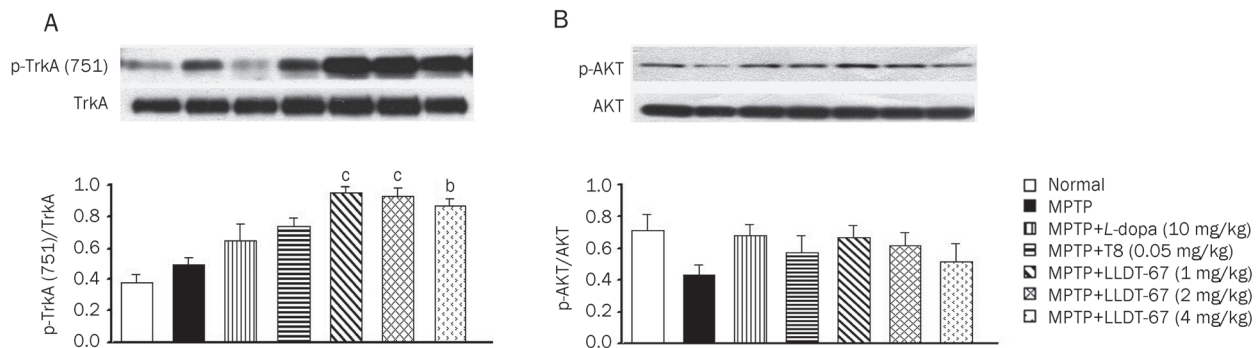

Figure 6. Effect of LLDT-67 on the phosphorylation of the TrkA tyrosine 751 site and AKT in the SN. (A) Effect of LLDT-67 on the phosphorylation of the TrkA tyrosine 751 site in the SN of MPTP-treated mice. Each column represents the mean±SEM of the results from six mice. $^{b}P<0.05$, $^{c}P<0.01$ compared with MPTP-treated mice (one-way ANOVA followed by Dunnett's *post hoc* comparison). (B) Effect of LLDT-67 on the phosphorylation of AKT in the SN of MPTP-treated mice. Each column represents the mean±SEM of the results from six mice (one-way ANOVA followed by Dunnett's *post hoc* comparison).

In conclusion, our study demonstrates that LLDT-67 possesses potent neutrophic effects and protects dopaminergic neurons from degeneration induced by MPTP. Immunohistochemistry staining and ELISA data show that LLDT-67 can stimulate the expression of NGF, which may contribute to its neuroprotective effects. We propose that LLDT-67 may be a promising drug for the treatment of Parkinson's disease.

Acknowledgements

Author contribution

Linyin FENG and Dong-dong WU designed the study; Dong-dong WU, Li HUANG, Lei ZHANG, and Le-yu WU performed the experiments; Yuan-chao LI contributed new reagents; Dong-dong WU analyzed the data; Linyin FENG and Dong-dong WU wrote the paper.

References

1 Bernheimer H, Birkmayer W, Hornykiewicz O, Jellinger K, Seitelberger F. Brain dopamine and the syndromes of Parkinson and Huntington. Clinical, morphological and neurochemical correlations. J Neurol Sci 1973; 20: 415–55.

2 Agid Y. Parkinson's disease: pathophysiology. Lancet 1991; 337: 1321–4.

3 Ren YX, Zhou R, Tang W, Wang WH, Li YC, Yang YF, *et al*. (*5R*)-5-hydroxytriptolide (LLDT-8) protects against bleomycin-induced lung fibrosis in mice. Acta Pharmacol Sin 2007; 28: 518–25.

4 Zhao F, Chen Y, Zeng LL, Li R, Zeng R, Wen L, *et al*. Effects of triptolide on RIZ1 expression, proliferation, and apoptosis in multiple myeloma U266 cells. Acta Pharmacol Sin 2010; 31: 733–40.

5 Wen L, Chen Y, Zeng LL, Zhao F, Li R, Liu Y, *et al*. Triptolide induces cell-cycle arrest and apoptosis of human multiple myeloma cells *in vitro* via altering expression of histone demethylase LSD1 and JMJD2B. Acta Pharmacol Sin 2012; 33: 109–19.

6   Li FQ, Cheng XX, Liang XB, Wang XH, Xue B, He QH, *et al*.   Neurotrophic and neuroprotective effects of tripchlorolide, an extract of Chinese herb *Tripterygium wilfordii* Hook F, on dopaminergic neurons.   Exp Neurol 2003; 179: 28–37.

7   Meredith GE, Sonsalla PK, Chesselet MF.   Animal models of Parkinson's disease progression.   Acta Neuropathol 2008; 115: 385–98.

8   Przedborski S, Jackson-Lewis V, Naini AB, Jakowec M, Petzinger G, Miller R, *et al*.   The parkinsonian toxin 1-methyl-4-phenyl-1,2,3,6-tetrahydropyridine (MPTP): a technical review of its utility and safety.   J Neurochem 2001; 76: 1265–74.

9   Matsuura K, Kabuto H, Makino H, Ogawa N.   Pole test is a useful method for evaluating the mouse movement disorder caused by striatal dopamine depletion.   J Neurosci Methods 1997; 73: 45–8.

10   Kato H, Kurosaki R, Oki C, Araki T.   Arundic acid, an astrocyte-modulating agent, protects dopaminergic neurons against MPTP neurotoxicity in mice.   Brain Res 2004; 1030: 66–73.

11   Meredith GE, Kang UJ.   Behavioral models of Parkinson's disease in rodents: a new look at an old problem.   Mov Disord 2006; 21: 1595–606.

12   Menet V, Gimenez y Ribotta M, Chauvet N, Drian MJ, Lannoy J, Colucci-Guyon E, *et al*.   Inactivation of the glial fibrillary acidic protein gene, but not that of vimentin, improves neuronal survival and neurite growth by modifying adhesion molecule expression.   J Neurosci 2001; 21: 6147–58.

13   Titov DV, Gilman B, He QL, Bhat S, Low WK, Dang Y, *et al*.   XPB, a subunit of TFIIH, is a target of the natural product triptolide.   Nat Chem Biol 2011; 7: 182–8.

14   Wang Y, Lu JJ, He L, Yu Q.   Triptolide (TPL) inhibits global transcription by inducing proteasome-dependent degradation of RNA polymerase II (Pol II).   PLoS One 2011; 6: e23993.

15   Meng HT, Zhu L, Ni WM, You LS, Jin J, Qian WB.   Triptolide inhibits the proliferation of cells from lymphocytic leukemic cell lines in association with downregulation of NF-kappaB activity and miR-16-1.   Acta Pharmacol Sin 2011; 32: 503–11.

16   Qiu D, Zhao G, Aoki Y, Shi L, Uyei A, Nazarian S, *et al*.   Immuno-suppressant PG490 (triptolide) inhibits T-cell interleukin-2 expression at the level of purine-box/nuclear factor of activated T-cells and NF-kappaB transcriptional activation.   J Biol Chem 1999; 274: 13443–50.

17   Phillips PA, Dudeja V, McCarroll JA, Borja-Cacho D, Dawra RK, Grizzle WE, *et al*.   Triptolide induces pancreatic cancer cell death via inhibition of heat shock protein 70.   Cancer Res 2007; 67: 9407–16.

18   Freeman RS, Burch RL, Crowder RJ, Lomb DJ, Schoell MC, Straub JA, *et al*.   NGF deprivation induced gene expression: after ten years, where do we stand?   Prog Brain Res 2004; 146: 111–26.

19   Madduri S, Papaloizos M, Gander B.   Synergistic effect of GDNF and NGF on axonal branching and elongation *in vitro*.   Neurosci Res 2009; 65: 88–97.

20   Wang WX, Hu XY, Xie XJ, Liu XB, Wu RR, Wang YP, *et al*.   Nerve growth factor induces cord formation of mesenchymal stem cell by promoting proliferation and activating the PI3K/Akt signaling pathway.   Acta Pharmacol Sin 2011; 32: 1483–90.

21   Crowder RJ, Freeman RS.   Phosphatidylinositol 3-kinase and Akt protein kinase are necessary and sufficient for the survival of nerve growth factor-dependent sympathetic neurons.   J Neurosci 1998; 18: 2933–43.

22   McMahon SB, Priestley JV.   Peripheral neuropathies and neurotrophic factors: animal models and clinical perspectives.   Curr Opin Neurobiol 1995; 5: 616–24.

23   Tuszynski MH, Thal L, Pay M, Salmon DP, U HS, Bakay R, *et al*.   A phase 1 clinical trial of nerve growth factor gene therapy for Alzheimer disease.   Nat Med 2005; 11: 551–5.

24   Shimoke K, Chiba H.   Nerve growth factor prevents 1-methyl-4-phenyl-1,2,3,6-tetrahydropyridine-induced cell death via the Akt pathway by suppressing caspase-3-like activity using PC12 cells: relevance to therapeutical application for Parkinson's disease.   J Neurosci Res 2001; 63: 402–9.

25   Thorne RG, Frey WH.   Delivery of neurotrophic factors to the central nervous system: pharmacokinetic considerations.   Clin Pharmacokinet 2001; 40: 907–46.

26   Miller G.   Drug targeting.   Breaking down barriers.   Science 2002; 297: 1116–8.

27   Chen XQ, Fawcett JR, Rahman YE, Ala TA, Frey IW.   Delivery of nerve growth factor to the brain via the olfactory pathway.   J Alzheimers Dis 1998; 1: 35–44.

28   Tuszynski MH, Thal L, U HS, Pay MM, Blesch A, Conner J, *et al*.   Nerve growth factor gene therapy for Alzheimer's disease.   J Mol Neurosci 2002; 19: 207.

29   Saragovi HU, Gehring K.   Development of pharmacological agents for targeting neurotrophins and their receptors.   Trends Pharmacol Sci 2000; 21: 93–8.

30   Kaplan DR, Miller FD.   Neurotrophin signal transduction in the nervous system.   Curr Opin Neurobiol 2000; 10: 381–91.

31   Culmsee C, Gerling N, Lehmann M, Nikolova-Karakashian M, Prehn JH, Mattson MP, *et al*.   Nerve growth factor survival signaling in cultured hippocampal neurons is mediated through TrkA and requires the common neurotrophin receptor P75.   Neuroscience 2002; 115: 1089–108.

32   Huang EJ, Reichardt LF.   Trk receptors: roles in neuronal signal transduction.   Annu Rev Biochem 2003; 72: 609–42.

33   Xiao J, Liu Y.   Differential roles of ERK and JNK in early and late stages of neuritogenesis: a study in a novel PC12 model system.   J Neurochem 2003; 86: 1516–23.

npg

Original Article

Emodin, an 11β-hydroxysteroid dehydrogenase type 1 inhibitor, regulates adipocyte function *in vitro* and exerts anti-diabetic effect in *ob/ob* mice

Yue-jing WANG, Su-ling HUANG, Ying FENG, Meng-meng NING, Ying LENG*

State Key Laboratory of Drug Research, Shanghai Institute of Materia Medica, Chinese Academy of Sciences, Shanghai 201203, China

Aim: Emodin (1,3,8-trihydroxy-6-methylanthraquinone) is a potent and selective inhibitor of 11β-hydroxysteroid dehydrogenase type 1 (11β-HSD1) with the ability to ameliorate metabolic disorders in diet-induced obese mice. In the present study, we investigated the effects of emodin on adipocyte function and the underlying mechanisms *in vitro*, and its anti-diabetic effects in *ob/ob* mice.
Methods: 3T3-L1 adipocytes were used for *in vitro* studies. 11β-HSD1A activity was evaluated with a scintillation proximity assay. The adipogenesis, glucose uptake, lipolysis and adiponectin secretion were investigated in 3T3-L1 adipocytes treated with emodin in the presence of active (corticosterone) or inactive glucocorticoid (11-dehydrocorticosterone). For *in vivo* studies, *ob/ob* mice were administered emodin (25 and 50 mg·kg^{-1}·d^{-1}, ip) for 26 d. On the last day of administration, the serum was collected and the mesenteric and perirenal fat were dissected for analyses.
Results: Emodin inhibited the 11β-HSD1 activity in 3T3-L1 adipocytes in concentration- and time-dependent manners (the IC$_{50}$ values were 7.237 and 4.204 μmol/L, respectively, after 1 and 24 h treatment. In 3T3-L1 adipocytes, emodin (30 μmol/L) suppressed 11-dehydrocorticosterone-induced adipogenesis without affecting corticosterone-induced adipogenesis; emodin (3 μmol/L) reduced 11-dehydrocorticosterone-stimulated lipolysis, but had no effect on corticosterone-induced lipolysis. Moreover, emodin (3 μmol/L) partly reversed the impaired insulin-stimulated glucose uptake and adiponectin secretion induced by 11-dehydrocorticosterone but not those induced by corticosterone. In *ob/ob* mice, long-term emodin administration decreased 11β-HSD1 activity in mesenteric adipose tissues, lowered non-fasting and fasting blood glucose levels, and improved glucose tolerance.
Conclusion: Emodin improves the inactive glucocorticoid-induced adipose tissue dysfunction by selective inhibition on 11β-HSD1 in adipocyte *in vitro* and improves glycemic control in *ob/ob* mice.

Keywords: emodin; 11β-hydroxysteroid dehydrogenase type 1; adipocyte; glucocorticoid; type 2 diabetes; *ob/ob* mice

Introduction

Adipose tissue plays a key role in regulating energy balance and glucose homeostasis. As an energy storage depot, adipose tissue responds to the body's metabolic signaling by regulating lipid storage and mobilization. Adipocytes release free fatty acid (FFA) as a nutrient source when glucose is limiting, whereas they store abundant energy as triglycerides in energy excess states. Insulin resistance can elevate the FFA level, and excessive FFA induces a deterioration in the metabolic state by accelerating liver glucose output and by inhibiting glucose uptake by peripheral tissues and the generation of reactive oxygen system (ROS), which, in turn, aggravates insulin resis-

tance[1]. Adipose tissue is an endocrine organ that releases several adipokines, such as leptin, adiponectin, visfatin, omentin, and resistin, to regulate glucose homeostasis and whole body insulin sensitivity [1]. Thus, adipocyte dysfunction is thought to be involved in the pathogenesis of obesity and metabolic diseases such as type 2 diabetes[2].

Glucocorticoid (GC) is an insulin-antagonizing hormone that stimulates hepatic glucose production and suppresses insulin-mediated glucose uptake in peripheral tissues such as adipose tissue and skeletal muscle. Glucocorticoid excess, which is well-characterized in Cushing's syndrome, produces central obesity and several clinical features associated with insulin resistance, such as type 2 diabetes, dyslipidemia, and hypertension[3]. The action of glucocorticoid on target tissue is determined not only by the circulating glucocorticoid level but also by the local glucocorticoid activation, which is regulated

by the 11β-hydroxysteroid dehydrogenase type 1 (11β-HSD1) and 11β-HSD2. 11β-HSD1, which is highly expressed in the liver, adipose tissue, gonads and brain, catalyze the activation of glucocorticoid (cortisol in human and corticosterone in rodents) from inactive 11-kero steroids (cortisone in human and 11-dehydrocorticosterone in rodents). This process amplifies local glucocorticoid action, whereas 11β-HSD2 is predominantly expressed in aldosterone-sensitive target tissues (in the kidney, colon, salivary glands and placenta) and catalyzes the opposite reaction[4].

Excess glucocorticoid in adipocytes decreases insulin-induced glucose uptake, promotes FFA secretion and affects adipokine profiles, thus causing insulin resistance[5]. Therefore, 11β-HSD1 is expected to play an important role in the regulation of glucose and lipid metabolism in adipose tissue. Several human studies have reported two- to three-fold increases in 11β-HSD1 activity in the adipose tissue of obese individuals, and the expression of 11β-HSD1 in adipose tissue was positively correlated with the degree of obesity[6, 7]. The contribution of 11β-HSD1 to the development of insulin resistance and obesity has been further confirmed in animal studies. Mice overexpressing adipose-specific 11β-HSD1 showed increased corticosterone in adipose tissue and developed insulin resistance, central obesity, hyperlipidemia, and other features of metabolism syndrome[8,9], whereas mice overexpressing liver-specific 11β-HSD1 only showed mild insulin resistance and dyslipidemia[10]. 11β-HSD1 knockout mice showed improved glucose tolerance, an elevated HDL, and protection from weight gain during a high-fat diet[11-13]. Moreover, overexpressing 11β-HSD2 to inactivate glucocorticoid in the adipose tissue of mice caused decreased food intake and improved glucose tolerance and insulin sensitivity under conditions of a high-fat diet[14]. Considering the above findings, the pharmacological inhibition of 11β-HSD1, especially in adipose tissue, could be a therapy for type 2 diabetes or metabolic diseases.

Emodin is an anthraquinone compound isolated mainly from the root and rhizome of *Rheum palmatum*. It demonstrates a variety of biological activities, such as anti-virus activities, anti-tumor activities, anti-inflammatory activities, and immune suppression, and it can also serve as a potential agent in therapy for liver cirrhosis, diabetic nephropathy and atherosclerosis[15-20]. Our previous study showed that emodin is a potent and selective 11β-HSD1 inhibitor and can ameliorate metabolic disorders in diet-induced obese mice[21]. In the present study, we investigated the effect of emodin on adipocyte function and the underlying mechanisms involving inhibition of 11β-HSD1. The anti-diabetic effect of emodin was also investigated in *ob/ob* mice, a genetic animal model of type 2 diabetes.

Materials and methods
Materials
Emodin was purchased from Nanjing Zelang Medical Technology Co Ltd (Nanjing, China). Corticosterone, dexamethasone, insulin, glycyrrhetinic acid and 3-isobutyl-1-methylxanthine

were purchased from Sigma (St Louis, MO, USA). 11-Dehydrocorticosterone was purchased from Steraloids (Newport, RI, USA). Fetal bovine serum (FBS), penicillin/streptomycin, HEPES and high glucose Dulbecco's modified Eagle's medium (DMEM) were purchased from GibcoBRL (Grand island, NY, USA). TRIzol Reagent was purchased from Invitrogen (Carlsbad, CA, USA). The M-MLV reverse transcriptional enzyme and SYBR® Premix Ex Taq™ were obtained from Takara (Dalian, China). All the primers were synthesized by Sangon Corporation (Shanghai, China). [1,2-(n)^{3}H]-Cortisone was obtained from Amersham (Buckinghamshire, UK). SPA beads were purchased from GE (Piscataway, NJ, USA). SuperBlock Blocking Buffer was obtained from Pierce (Rockford, IL, USA). The murine monoclonal anti-cortisol antibody was purchased from East Coast Biologics (North Berwick, ME, USA).

3T3-L1 cell culture and differentiation
3T3-L1 preadipocytes were cultured and differentiated as previously described[22]. In brief, 3T3-L1 preadipocytes were maintained at ~70% confluence in DMEM supplemented with 10% FBS, 25 mmol/L glucose and antibiotics (DMEM/FBS). Cells were grown for 2 d post-confluence and cultured in DMEM/FBS supplemented with 1 μmol/L insulin, 0.25 μmol/L dexamethasone, and 0.5 mmol/L 3-isobutyl-1-methylxanthine for 3 d. The medium was replaced with DMEM/FBS supplemented with only 1 μmol/L insulin for 3 d and then DMEM/FBS alone for 2 d. Cytoplasmic triacylglycerol droplets were visible on d 5 after initiation of differentiation. The differentiated cells were used when ~90% of the cells showed an adipocyte phenotype.

11β-HSD1 enzyme activity assay
The reductase activity of 11β-HSD1 in intact 3T3-L1 adipocytes was determined by measuring the rate of conversion of cortisone to cortisol. 3T3-L1 adipocytes were incubated for 1 h at 37 °C in serum-free DMEM containing 6.25 nmol/L [1,2-(N)^{3}H]-cortisone and different concentrations of emodin, according to experimental design, and 0.1% DMSO was set as the vehicle control. To explore the effect of emodin on 11β-HSD1 reductase activity after 24 h of treatment, the adipocytes were pretreated with emodin for 23 h before incubation. At the end of the incubation, 80 μL of medium was pipetted into a transparent bottom 96-well plate, and 35 μL of SuperBlock Blocking Buffer containing 10 g/L of protein A-coated yttrium silicate beads and 3 mg/L of anti-cortisol antibodies was added. The mixtures were shaken in the dark for 2 h and then used for liquid scintillation readings.

Adipogenesis measurement
To observe the effect of emodin on adipocyte adipogenesis, 3T3-L1 preadipocytes were initiated to differentiate with 1 μmol/L insulin, 0.5 mmol/L IBMX and different types of glucocorticoids (0.25 μmol/L dexamethasone, 0.25 μmol/L 11-DHC or 0.25 μmol/L corticosterone). The emodin or vehicle control containing 0.1% DMSO was added on the first day of differentiation, and the medium was changed every

2 d until d 8. The triglyceride content of cells was measured on d 8. After washing with ice-cold PBS, the adipocytes were collected and sonicated in distilled water. The triglyceride content of the cell lysate was measured using the GPO-PAP method, and the absorbance was monitored at 546 nm in a spectrophotometer.

Glucose uptake

3T3-L1 adipocytes were pretreated with 3 µmol/L emodin for 2 h and then incubated with 10 nmol/L corticosterone, 10 nmol/L 11-DHC or 0.1% ethanol for another 24 h. The medium containing 0.1% DMSO was used as the vehicle. At the last 0.5 h of treatment, glucose uptake was determined. The adipocytes were washed twice with pre-warmed (37 °C) PBS and incubated with Krebs-BSA buffer (140 mmol/L NaCl, 5 mmol/L KCl, 2.5 mmol/L $MgSO_4$, 1 mmol/L $CaCl_2$, 20 mmol/L HEPES, and 0.5% BSA, pH 7.4) with or without insulin (basal state) for 25 min, followed by the addition of 0.05 mmol/L 2-deoxy-*D*-glucose and $1.85×10^4$ Bq/mL 2-deoxy-*D*-[1,2-^{3}H]glucose for 5 min. The assay was terminated by washing the cells three times with ice-cold PBS. The cells were solubilized with 0.1% Triton X-100, and radioactivity was determined in a liquid scintillation counter (Beckman LS6500, Fullerton, CA, USA). Total cellular protein concentration was measured by the Bradford method (BioRad, Richmond, CA, USA). Glucose uptake assays were performed in duplicate at least three times.

Lipolysis

3T3-L1 adipocytes were pretreated with 3 µmol/L emodin or 0.1% DMSO for 2 h and then incubated with 10 nmol/L corticosterone, 10 nmol/L 11-DHC or 0.1% ethanol in phenol-red free DMEM for another 48 h. The medium was collected, and the free glycerol (index of lipolysis) was measured using a Free Glycerol Determination Kit (Sigma, St Louis, MO, USA).

Adiponectin release

3T3-L1 adipocytes were pretreated with 3 µmol/L emodin or 0.1% DMSO for 2 h in serum-free DMEM and were then incubated with 50 nmol/L corticosterone, 50 nmol/L 11-DHC or 0.1% ethanol for another 48 h. After treatment, the cell medium was collected and added to 5×Laemmli Buffer. The medium was then degenerated at 56 °C for 20 min. Equal amounts of the medium were subjected to 10% SDS polyacrylamide gel electrophoresis, and the separated proteins were transferred to polyvinylidene difluoride membranes. Then, the membranes were blocked for 1 h with 7.5% non-fat milk at room temperature and incubated with an antibody against adiponectin (R&D, MN, USA) at 4 °C. After overnight incubation with the primary antibody, the blots were repeatedly washed in 0.1% TBS-Tween and incubated with a 1:10 000 dilution of an HRP-conjugated secondary antibody in 0.1% TBS-Tween for 1 h. Following further washes, proteins were detected using an ECL Plus Western Blotting Detection System (Amersham, Arlington Heights, IL, USA) and quantified by densitometry.

Animals and treatments

B6.V-*Lep*^{ob}/*Lep*^{ob} (*ob/ob*) mice and their lean littermates$^{+/+}$ (from Jackson Laboratory, Bar Harbor, ME, USA) were bred at the Shanghai Institute of Materia Medica (SIMM), Chinese Academy of Sciences. The animals were maintained under a 12-h light-dark cycle with free access to water and food. The animal experiments were approved by the Animal Care and Use Committee, Shanghai Institute of Materia Medica, Chinese Academy of Sciences.

Based on fasting blood glucose values (first criterion) and initial body weights (second criterion), the *ob/ob* mice were assigned to four groups. The *ob/ob* mice were subjected to intraperitoneal injection treatment twice daily with the vehicle (0.5% Tween 80), emodin (25 mg/kg) or emodin (50 mg/kg) for 26 d. We subjected the fourth group of *ob/ob* mice to pair feeding (providing the mice each day with the amount of food eaten by the freely fed mice treated with 50 mg/kg of emodin) on d 7. The lean mice were treated with the vehicle (0.5% Tween 80). The blood glucose levels were measured via blood drops obtained by clipping the tail of the mice using a ONE TOUCH BASIC plus Glucose Monitor (Lifescan, Milpitas, CA, USA). The food intake and body weight of the animals were recorded every 3 d. A glucose tolerance test was performed for mice deprived of food for 5 h (2.5 g/kg of glucose administered by gavage) on d 20 of the treatment. On the last day of administration, the mice were anaesthetized with an ip injection of sodium pentobarbital (40 mg/kg). The serum was collected for the determination of triacylglycerol, cholesterols and the non-esterified free fatty acid (NEFA) concentration. The mesenteric and perirenal fat were dissected, weighed, immediately frozen in liquid nitrogen and stored at -80 °C.

Real-time PCR

The mesenteric fat was homogenized in TRIZOL solution, and the total mRNA was extracted following the manufacturer's instructions. One microgram of total mRNA was reverse-transcribed in a 20-µL reaction mixture containing 4 µL 5×PrimeScript Buffer, 1 µL Primescript RT Enzyme Mix I, 1 µL Random 6 mers (100 µmol/L), 1 µL Oligo dT Primer (50 µmol/L), and 11 µL RNAse-free H_2O. The mixture was incubated at 37 °C for 15 min, then at 85 °C for 5 s. Then, real-time PCR was performed in an ABI 7500 Fast Real-Time PCR System (Applied Biosystems, CA, USA) using the SYBR® Premix Ex Taq™, and 2 µL of cDNA was amplified in a 25-µL reaction mixture containing 12.5 µL of the SYBR Premix Ex Taq, 0.5 µL of the forward primer (10 µmol/L), 0.5 µL of the reverse primers (10 µmol/L), 0.5 µL of the ROX Reference Dye II, and 9 µL of dH_2O. The amplifications were as follows: 95 °C for 30 s, followed by 40 cycles at 95 °C for 5 s, 57 °C for 20 s, and 72 °C for 15 s. The forward and reverse primers for adiponectin are 5'-AATCATTATGACGGCAGCAC-3' and 5'-CCAGATG-GAGGAGCACAGAG-3', respectively; those for PPARγ are 5'-GGCCATCCGAATTTTTCAAG-3' and 5'-GGGATATTTT-GGCATACTCTGTGA-3', respectively; and those for β-actin are 5'-TGCTGTCCCTGTATGCCTCTG-3' and 5'-TTGAT-GTCACGCACGATTTCC-3', respectively. The reverse-tran-

scribed cDNA samples were amplified, and cycle threshold (C_t) values were determined. The mRNA levels of adiponectin were normalized to the mRNA levels of the housekeeping gene β-actin. The comparative C_t method ($2^{-\Delta\Delta Ct}$) was used to analyze the differences in the level of adiponectin mRNA between each group.

11β-HSD1 activity assay in mesenteric fat

A weight of 200 mg of mesenteric fat was homogenized in 200 µL of cold homogenization buffer (20 mmol/L Na_2HPO_4, 5% glycerol, 1 mmol/L EDTA, pH 7.0) at 4 °C. The protein concentration of homogenate was determined using the Bradford method. A total of 10 µg of homogenate was pipetted into 96-well microtitre plates, and 70 µL of buffer (25 nmol/L [1,2-(N)^{3}H]-cortisone, 1.25 mmol/L NADPH and l50 mmol/L HEPES, pH 7.4) was added. The microtitre plates were shaken in the dark at 37 °C at 140 rounds per minute for 1 h. Then, 35 µL of SuperBlocking buffer (10 g/L of protein A-coated yttrium silicate beads, 3 g/L of anti-cortisol antibody and 314 µmol/L of glycyrrhetinic acid) was added. After shaking for another 2 h, the amount of [1,2-(N)^{3}H]-cortisol generated in the 11β-HSD1 reaction was captured by beads and determined in a microplate liquid scintillation counter.

Statistical analysis

The results are expressed as the mean±SEM. The differences between the two groups were analyzed by Student's *t*-test. Statistical analysis was carried out using the Prism program from GraphPad Software. Values of *P*<0.05 were considered statistically significant.

Results

Emodin inhibited 11β-HSD1 activity in 3T3-L1 adipocytes

Emodin showed strong inhibitory effects on 11β-HSD1 activity in 3T3-L1 adipocytes. The IC_{50}s were 7.237 and 4.204 µmol/L after 1 h and 24 h of treatment, respectively (Figure 1A and 1B).

Emodin regulated adipogenesis and energy metabolism in 3T3-L1 cells

It is well documented that glucocorticoids promote preadipocyte differentiation. The triglyceride content of adipocytes was used as a marker of the adipogenesis of 3T3-L1 cells. We found that all active glucocorticoids (dexamethasone and corticosterone) and inactive glucocorticoids (11-dehydrocorticosterone, 11-DHC) enhanced adipogenesis in 3T3-L1 preadipocytes. Incubation with 30 µmol/L of emodin reduced the triglyceride levels of 3T3-L1 adipocytes induced by 11-DHC by 19.8% (*P*<0.01), but it had no significant effect on the triglyceride levels in 3T3-L1 adipocytes treated with dexamethasone or corticosterone. Therefore, emodin suppressed inactive glucocorticoid-induced adipogenesis but not active glucocorticoid-induced adipogenesis in 3T3-L1 cells, which might be mediated by the inhibition of 11β-HSD1 activity (Figure 2A).

To determine whether emodin affects lipolysis through 11β-HSD1 inhibition, 11-DHC and corticosterone were used to
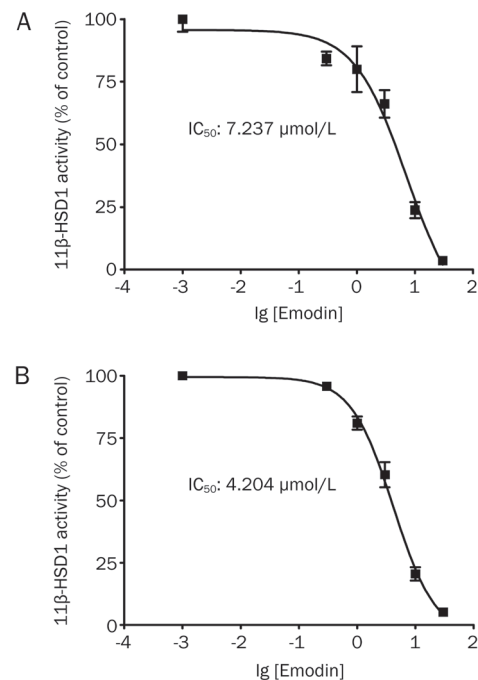

Figure 1. Emodin inhibited 11β-HSD1 activity in 3T3-L1 adipocytes after 1 h (A) or 24 h (B) of treatment. Differentiated 3T3-L1 adipocytes were incubated with the indicated concentrations of emodin or 0.1% DMSO for 1 h or 24 h. 11β-HSD1 enzyme activity was determined by scintillation proximity assay. Each point represents the mean±SEM. *n*=3.

induce lipolysis, and the effects of emodin were studied. Figure 2B indicates that 11-DHC and corticosterone significantly increased the glycerol release by 17.8% and 18.5% (*P*<0.01), respectively. Incubation with 3 µmol/L of emodin significantly decreased the glycerol release induced by 11-DHC but not by corticosterone. These results suggest that emodin suppressed lipolysis by inhibiting 11β-HSD1 activity.

Both 11-DHC and corticosterone attenuated insulin-stimulated glucose uptake in 3T3-L1 adipocytes (Figure 2C). Incubation with 3 µmol/L of emodin significantly reversed the impaired insulin-stimulated glucose uptake induced by 11-DHC. Although emodin treatment alone caused an 11.2% reduction in insulin-stimulated glucose uptake, it increased the insulin-stimulated glucose uptake by 17.7% when compared with 11-DHC-treated group. However, emodin had no effect on the impaired-insulin stimulated glucose uptake induced by corticosterone (Figure 2C).

Both 11-DHC and corticosterone significantly decreased adiponectin release from 3T3-L1 adipocytes. The reduced adiponectin secretion caused by 11-DHC was partly reversed by treatment with 3 µmol/L of emodin, whereas emodin exerted no effect on the impaired adiponectin secretion induced by corticosterone (Figure 2D).

Emodin suppressed 11β-HSD1 activity in adipose tissue and ameliorated metabolic disorders in *ob/ob* mice

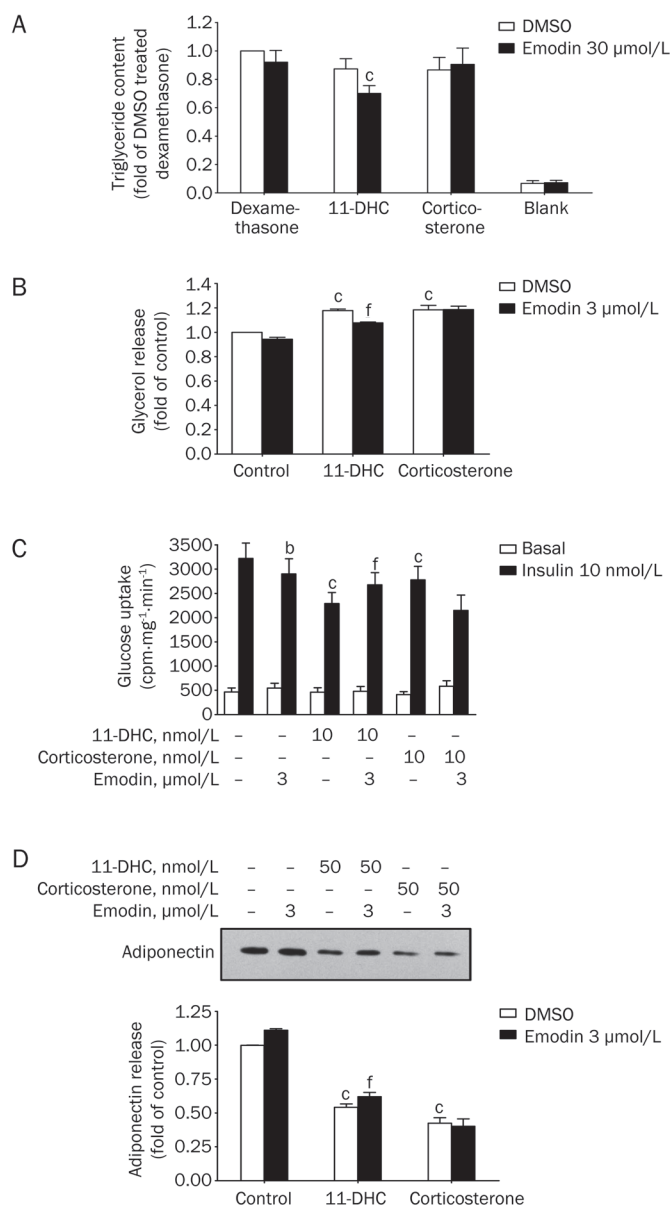To evaluate the long-term effect of emodin on metabolic disor-

Figure 2. Emodin regulated adipogenesis and energy metabolism in 3T3-L1 adipocytes. (A) Emodin inhibited the adipogenesis induced by 11-DHC (an inactive glucocorticoid) but not by corticosterone (an active glucocorticoid). The values are expressed as the fold increase over the values for the dexamethasone-treated DMSO group. [c]$P<0.01$ *vs* DMSO-treated 11-DHC group; $n=4$. (B) Emodin inhibited the glycerol release induced by 10 nmol/L 11-DHC but not by 10 nmol/L corticosterone. The values are expressed as the fold increase over the values for the DMSO-treated control group. [c]$P<0.01$ *vs* DMSO-treated control group, [f]$P<0.01$ *vs* DMSO-treated 11-DHC group; $n=3$. (C) Emodin significantly reversed the impaired insulin-stimulated glucose uptake induced by 11-DHC but not by corticosterone. [b]$P<0.05$, [c]$P<0.01$ *vs* insulin-stimulated control group, [f]$P<0.01$ *vs* insulin stimulated 11-DHC group; $n=6$. (D) 11-DHC- but not corticosterone-impaired adiponectin release was reversed by 3 µmol/L of emodin in 3T3-L1 adipocytes. Values are expressed as the fold increase over the values for the DMSO-treated control group. [c]$P<0.01$ *vs* DMSO-treated control group, [f]$P<0.01$ *vs* DMSO-treated 11-DHC group; $n=3$.

ders, *ob/ob* mice were treated twice daily with 25 or 50 mg/kg of emodin by intraperitoneal injection for 26 d. The enzymatic activity of 11β-HSD1 in mesenteric fat was measured at the end of the experiment. As shown in Figure 3, a significant decrease in 11β-HSD1 activity, by 44.5%, was observed in the mesenteric adipose tissues of *ob/ob* mice treated with 50 mg/kg of emodin ($P<0.05$).
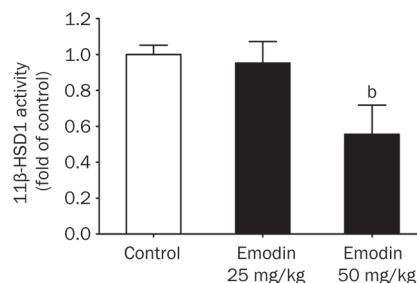

Figure 3. Emodin suppressed 11β-HSD1 activity in the mesenteric fat of *ob/ob* mice. *Ob/ob* mice were subjected to intraperitoneal injection treatment twice daily with vehicle (0.5% Tween 80), 25 mg/kg emodin or 50 mg/kg emodin for 26 d. 11β-HSD1 activity in the mesenteric fat was measured by SPA at the end of the treatment period. Values are expressed as fold of the values for the vehicle group. [b]$P<0.05$ *vs* vehicle group; $n=6$.

The genetic type 2 diabetic *ob/ob* mice showed obesity, hyperglycemia, dyslipidemia and insulin resistance. Long-term treatment with emodin significantly decreased the random-fed and fasting blood glucose levels in *ob/ob* mice, whereas the pair-fed group of mice showed no significant changes in blood glucose levels. As shown in Figures 4A and 4B, 16 or 20 d of treatment with 50 mg/kg of emodin significantly reduced the random-fed blood glucose concentrations in *ob/ob* mice by 32.53% and 32.68% ($P<0.05$), respectively, and the fasting blood glucose levels of *ob/ob* mice were also decreased by 38.29% ($P<0.01$) and 31.61% ($P<0.05$), respectively, when compared with the vehicle control mice. After 20 d of treatment with 50 mg/kg of emodin, glucose tolerance was improved. The emodin-treated mice exhibited significant reductions in blood glucose levels at 15, 60, and 120 min following an oral glucose challenge, and the glucose AUC$_{0-120 min}$ value decreased by 29.11% when compared with the vehicle control group (Figure 4C and 4D, $P<0.05$). There was no significant difference in the blood glucose level or the AUC$_{0-120 min}$ value between the emodin pair-fed and vehicle control groups. Moreover, the random-fed, fasting blood glucose levels at the treatments on d 16 and d 20 and the blood glucose levels and AUC$_{0-120 min}$ values in OGTT of the 50-mg/kg emodin-treated group were significantly lower than in the pair-fed group ($P<0.05$, $P<0.01$).

Emodin also improved the lipid profiles in *ob/ob* mice. After 26 d of treatment with 50 mg/kg of emodin, the serum triglyceride was significantly reduced by 26.0% ($P<0.01$) compared
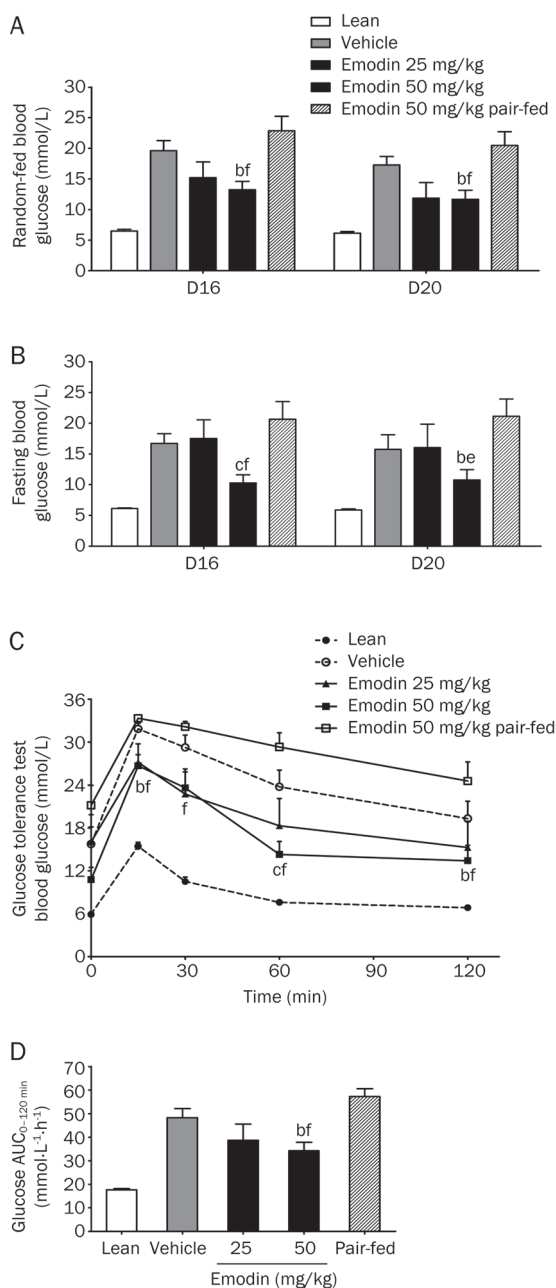
Figure 4. Emodin lowered blood glucose and improved the glucose tolerance of *ob/ob* mice. *ob/ob* mice were subjected to intraperitoneal injection twice daily with vehicle (0.5% Tween 80), 25 mg/kg emodin or 50 mg/kg emodin for 26 d. A pair-fed group was set by providing the *ob/ob* mice each day with the amount of food eaten by freely fed 50-mg/kg emodin-treated mice. Random-fed blood glucose concentrations (A) and fasting blood glucose concentrations (B) were measured on day 16 and day 20. Glucose tolerance (C and D) was determined on day 20 of the treatment. Values are expressed as the mean±SEM. [b]$P<0.05$, [c]$P<0.01$ *vs* vehicle group; [e]$P<0.05$, [f]$P<0.01$ *vs* 50-mg/kg emodin pair-fed group; $n=8$.

with the vehicle control mice (Figure 5A). The total cholesterol levels of emodin and pair-fed mice showed mild reductions but did not reach statistical significance (Figure 5B). Emodin (25 mg/kg) caused a 15.25% reduction of the NEFA level
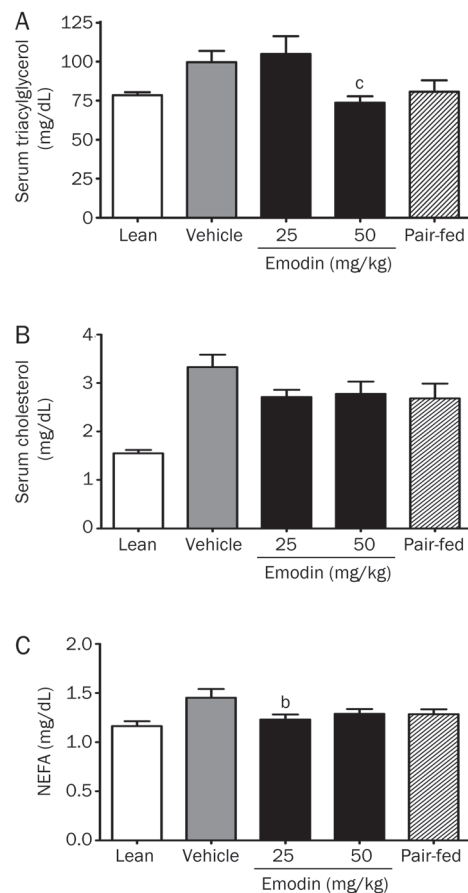

Figure 5. Effects of emodin on serum lipids of *ob/ob* mice. *ob/ob* mice were subjected to intraperitoneal injection twice daily with vehicle (0.5% Tween 80), 25 mg/kg emodin or 50 mg/kg emodin for 26 d. A pair-fed group was set by providing the *ob/ob* mice each day with the amount of food eaten by freely fed 50-mg/kg emodin-treated mice. Serum triacylglycerol (A), cholesterols (B) and NEFA (C) concentrations were evaluated at the end of the treatment period. Data are expressed as the mean±SEM. [b]$P<0.05$, [c]$P<0.01$ *vs* vehicle group; $n=8$.

($P<0.05$). The NEFA concentrations of 50-mg/kg emodin-treated and pair-fed mice were reduced by 11.15% and 11.60%, respectively, although these values did not reach statistical significance (Figure 5C).

Long-term treatment with emodin lowered the appetite and body weight of *ob/ob* mice. The food intakes of the 25- and 50-mg/kg emodin-treated mice were significantly decreased, by 26.26% and 26.31% ($P<0.01$), respectively, compared with the vehicle-treated animals (Figure 6A). The *ob/ob* mice treated with 25 or 50 mg/kg of emodin showed steady declines in body weight; the body weight gains on day 20 were reduced by 63.30% and 66.06% ($P<0.01$), respectively, and the emodin pair-fed mice also showed a similar decreased body weight gain (Figure 6B). Furthermore, both 25 and 50 mg/kg of emodin caused a reduction in mesenteric fat pad weights by 37.8% ($P<0.01$), whereas the pair-fed mice showed a reduction of 28.48% ($P<0.01$) (Figure 6C). The perirenal fat pad weight in the 50-mg/kg emodin-treated *ob/ob* mice was reduced by
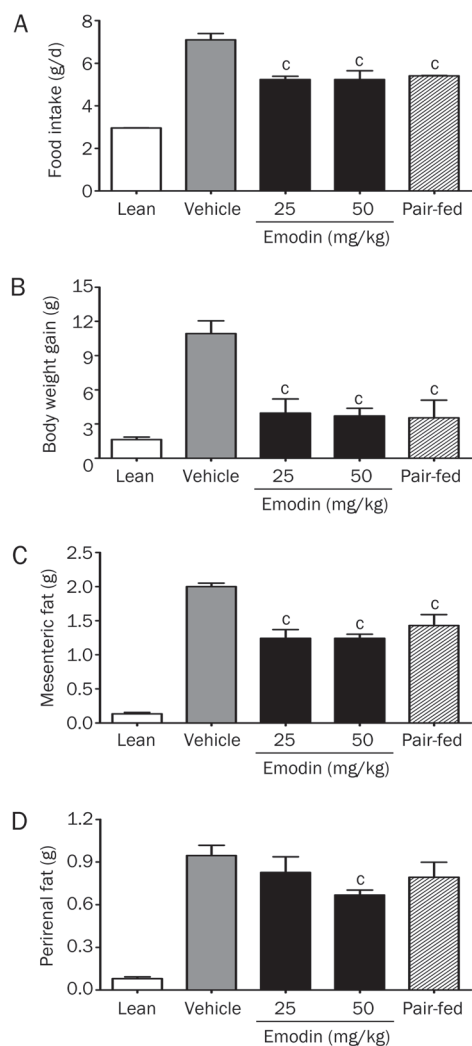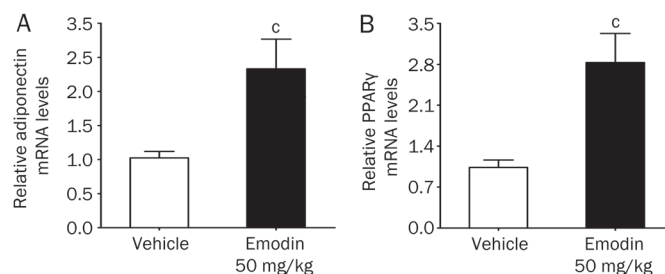
Figure 7. Emodin increased the mRNA levels of adiponectin (A) and PPARγ (B) in the mesenteric fat of *ob/ob* mice. *ob/ob* mice were subjected to intraperitoneal injection twice daily with vehicle (0.5% Tween 80) or emodin (50 mg/kg) for 26 d. The relative mRNA levels of adiponectin and PPARγ in the mesenteric fat were determined by real-time PCR at the end of the treatment period. Values are expressed as the fold increase over the values for the vehicle group. $^{c}P<0.01$ *vs* vehicle group; *n*=7.

Figure 6. Emodin decreased the food intake (A), body weight gain (B), mesenteric fat weight (C) and perirenal fat weight (D) of *ob/ob* mice. *ob/ob* mice were subjected to intraperitoneal injection twice daily with vehicle (0.5% Tween 80), 25 mg/kg emodin or 50 mg/kg emodin for 26 d. A pair-fed group was set by providing the *ob/ob* mice each day with the amount of food eaten by freely fed 50-mg/kg emodin-treated mice. Values are expressed as the mean±SEM. $^{c}P<0.01$ *vs* vehicle group; *n*=8.

29.26% ($P<0.01$) compared with the vehicle-treated mice, whereas no significant reduction was found in the pair-fed mice (Figure 6D).

The effects of long-term treatment with emodin on the mRNA expression of adiponectin and PPARγ in the mesenteric fat of *ob/ob* mice were also studied. As shown in Figures 7A and 7B, the treatment of *ob/ob* mice with 50 mg/kg of emodin for 26 d significantly increased adiponectin and PPARγ mRNA levels by 233.2% and 282.9%, respectively, compared with the vehicle group ($P<0.01$).

Discussion

Adipocyte dysfunction has been shown to play key roles in the development of insulin resistance, obesity and type 2 diabetes.

The inhibition of 11β-HSD1 in adipose tissue was expected to ameliorate adipocyte dysfunction and exert a beneficial effect on type 2 diabetes or metabolic diseases[5, 13]. In our previous study, emodin was demonstrated to be a potent and selective 11β-HSD1 inhibitor and ameliorate metabolic disorders in diet-induced obese mice[21]. However, its effect on adipocyte dysfunction has been unclear until now. In the present study, we demonstrated that emodin inhibited 11β-HSD1 activity in 3T3-L1 adipocytes and ameliorated inactive glucocorticoid-caused adipocyte dysfunction. Moreover, emodin improved the glycemic control and ameliorated other metabolic disorders in *ob/ob* mice.

11β-HSD1 is a bidirectional enzyme (dehydrogenase and oxoreductase) that functions predominantly as an oxoreductase in intact cells and catalyzes glucocorticoids to become active; its action is dependent on the NAPDH concentration in the endoplasmic reticulum[23]. Our previous study showed that emodin inhibited recombinant 11β-HSD1 activity in microsome fractions prepared from HEK-293 cells stably transfected with either mouse or human 11β-HSD1, with IC_{50} values of 86 and 186 nmol/L, respectively. Emodin also exhibited low inhibitory activity against mouse or human 11β-HSD2 with the IC_{50} higher than 1 mmol/L[21]. In this study, the inhibitory effect of emodin on the oxoreductase activity of 11β-HSD1 was determined in 3T3-L1 adipocytes in the absence of exogenous NAPDH, and the IC_{50} values after 1 h or 24 h of treatment were 7.24 and 4.20 μmol/L, respectively. Therefore, emodin inhibited the oxoreductase activity of 11β-HSD1 in intact 3T3-L1 adipocytes, although its efficacy is less than that against recombinant mouse 11β-HSD1 in microsome fractions; this lower efficacy might be due to the compound's limited penetration of the cell membrane or the restricted NADPH levels in intact cells.

Excess glucocorticoid causes visceral obesity owing to the acceleration of preadipocyte differentiation and adipocyte fat accumulation[24]. It has been demonstrated that the differentiation of 3T3-L1 preadipocytes can be induced by both active and inactive glucocorticoids, such as dexamethasone,

corticosterone and 11-DHC, and endogenous 11β-HSD1 oxore-ductase activity was expected to be required for differentiation induced by 11-DHC, an inactive glucocorticoid[25]. Thus, we examined the effect of emodin on the differentiation of 3T3-L1 preadipocytes induced by dexamethasone, corticosterone and 11-DHC. Emodin suppressed the adipogenesis induced by 11-DHC but not by corticosterone or dexamethasone in 3T3-L1 cells, which further confirms that emodin inhibits the oxore-ductase activity of 11β-HSD1 in 3T3-L1 cells.

Glucocorticoid receptors are highly expressed in adipocytes. Excessive glucocorticoid action in adipose tissue caused by either high circulating glucocorticoid levels or high local 11β-HSD1 expression and activity can negatively regulate a number of cellular glucose and lipid metabolic processes in adipocytes[5]. Glucocorticoids directly induce insulin resistance, which is mainly associated with the manifestation of impaired insulin-stimulated glucose uptake[26] and increased lipolysis, leading to elevated FFA release[27]; glucocorticoids also cause abnormalities in the release of adipokines, such as adiponectin[28]. Our present study showed that both corticosterone and 11-DHC can impair the insulin-stimulated glucose uptake, enhance lipolysis, and suppress adiponectin release in 3T3-L1 adipocytes. All cellular disorders caused by 11-DHC were partly reversed by emodin, whereas no significant changes were observed in the corticosterone-treated group. Because 11β-HSD1 is highly expressed in mature adipocytes[25], these results suggest that emodin can diminish adipocyte dysfunction by reducing local glucocorticoid action through inhibition of 11β-HSD1, which may ameliorate the whole body metabolic disorders in obesity or type 2 diabetes.

Our previous studies showed that emodin lowered blood glucose, improved insulin resistance and dyslipidemia, and decreased body weight and central fat mass in DIO mice[21]. In the present study, we further evaluated the *in vivo* effects of emodin on *ob/ob* mice, a genetic murine model of type 2 diabetes, which displayed hyperglycemia, hyperinsulinemia, dyslipidemia, obesity and insulin resistance[29]. The results showed that 26 days of treatment with emodin caused a significant reduction in 11β-HSD1 activity in the mesenteric fat of *ob/ob* mice, which confirmed that emodin inhibits 11β-HSD1 in adipose tissues *in vivo*. Moreover, emodin lowered the blood glucose levels, improved glucose tolerance, ameliorated dyslipidemia, and decreased body weight and food intake in *ob/ob* mice. Because glucocorticoids are orexigenic and adipose tissue-specific overexpression of 11β-HSD1 has been shown to cause hyperphagia[8, 30], the reduced food intake caused by emodin was expected. This finding is in line with our previous findings in DIO mice and other reports on the 11β-HSD1 inhibitor[31]. To exclude the metabolic changes caused by the reduced food intake, a pair-fed group corresponding to the 50-mg/kg emodin-treated group was set up. The beneficial changes in lipid profile, body weight, and fat mass in the 50-mg/kg emodin group were similar to those in the pair-fed group, which suggests that those improvements might be due to the reduced food intake. However, although the food intakes were similar, 50 mg/kg of emodin still significantly

decreased both the random-fed and fasting blood glucose levels, and it also resulted in an improved oral glucose tolerance compared with the pair-fed group, which indicated that the glucose lowering effect of emodin on *ob/ob* mice is not only due to reduced food intake; other mechanisms, such as the inhibition of 11β-HSD1, were also involved.

It has been reported that the mRNA expression of adiponectin and PPARγ are increased in epididymal adipose tissue in 11β-HSD1 knockout mice[13]. Owing to the role of glucocorticoids in adiponectin secretion decreases[28], it was not surprising to find that 11β-HSD1 inhibition is involved in increasing adiponectin content. The present study demonstrates that long-term treatment with emodin increased adiponectin mRNA expression in mesenteric adipose tissue, which may be attributable to the amelioration of metabolic disorders by emodin in *ob/ob* mice. PPARγ is a transcription factor closely related to insulin sensitivity, and its activation promotes preadipocyte differentiation and increases adipocyte glucose uptake[32]. Chronic emodin administration increased PPARγ mRNA expression in mesenteric adipose tissue. Although the correlation between the increased PPARγ expression and the 11β-HSD1-inhibitory effect of emodin is unclear, PPARγ is clearly involved in the anti-diabetic effect of emodin.

In conclusion, our study demonstrates that emodin inhibits 11β-HSD1 activity in 3T3-L1 adipocytes and improves inactive glucocorticoid-induced adipocyte dysfunction. The administration of emodin improved glycemic control and ameliorated other metabolic disorders in *ob/ob* mice, possibly owing to the inhibition of 11β-HSD1 activity in adipose tissue.

Author contribution
Ying LENG designed the study; Yue-jing WANG, Su-ling HUANG, Ying FENG, and Meng-meng Ning performed the research; and Yue-jing WANG, Su-ling HUANG, and Ying LENG wrote the paper.

References
1 Rosen ED, Spiegelman BM. Adipocytes as regulators of energy balance and glucose homeostasis. Nature 2006; 444: 847–53.
2 Guilherme A, Virbasius JV, Puri V, Czech MP. Adipocyte dysfunctions linking obesity to insulin resistance and type 2 diabetes. Nat Rev Mol Cell Biol 2008; 9: 367–77.
3 Beauregard C, Dickstein G, Lacroix A. Classic and recent etiologies of Cushing's syndrome: diagnosis and therapy. Treat Endocrinol 2002; 1: 79–94.
4 Seckl JR, Walker BR. Minireview: 11beta-hydroxysteroid dehydrogenase type 1- a tissue-specific amplifier of glucocorticoid action. Endocrinology 2001; 142: 1371–6.
5 Morton NM. Obesity and corticosteroids: 11beta–hydroxysteroid type 1 as a cause and therapeutic target in metabolic disease. Mol Cell

Endocrinol 2010; 316: 154–64.

6   Hollis G, Huber R.   11beta-Hydroxysteroid dehydrogenase type 1 inhibition in type 2 diabetes mellitus.   Diabetes Obes Metab 2011; 13: 1–6.

7   Westerbacka J, Yki-Jarvinen H, Vehkavaara S, Hakkinen AM, Andrew R, Wake DJ, *et al*.   Body fat distribution and cortisol metabolism in healthy men: enhanced 5beta-reductase and lower cortisol/cortisone metabolite ratios in men with fatty liver.   J Clin Endocrinol Metab 2003; 88: 4924–31.

8   Masuzaki H, Paterson J, Shinyama H, Morton NM, Mullins JJ, Seckl JR, *et al*.   A transgenic model of visceral obesity and the metabolic syndrome.   Science 2001; 294: 2166–70.

9   Masuzaki H, Yamamoto H, Kenyon CJ, Elmquist JK, Morton NM, Paterson JM, *et al*.   Transgenic amplification of glucocorticoid action in adipose tissue causes high blood pressure in mice.   J Clin Invest 2003; 112: 83–90.

10   Paterson JM.   Metabolic syndrome without obesity: Hepatic over-expression of 11-hydroxysteroid dehydrogenase type 1 in transgenic mice.   Proc Natl Acad Sci U S A 2004; 101: 7088–93.

11   Kotelevtsev Y, Holmes MC, Burchell A, Houston PM, Schmoll D, Jamieson P, *et al*.   11Beta-hydroxysteroid dehydrogenase type 1 knockout mice show attenuated glucocorticoid-inducible responses and resist hyperglycemia on obesity or stress.   Proc Natl Acad Sci U S A 1997; 94: 14924–9.

12   Morton NM, Holmes MC, Fievet C, Staels B, Tailleux A, Mullins JJ, *et al*.   Improved lipid and lipoprotein profile, hepatic insulin sensitivity, and glucose tolerance in 11beta-hydroxysteroid dehydrogenase type 1 null mice.   J Biol Chem 2001; 276: 41293–300.

13   Morton NM, Paterson JM, Masuzaki H, Holmes MC, Staels B, Fievet C, *et al*.   Novel adipose tissue-mediated resistance to diet-induced visceral obesity in 11beta-hydroxysteroid dehydrogenase type 1-deficient mice.   Diabetes 2004; 53: 931–8.

14   Kershaw EE, Morton NM, Dhillon H, Ramage L, Seckl JR, Flier JS.   Adipocyte-specific glucocorticoid inactivation protects against diet-induced obesity.   Diabetes 2005; 54: 1023–31.

15   Wang HH, Chung JG.   Emodin-induced inhibition of growth and DNA damage in the *Helicobacter pylori*.   Curr Microbiol 1997; 35: 262–6.

16   Huang Q, Lu G, Shen HM, Chung MC, Ong CN.   Anti-cancer properties of anthraquinones from rhubarb.   Med Res Rev 2007; 27: 609–30.

17   Chang CH, Lin CC, Yang JJ, Namba T, Hattori M.   Anti-inflammatory effects of emodin from ventilago leiocarpa.   Am J Chin Med 1996; 24: 139–42.

18   Huang HC, Chang JH, Tung SF, Wu RT, Foegh ML, Chu SH.   Immunosuppressive effect of emodin, a free radical generator.   Eur J Pharmacol 1992; 211: 359–64.

19   Woo SW, Nan JX, Lee SH, Park EJ, Zhao YZ, Sohn DH.   Aloe emodin suppresses myofibroblastic differentiation of rat hepatic stellate cells in primary culture.   Pharmacol Toxicol 2002; 90: 193–8.

20   Heo SK, Yun HJ, Park WH, Park SD.   Emodin inhibits TNF-alpha-induced human aortic smooth-muscle cell proliferation via caspase- and mitochondrial-dependent apoptosis.   J Cell Biochem 2008; 105: 70–80.

21   Feng Y, Huang SL, Dou W, Zhang S, Chen JH, Shen Y, *et al*.   Emodin, a natural product, selectively inhibits 11beta-hydroxysteroid dehydrogenase type 1 and ameliorates metabolic disorder in diet-induced obese mice.   Br J Pharmacol 2010; 161: 113–26.

22   Hu X, Feng Y, Liu X, Zhao XF, Yu JH, Yang YS, *et al*.   Effect of a novel non-thiazolidinedione peroxisome proliferator-activated receptor alpha/gamma agonist on glucose uptake.   Diabetologia 2007; 50: 1048–57.

23   Hewitt KN, Walker EA, Stewart PM.   Minireview: hexose-6-phosphate dehydrogenase and redox control of 11{beta}-hydroxysteroid dehydrogenase type 1 activity.   Endocrinology 2005; 146: 2539–43.

24   Seckl JR, Morton NM, Chapman KE, Walker BR.   Glucocorticoids and 11beta–hydroxysteroid dehydrogenase in adipose tissue.   Recent Prog Horm Res 2004; 59: 359–93.

25   Kim J, Temple KA, Jones SA, Meredith KN, Basko JL, Brady MJ.   Differential modulation of 3T3-L1 adipogenesis mediated by 11beta-hydroxysteroid dehydrogenase-1 levels.   J Biol Chem 2007; 282: 11038–46.

26   Sakoda H, Ogihara T, Anai M, Funaki M, Inukai K, Katagiri H, *et al*.   Dexamethasone-induced insulin resistance in 3T3-L1 adipocytes is due to inhibition of glucose transport rather than insulin signal transduction.   Diabetes 2000; 49: 1700–8.

27   Divertie GD, Jensen MD, Miles JM.   Stimulation of lipolysis in humans by physiological hypercortisolemia.   Diabetes 1991; 40: 1228–32.

28   Shi JH, Du WH, Liu XY, Fan YP, Hu XL, Zhou HY, *et al*.   Glucocorticoids decrease serum adiponectin level and WAT adiponectin mRNA expression in rats.   Steroids 2010; 75: 853–8.

29   Herberg L, Leiter EH, editor.   Obesity/diabetes in mice with mutations in the leptin or leptin receptor genes.   Amsterdam Harwood Academic 2001.

30   Cavagnini F, Croci M, Putignano P, Petroni ML, Invitti C.   Glucocorticoids and neuroendocrine function.   Int J Obes Relat Metab Disord 2000; 24: S77–9.

31   Wang SJ, Birtles S, de Schoolmeester J, Swales J, Moody G, Hislop D, *et al*.   Inhibition of 11beta-hydroxysteroid dehydrogenase type 1 reduces food intake and weight gain but maintains energy expenditure in diet–induced obese mice.   Diabetologia 2006; 49: 1333–7.

32   Ferre P.   The biology of peroxisome proliferator-activated receptors: relationship with lipid metabolism and insulin sensitivity.   Diabetes 2004; 53: S43–50.

Original Article

A novel small molecule, HK-156, inhibits lipopoly-saccharide-induced activation of NF-κB signaling and improves survival in mouse models of sepsis

Jian-ping FANG[1, #], Yang LIU[2, #], Jie LI[1], Wen-feng LIAO[1], You-hong HU[2, *], Kan DING[1, *]

[1]Glycochemistry & Glycobiology Lab, Shanghai Institute of Materia Medica, Chinese Academy of Sciences, Shanghai 201203, China; [2]State Key Laboratory of Drug Research, Shanghai Institute of Materia Medica, Chinese Academy of Sciences, Shanghai 201203, China

Aim: To characterize a small molecule compound HK-156 as a novel inhibitor of the nuclear factor κB (NF-κB) signaling pathway.
Methods: THP-1 monocytes and HEK293/hTLR4A-MD2-CD14 cells were tested. HK-156 and compound **809**, an HK-156 analogue, were synthesized. A luciferase assay was used to evaluate the transcriptional activity of NF-κB. The levels of cytokines were measured with cytokine arrays, ELISA and quantitative PCR. An electrophoretic mobility shift assay (EMSA), immunofluorescence, Western blot and mass spectrometry were used to investigate the molecular mechanisms underlying the actions of the agent. BALB/c mice challenged with lipopolysaccharide (LPS, 15 mg/kg, ip) were used as a mouse experimental endotoxemia model.
Results: In HEK293hTLR4/NF-κB-luc cells treated with LPS (1000 ng/mL), HK-156 inhibited the transcriptional activity of NF-κB in a concentration-dependent manner (IC_{50}=6.54±0.37 μmol/L). Pretreatment of THP-1 monocytes with HK-156 (5, 10 and 20 μmol/L) significantly inhibited LPS-induced release and production of TNF-α and IL-1β, attenuated LPS-induced translocation of NF-κB into the nucleus and its binding to DNA, and suppressed LPS-induced phosphorylation and degradation of IκBα, and phosphorylation of IKKβ and TGFβ-activated kinase (TAK1). Meanwhile, HK-156 (5, 10 and 20 μmol/L) slightly suppressed LPS-induced activation of p38. The effect of HK-156 on LPS-induced activation of NF-κB signaling was dependent on thiol groups of cysteines in upstream proteins. In mouse models of sepsis, pre-injection of HK-156 (50 mg/kg, iv) significantly inhibited TNFα production and reduced the mortality caused by the lethal dose of LPS.
Conclusion: HK-156 inhibits LPS-induced activation of NF-κB signaling by suppressing the phosphorylation of TAK1 *in vitro*, and exerts beneficial effects in a mouse sepsis model. HK-156 may therefore be a useful therapeutic agent for treating sepsis.

Keywords: HK-156; NF-κB; NF-κB inhibitor; monocyte; lipopolysaccharide; TAK1; IKKβ; p38; sepsis

Introduction

The nuclear factor κB (NF-κB) family of transcription factors consists of five members in mammalian cells — p65/RelA, c-Rel, RelB, p50, and p52 — and these members can form homodimers or heterodimers[1]. Of the various dimeric combinations, the p50/p65 heterodimer is the most frequently detected. The activation of NF-κB is controlled by the IκB kinase (IKK) complex, which consists of two catalytic subunits, named IKK1/IKKα and IKK2/IKKβ, and the NEMO/IKKγ regulatory protein[2]. In resting cells, NF-κB is located in the cytosol in complex with the inhibitory proteins of the IκB family, mainly IκBα[1]. In the canonical activation pathway, following the presentation of stimuli such as lipopolysaccharide (LPS) or the cytokines tumor necrosis factor (TNF)α and interleukin (IL)-1β, which act through different receptors, signal transduction leads to the activation of IKKβ. IKKβ predominantly phosphorylates IκBα, leading to its subsequent ubiquitination and degradation by the proteasome. The NF-κB complex is then released and translocates into the nucleus, where it triggers the transcription of multiple proinflammatory genes, including cytokines, chemokines and adhesion molecules that are essential for both the innate and adaptive immune response through the binding of a *cis*-acting κB element[3]. NF-κB is a central mediator of the human immune response. It has been demonstrated that a large variety of pathogens and cytokines activate NF-κB signaling, and almost all of the proin-

flammatory cytokines that participate in the inflammatory and immune responses are target genes of NF-κB[4]. Furthermore, constitutively activated NF-κB is often found to be involved in the pathogenesis of inflammatory diseases[5]. Gene knockout and knock-in mice have further proven the important role of NF-κB in inflammation[6, 7]. The inhibition of NF-κB activation is now widely recognized as a valid drug-targeting strategy to combat inflammatory diseases[8–10].

Sepsis is an acute inflammatory syndrome that leads to multiple organ failure and remains a leading cause of mortality and morbidity in intensive care units[11]. An uncontrolled hyperinflammatory response and inappropriate cytokine response during early sepsis have been proposed as the cause of the multiple organ dysfunction syndrome that occurs during sepsis. Control of inflammation during the early stages of sepsis may therefore reduce organ injury and prevent death after septic insult. Fatal clinical instances of sepsis were originally attributed to LPS or endotoxin, a major constituent of the outer membrane of Gram negative bacteria[12]. When a bacterial infection occurs, LPS is released into the lymphatic and circulatory systems, which induces the activation of monocytes and macrophages via the production of proinflammatory cytokines, including TNFα and IL-1β, and initiates the pathogenetic process of sepsis[13]. Multiple signaling events, especially through the NF-κB signaling pathway, play a critical role in this process[14]. With the help of the LPS binding protein (LBP) and CD14, LPS is transferred to the toll like receptor (TLR) 4/MD-2 receptor complex, resulting in NF-κB activation via an early myeloid differentiation factor 88 (MyD88)-dependent pathway and a late Toll/Interleukin-1 receptor (TIR) domain-containing adapter-inducing interferon (IFN)β (TRIF)-dependent pathway[2, 15]. In the end, both pathways lead to the activation of TGFβ-activated kinase 1 (TAK1) through phosphorylation[2, 16]. Phosphorylated TAK1 kinase then directly phosphorylates the IKKβ subunit of the IKK complex to activate the canonical NF-κB pathway, giving rise to the expression of numerous proinflammatory genes that are known to play important roles in septic pathophysiology[15, 17–20]. Proinflammatory cytokines such as TNFα and IL-1β also enlarge this cascade through positive feedback by activating NF-κB signaling through their respective receptors[2]. This unregulated systemic response progresses to multiple organ failure, which is associated with a high mortality rate in humans[14]. NF-κB activation has been proposed as a pathological mechanism of septic shock, and the inhibition of NF-κB activation has been suggested to be a useful strategy for the treatment of sepsis[14, 21].

Many inhibitors of the NF-κB pathway have been identified, including a variety of natural and synthetic molecules such as antioxidants, peptides, small RNA/DNA molecules, and flavonoids[22]. These compounds act on NF-κB signaling at different points and have been shown to have an anti-inflammatory effect *in vitro* and *in vivo*, including in sepsis[23]. Many clinically used anti-inflammatory drugs, such as glucocorticoids, non-steroidal anti-inflammatory drugs (NSAIDs), and other immunosuppressants, have also been shown to act as inhibi-

tors of the NF-κB pathway[22]. Several thiol-reactive compounds, such as parthenolide, cyclopentenone prostanglandins, sesquiterpene lactones, certain epoxyquinoids and arsenite, have been shown to inhibit the activity of IKKβ or the binding of NF-κB to DNA, probably through direct conjugation to the thiol group of cysteine[22]. Many NF-κB inhibitors have been shown to reduce the expression of multiple proinflammatory genes, diminish intravascular coagulation, and eventually prevent multiple organ injury and improve survival in rodent models of septic shock[24]. However, because of the complex nature of sepsis, to date, activated protein C is the only drug on the market[11, 21], although some TLR4 antagonists are still in clinical trials[25, 26].

In this study, we found the synthetic compound HK-156 (Figure 1A) to be a novel NF-κB inhibitor using cell-based screening assays. In addition, its mechanism of action and direct target were investigated in human monocytes. The protective effects of HK-156 against sepsis were also evaluated in a sepsis animal model challenged with a lethal dose of LPS.

Materials and methods
Materials
Phorbol-12-myristate-13-acetate (PMA) and LPS (isolated from *E coli* strain 055: B5) were purchased from Sigma-Aldrich (St Louis, MO, USA). Cytokine array and ELISA kits were from R&D systems (Minneapolis, MN, USA). Antibodies for IKKα, IKKβ, p-IκBα, IκBα, p65, p-IKKα (Ser176)/IKKβ (Ser177), p-IKKα (Ser180)/IKKβ (Ser181), p-IKKα (Ser176, Ser180)/IKKβ (Ser177, Ser181), p-TAK1, TAK1, Lamin A, p-p38, p38, p-ERK1/2, and ERK1/2 were obtained from Cell Signaling Technology (Danvers, MA, USA), and the β-actin antibody used as internal reference was from Sigma-Aldrich.

Compound HK-156 (N-(2-methylfuro[2,3-d]pyrimidin-4-yl)acrylamide) (Figure 1A) and **809** (N-(2-methylfuro[2,3-d]pyrimidin-4-yl)propionamide) (Figure 1B) were synthesized according to the procedure described in the supplementary data (Supplementary Figure 1). Their structures were characterized by ^{1}H-NMR, ^{13}H-NMR, and MS spectra (Supplementary Figure 2). The purity of them determined by HPLC was above 98%. For *in vitro* experiments, HK-156 and compound **809** were dissolved in dimethylsulfoxide (DMSO) and diluted in cell culture medium at different concentrations as specified in the text. The final concentration of DMSO was less than or equal to 0.1% *v/v*. For *in vivo* studies, HK-156 was prepared in a vehicle consisting of 10% DMSO and 10% Cremophor EL (Sigma-Aldrich) in normal saline (NS), whereas the vehicle without HK-156 was used in parallel as a control group.

Cell culture and transfection
THP-1 cells (American Type Culture Collection, Manassas, VA, USA) were cultured in RPMI-1640 (Thermo Scientific, Rockford, IL, USA) containing 0.05 mmol/L 2-mercaptoethanol. HEK293/hTLR4A-MD2-CD14 cells stably transfected with the human TLR4A, MD2 and CD14 genes (Invivogen, San Diego, CA, USA) were cultured in DMEM (Thermo Scientific). The culture media were supplemented with 10% FBS and 100
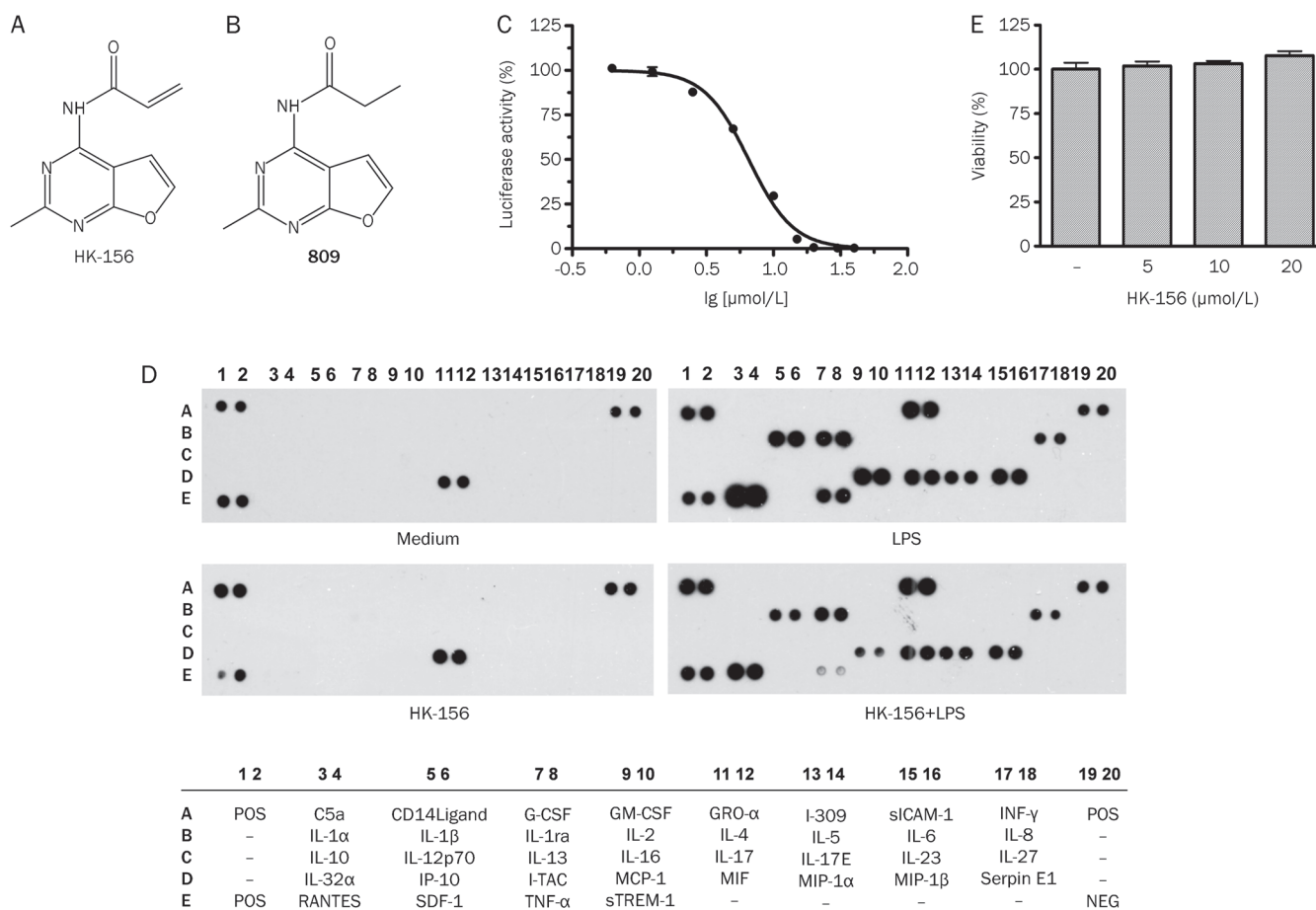
Figure 1. Dose response inhibition by HK-156 of NF-κB transcriptional activity. (A) Chemical structure of HK-156. (B) Chemical structure of compound **809**. (C) After pretreatment with various doses of HK-156 (0.625, 1.25, 2.5, 5, 10, 15, 20, 30, and 40 μmol/L) for 20 min, HEK293hTLR4/NF-κB-luc cells were treated with LPS (1000 ng/mL) in the presence or absence of HK-156 for 6 h. The cell lysates were subjected to luciferase assays to evaluate the transcriptional activity of NF-κB. The results are expressed as relative luciferase activity compared with the cells treated with LPS alone and analyzed using the nonlinear regression curve-fitting program in GraphPad Prism software. Values represent mean±SEM. (D) After being pretreated with or without HK-156 (5 μmol/L) treatment for 20 min, THP-1 monocytes were incubated with or without LPS (1000 ng/mL) in the presence or absence of HK-156 for 16 h, followed by immunodetection of multiplex cytokines in the medium with cytokine array. The positions of the respective cytokines and controls on the array are shown below. (E) THP-1 monocytes were treated with the indicated concentration of HK-156 for 48 h, and the cell viability was determined by a CCK-8 assay. Mean±SEM. *n*=3.

U/mL penicillin plus 100 mg/mL streptomycin at 37 °C in a humidified atmosphere containing 5% CO_2. Transfection of pNFκB-TA-Luc with co-transfection of pCDNA3.1 as a screening tag (Clontech, Mountain View, CA, USA) into HEK293/hTLR4A-MD2-CD14 cells was performed using Lipofectamine 2000 (Invitrogen, Carlsbad, CA, USA). After reaching confluence, cells were split into complete medium with 0.8 mg/mL G418 (Merck KGaA, Darmstadt, Germany). Three weeks later, independent clones were isolated. Stable transfected clones were evaluated using NF-κB transcriptional activity assay with LPS (1000 ng/mL) as a stimulus. About 2 months later, stable cell line HEK293hTLR4/NF-κB-luc was achieved.

NF-κB transcriptional activity assay

The NF-κB transcriptional activity assay was performed with the NF-κB reporter plasmid stably transfected cell line HEK-293hTLR4/NF-κB-luc using the Luciferase Assay System (Promega, Madison, WI, USA) according to the manufacturer's instructions. Briefly, untreated cells or cells that were incubated with the compound were lysed with CCLR buffer, and the cell lysates were transferred to Lumitrac 200 flat-bottomed 96-well plates (Greiner, Frickenhausen, Germany). The relative luciferase activity, recorded as relative light units (RLU), was read immediately after the substrate was added on a NOVOstar Microplate Reader (BMG Labtech, Offenburg, Germany). All experiments were performed in triplicate.

Cell viability assay

The cell viability after treatment with or without HK-156 was measured by a Cell Counting Kit-8 (CCK-8) assay following the manufacturer's instructions (Dojindo, Tokyo, Japan). THP-1 cells were suspended at a final concentration of 1×10^5

cells/well and cultured in a 96-well flat-bottomed microplate. After exposure to HK-156 for 48 h, CCK-8 (10 µL) was added to each well, followed by incubation for 2 h at 37 °C. Viable cells were counted by absorbance measurement at 450 nm using a NOVOstar Microplate Reader, and the viability was expressed as a percentage relative to untreated control cells. All experiments were performed in triplicate on three independent occasions.

Immunodetection of cytokines
Relative levels of complex cytokines in the medium of the cell culture or the serum of a mouse were measured using a cytokine array kit, while the quantitative cytokine contents were determined using sandwich ELISA kits for TNFα and IL-1β following the manufacturers' instructions. Briefly, cell cultures or sera were collected and centrifuged ($500 \times g$) for 5 min. The supernatant was subjected to a cytokine array or ELISA assay.

RNA isolation and measurement of mRNA by quantitative real-time PCR
For real-time PCR, total RNA was isolated from monocytes with Trizol (Invitrogen) following the manufacturer's instructions. Briefly, 1–2 µg of total RNA was reverse transcribed to cDNA with MMLV reverse transcriptase (Takara, Otsu, Shiga, Japan) and diluted to a final volume of 100 µL. A 20 µL reaction mixture containing 2 µL of cDNA (20–60 ng) template, 0.25 µmol/L primers and 10 µL SYBR Ex Taq Premix (Takara, Otsu, Shiga, Japan) was added to EU optical PCR tubes (Gene Chain Scientific, New York, USA) in a 96-well plate format. Real-time PCR was performed using an ABI 7500 Fast Real-Time PCR system with the Sequence Detection software version 1.4 (Applied Biosystems, Foster City, CA, USA). The following primers were used: for TNFα: sense: 5′-GCTTGT-TCCTCAGCCTCTTCT-3′ and anti-sense: 5′-GGTTTGCTA-CAACATGGGCTA-3′; for IL-1β: sense: 5′-CCAGTGAAAT-GATGGCTTATTAC-3′ and anti-sense: 5′-CTGTAGTGGTG-GTCGGAGATT-3′. Conditions for amplification were 95 °C for 10 s and 40 cycles of 95 °C for 5 s followed by 60 °C for 30 s. The fold change of mRNA was evaluated by the relative copy number (RCN) and expression ratios of selected genes normalized to the expression of the housekeeping gene GAPDH (primers: sense: 5′-ACTTTGGTATCGTGGAAGGACT-3′ and anti-sense: 5′-GTAGAGGCAGGGATGATGTTCT-3′) and calculated by the relative quantification method using Sequence Detection software with the equation RCN=$2^{-\Delta\Delta Ct}$, where $\Delta Ct=Ct_{target}-Ct_{reference}$, and $\Delta\Delta Ct=\Delta Ct_{test sample}-\Delta Ct_{calibrator sample}$.

Nuclear protein extraction and electrophoretic mobility shift assay (EMSA)
Nuclear protein extraction was performed using the hypotonic method with a nuclear extraction kit according to the manufacturer's instructions (Active Motif, Carlsbad, CA, USA). Briefly, cells were resuspended in hypotonic buffer after being washed with ice-cold PBS containing phosphatase inhibitors and incubated on ice for 15 min. Detergent was added, and

the mixture was vortexed at the highest speed. After centrifugation, the nuclear pellet was resuspended in complete lysis buffer and rocked at 4 °C for 30 min with vortexing at intervals, followed by centrifugation at $14\,000 \times g$ for 10 min. The supernatant contained the nuclear extract. After the concentration was determined by the BCA method (Beyotime, Haimen, China), the nuclear protein extract was subjected to EMSA following the manufacturer's instructions (Pierce, Rockford, IL, USA). In short, equivalent amounts of nuclear extracts (10 µg of protein) prepared from cells stimulated with LPS (1000 ng/mL) in the presence or absence of HK-156 for 20 min were incubated with a 5′-biotin end-labeled double-stranded NF-κB-specific probe (5′-AGTTGAGGGGACTTTC-CCAGGC-3′) synthesized by Sangon (Shanghai, China) and poly (dI-dC) in the presence or absence of a 100-fold excess of cold non-biotin labeled probe for the NF-κB p65 subunit for 20 min at room temperature. Samples were resolved on a native 4.5% polyacrylamide gel and transferred to a nylon membrane, followed by crosslinking at 120 mJ/cm² using an ultraviolet crosslinker (UVP, Upland, CA, USA). After blockade and incubation with streptavidin-conjugated HRP for 15 min, the membrane was exposed to the ECL substrate to detect biotin-labeled DNA bands.

Immunoblotting
Cells were lysed with SDS-PAGE sample loading buffer followed by denaturation at 95 °C for 15 min. After centrifugation, the supernatant protein samples were subjected to 10% SDS-PAGE and incubation with specific antibodies. After three washes, secondary antibodies were applied, and blots were developed.

Immunofluorescence
Nuclear translocation of the p65 subunit of NF-κB was examined by immunofluorescence. Briefly, THP-1 cells were induced to adhesion for 12 h with a low concentration of PMA (10 ng/mL), followed by treatment with HK-156 and LPS. The cells were fixed with 3% formaldehyde and permeabilized with ice-cold methanol. After washing with PBS, the slides were blocked with 3% bovine serum albumin in PBS/Triton (PBS/0.3% Triton X-100) for 1 h and incubated with rabbit anti-p65 antibody diluted in PBS/Triton at 4 °C overnight. The cells were washed and incubated with AlexaFluor 488 goat anti-rabbit IgG antibody in PBS/Triton (1:200, Molecular Probe, Carlsbad, CA, USA) and propidium iodide (PI, 100 µg/mL, Sigma-Aldrich) for 1 h. After staining, the cells were mounted with fluorescent mounting medium (Dako, Carpinteria, CA, USA) and observed with a Leica SP2 laser scanning confocal microscope (Leica Microsystems CMS GmbH, Mannheim, Germany).

Conjugation of HK-156 with glutathione
HK-156 (20 nmol) in DMSO was incubated with 4 eq of reduced glutathione in 20 mmol/L Tris-HCl (pH 7.5) for 1 h at 37 °C. The sample was directly injected into a LCQ Deca ion trap mass spectrometer (Thermo Finnigan), and mass spectra

were recorded in ESI-positive mode.

Animal test

Female BALB/c mice, 6–8 weeks old, were purchased from the Shanghai SLAC Laboratory Animal Center and maintained in a specific pathogen-free (SPF) environment and used in accordance with approved regulations of the Institutional Animal Care and Use Committee of the Shanghai Institute of Materia Medica, Chinese Academy of Sciences (Approval ID: SIMM-AE-DK-2010-03) after 10 d of acclimatization. Mice were injected iv with HK-156 or vehicle consisting of 10% DMSO and 10% Cremophor EL in normal saline 2 h before the ip administration of a lethal dose of LPS (15 mg/kg) or normal saline. Mice were monitored hourly. In experiments used to determine the cytokine level, mice were treated with LPS and/or HK-156 as outlined above. Blood was drawn via a retro-orbital puncture at 2 h post challenge and clotted for 1 h at 4 °C. The serum was collected through centrifugation and stored at -80 °C for future analysis. A Mantel-Haenszel log rank test was performed, and a Kaplan-Meier survival curve was generated using Graph-Pad Prism (version 5.01 for Windows, GraphPad Software, www.graphpad.com).

Statistical analysis

All data were managed with GraphPad Prism 5.01 software and expressed as mean±SEM. The significance (*P* value) of the difference was evaluated based on an unpaired Student's *t* test for the comparison of two groups or a one-way ANOVA analysis method for multiple comparisons. Values of *P*<0.05 were considered statistically significant.

Results

HK-156 inhibits LPS induced transcriptional activation of NF-κB and cytokine release

To identify a new NF-κB signaling inhibitor, we established a cell-based screening panel on the stable cell line HEK293-hTLR4/NF-κB-luc. Using LPS as an inducer and luciferase as a reporter gene, we found that the novel small molecule HK-156 (Figure 1A) significantly inhibited NF-κB transcriptional activation stimulated by LPS in a dose-dependent manner. When pretreated with HK-156 for 20 min and cocultured with LPS (1 µg/mL) for another 6 h, the half inhibitory concentration (IC$_{50}$) was 6.54±0.37 µmol/L (Figure 1C). When the cell viability was evaluated with MTT, HK-156 had no observable effect on the proliferation of HEK293hTLR4/NF-κB-luc cells at concentrations up to 40 µmol/L (data not shown). These results showed that HK-156 was a significant NF-κB signaling inhibitor based on HEK293hTLR4/NF-κB-luc cells treated with LPS.

Inhibition of NF-κB activation should lead to the attenuation of the transcription and expression of target genes regulated by NF-κB. To evaluate whether this occurs, human THP-1 monocytes were pretreated with HK-156 (5 µmol/L) and cocultured with LPS (1 µg/mL) for 16 h. The medium was then subjected to a cytokine array assay. We found that the release of cytokines such as GROα, IL-1β, IL-1rα, IL-8, MCP-1,

MIP-1α, MIP-1β, RANTES, and TNFα induced by LPS was inhibited to different degrees, and IL-1β, RANTES, and TNFα were most obviously attenuated (Figure 1D). In comparison with the control medium group, HK-156 treatment alone did not induce any cytokines other than MIF in the medium, which was considered to be background (Figure 1D). As all of the cytokines above are target genes of NF-κB[4], which indicated that HK-156 could inhibit NF-κB targeted cytokine release in LPS-induced THP-1 cells.

To determine whether the ability of HK-156 to reduce the release of proinflammatory cytokines was caused by its cytotoxicity, the CCK-8 method was employed to evaluate cell survival. As shown in Figure 1E, the viability of THP-1 cells treated by HK-156 at a concentration of 20 µmol/L for 48 h was almost the same as that of untreated cells, suggesting that HK-156 had no observable effect on cell survival, at least at concentrations less than 20 µmol/L.

All of these experiments indicated that HK-156 inhibited the transcriptional activation of NF-κB and the release of several NF-κB targeted inflammatory cytokines stimulated by LPS.

HK-156 arrests the release and production of inflammatory cytokines in THP-1 monocytes stimulated by LPS

To further quantitatively evaluate the effect of HK-156 on cytokine release in THP-1 cells stimulated by LPS, the ELISA method was adopted, and different concentrations of HK-156 were used. We found that TNFα and IL-1β release was dramatically induced by LPS and was undetectable in untreated THP-1 cells. However, when pretreated with HK-156, the release of cytokines was significantly reduced in a dose-dependent manner, and 20 µmol/L of HK-156 almost completely abrogated the release of TNFα and IL-1β (Figure 2A and 2B). In addition, HK-156 alone had no effect on the release of TNFα and IL-1β (Figure 2A and 2B).

Next, to determine the level at which HK-156 affected the production of proinflammatory cytokines, we compared the mRNA levels of inflammatory cytokines in THP-1 monocytes. Real-time PCR was performed after the mRNA was isolated from untreated THP-1 monocytes, monocytes treated with LPS alone (1000 ng/mL), pretreated with different concentrations of HK-156 and cocultured with LPS, or treated with HK-156 alone (20 µmol/L) for 2 h. Compared with untreated monocytes, an 80-fold increase in TNFα was induced by LPS. The accumulation of TNFα mRNA after stimulation by LPS was decreased by HK-156 in a dose-dependent manner (Figure 2C). Similarly, the production of IL-1β mRNAs in LPS-stimulated monocytes was also inhibited by HK-156 in a dose-dependent manner, by 2000-fold in some cases (Figure 2D). Moreover, treatment with 20 µmol/L of HK-156 almost completely abrogated the accumulation of both proinflammatory cytokine mRNAs from LPS-stimulated THP-1 monocytes (Figure 2C and 2D). These experiments indicated that HK-156 affected the transcript levels of the previously described proinflammatory cytokines.

Taken together, these results indicated that HK-156 inhibited the release and production of inflammatory cytokines
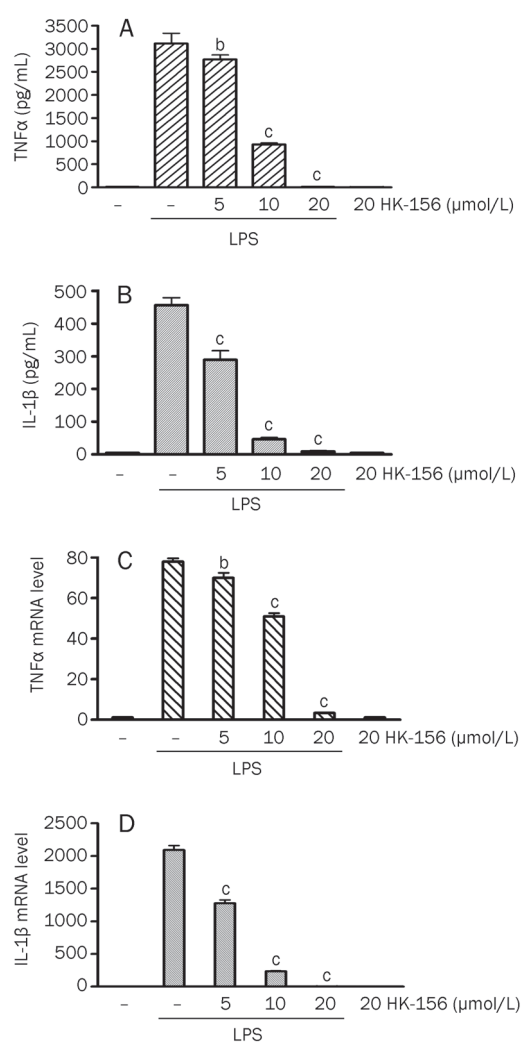
release and production of TNFα and IL-1β in THP-1 cells stimulated by LPS, we asked if HK-156 could inhibit LPS-induced translocation of the NF-κB complex into the nucleus and its binding to DNA. To address this question, after 20 min pretreatment with or without different doses of HK-156, THP-1 cells were stimulated with or without LPS for another 20 min, and then nuclear extracts were prepared and analyzed by EMSA. We found that HK-156 significantly inhibited the formation of the NF-κB-DNA complex in LPS-stimulated human monocytes in a dose-dependent manner, and HK-156 did not induce the DNA-binding activity of NF-κB (Figure 3A). Next, we investigated whether HK-156 directly interfered with the interaction of NF-κB and DNA or inhibited the translocation
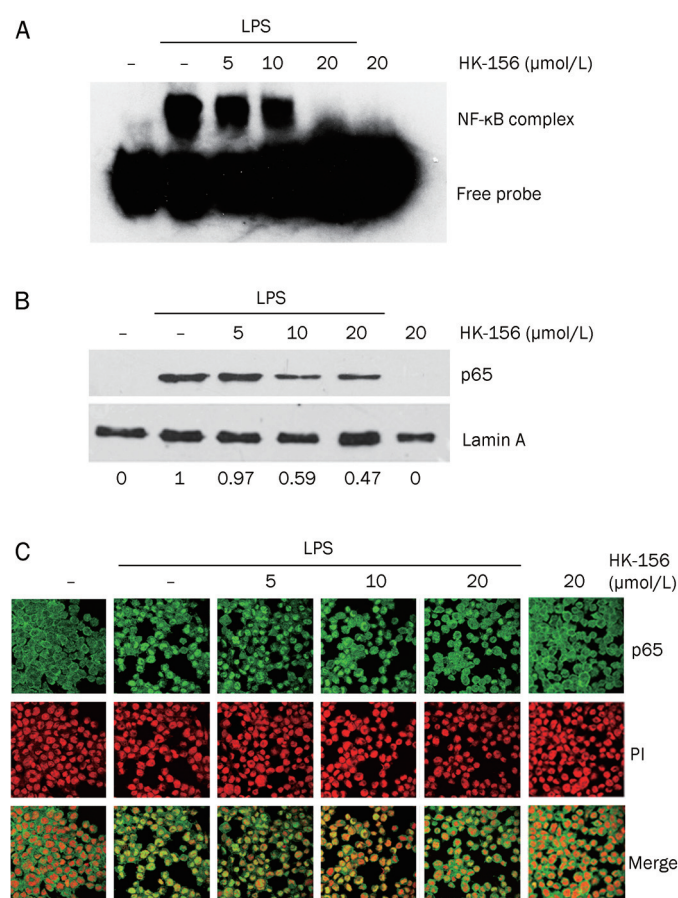

Figure 2. Effect of HK-156 on the release and production of inflammatory cytokines. (A–B) THP-1 monocytes were pretreated with or without different doses of HK-156 for 20 min, followed by the addition of LPS (1000 ng/mL) or PBS to incubate for another 16 h. The supernatant of the medium was collected and subjected to immunodetection of TNFα (A) and IL-1β (B) with an ELISA kit. (C–D) THP-1 monocytes were pretreated with or without the indicated doses of HK-156 20 min prior to the addition of LPS (1000 ng/mL) or PBS for another 2 h, then total RNA was isolated and the mRNA levels of TNFα (C) and IL-1β (D) were determined by quantitative real-time PCR. Values represent mean±SEM (*n*=3; [b]*P*<0.05, [c]*P*<0.01 compared with LPS treatment alone).

Figure 3. Effect of HK-156 on LPS-induced translocation of NF-κB complex into the nucleus and its binding to DNA. (A–B) THP-1 monocytes were pretreated with or without different doses of HK-156 for 20 min, followed by the addition of LPS (1000 ng/mL) or PBS and incubated for another 20 min. The cells were lysed and nuclear protein was extracted, followed by an (A) EMSA assay, or (B) immunoblotting assay with anti-p65 antibody, whereas equal protein loading was verified using an anti-Lamin A antibody. The numbers below the blots depict densitometric values (ratio of p65/Lamin A, normalized to LPS treated alone). (C) After adhesion onto a cover slip was induced by PMA (10 ng/mL) for 12 h, THP-1 monocytes were treated as described above. The cells were then fixed, stained with a monoclonal anti-p65 antibody (upper panel, green) and examined by confocal microscopy. Merged images with nuclei counterstaining with PI (middle panel, red) are shown in the lower panels.

in human THP-1 monocytes at the protein and mRNA levels when stimulated by LPS.

HK-156 impairs LPS-induced translocation of NF-κB complex into the nucleus and the formation of an NF-κB-DNA complex

Canonical NF-κB pathway activation by LPS results in the translocation of the NF-κB complex from the cytosol into the nucleus to bind the DNA of target genes and initiate the transcription and expression of proinflammatory cytokines. Since HK-156 inhibited the transcriptional activation of NF-κB in HEK293hTLR4/NF-κB-luc cells induced by LPS and the

of NF-κB complex into the nucleus, leading to the decreased accumulation of NF-κB in nucleus. For this purpose, nuclear lysates from THP-1 monocytes treated as described above were analyzed by immunoblotting. As shown in Figure 3B, the p65 subunit of the NF-κB complex translocated into the nucleus upon stimulation by LPS. In addition, HK-156 could significantly inhibit the translocation in a dose-dependent manner, and HK-156 alone could not induce the translocation of NF-κB complex into nucleus. The dose-dependent inhibitory effect of HK-156 on the translocation of NF-κB complex into the nucleus was further confirmed by immunofluorescence (Figure 3C). These results demonstrated that HK-156 could inhibit the LPS-induced translocation of NF-κB complex into the nucleus and subsequent binding to DNA in THP-1 cells in a dose-dependent manner, but HK-156 alone had no effect.

Effect of HK-156 on LPS-activated NF-κB and MAPKs signaling pathways

HK-156 could inhibit the LPS-induced translocation of NF-κB complex into the nucleus, which suggested that HK-156 might inhibit the activation of the NF-κB pathway upstream of the NF-κB complex. To examine the molecular mechanisms by which HK-156 inhibited the LPS-stimulated translocation of NF-κB complex into the nucleus in THP-1 monocytes and to determine the target of HK-156, we investigated the effect of HK-156 on the components of the NF-κB signaling pathway from the downstream targets to the upstream regulators along LPS/TLR4/NF-κB.

First, to determine whether the inhibitory effect of HK-156 on the translocation of NF-κB complex into the nucleus induced by LPS resulted from direct interference with the translocation of NF-κB complex or the inhibition of the activation of upstream regulators, THP-1 monocytes pretreated with different doses of HK-156 (0, 5, 10, and 20 μmol/L) for 20 min were incubated with LPS (1000 ng/mL) for another 20 min, and cell lysates were subjected to immunoblotting assay. We found that the phosphorylation of IκBα stimulated by LPS was significantly inhibited by HK-156, leading to the reduced degradation of IκBα (Figure 4A). When phosphorylation of the IKK complex was detected, HK-156 blocked the LPS-induced phosphorylation of IKKβ at Serine181, Serine177 or both simultaneously (Figure 4A). However, the induction of phosphorylation of IKKα at Ser180 by HK-156 in a dose-dependent manner was also observed (Figure 4A). Furthermore, TAK1 phosphorylation as a result of LPS stimulation was also inhibited by HK-156 in a dose-dependent manner (Figure 4A). Treatment with HK-156 alone (20 μmol/L) had no effect on the activation of the NF-κB signaling pathway other than phosphorylation of IKKα at Ser180 (Figure 4A).

Second, mitogen-activated protein kinases (MAPKs) are families of serine/threonine protein kinases, including c-Jun NH2-terminal kinase (JNK), ERK, and p38. MAPK signaling is another important signaling pathway induced by LPS[15, 17]. To explore whether HK-156 affected LPS-induced MAPK signaling, THP-1 monocytes were lysed and subjected to an immu-
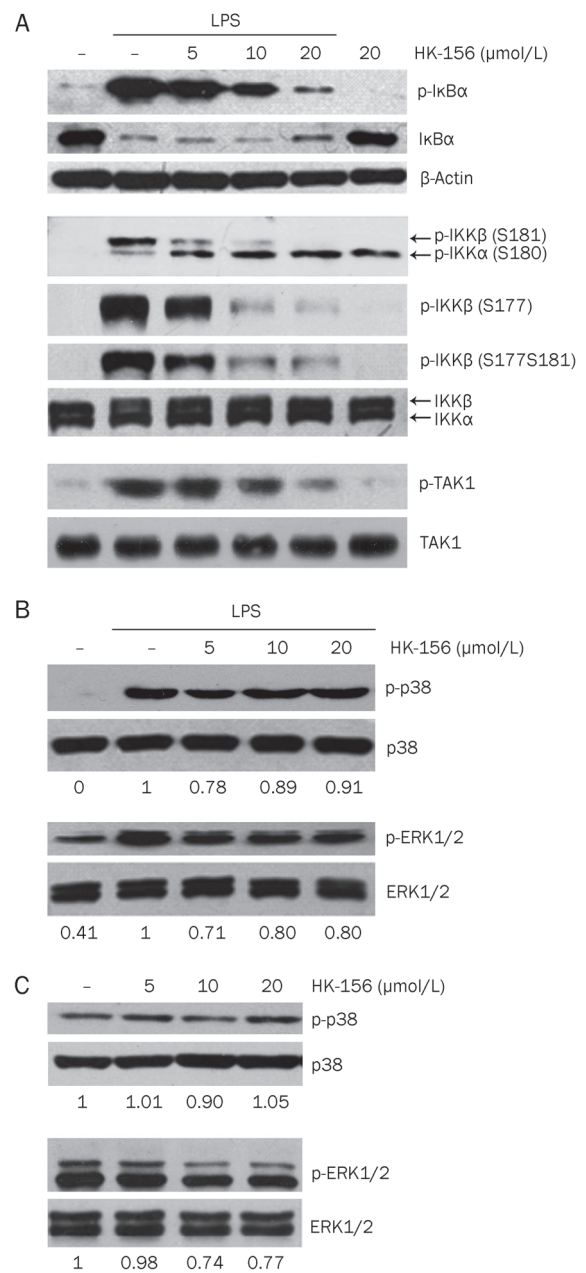

Figure 4. Effect of HK-156 on LPS-activated NF-κB and MAPKs signaling pathways. (A) THP-1 monocytes were pretreated with or without different doses of HK-156 for 20 min, followed by the addition of LPS (1 μg/mL) or PBS and incubated for another 20 min. The cells were lysed and subjected to an immunoblotting assay with anti-p-IκBα, IκBα, p-IKKβ (Ser181)/p-IKKα (Ser180), p-IKKβ (Ser177), p-IKKβ (Ser177Ser181), and p-TAK1 antibodies. The expression of β-actin, IKKβ/IKKα, or TAK1, respectively, served as the loading control. (B) The cells were treated with HK-156 and LPS as described in (A), followed by an immunoblotting assay probed by p-p38 and p-ERK1/2 antibodies, whereas total p38 and total ERK1/2, respectively, served as controls. The numbers below the blots depict densitometric values (ratio of p-p38 to p38 or p-ERK1/2 to ERK1/2, respectively, normalized to LPS treated alone). (C) Lysates of THP-1 monocytes treated with the indicated doses of HK-156 for 20 min were subjected to immunoblotting with p-p38 or p-ERK1/2 antibodies, whereas total p38 and total ERK1/2, respectively, served as controls. The numbers below the blots depict the densitometric values (ratio of p-p38 to p38 or p-ERK1/2 to ERK1/2, respectively, normalized to control).

noblotting assay after pretreatment by HK-156 (0, 5, 10, and 20 µmol/L) for 20 min prior to the addition of LPS (1 µg/mL) for another 20 min. As shown in Figure 4B, the phosphorylation of both p38 and ERK1/2 induced by LPS was slightly inhibited by treatment of HK-156. Meanwhile, when the cells were treated with HK-156 in the absence of LPS at various concentrations (0, 5, 10, and 20 µmol/L), the phosphorylation of p38 was not apparently altered, but the phosphorylation of ERK1/2 was slightly decreased (Figure 4C). Considering that HK-156 could inhibit the phosphorylation of ERK1/2 to almost the same degree when THP-1 cells were treated with or without LPS, HK-156 itself might have no influence on the phosphorylation of ERK1/2 induced by LPS.

Overall, HK-156 blocked LPS activated NF-κB signaling through inhibiting the phosphorylation of TAK1 and slightly inhibiting p38 signaling induced by LPS, whereas it might not affect the phosphorylation of ERK1/2 stimulated by LPS.

Effect of HK-156 on LPS-induced activation of NF-κB signaling is thiol dependent

Considering the structure of HK-156 (Figure 1A), HK-156 is a Michael reaction acceptor molecule because it has an α,β-unsaturated carbonyl group. We speculated that the α,β-unsaturated carbonyl group is the functional group. To address this question, compound **809**, an HK-156 analogue with only a carbonyl group, was used as a reference. As shown in Figure 5A, compound **809** could not inhibit LPS-induced transcription activation of NF-κB. This result suggested that the α,β-unsaturated carbonyl group is required for HK-156 to have an effect on the activation of the NF-κB pathway. Furthermore, as α,β-unsaturated carbonyl groups react with thiols, it is possible that the inhibition of the LPS-based activation of the NF-κB pathway by HK-156 was through a reaction with thiol groups of the cysteines in the component proteins of the NF-κB pathway. If so, other thiol-containing reagents might compete with HK-156 for the cysteines of the target protein(s) and alleviate the effects of HK-156 on the LPS-induced activation of the NF-κB pathway. As shown in Figure 5B, the inhibition of the LPS-induced transcriptional activation of NF-κB by HK-156 was indeed abrogated in the presence of the thiol-containing reagent reduced glutathione (GSH). Furthermore, the HK-156-mediated inhibition of LPS-induced IKKβ and IκBα phosphorylation was also abolished in the presence of GSH (Figure 5C), as was the inhibition of LPS-induced TNFα release (Figure 5D). In addition, the reference compound **809** did not alter the LPS-induced phosphorylation of IKKβ and IκBα or the release of TNFα. These results showed that HK-156 inhibited the LPS-induced NF-κB signaling pathway through interacting with the cysteine thiol groups of an unknown protein upstream of the IKK complex. To further understand the HK-156-thiol interaction, HK-156 was incubated with GSH, and the products were examined using mass spectrometry (MS). The analysis detected one major component at *m/z* 511.3 [HK-156+GSH+H]$^+$, indicating the addition of one molecule of GSH to one molecule of HK-156 (Figure 5D). The proposed reaction site of HK-156 is illustrated in Figure 5D.

Taken together, the results provided strong evidence indicating that a Michael reaction acceptor is required for the inhibitory activity of HK-156 against NF-κB signaling, and this group reacts with thiols and inhibits the LPS-induced activation of the NF-κB signaling pathway.

HK-156 inhibits LPS-induced secretion of TNFα *in vivo* and increases mouse survival in a model of sepsis

Because HK-156 efficiently inhibited the LPS-induced activation of the NF-κB pathway and the release of proinflammatory cytokines *in vitro*, we next investigated whether HK-156 could reduce the secretion of proinflammatory cytokines *in vivo* and be effective in protecting mice from lethality in a mouse endotoxemia model of sepsis as a model of systemic inflammation. BALB/c mice were injected iv with different doses of HK-156 (10, 30, and 50 mg/kg) or vehicle control, and 2 h later they were challenged ip with LPS (15 mg/kg) or NS. Mice that received HK-156 alone had no detectable serum TNFα. However, pretreatment of mice with HK-156 before the LPS challenge attenuated the increase in serum TNFα levels elicited after 2 h of LPS challenge in a dose-dependent manner, with treatment of 50 mg/kg of HK-156 yielding statistically significant results (Figure 6A, 8174±1872 pg/mL for the LPS group *vs* 1146±444 pg/mL for the HK-156 plus LPS group, *n*=3, 12 animals per treatment. *P*<0.05). When the relative cytokine level in the serum was further detected with a cytokine array assay, as shown in Figure 6B, HK-156 alone had no effect on the induced serum cytokine release, whereas LPS induced the secretion of many proinflammatory cytokines, including G-CSF, IL-6, MIP-1, TNFα, and RANTES[27]. Pretreatment of mice with HK-156 (50 mg/kg) attenuated the increase of some of these cytokines and reduced the TNFα level in the serum (Figure 6B).

We next investigated whether HK-156 could increase the survival of mice treated with a lethal dose of LPS. Animals were injected iv with 50 mg/kg of HK-156 (or vehicle control) 2 h prior to injecting a lethal dose of LPS (as described above). Mice receiving HK-156 alone exhibited no lethality. In contrast, all of the mice that received LPS alone died within 69 h post challenge. Pretreatment with HK-156 resulted in an extended survival time of up to 200 h in 25% of the mice (Figure 6C).

These results suggested that HK-156 inhibited the LPS-induced secretion of TNFα *in vivo* and enhanced survival in a mouse model of sepsis.

Discussion

Accumulating evidence indicates that constitutively activated NF-κB signaling and uncontrolled expression of proinflammatory cytokines are correlated with the pathogenesis of inflammatory disease. The inhibition of NF-κB signaling has become a well-recognized strategy for anti-inflammatory therapy. In the present study, using an NF-κB luciferase reporter system consisting of the stably transfected cell line HEK293hTLR4/NF-κB-luc, we found that the small molecule HK-156 could
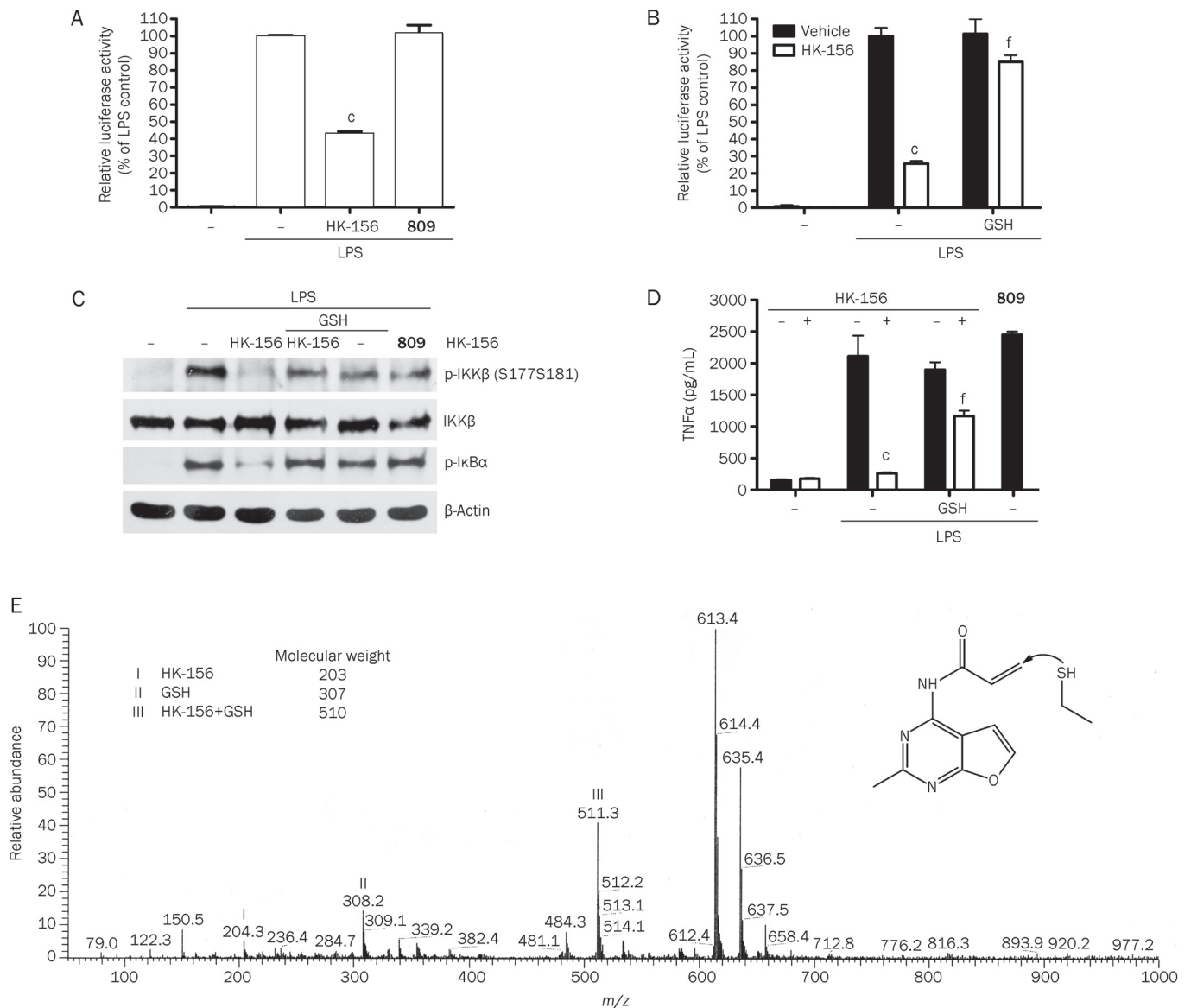
Figure 5. Inhibition of LPS/NF-κB signaling by HK-156 is thiol dependent. (A) HEK293hTLR4/NF-κB-luc cells were pretreated with HK-156 (10 μmol/L) or **809** (10 μmol/L) for 20 min and then stimulated with LPS for 6 h. Cells were harvested for the luciferase assay. (B) HEK293hTLR4/NF-κB-luc cells were pretreated with GSH, HK-156 (10 μmol/L) or a mixture (HK-156 and GSH were premixed for 1 h at 37 °C) for 20 min and then stimulated with LPS for 6 h. Cells were harvested for the luciferase assay. (C) THP-1 cells were pretreated with GSH, HK-156 (10 μmol/L), the mixture or **809** (10 μmol/L) for 20 min and then stimulated with LPS for 20 min. Whole cell lysates were processed for Western blotting analysis using antibodies as indicated. (D) THP-1 cells were pretreated with GSH, HK-156 (10 μmol/L), the mixture or **809** (10 μmol/L) for 20 min and then stimulated with LPS for 16 h. The cell culture media were collected and subjected to an ELISA for TNFα. (E) HK-156 was incubated with 4 eq of GSH for 60 min at 37 °C, and the mixture was resolved by mass spectrometry. The molecular weights of the molecules are indicated. An arrow indicates the functional group of HK-156, which may react with thiol nucleophiles. $n=3$. Mean±SEM. $^c P<0.01$ vs vehicle. $^f P<0.01$ vs HK-156 10 μmol/L.

inhibit the LPS-induced transcriptional activity of NF-κB in a dose-dependent fashion. HK-156 significantly inhibited the LPS-stimulated production of proinflammatory cytokines in human monocytes through the inactivation of NF-κB, via suppressing the LPS-induced phosphorylation of TAK1. In addition, we showed *in vivo* that HK-156 inhibited LPS-stimulated TNFα secretion and enhanced survival in a mouse model of lethal LPS-induced sepsis.

To discover a novel NF-κB inhibitor, we established an NF-κB luciferase reporter system, the stably transfected cell line HEK293hTLR4/NF-κB-luc, which expresses TLR4, MD-2 and CD14. Using cell-based high-throughput screening with LPS as a stimulus, we found that the small molecule HK-156 could inhibit the LPS-induced transcriptional activity of NF-κB in a dose-dependent fashion (Figure 1C). Monocytes play a critical role in the pathogenesis of various infectious and
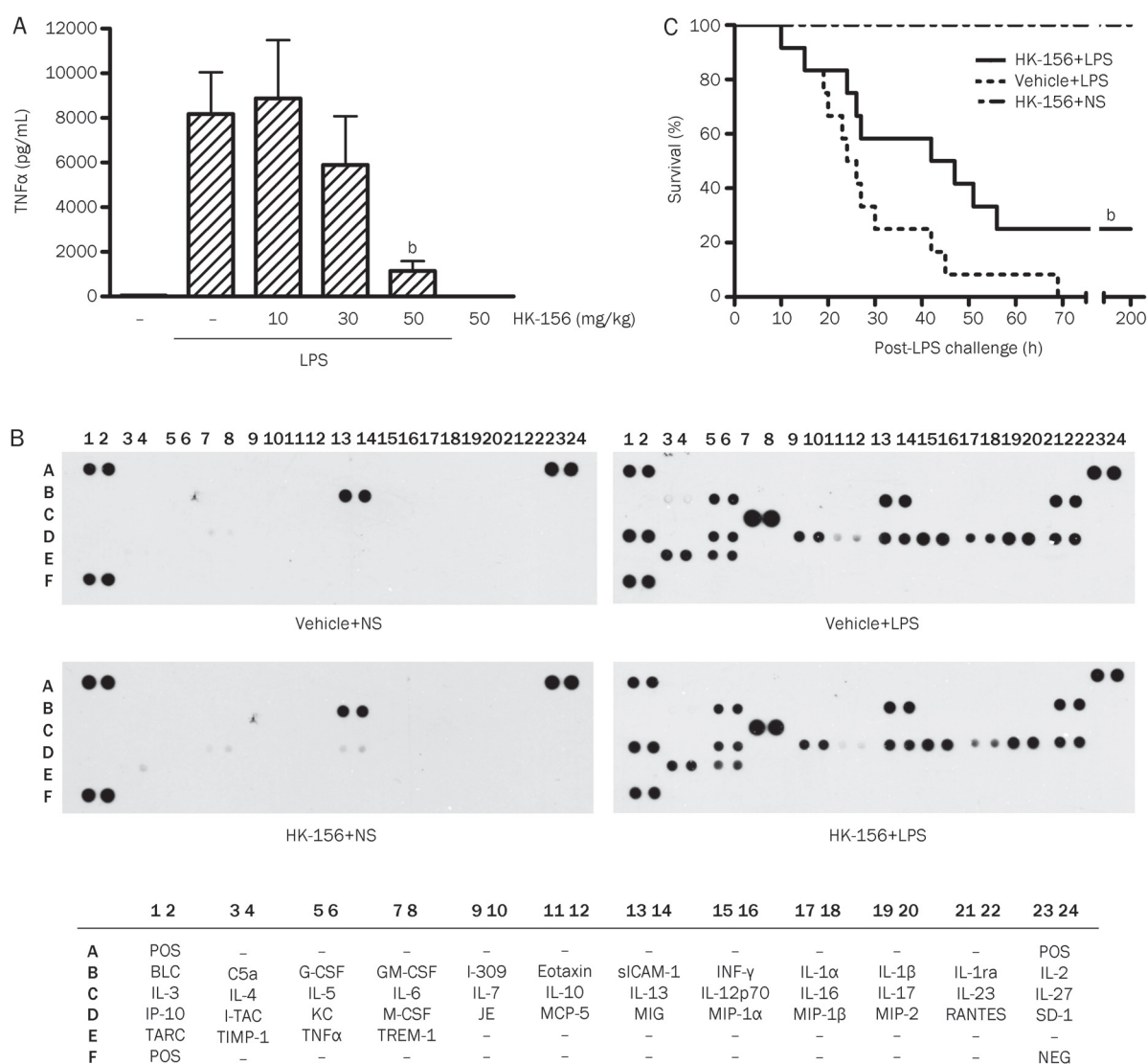
Figure 6. Effect of HK-156 on LPS-induced secretion of inflammatory cytokines and mortality *in vivo*. BALB/c mice (12 mice/group) were administered iv with the indicated doses of HK-156 (10, 30, and 50 mg/kg body weight) or vehicle 2 h before ip administration of LPS (15 mg/kg body weight). (A) The serum level of TNFα was determined 2 h after the LPS or NS injection with ELISA assays. Results represent the mean±SEM of three independent experiments (using 12 animals per experimental group. Mean±SEM. bP<0.05 compared with LPS treated alone). (B) The mixture of equal volume of serum from each mouse per group 2 h after the LPS or NS injection was subjected to cytokine array analysis. The positions of the respective cytokines and controls on the array are shown below. (C) Survival was monitored every 1 h over the course of 200 h. Experiments were performed three times using 12 animals per group and reported in a Kaplan-Meier survival curve. bP<0.05 vs Vehicle+LPS.

inflammatory diseases[28]. Thus, the human monocyte cell line THP-1 was employed to study the efficacy and mechanism of action of HK-156. LPS induced the release of many NF-κB targeted cytokines (Figure 1D), consistent with previously reported results[29]. However, HK-156 reduced the expression of these cytokines after treatment of the cells with LPS. IL-1β, RANTES and TNFα were the most apparently attenuated. The incomplete attenuation might be explained by the fact that the expression of proinflammatory cytokines is not exclusively regulated by NF-κB but is also affected by the integration of several other transcription factors.

The inhibition of the production and release of proinflam-matory cytokines from LPS-stimulated THP-1 cells in a dose-dependent manner indicated that HK-156 significantly inhibited the transcription of cytokines TNFα and IL-1β at the mRNA level and then resulted in reduced secretion of cytokines at the protein level (Figure 2). HK-156 significantly impaired LPS-stimulated translocation of NF-κB into the nucleus and its binding with DNA concomitant with the phosphorylation and degradation of IκBα (Figure 3). It also inhibited the phosphorylation of IKKβ and TAK1 in THP-1 cells stimulated by LPS in a dose-dependent manner to almost the same degree seen for the transcriptional activation of NF-κB in HEK293hTLR4/NF-κB-luc cells (Figure 1C, 4A). All

of these data suggested that HK-156 is an NF-κB inhibitor. It inhibited the LPS-induced phosphorylation of TAK1, resulting in IKKβ inactivation, and subsequently reduced the phosphorylation and degradation of IκBα, blocking the translocation of the NF-κB complex into the nucleus and binding to the κB enhancer sequence of the targeted genes. As a consequence, HK-156 decreased the production and secretion of proinflammatory cytokines such as TNFα and IL-1β in THP-1 cells.

The impaired phosphorylation of TAK1 caused by HK-156 indicated that a molecule upstream of TAK1 in the LPS-induced NF-κB signaling pathway might be a potential target of HK-156. The activation of TAK1 is a prerequisite not only for the activation of IKKβ but also for the activation of MAPKs such as mitogen-activated protein kinase kinase 6 (MKK6, also known as MAP2K6), which is stimulated by LPS, which, in turn, phosphorylates JNK and p38 kinase[20, 30–32]. However, the activation of another MAPK kinase (*ie*, ERK) following TLR4 stimulation by LPS does not seem to require the activation of TAK1. It has been reported that LPS induced the activation of ERK in THP-1 cells, leading to the phosphorylation of Elk-1 and the expression of Erg-1, which acted together with independently activated NF-κB to induce gene expression[33]. The phosphorylation of IKKβ and MAPK p38 in THP-1 cells stimulated by LPS was weakened by HK-156 (Figure 4A, 4B), further showing that HK-156 might target a protein upstream of TAK1 within the LPS/TLR4/TAK1/NF-κB signaling pathway, perhaps by interfering with the protein-protein interaction between adapters. This information is consistent with the fact that the highly selective IKKβ inhibitor TPCA-1[24] did not inhibit the phosphorylation of TAK1 induced by LPS (data not shown). HK-156 might have no influence on the phosphorylation of ERK1/2 induced by LPS, and because activation of ERK is independent of NF-κB signaling, the influence of HK-156 on the phosphorylation of ERK1/2 induced by LPS might not affect the effect of HK-156 on NF-κB signaling. All of these results suggest that the inhibition of the LPS-induced production of proinflammatory mediators by HK-156 might occur through targeting a protein upstream of TAK1 and then downregulating the TAK1/IKK and TAK1/p38 MAPK pathways.

The release of proinflammatory cytokines induced by LPS through the activation of NF-κB signaling is the major pathological mechanism of sepsis[14]. Experimental models of sepsis have also shown increased levels of TNFα in the serum preceding organ failure[34]. TNFα is the major contributor to organ failure and death in the progression of sepsis[35], and anti-TNF-mAb therapy (Afelimomab) in clinical trials has had a little positive effect[21]. During sepsis *in vivo*, the upregulation of proinflammatory cytokines initiates and contributes to organ dysfunction syndrome. The inhibition of the expression of these molecules may ameliorate inflammation. In our study, HK-156 protected mice from LPS-induced lethal toxicity *in vivo* (Figure 6C). This effect was accompanied by a decrease in the LPS-stimulated production of TNFα, demonstrating the anti-inflammatory potential of HK-156 *in vivo*. The increased survival of mice pretreated with HK-156 is in agreement with

our *in vitro* experiments. Moreover, attenuation of many proinflammatory cytokines release besides TNFα induced by LPS *in vivo* showed that HK-156 might have better effect than anti-TNF-mAb. However, recent studies showed that the elevated serum level of a late mediator, high mobility group box 1 (HMGB1), is highly correlated with the lethal outcome of human sepsis[36, 37]. The effect of HK-156 on sepsis might be further assessed based on levels of this mediator rather than the inhibition of the release of early proinflammatory cytokines.

Interestingly, we found that HK-156 inhibited the LPS-stimulated phosphorylation of IKKβ at Ser177 and Ser181 in the T-loop but induced the phosphorylation of IKKα at Ser180 (Figure 4A). As a core element of NF-κB signaling, the IKK complex primarily consists of IKKα, IKKβ and the regulatory subunit IKKγ/NEMO[3]. Until the present study, the fact that IKKβ but not IKKα plays a key role in the activation of classic NF-κB signaling had been clearly elucidated[1]. The simultaneous blockage of the phosphorylation of IKKβ at Ser177 and Ser181 completely inhibits the transduction of NF-κB signaling[38]. The phosphorylation of both sites of IKKβ that is induced by LPS was blocked by HK-156, showing that HK-156 is an effective inhibitor of NF-κB signaling (Figure 4A). However, the function of IKKα in the activation of classic NF-κB signaling is still ambiguous and has not been clearly described to date[1]. There are two paradoxical conclusions that can be drawn regarding the role of IKKα in the activation of NF-κB signaling during the process of inflammation. Some reports demonstrated that activation of IKKα through phosphorylation was essential for the expression of cytokines induced by stimuli. Activation of IKKα, resulting in the phosphorylation of p65 and histones, gives rise to the positive regulation of transcriptional activation of NF-κB[39–41]. In contrast, a negative regulatory function of IKKα in the activation of NF-κB signaling has also been reported[42, 43]. Manipulations that inactivate IKKα cause the suppression of NF-κB activity by accelerating both the turnover of the NF-κB subunits RelA and c-Rel and their removal from proinflammatory gene promoters[42]. Liu *et al* also reported that proinflammatory stimuli induced the activation and translocation of IKKα into the nucleus and then phosphorylated PIAS1 [protein inhibitor of activated STAT1 (signal transducer and activator of transcription 1)] to restrict inflammation and immune response[43]. Based on the function of IKKα, the author further proposed that small molecules that could enhance the phosphorylation of PIAS1 by activating IKKα might prove effective in reducing inflammation[44]. Usually, the activation of the kinase can be induced only when both sites in the T-loop of IKK are phosphorylated[38]. However, the kinase will be partly activated when a single site is phosphorylated. The role of the phosphorylation site of IKKβ at Ser181 is more important than that at Ser177[38]. As for IKKα, phosphorylation at Ser176 plays a critical role in NIK (NF-κB-inducing kinase)-induced nonclassical NF-κB signaling[45] and the expression of interferon-α through the activation of interferon regulatory factor 3/7 (IRF3/7) by NIK[46]. IKKα phosphorylated only at Ser180 has partial kinase

activity[46]. The phosphorylation of IKKα induced by HK-156 only at Ser180 might suggest that HK-156 can partially activate the kinase activity of IKKα (Figure 4A). In contrast, LPS could induce weak phosphorylation of IKKα at Ser180 but not at Ser176 in THP-1 cells (Figure 4A). The real function of the partial activation of IKKα by HK-156 and LPS in THP-1 cells needs to be further investigated, although the possible positive regulation of NF-κB by HK-156 was disproved by the finding that HK-156 alone did not induce the transcriptional activation of NF-κB and expression of proinflammatory cytokines.

Many natural products that are thiol-reactive compounds with Michael reaction acceptor groups have been reported to inhibit NF-κB signaling. Eriocalyxin B (Eri-B), an ent-kauranoid isolated from *Isodon eriocalyx*, can selectively block the binding between NF-κB and the response elements in a noncompetitive manner through its functional Michael reaction acceptor without affecting the nuclear translocation of the transcription factor[47]. Several diterpenoids isolated from *Isodon rubescens* have also been shown to impact the translocation of NF-κB from the cytoplasm to nuclei without affecting IκBα phosphorylation and degradation[48]. Caffeic acid phenethyl ester (CAPE), an active component of propolis from honeybees, was shown to directly inhibit the activity of IKKβ at 25 μmol/L without influencing the TNFα-induced phosphorylation of IKKβ, in which the electrophilic Michael reaction acceptor might be involved[49]. Moreover, a cyclopentanone prostaglandin was found to inhibit the activity of IKKβ through the interaction of the thiol of cysteine 179 in IKKβ with a Michael reaction acceptor in the prostaglandin[50]. In our studies, HK-156 was shown to be more effective than CAPE and to inhibit LPS-induced NF-κB signaling dependent on the presence of the Michael reaction acceptor group. Furthermore, the effect of HK-156 is thiol dependent. Because HK-156 can attenuate the phosphorylation of TAK1 and IKKβ and the translocation of the NF-κB complex into the nucleus and the formation of the NF-κB-DNA complex in a dose-dependent manner, it is not likely that HK-156 could inhibit the activity of IKKβ or binding of NF-κB with DNA. The cellular target of HK-156 might be a cysteine-containing protein upstream of TAK1 whose identity is still under investigation.

In summary, our study discovered that a novel synthetic small molecule HK-156 is a potent inhibitor of the LPS/NF-κB signaling pathway. HK-156 potently inhibited the LPS-induced transcriptional activation of NF-κB. Morever, HK-156 could inhibit TNFα production, possibly through targeting a protein upstream of TAK1 that might contain cysteine, resulting in the inhibition of LPS-induced activation of NF-κB signaling *in vitro* in THP-1 monocytes. In addition, HK-156 could protect mice from LPS-induced lethality, accompanied by decreased TNFα production *in vivo*. Our study provides a novel NF-κB inhibitor with potential application for the treatment of sepsis. Furthermore, given the novel structure of HK-156, HK-156 might be used as a lead compound for developing new drugs for the treatment of sepsis and other inflammatory diseases.

Author contribution

Dr Kan DING and Dr You-hong HU designed the research; Jian-ping FANG, Jie LI, and Wen-feng LIAO performed the research; Yang LIU contributed new agents; Jian-ping FANG wrote the paper; Dr Kan DING revised the paper.

Supplementary information

Supplementary figures are available at website of Acta Pharmacologica Sinica on NPG.

References

1 Hayden MS, Ghosh S. Shared principles in NF-kappaB signaling. Cell 2008; 132: 344–62.

2 Vallabhapurapu S, Karin M. Regulation and function of NF-kappaB transcription factors in the immune system. Annu Rev Immunol 2009; 27: 693–733.

3 Huxford T, Ghosh G. A structural guide to proteins of the NF-kappaB signaling module. Cold Spring Harb Perspect Biol 2009; 1: a000075.

4 Pahl HL. Activators and target genes of Rel/NF-kappaB transcription factors. Oncogene 1999; 18: 6853–66.

5 Yamamoto Y, Gaynor RB. Role of the NF-kappaB pathway in the pathogenesis of human disease states. Curr Mol Med 2001; 1: 287–96.

6 Gerondakis S, Grumont R, Gugasyan R, Wong L, Isomura I, Ho W, *et al*. Unravelling the complexities of the NF-kappaB signalling pathway using mouse knockout and transgenic models. Oncogene 2006; 25: 6781–99.

7 Dong J, Jimi E, Zeiss C, Hayden MS, Ghosh S. Constitutively active NF-kappaB triggers systemic TNFalpha-dependent inflammation and localized TNFalpha-independent inflammatory disease. Genes Dev 2010; 24: 1709–17.

8 Ivanenkov YA, Balakin KV, Tkachenko SE. New approaches to the treatment of inflammatory disease: focus on small-molecule inhibitors of signal transduction pathways. Drugs R D 2008; 9: 397–434.

9 O'Neill LA. Targeting signal transduction as a strategy to treat inflammatory diseases. Nat Rev Drug Discov 2006; 5: 549–63.

10 Sarkar FH, Li Y, Wang Z, Kong D. NF-kappaB signaling pathway and its therapeutic implications in human diseases. Int Rev Immunol 2008; 27: 293–319.

11 Suffredini AF, Munford RS. Novel therapies for septic shock over the past 4 decades. JAMA 2011; 306: 194–9.

12 Bone RC, Grodzin CJ, Balk RA. Sepsis: a new hypothesis for pathogenesis of the disease process. Chest 1997; 112: 235–43.

13 Munford RS. Severe sepsis and septic shock: the role of gram-negative bacteremia. Annu Rev Pathol 2006; 1: 467–96.

14 Liu SF, Malik AB. NF-kappa B activation as a pathological mechanism of septic shock and inflammation. Am J Physiol Lung Cell Mol Physiol 2006; 290: L622–45.

15 Lu YC, Yeh WC, Ohashi PS. LPS/TLR4 signal transduction pathway. Cytokine 2008; 42: 145–51.

16 Sato S, Sanjo H, Takeda K, Ninomiya-Tsuji J, Yamamoto M, Kawai T, *et al*. Essential function for the kinase TAK1 in innate and adaptive

npg
www.nature.com/aps
Fang JP *et al*

1216

immune responses. Nat Immunol 2005; 6: 1087–95.

17 Guha M, Mackman N. LPS induction of gene expression in human monocytes. Cell Signal 2001; 13: 85–94.

18 Kawai T, Akira S. The role of pattern-recognition receptors in innate immunity: update on Toll-like receptors. Nat Immunol 2010; 11: 373–84.

19 Miggin SM, O'Neill LA. New insights into the regulation of TLR signaling. J Leukoc Biol 2006; 80: 220–6.

20 Beutler B. Microbe sensing, positive feedback loops, and the pathogenesis of inflammatory diseases. Immunol Rev 2009; 227: 248–63.

21 Wheeler DS, Zingarelli B, Wheeler WJ, Wong HR. Novel pharmacologic approaches to the management of sepsis: targeting the host inflammatory response. Recent Pat Inflamm Allergy Drug Discov 2009; 3: 96–112.

22 Gilmore TD, Herscovitch M. Inhibitors of NF-kappaB signaling: 785 and counting. Oncogene 2006; 25: 6887–99.

23 Calzado MA, Bacher S, Schmitz ML. NF-kappaB inhibitors for the treatment of inflammatory diseases and cancer. Curr Med Chem 2007; 14: 367–76.

24 Bamborough P, Callahan JF, Christopher JA, Kerns JK, Liddle J, Miller DD, *et al*. Progress towards the development of anti-inflammatory inhibitors of IKKbeta. Curr Top Med Chem 2009; 9: 623–39.

25 Leon CG, Tory R, Jia J, Sivak O, Wasan KM. Discovery and development of toll-like receptor 4 (TLR4) antagonists: a new paradigm for treating sepsis and other diseases. Pharm Res 2008; 25: 1751–61.

26 Barochia A, Solomon S, Cui X, Natanson C, Eichacker PQ. Eritoran tetrasodium (E5564) treatment for sepsis: review of preclinical and clinical studies. Expert Opin Drug Metab Toxicol 2011; 7: 479–94.

27 Abraham E. Nuclear factor-kappaB and its role in sepsis-associated organ failure. J Infect Dis 2003; 187: S364–9.

28 Robbins CS, Swirski FK. The multiple roles of monocyte subsets in steady state and inflammation. Cell Mol Life Sci 2010; 67: 2685–93.

29 Suzuki T, Hashimoto S, Toyoda N, Nagai S, Yamazaki N, Dong HY, *et al*. Comprehensive gene expression profile of LPS-stimulated human monocytes by SAGE. Blood 2000; 96: 2584–91.

30 Palsson-McDermott EM, O'Neill LA. Signal transduction by the lipopolysaccharide receptor, Toll-like receptor-4. Immunology 2004; 113: 153–62.

31 Landstrom M. The TAK1-TRAF6 signalling pathway. Int J Biochem Cell Biol 2010; 42: 585–9.

32 Hayden MS, Ghosh S. Signaling to NF-kappaB. Genes Dev 2004; 18: 2195–224.

33 Guha M, O'Connell MA, Pawlinski R, Hollis A, McGovern P, Yan SF, *et al*. Lipopolysaccharide activation of the MEK-ERK1/2 pathway in human monocytic cells mediates tissue factor and tumor necrosis factor alpha expression by inducing Elk-1 phosphorylation and Egr-1 expression. Blood 2001; 98: 1429–39.

34 Tracey KJ, Cerami A. Tumor necrosis factor, other cytokines and disease. Annu Rev Cell Biol 1993; 9: 317–43.

35 Secher T, Vasseur V, Poisson DM, Mitchell JA, Cunha FQ, Alves-Filho JC, *et al*. Crucial role of TNF receptors 1 and 2 in the control of poly-microbial sepsis. J Immunol 2009; 182: 7855–64.

36 Huang W, Tang Y, Li L. HMGB1, a potent proinflammatory cytokine in sepsis. Cytokine 2010; 51: 119–26.

37 Wang H, Bloom O, Zhang M, Vishnubhakat JM, Ombrellino M, Che J, *et al*. HMG-1 as a late mediator of endotoxin lethality in mice. Science 1999; 285: 248–51.

38 Delhase M, Hayakawa M, Chen Y, Karin M. Positive and negative regulation of IkappaB kinase activity through IKKbeta subunit phosphorylation. Science 1999; 284: 309–13.

39 Yang F, Tang E, Guan K, Wang CY. IKK beta plays an essential role in the phosphorylation of RelA/p65 on serine 536 induced by lipopolysaccharide. J Immunol 2003; 170: 5630–5.

40 Anest V, Hanson JL, Cogswell PC, Steinbrecher KA, Strahl BD, Baldwin AS. A nucleosomal function for IkappaB kinase-alpha in NF-kappaB-dependent gene expression. Nature 2003; 423: 659–63.

41 Yamamoto Y, Verma UN, Prajapati S, Kwak YT, Gaynor RB. Histone H3 phosphorylation by IKK-alpha is critical for cytokine-induced gene expression. Nature 2003; 423: 655–9.

42 Lawrence T, Bebien M, Liu GY, Nizet V, Karin M. IKKalpha limits macrophage NF-kappaB activation and contributes to the resolution of inflammation. Nature 2005; 434: 1138–43.

43 Liu B, Yang Y, Chernishof V, Loo RR, Jang H, Tahk S, *et al*. Proinflammatory stimuli induce IKKalpha-mediated phosphorylation of PIAS1 to restrict inflammation and immunity. Cell 2007; 129: 903–14.

44 Liu B, Shuai K. Targeting the PIAS1 SUMO ligase pathway to control inflammation. Trends Pharmacol Sci 2008; 29: 505–9.

45 Ling L, Cao Z, Goeddel DV. NF-kappaB-inducing kinase activates IKK-alpha by phosphorylation of Ser-176. Proc Natl Acad Sci U S A 1998; 95: 3792–7.

46 Wang RP, Zhang M, Li Y, Diao FC, Chen D, Zhai Z, *et al*. Differential regulation of IKK alpha-mediated activation of IRF3/7 by NIK. Mol Immunol 2008; 45: 1926–34.

47 Leung CH, Grill SP, Lam W, Gao W, Sun HD, Cheng YC. Eriocalyxin B inhibits nuclear factor-kappaB activation by interfering with the binding of both p65 and p50 to the response element in a noncompetitive manner. Mol Pharmacol 2006; 70: 1946–55.

48 Leung CH, Grill SP, Lam W, Han QB, Sun HD, Cheng YC. Novel mechanism of inhibition of nuclear factor-kappa B DNA-binding activity by diterpenoids isolated from *Isodon rubescens*. Mol Pharmacol 2005; 68: 286–97.

49 Lee Y, Shin DH, Kim JH, Hong S, Choi D, Kim YJ, *et al*. Caffeic acid phenethyl ester-mediated Nrf2 activation and IkappaB kinase inhibition are involved in NFkappaB inhibitory effect: structural analysis for NFkappaB inhibition. Eur J Pharmacol 2010; 643: 21–8.

50 Rossi A, Kapahi P, Natoli G, Takahashi T, Chen Y, Karin M, *et al*. Anti-inflammatory cyclopentenone prostaglandins are direct inhibitors of IkappaB kinase. Nature 2000; 403: 103–8.